


December 2015

# Arylboronates as H<sub>2</sub>O<sub>2</sub> or Photo-Inducible DNA Cross-Linking Agents: Design, Synthesis, Mechanism, and Anticancer Activity

Yibin Wang

*University of Wisconsin-Milwaukee*

Follow this and additional works at: <https://dc.uwm.edu/etd>

 Part of the [Biochemistry Commons](#), and the [Organic Chemistry Commons](#)

---

## Recommended Citation

Wang, Yibin, "Arylboronates as H<sub>2</sub>O<sub>2</sub> or Photo-Inducible DNA Cross-Linking Agents: Design, Synthesis, Mechanism, and Anticancer Activity" (2015). *Theses and Dissertations*. 1103.  
<https://dc.uwm.edu/etd/1103>

This Dissertation is brought to you for free and open access by UWM Digital Commons. It has been accepted for inclusion in Theses and Dissertations by an authorized administrator of UWM Digital Commons. For more information, please contact [open-access@uwm.edu](mailto:open-access@uwm.edu).

ARYLBORONATES AS H<sub>2</sub>O<sub>2</sub> OR PHOTO-INDUCIBLE DNA CROSS-LINKING AGENTS:  
DESIGN, SYNTHESIS, MECHANISM, AND ANTICANCER ACTIVITY

by

Yibin Wang

A Dissertation Submitted in  
Partial Fulfillment of the  
Requirements for the Degree of

Doctor of Philosophy

in Chemistry

at

The University of Wisconsin-Milwaukee

December 2015

## ABSTRACT

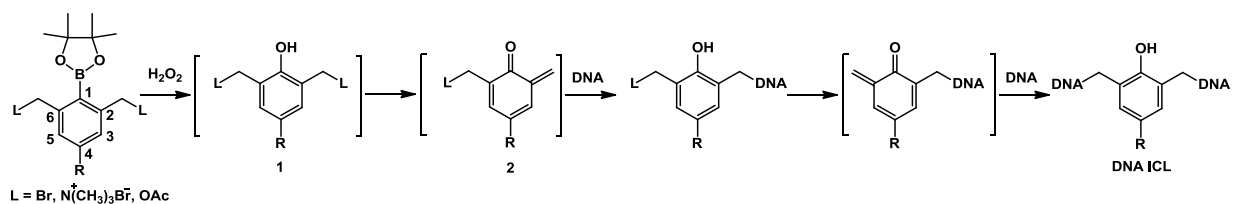
### ARYLBORONATES AS H<sub>2</sub>O<sub>2</sub> OR PHOTO-INDUCIBLE DNA CROSS-LINKING AGENTS: DESIGN, SYNTHESIS, MECHANISM, AND ANTICANCER ACTIVITY

by

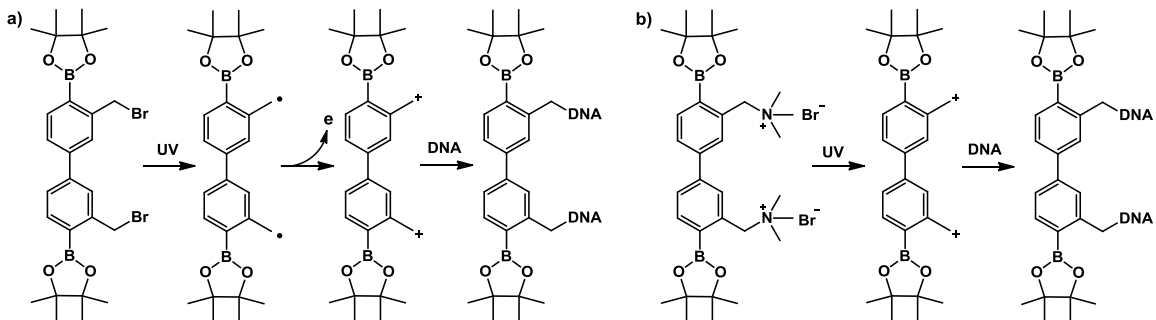
Yibin Wang

The University of Wisconsin-Milwaukee, 2015  
Under the Supervision of Professor Xiaohua Peng

Interest in the development of cancer therapies with improved selectivity and reduced host toxicity has been growing. In this thesis, we designed and synthesized a series of novel non-toxic arylboronic ester and biarylboronic ester derivatives that can be activated by hydrogen peroxide (H<sub>2</sub>O<sub>2</sub>) to induce DNA interstrand cross-link formation. The mechanism of DNA cross-linking induced by these arylboronates involves generation of phenol intermediates **1** followed by departure of leaving group (L) leading to quinone methides (QMs) **2**, which directly cross-link DNA via alkylation. The QM formation is the rate-determining step for DNA cross-linking. The activity and selectivity of these compounds towards H<sub>2</sub>O<sub>2</sub> were investigated and the activation mechanism was determined by NMR analysis and QM trapping experiments. The oxidative activation of these compounds by H<sub>2</sub>O<sub>2</sub> produced an electron rich aromatic ring that facilitated QM formation and release of the leaving group.



We also evaluated the effects of the benzylic leaving groups (L), the core structures of the arylboronates, and the aromatic substituents (R) on H<sub>2</sub>O<sub>2</sub>-induced formation of bisquinone methides (bisQMs) for DNA interstrand cross-linking. A better leaving group (Br) and stepwise bisquinone methide formation increased interstrand cross-linking efficiency. The electron-donating groups (OMe or OH) on the aromatic ring greatly favored QM formation and improved interstrand cross-link (ICL) formation. An *in vitro* cytotoxicity assay showed that the arylboronic esters with OMe or OH at position 4 dramatically inhibited the growth of various cancer cell lines. These findings provide essential guidelines for designing novel anticancer prodrugs.



Furthermore, the photochemical reactivity of these arylboronates, including phenyl boronates and naphthalene boronates, towards DNA has been investigated. The results indicated that most arylboronates induced DNA ICL formation upon 350 nm irradiation. Two mechanisms were involved for photo-inducible DNA ICL formation: a) UV-irradiation of the arylboronates produced a methyl radical which was oxidized to a methyl cation capable of alkylating DNA; b) a methyl cation was directly generated by UV-irradiation of the arylboronates via heterolysis of CH<sub>2</sub>-L (L= Br or NMe<sub>3</sub><sup>+</sup>Br<sup>-</sup>) bond. The activation mechanism was determined using the orthogonal traps, 2,2,6,6-tetramethylpiperidin-1-oxyl (TEMPO) and methoxyamine. The TEMPO reacts with free radicals while methoxyamine acts as a carbocation trap.

## TABLE OF CONTENTS

<b>Abstract</b> .....	ii
<b>Table of Contents</b> .....	iv
<b>List of Figures</b> .....	viii
<b>List of Tables</b> .....	xv
<b>List of Schemes</b> .....	xvi
<b>List of Abbreviations</b> .....	xviii
<b>Acknowledgements</b> .....	xxi

CHAPTER	PAGE
<b>1. Introduction</b> .....	1
1.1. The structure and function of deoxyribonucleic acid (DNA) .....	1
1.2. DNA interstrand cross-linking agents .....	3
1.2.1. Commonly used chemotherapeutic agents.....	4
1.2.2. Chemical methods for inducing DNA cross-link formation .....	9
1.2.2.1. Photo-activated ICL agents .....	9
1.2.2.2. DNA ICL agents activated by reduction .....	10
1.2.2.3. DNA ICL agents activated by oxidation .....	12
1.3. Reactive Oxygen Species.....	14
1.3.1. High levels of reactive oxygen species in cancer cell.....	14
1.3.2. Hydrogen peroxide and its detection .....	16
1.4. Quinone Methides.....	20
1.4.1. The characterization and reactivity of quinone methides .....	20

1.4.2. Chemical methods to produce quinone methides .....	22
1.5. References.....	26
<b>2. Synthesis and Biological Investigation of H<sub>2</sub>O<sub>2</sub>-Inducible DNA Cross-Linking Agents.....</b>	<b>36</b>
2.1. Introduction.....	36
2.2. Arylboronic ester as H <sub>2</sub> O <sub>2</sub> -inducible ICL agents.....	38
2.2.1. Synthesis of <b>1a,b</b> .....	38
2.2.2. The reactivity of <b>1-4</b> toward DNA .....	39
2.2.3. The mechanism of ICL formation.....	44
2.2.4. Determination of cross-linking site .....	46
2.2.5. The kinetics of ICL formation.....	51
2.3. Cytotoxicity towards cancers cells and future work .....	63
2.4. Experimental Section.....	64
2.5. References.....	70
2.6. Appendices A: Characterization of Compounds .....	74
<b>3. Optimization of H<sub>2</sub>O<sub>2</sub>-Activated Quinone Methide Prodrugs to Improve DNA Cross-Linking Efficiency and Cytotoxicity towards Cancer Cells.....</b>	<b>79</b>
3.1. Introduction.....	79
3.2. Modification of <b>1a</b> to improve DNA cross-linking efficiency .....	81
3.2.1. Design and Synthesis of arylboronic ester <b>9-12</b> .....	81
3.2.2. DNA cross-linking assay.....	84
3.2.3. The effect of substituents on the DNA cross-link formation .....	85
3.2.3.1. The electron-donating group favors the ICL formation.....	85
3.2.3.2. The kinetics of ICL formation induced by <b>1a, 9a</b> and <b>12a</b> .....	90

3.2.4.	The effect of leaving group on the DNA cross-link formation .....	96
3.3.	Cytotoxicity of <b>9a</b> and <b>12a</b> towards cancer cell lines.....	103
3.4.	Identification of biological quinone methide prodrug targets .....	110
3.4.1.	Synthesis and DNA cross-linking study with alkyne-modified arylboronic ester <b>13</b> .....	111
3.4.2.	Fluorescence detection of <b>13</b> -labelled DNA .....	113
3.5.	Experimental Section.....	116
3.6.	References.....	133
3.7.	Appendices B: Characterization of Compounds.....	135
4.	<b>Photo-Induced Interstrand Cross-Link Formation by Naphthalene Boronates and its Mechanism Study</b> .....	151
4.1.	Introduction.....	151
4.2.	DNA cross-linking ability of binaphthalene boronate esters <b>14a</b> and <b>14b</b> .....	152
4.2.1.	Synthesis of <b>14a</b> and <b>14b</b> .....	152
4.2.2.	DNA cross-linking ability of <b>14a</b> and <b>14b</b> .....	153
4.2.3.	Determination of cross-linking site .....	158
4.3.	The mechanism of ICL formation induced by <b>14a,b</b> .....	159
4.3.1.	QM formation in the presence of H <sub>2</sub> O <sub>2</sub> .....	159
4.3.2.	Radical formation upon UV irradiation.....	160
4.3.3.	Cation formation from radical through electron transfer .....	162
4.3.4.	The effect of trapping agent on DNA cross-link formation .....	165
4.3.5.	Proposed mechanism for ICL formation induced by <b>14a</b> and <b>14b</b> .....	169
4.4.	Experimental Section.....	170
4.5.	References.....	178

4.6. Appendices C: Characterization of Compounds.....	181
<b>5. Photo-Induced Interstrand Cross-Link Formation by Phenyl boronates.....</b>	<b>196</b>
5.1. Introduction.....	196
5.2. DNA cross-linking assay .....	196
5.2.1. DNA cross-linking ability of <b>1-3a,b</b> upon photo-irradiation .....	196
5.2.2. Determination of cross-linking site .....	199
5.2.3. The mechanism of ICL formation induced by <b>3a,b</b> .....	202
5.2.4. DNA cross-linking ability of <b>9a</b> and <b>9b</b> .....	208
5.3. Experimental Section.....	214
<b>Curriculum Vitae .....</b>	<b>217</b>



## LIST OF FIGURES

<b>Figure 1-1.</b> DNA double helix structures and Watson-Crick base pairing.....	2
<b>Figure 1-2.</b> DNA lesions induced by interstrand cross-linking agents .....	3
<b>Figure 1-3.</b> Mechanism of ICL formation by mitomycin C .....	5
<b>Figure 1-4.</b> Structures of psoralens and ICL formation by methoxsalen .....	6
<b>Figure 1-5.</b> Structures of nitrogen mustard compounds and mechanism of ICL formation.	7
<b>Figure 1-6.</b> Mechanism of ICL formation by cisplatin .....	8
<b>Figure 1-7.</b> Structure of psoralen analog.....	9
<b>Figure 1-8.</b> ICL formation by biquaternary ammonium salts .....	10
<b>Figure 1-9.</b> ICL formation by binol quaternary ammonium salts .....	10
<b>Figure 1-10.</b> ICL formation by aziridinybenzoquinones .....	11
<b>Figure 1-11.</b> Mechanism of activation of <i>o</i> -nitrobenzyl compounds .....	12
<b>Figure 1-12.</b> Reductive activation of nitrophenyl mustard .....	12
<b>Figure 1-13.</b> Oxidative activation of cyclophosphamide .....	13
<b>Figure 1-14.</b> Oxidative activation of hexamethylmelamine.....	14
<b>Figure 1-15.</b> Generation of reactive oxygen species.....	16
<b>Figure 1-16.</b> Activation of H <sub>2</sub> O <sub>2</sub> probes PF1 .....	18
<b>Figure 1-17.</b> Spectroscopic response and selectivity of H <sub>2</sub> O <sub>2</sub> probes PF1 .....	18
<b>Figure 1-18.</b> A. Activation and spectroscopic responses of H <sub>2</sub> O <sub>2</sub> probes PG1 and PC1 .....	18

<b>Figure 1-19.</b> Activation of H <sub>2</sub> O <sub>2</sub> probe MitoPY1.....	19
<b>Figure 1-20.</b> Activation of H <sub>2</sub> O <sub>2</sub> probe <b>38</b> .....	19
<b>Figure 1-21.</b> Design arylboronic ester H <sub>2</sub> O <sub>2</sub> -selective ICL agent.....	20
<b>Figure 1-22.</b> <i>o</i> -, <i>m</i> - and <i>p</i> -quinone methide and nucleophilic addition.....	21
<b>Figure 1-23.</b> Nucleophiles in dC, dG and dA .....	22
<b>Figure 1-24.</b> Nucleoside adducts formed by <i>o</i> -QM .....	22
<b>Figure 1-25.</b> Photochemical, base catalyzed and fluoride induced QM generation.....	23
<b>Figure 1-26.</b> ICL formation by silyl-protected bis(acetoxymethyl)phenol.....	23
<b>Figure 1-27.</b> Formation of QM by oxidation of tamoxifen.....	24
<b>Figure 1-28.</b> Formation of diquinone methide and classical acolbifene quinone methide by enzymatic oxidation.....	25
<b>Figure 1-29.</b> Formation of biquinone methide by oxidation of biphenyl selenide.....	26
<b>Figure 2-1.</b> A. H <sub>2</sub> O <sub>2</sub> selectivity of ICL formation. B. Cytotoxicity towards different cancer cell lines .....	38
<b>Figure 2-2.</b> 5'-end oligonucleotide labeling reaction .....	40
<b>Figure 2-3.</b> H <sub>2</sub> O <sub>2</sub> -induced DNA ICL formation by <b>1a</b> .....	41
<b>Figure 2-4.</b> Concentration dependence of ICL formation by <b>1a</b> .....	41
<b>Figure 2-5.</b> pH dependence of ICL formation by <b>1a</b> .....	42
<b>Figure 2-6.</b> H <sub>2</sub> O <sub>2</sub> -induced DNA ICL formation by compounds <b>1-4</b> .....	42
<b>Figure 2-7.</b> Determination of the reaction sites of <b>1a</b> .....	47
<b>Figure 2-8.</b> ICL formation from duplex <b>7</b> induced by <b>1a</b> upon H <sub>2</sub> O <sub>2</sub> activation.....	48

<b>Figure 2-9.</b> HPLC profiles of the enzymatic analysis .....	49
<b>Figure 2-10.</b> Mass spectrum of enzymatic digestion product corresponded to retention time about 7.9 min on HPLC chromatography.....	50
<b>Figure 2-11.</b> Kinetic rate of ICL formation from <b>5</b> upon treatment with bromides/H <sub>2</sub> O <sub>2</sub> ....	51
<b>Figure 2-12.</b> <sup>1</sup> H NMR analysis of <b>1a</b> in deuterated DMSO, D <sub>2</sub> O, and H <sub>2</sub> O <sub>2</sub> .....	55
<b>Figure 2-13.</b> <sup>1</sup> H NMR analysis of <b>2a</b> in deuterated DMSO, D <sub>2</sub> O, and H <sub>2</sub> O <sub>2</sub> .....	56
<b>Figure 2-14.</b> <sup>1</sup> H NMR analysis of <b>3a</b> in deuterated DMSO, D <sub>2</sub> O, and H <sub>2</sub> O <sub>2</sub> .....	57
<b>Figure 2-15.</b> <sup>1</sup> H NMR analysis of <b>4a</b> in deuterated DMSO, D <sub>2</sub> O, and H <sub>2</sub> O <sub>2</sub> .....	58
<b>Figure 2-16.</b> <sup>1</sup> H NMR analysis of <b>4b</b> in deuterated DMSO, D <sub>2</sub> O, and H <sub>2</sub> O <sub>2</sub> .....	59
<b>Figure 2-17.</b> <sup>1</sup> H NMR analysis of <b>4c</b> in deuterated DMSO, D <sub>2</sub> O, and H <sub>2</sub> O <sub>2</sub> .....	60
<b>Figure 2-18.</b> Rate constant for the disappearance of starting material ( <b>A-C</b> , <b>G</b> and <b>H</b> ) and the formation of hydrolyzed product ( <b>D-F</b> ) in NMR analysis .....	61
<b>Figure 2-19.</b> Effect of <b>1a</b> on cancer cells .....	64
<b>Figure 3-1.</b> H <sub>2</sub> O <sub>2</sub> -induced DNA ICL formation by compounds <b>9-12</b> .....	85
<b>Figure 3-2.</b> Compound/H <sub>2</sub> O <sub>2</sub> ratio dependence of ICL formation by <b>10a</b> .....	86
<b>Figure 3-3.</b> pH dependence of ICL formation by <b>11a</b> .....	87
<b>Figure 3-4.</b> Compound/H <sub>2</sub> O <sub>2</sub> ratio dependence of ICL formation by <b>9a</b> .....	88
<b>Figure 3-5.</b> Concentration dependence of ICL formation by <b>9a</b> .....	88
<b>Figure 3-6.</b> pH dependence for of ICL formation by <b>9a</b> .....	89
<b>Figure 3-7.</b> Compound/H <sub>2</sub> O <sub>2</sub> ratio dependence of ICL formation by <b>12a</b> .....	89
<b>Figure 3-8.</b> Concentration dependence of ICL formation by <b>12a</b> .....	90

<b>Figure 3-9.</b> pH dependence of ICL formation by <b>12a</b> .....	90
<b>Figure 3-10.</b> Kinetic rate of ICL formation from <b>5</b> upon treatment with bromides/H <sub>2</sub> O <sub>2</sub> ....	91
<b>Figure 3-11.</b> <sup>1</sup> H NMR analysis of <b>9a</b> in deuterated DMSO, D <sub>2</sub> O, and H <sub>2</sub> O <sub>2</sub> .....	93
<b>Figure 3-12.</b> <sup>1</sup> H NMR analysis of <b>12a</b> in deuterated DMSO, D <sub>2</sub> O, and H <sub>2</sub> O <sub>2</sub> .....	94
<b>Figure 3-13.</b> Rate constant for the disappearance of starting material ( <b>A</b> and <b>B</b> ) and the formation of hydrolyzed product ( <b>C</b> and <b>D</b> ) in NMR analysis.....	95
<b>Figure 3-14.</b> ICL formation induced by <b>9b</b> by extend the incubation time to 3 days.....	97
<b>Figure 3-15.</b> <sup>1</sup> H NMR analysis of <b>9b</b> in deuterated DMSO, D <sub>2</sub> O, and H <sub>2</sub> O <sub>2</sub> .....	97
<b>Figure 3-16.</b> <sup>1</sup> H NMR analysis of <b>12b</b> in deuterated DMSO, D <sub>2</sub> O, and H <sub>2</sub> O <sub>2</sub> .....	98
<b>Figure 3-17.</b> Kinetic rate of ICL formation from <b>5</b> upon treatment with bromides/H <sub>2</sub> O <sub>2</sub> ....	100
<b>Figure 3-18.</b> <sup>1</sup> H NMR analysis of <b>9c</b> in deuterated DMSO, D <sub>2</sub> O, and H <sub>2</sub> O <sub>2</sub> .....	101
<b>Figure 3-19.</b> <sup>1</sup> H NMR analysis of <b>12c</b> in deuterated DMSO, D <sub>2</sub> O, and H <sub>2</sub> O <sub>2</sub> .....	102
<b>Figure 3-20.</b> Cytotoxicity of <b>1a</b> towards 60 human tumor cell lines .....	104
<b>Figure 3-21.</b> Cytotoxicity of <b>9a</b> towards 60 human tumor cell lines .....	105
<b>Figure 3-22.</b> Cytotoxicity of <b>1a</b> , <b>9a</b> and <b>12a</b> towards ovarian cell line SKOV3 .....	108
<b>Figure 3-23.</b> Cytotoxicity of <b>1a</b> , <b>9a</b> and <b>12a</b> towards renal cell lines and breast cell line MDA-MB-468 .....	108
<b>Figure 3-24.</b> Compound/H <sub>2</sub> O <sub>2</sub> ratio dependence of ICL formation by <b>13</b> .....	112
<b>Figure 3-25.</b> Concentration dependence of ICL formation by <b>13</b> .....	112
<b>Figure 3-26.</b> pH dependence of ICL formation by <b>13</b> .....	113
<b>Figure 3-27.</b> Kinetic rate of ICL formation from <b>5</b> upon treatment with <b>13</b> /H <sub>2</sub> O <sub>2</sub> .....	113

<b>Figure 3-28.</b> Fluorescence detected ICL formation by <b>13</b> using a 635 nm laser line .....	114
<b>Figure 3-29.</b> Cytotoxicity of <b>9a</b> , <b>12a</b> and <b>13</b> toward ovarian cell line SKOV3 .....	115
<b>Figure 3-30.</b> Purified genomic DNA and total RNA from <b>13</b> treated SKOV3 cell.....	115
<b>Figure 3-31.</b> Fluorescence detection of genomic DNA and total RNA from <b>13</b> treated SKOV3 cell.....	116
<b>Figure 4-1.</b> H <sub>2</sub> O <sub>2</sub> and UV induced ICL formation by <b>14a,b</b> .....	154
<b>Figure 4-2.</b> Concentration dependence of ICL formation by <b>14a</b> upon H <sub>2</sub> O <sub>2</sub> activation.....	155
<b>Figure 4-3.</b> Concentration dependence of ICL formation by <b>14b</b> upon H <sub>2</sub> O <sub>2</sub> activation.....	155
<b>Figure 4-4.</b> Concentration dependence of ICL formation by <b>14a</b> upon UV irradiation .....	156
<b>Figure 4-5.</b> Concentration dependence of ICL formation by <b>14b</b> upon UV irradiation .....	156
<b>Figure 4-6.</b> Time dependence of ICL formation by <b>14a</b> upon UV irradiation.....	157
<b>Figure 4-7.</b> Time dependence of ICL formation by <b>14b</b> upon UV irradiation .....	157
<b>Figure 4-8.</b> Determination of cross-linking site of <b>14a</b> .....	158
<b>Figure 4-9.</b> ICL formation from duplex <b>7</b> induced by <b>14a</b> upon UV irradiation.....	159
<b>Figure 4-10.</b> Effect of methoxyamine on ICL formation by <b>14a</b> upon UV irradiation .....	166
<b>Figure 4-11.</b> Effect of TEMPO on ICL formation by <b>14a</b> upon UV irradiation.....	166
<b>Figure 4-12.</b> Effect of methoxyamine on ICL formation by <b>14b</b> upon UV irradiation .....	167
<b>Figure 4-13.</b> Effect of TEMPO on ICL formation by <b>14b</b> upon UV irradiation .....	167
<b>Figure 4-14.</b> Effect of methoxyamine and TEMPO on ICL formation by <b>14a</b> .....	168
<b>Figure 4-15.</b> Effect of methoxyamine and TEMPO on ICL formation by <b>14b</b> .....	168

<b>Figure 5-1.</b> UV-induced DNA cross-link formation by <b>1a,b-3a,b</b> .....	197
<b>Figure 5-2.</b> Concentration dependence of ICL formation by <b>3a</b> upon UV irradiation .....	198
<b>Figure 5-3.</b> Concentration dependence of ICL formation by <b>3b</b> upon UV irradiation .....	198
<b>Figure 5-4.</b> Time dependence of ICL formation by <b>3a</b> upon UV irradiation.....	199
<b>Figure 5-5.</b> Time dependence of ICL formation by <b>3b</b> upon UV irradiation .....	199
<b>Figure 5-6.</b> Determination of cross-linking site of <b>3a</b> .....	200
<b>Figure 5-7.</b> Determination of cross-linking site of <b>3b</b> .....	201
<b>Figure 5-8.</b> ICL formation from duplex <b>7</b> induced by <b>3b</b> upon UV irradiation.....	202
<b>Figure 5-9.</b> Effect of TEMPO on ICL formation by <b>3a</b> upon UV irradiation.....	203
<b>Figure 5-10.</b> Effect of BME on ICL formation by <b>3a</b> upon UV irradiation .....	203
<b>Figure 5-11.</b> Effect of TEMPO on ICL formation by <b>3b</b> upon UV irradiation .....	204
<b>Figure 5-12.</b> Effect of BME on ICL formation by <b>3b</b> upon UV irradiation .....	204
<b>Figure 5-13.</b> Effect of methoxyamine on ICL formation by <b>3a</b> upon UV irradiation .....	205
<b>Figure 5-14.</b> Effect of methoxyamine on ICL formation by <b>3b</b> upon UV irradiation .....	205
<b>Figure 5-15.</b> Effect of TEMPO and methoxyamine on ICL formation by <b>3a</b> and <b>3b</b> .....	206
<b>Figure 5-16.</b> Absorbance of <b>1b, 2b</b> and <b>3a,b</b> .....	207
<b>Figure 5-17.</b> Absorbance of <b>9b</b> .....	209
<b>Figure 5-18.</b> Concentration dependence of ICL formation by <b>9a</b> upon UV irradiation .....	209
<b>Figure 5-19.</b> Concentration dependence of ICL formation by <b>9b</b> upon UV irradiation .....	210
<b>Figure 5-20.</b> Time dependence of ICL formation by <b>9a</b> upon UV irradiation.....	210

<b>Figure 5-21.</b> Time dependence of ICL formation by <b>9b</b> upon UV irradiation .....	211
<b>Figure 5-22.</b> Effect of TEMPO on ICL formation by <b>9a</b> upon UV irradiation.....	212
<b>Figure 5-23.</b> Effect of methoxyamine on ICL formation by <b>9a</b> upon UV irradiation .....	212
<b>Figure 5-24.</b> Effect of TEMPO on ICL formation by <b>9b</b> upon UV irradiation .....	213
<b>Figure 5-25.</b> Effect of methoxyamine on ICL formation by <b>9a</b> upon UV irradiation .....	213
<b>Figure 5-26.</b> Effect of TEMPO and methoxyamine on ICL formation by <b>9a</b> and <b>9b</b> .....	214

## LIST OF TABLES

<b>Table 1-1.</b> Chemical properties of different ROS.....	17
<b>Table 2-1.</b> Rate of ICL formation from <b>5</b> upon treatment with bromides and salts.....	52
<b>Table 2-2.</b> Rate of starting material disappearance and QM formation .....	62
<b>Table 3-1.</b> Rate of ICL formation from <b>5</b> upon treatment with bromides.....	91
<b>Table 3-2.</b> Rate of starting material disappearance and QM formation .....	96
<b>Table 3-3.</b> Kinetics of ICL formation and monomer reaction.....	100
<b>Table 3-4.</b> The Cytotoxicity of <b>9a</b> in 60 cell lines .....	106
<b>Table 3-5.</b> IC <sub>50</sub> of <b>1a</b> , <b>9a</b> and <b>12a</b> toward renal and breast cell lines.....	110



## LIST OF SCHEMES

<b>Scheme 1-1.</b> Structures of nucleobases .....	1
<b>Scheme 2-1.</b> ICL formation induced by aryboronates upon H <sub>2</sub> O <sub>2</sub> activation .....	37
<b>Scheme 2-2.</b> The structures of <b>1-4</b> .....	39
<b>Scheme 2-3.</b> Synthesis of <b>1a,b</b> .....	39
<b>Scheme 2-4.</b> DNA duplex <b>5</b> .....	40
<b>Scheme 2-5.</b> Synthesis of <b>4c</b> that contains mixed leaving groups.....	43
<b>Scheme 2-6.</b> Proposed mechanism of H <sub>2</sub> O <sub>2</sub> -induced ICL formation .....	44
<b>Scheme 2-7.</b> QM-trapping reaction of <b>1a,b</b> .....	45
<b>Scheme 2-8.</b> QM-trapping product was generated by <b>2-4</b> .....	45
<b>Scheme 2-9.</b> Proposed mechanism of H <sub>2</sub> O <sub>2</sub> -induced QM formation by <b>4b</b> .....	46
<b>Scheme 2-10.</b> Cleavage of N-7-alkylated purines upon heating in piperidine.....	48
<b>Scheme 2-11.</b> DNA duplex <b>6</b> and <b>7</b> .....	48
<b>Scheme 2-12.</b> Deglycosylation of N7 adduct of dG.....	51
<b>Scheme 2-13.</b> Hydrolysis and oxidization product of bromide analogues.....	53
<b>Scheme 3-1.</b> Structure of <b>1a</b> and the factors influence QM formation .....	79
<b>Scheme 3-2.</b> Effect of substituents on QM formation.....	80
<b>Scheme 3-3.</b> The structures of <b>9-12</b> .....	81
<b>Scheme 3-4.</b> Synthesis of <b>9a,b</b> .....	81
<b>Scheme 3-5.</b> Synthesis of <b>10a</b> .....	82

<b>Scheme 3-6.</b> Synthesis of <b>11a,b</b> .....	82
<b>Scheme 3-7.</b> Synthesis of <b>12a,b</b> .....	83
<b>Scheme 3-8.</b> Synthesis of <b>1c, 9c, and 12c</b> .....	84
<b>Scheme 3-9.</b> The mechanism of H <sub>2</sub> O <sub>2</sub> -induced ICL formation.....	92
<b>Scheme 3-10.</b> Hypercoordination of arylboronic derivatives.....	103
<b>Scheme 3-11.</b> Structure of <b>13</b> and Alexa Flour 647 azide and a scheme of a pull-down reaction using Cu[I]-catalyzed azides-alkynes cycloaddition.....	111
<b>Scheme 3-12.</b> Synthesis of <b>13</b> .....	112
<b>Scheme 4-1.</b> QM generation by binol quinone methide precursors .....	152
<b>Scheme 4-2.</b> Synthesis of compounds <b>14a</b> and <b>14b</b> .....	152
<b>Scheme 4-3.</b> QM Trapping reactions with ethyl vinyl ether .....	160
<b>Scheme 4-4.</b> Synthesis of compounds <b>15a</b> and <b>15b</b> .....	160
<b>Scheme 4-5.</b> Radical trapping reactions with BME or TEMPO .....	161
<b>Scheme 4-6.</b> Cation trapping reactions with methoxyamine.....	163
<b>Scheme 4-7.</b> Nucleophilic substitution occurred between <b>15a</b> and methoxyamine under heating without UV-irradiation.....	163
<b>Scheme 4-8.</b> Photo-irradiation of <b>15b</b> in the presence of TEMPO and D <sub>2</sub> O .....	164
<b>Scheme 4-9.</b> One-electron transfer occurred between the radical <b>16</b> and bromo radical.....	164
<b>Scheme 4-10.</b> Proposed mechanism for ICL formation induced by <b>14a</b> and <b>14b</b> .....	169
<b>Scheme 5-1.</b> The structures of arylboronates .....	196
<b>Scheme 5-2.</b> Proposed mechanism for ICL formation induced by <b>3a</b> and <b>3b</b> .....	208

## LIST OF ABBREVIATIONS

A	Adenine
AIBN	Azobisisobutyronitrile
ATP	Adenosine triphosphate
AZQ	2,5-Bis(1-aziridiny)-3,6-bis(carbethoxyamino)-1,4-benzoquinone
BME	2-Mercaptoethanol
C	Cytosine
CDDP	Cis-diamminedichloroplatinum or cisplatin
CP	Cyclophosphamide
CYPs	Cytochrome P-450
dA	Dexoyadonosine
dC	Deoxycytidine
dG	Deoxyguanosine
DMF	Dimethylformamide
DMSO	Dimethyl sulfoxide
DNA	2'-Deoxyribonucleic acid
DZQ	Diaziridinyquinone
dsDNA	Double-stranded DNA
EDTA	Ethylenediaminetetraacetic acid
ER $\alpha$	Estrogen receptor 1
ER $\beta$	Estrogen receptor 2
ESI	Electrospray ionization
EtOAc	Ethyl acetate
EtOH	Ethanol
EVE	Ethyl vinyl ether
FDA	Food and Drug Administration
G	Guanine
HMM	Hexamethylmelamine
HPLC	High-performance liquid chromatography

HRMS	High-resolution mass spectrometry
ICLs	Interstrand cross-links
<i>k</i>	Reaction rate constant
LC-MS	Liquid chromatography-mass spectrometry
MALDI-TOF	Matrix-assisted laser desorption/ionization - time of flight
MeCN	Acetonitrile
MeOH	Methanol
8-MOP	Methoxsalen
MitoPY1	Mitochondria peroxy yellow 1
<i>m</i> -QM	meta-Quinone methide
mRNA	Messenger ribonucleic acid
MS	Mass Spectrometry
NADPH	Nicotinamide adenine dinucleotide phosphate hydrogen
NBS	N-bromosuccinimide
NMR	Nuclear magnetic resonance
<i>o</i> -QM	ortho-Quinone methide
PAGE	Polyacrylamide gel electrophoresis
PC1	Peroxy crimson 1
PF1	Peroxyfluor-1
PG1	Peroxy green 1
<i>p</i> -QM	para-Quinone methide
QM	Quinine methide
ROS	Reactive oxygen species
RNA	Ribonucleic acid
SERM	Selective estrogen receptor modulator
SOD	Superoxide dismutase
T	Thymine
TEMPO	2,2,6,6-Tetramethylpiperidin-1-oxyl
THF	Tetrahydrofuran
TMP	4,5',8-Trimethylpsoralen

UV

Ultraviolet

UVA

Ultraviolet A

## ACKNOWLEDGMENTS

First and foremost, I would like to thank my advisor, Professor Xiaohua Peng, for the chance to work on this project. Her profound knowledge, patient mentoring, excellent advice and professional training lead me become a real scientist. It is my great pleasure to be one member of Professor Peng's Lab.

I greatly appreciate my committee, Professor Alexander A. Arnold, Professor Mark L. Dietz, Professor M. Mahmum Hossain, and Professor Nicholas Silvaggi for their nice support, encouragement and insightful comments for my research and dissertation. Especially thank Professor Alexander A. Arnold for his kind collaboration and professional training of cell culture study.

Thanks to all members of Professor Peng's Lab: Dr. Yunyan Kuang, Dr. Wenbing Chen, Dr. Yanyan Han, Dr. Yukai Fan, Dr. Mohammad Mojibul Haque, Dr. Huabing Sun and Heli Fan for their kind assistance and support not only in my study but also in my life; I'd especially like to thank Dr. Sheng Cao as the good collaborator for sharing knowledge and experience to solve chemical problems.

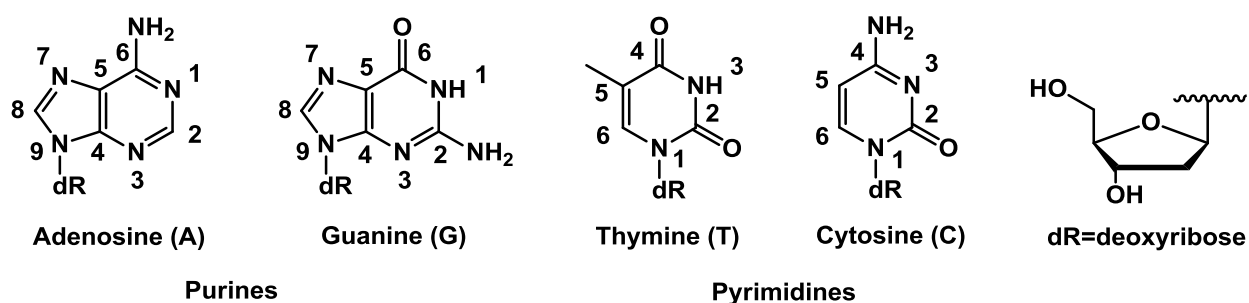
I also would like to express my gratitude to the faculty members and staffs of the Department of Chemistry and Biochemistry at University Wisconsin-Milwaukee.

Last but not the least, special thanks to my family for their unconditionally support and encouragement especially my wife, Yanyan Huang, provided trust and great support all the time. I could not have accomplished this without her restless inspiration. I also thank to my lovely daughter, Yajie Wang, who gives me endless energy. I really appreciate everything you have done for me all these years.

## Chapter 1. Introduction

### 1.1. The structure and function of deoxyribonucleic acid (DNA)

Deoxyribonucleic acid (DNA) is a basic biomolecule that carries genetic information used in the development and functioning of all living organisms. The structure of DNA was first identified by Watson and Crick in 1953.<sup>1</sup> DNA usually consists of two polynucleotide strands twisted around each other to form a double helix (Figure 1-1). The backbone of each strand is made up of alternating deoxyribose and phosphate groups. One of four nucleobases are attached to each deoxyribose in the DNA backbones, including the purines, adenine (A) and guanine (G), and the pyrimidines, thymine (T) and cytosine (C) (Scheme 1-1). The DNA double strands are bound together via Watson-Crick base pairing through hydrogen bonding, where A pairs with T through two hydrogen bonds, and G pairs with C via three hydrogen bonds (Figure 1-1). This base recognition results in a complementary relationship between the base sequences of the two DNA strands. The sequence of nucleobases in the DNA strands forms the genetic code.<sup>1-5</sup>



**Scheme 1-1.** Structures of nucleobases.

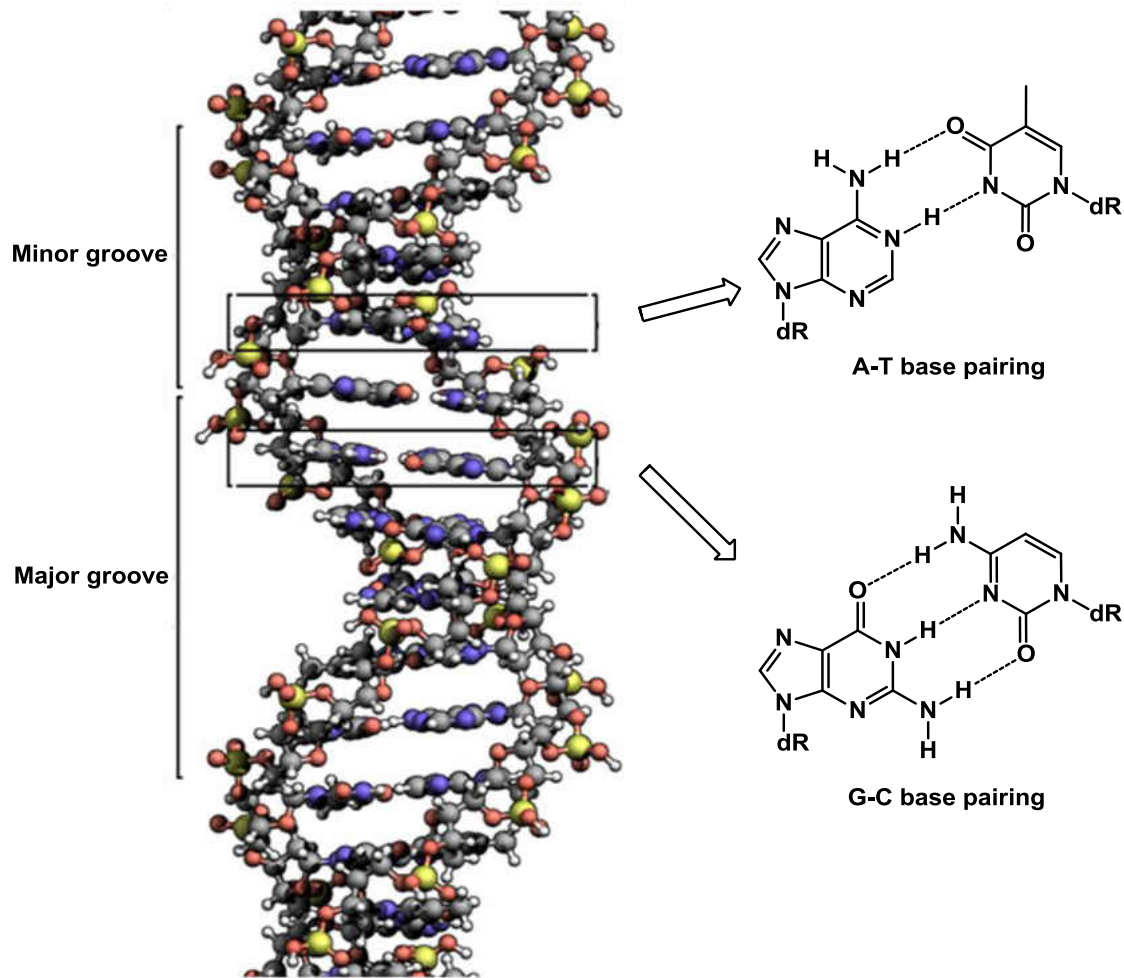


**Figure 1-1.** DNA double helix structures and Watson-Crick base pairing.

DNA is considered a very important target for biological study. Its replication and transcription are essential for cellular processes such as cell division.<sup>6</sup> DNA replication is the process of utilizing two separated single strands as templates to synthesize two daughter strand DNA.<sup>7,8</sup> While transcription is the first step of gene expression, in which a particular segment of DNA sequence is copied into messenger RNA (mRNA) which carries the genetic code needed for protein synthesis. The DNA structure can be chemically modified and the resulting structure change may induce gene mutations or even cause cell death. DNA alkylation is one of the widely occurred modifications which have been applied as an anticancer strategy. Broadly there are



three major types of DNA alkylation: interstrand cross-links, intrastrand cross-links and monoalkylation. Among these three kinds of alkylation, the interstrand cross-links (ICLs) are the most toxic DNA lesions because they directly and completely prevent the separation of the two strands by forming covalent linkages between DNA complementary strands.<sup>9-11</sup> The mechanisms of ICL formation are broadly similar in that bifunctional sites are required, which can be activated chemically and bond to specific bases residing on opposing DNA strands to form DNA interstrand cross-links. Apart from DNA interstrand cross-links formation, intrastrand cross-links are also possible, where the cross-linking agent bonds to adjacent bases in the same strand. Additionally, monoadducts could be formed when only one functional site bonds to a DNA strands (Figure 1-2).<sup>12</sup>

Therefore, DNA cross-linking agents have been considered an important class of clinically useful drugs that can be used for cancer treatment and other diseases over the years.

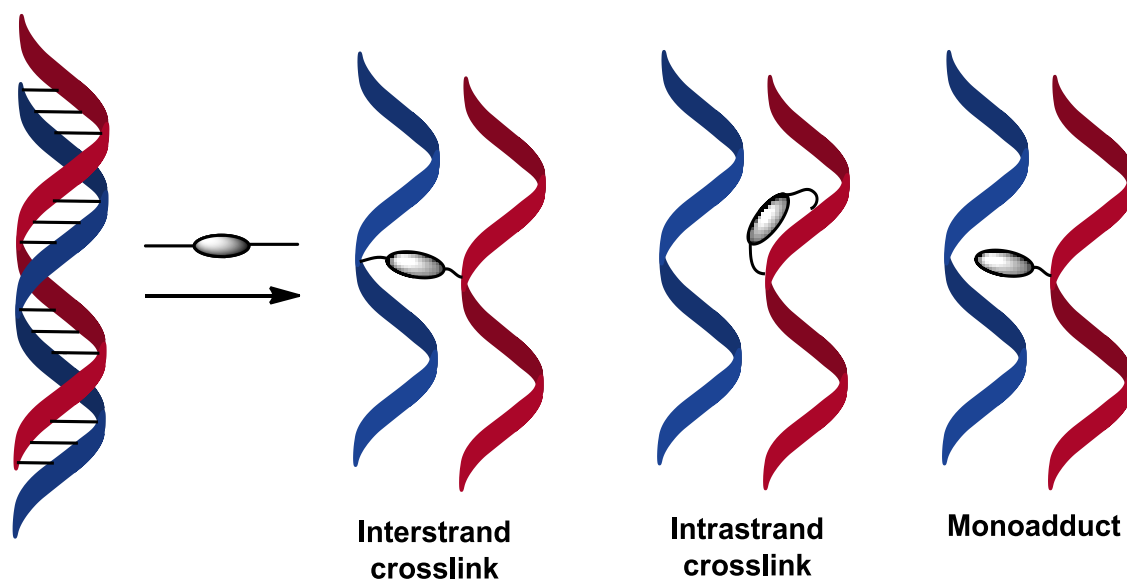


**Figure 1-2.** DNA lesions induced by alkylating agents.

## 1.2. DNA interstrand cross-linking agents

### 1.2.1. Commonly used chemotherapeutic agents

ICLs agents are one of the earliest anticancer drugs and some ICL-inducing agents, such as nitrogen mustard, mitomycin C and methoxsalen are still widely used in cancer therapy. There are four major classes of DNA cross-linking agents that are either naturally occurring or synthetically available, including mitomycins, methoxsalens, nitrogen mustards, and cisplatin.

Mitomycins belong to a family of aziridine-containing natural products originally derived from fungal sources, such as *streptomyces caespitosus*, or *streptomyces lavendulae*. Most mitomycins directly induce DNA cross-links formation. Some of them can be activated *in vivo* to cross-link DNA, therefore acting as prodrugs. For example, mitomycin C, a widely used chemotherapeutic anticancer drug, does not react with DNA by itself, but can be activated by photon-mediated or enzymatic reduction of the quinone leading to formation of a quinone methide-like specie **3** that cross-links DNA (Figure 1-3). Enzyme-induced two-electron reduction of the quinone ring ( $\rightarrow$ **1**) facilitates the loss of the methoxy group, which yields the unstable vinylogous quinone methide intermediate **2**. Tautomerization of **2** leads to formation of the QM-like structure **3**, which alkylates DNA at N2 of deoxyguanosine (dG) to produce the monoadduct **4**. The elimination of the carbamoyl leaving group produces the highly reactive intermediate **5**, which alkylates the second guanine in the complimentary strand to form the interstrand cross-link (Figure 1-3).<sup>13-15</sup> Mitomycin C commonly reacts with guanine residues through the minor groove of DNA. It is often used to treat esophageal carcinoma, breast cancers, and bladder cancers.

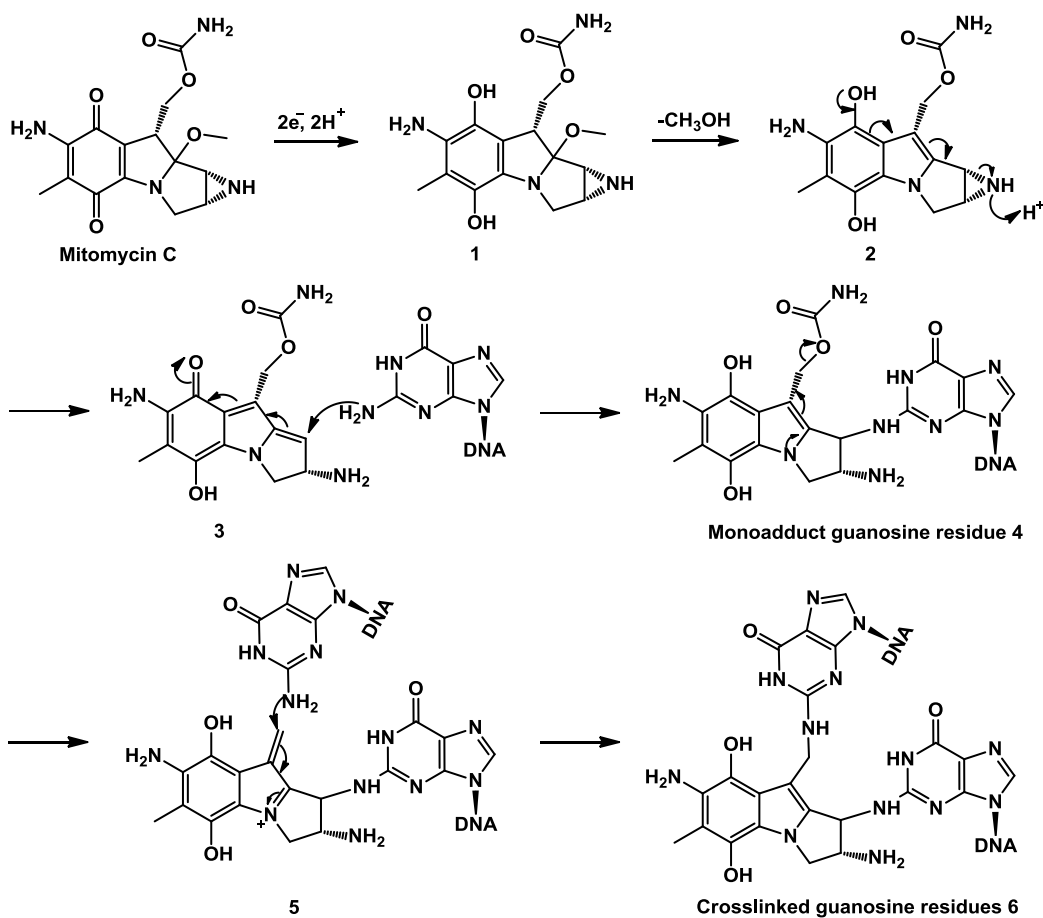


**Figure 1-3.** Mechanism of ICL formation by mitomycin C.

Methoxsalen and its parent compound psoralen are naturally occurring furocoumarins that are derived from plants. These compounds consist of a coumarin and a fused furan ring. Psoralen and its derivatives are well known photo-activated ICL agents that can form monoadducts and ICLs with thymines preferentially via [2 + 2] cycloaddition inducing apoptosis when exposed to long wavelength (320-410 nm) ultraviolet A (UVA) radiation (Figure 1-4).<sup>16-18</sup> Because of this unique feature, psoralens such as methoxsalen (8-MOP) and 4,5',8-trimethylpsoralen (TMP) have been used for the topical treatment of cutaneous T-cell lymphoma.<sup>19,20</sup>

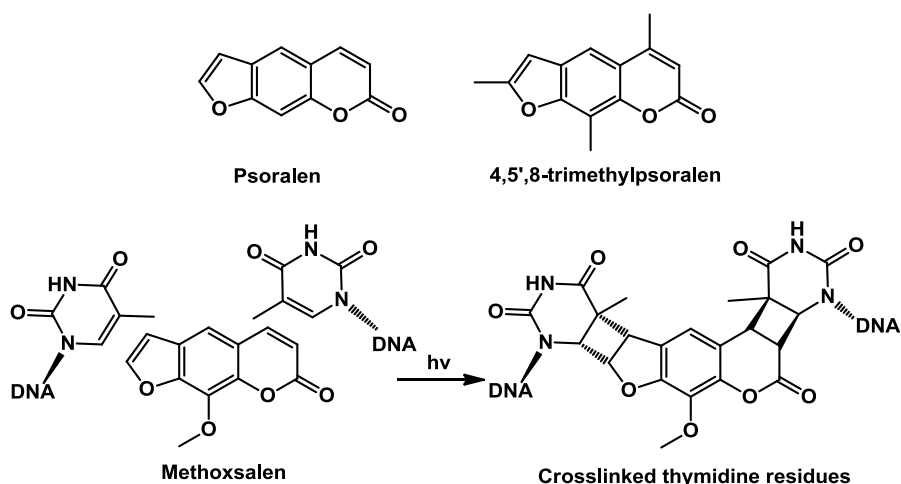


**Figure 1-4.** Structures of psoralens and ICL formation by methoxsalen.

The nitrogen mustard derivatives are the major kind of synthetic alkylating agents, which are widely used in the clinic for cancer treatment.<sup>12,21,22</sup> Nitrogen mustards contain a reactive *N,N*-bis-(2-chloroethyl)amine functional group that is highly active towards nucleophiles in DNA because a highly electrophilic aziridinium intermediate **7** can be formed by intramolecular displacement of the chloride by the amine nitrogen (Figure 1-5).<sup>23,24</sup> The aziridinium group greatly facilitates the DNA alkylation and cross-link formation. These compounds most commonly react with N7 of guanine residues to produce N7-alkylated derivatives **8** and **9**.

Nitrogen mustard gas was used as a chemical weapon during the Second World War. Exposure to nitrogen mustard drastically decreased white blood cell counts. After that, nitrogen mustards were used as a chemotherapeutic agent for leukemia and lymphoma. Since then, more nitrogen mustard derivatives such as melphalan and chlorambucil have been developed for cancer treatment. Melphalan is currently being used to treat multiple myeloma and ovarian cancer<sup>25</sup> and chlorambucil is used to treat chronic lymphocytic leukemia.

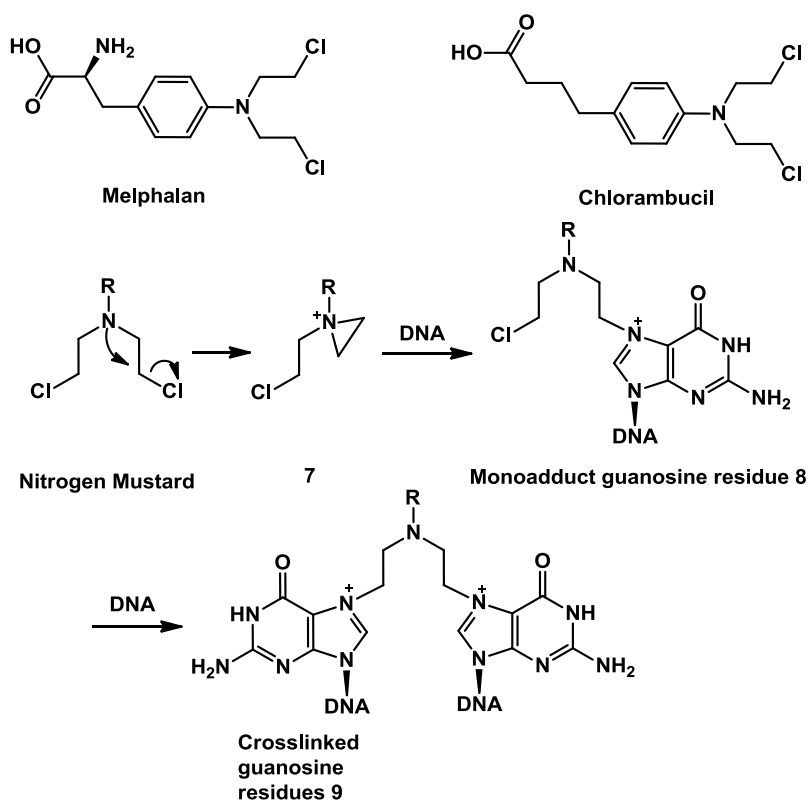


**Figure 1-5.** Structures of nitrogen mustard compounds and mechanism of ICL formation.

Cis-diamminedichloroplatinum II (CDDP or cisplatin) is the first member of the platinum-containing cross-linking agents. The mechanism of interstrand cross-link formation by cisplatin is similar to nitrogen mustard. One of the chloride ligands is slowly displaced by water to form the positively charged aquated species **10**, which easily binds with DNA and leads to replacement of water-ligand by N7 of guanosine to form monoadduct **11** or cross-linked product **12** (Figure 1-6).<sup>26-29</sup> Cisplatin was first identified as an inhibitor of bacterial division and is now widely used to treat a variety of solid tumors including lung cancer, ovarian cancer, lymphoma, and testicular cancer.<sup>30-32</sup>

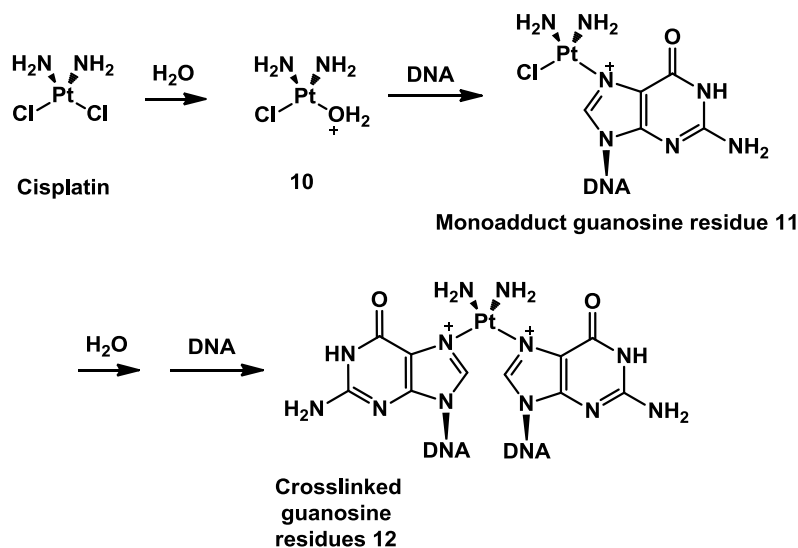


**Figure 1-6.** Mechanism of ICL formation by cisplatin.

In addition to DNA interstrand cross-links, these ICL-inducing agents also cause the formation of various DNA lesions due to their high reactivity, which lead to serious side effects. For example, a long term usage of mitomycin C can cause bone-marrow damage,<sup>29</sup> lung fibrosis, and renal damage. Methoxsalen usually causes nausea, headaches, and dizziness. Patients with high blood pressure or a history of liver problems are at risk for irreparable damage to both liver and skin. Nitrogen mustards are nonspecific DNA alkylating agents. The major side effect of nitrogen mustards is bone marrow suppression. Cisplatin, the most widely used DNA cross-linking drug, causes damage that is comprised of 90% intrastrand cross-links (mainly cross-links between adjacent purine residues on the same strand of the DNA double helix) and less than 5% ICLs.<sup>26,32</sup> The primary side effect for cisplatin is kidney damage.

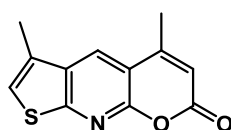
Overall, most of these existing cross-linking agents show poor selectivity towards cancer cells and lead to serious side effects. Host toxicity became a major concern of chemotherapeutic agents. The development of tumor-specific cross-linking agents is a novel approach to achieve therapeutic selectivity.

## 1.2.2. Chemical methods for inducing DNA cross-link formation

In recent decades, there has been increasing interest in the design of inducible DNA interstrand cross-linking agents with improved selectivity. The most common way is to mask the reactivity of the electrophiles, which are then activated by heat, photo-irradiation, or a chemical reduction or oxidation process.

### 1.2.2.1. Photo-activated ICL agents

The psoralens were the first photo-activated DNA cross-linking agents. UVA irradiation of psoralens leads to efficient DNA cross-linking. Recent research on psoralens has focused on improvement of drug absorption and solubility.<sup>33-35</sup> Several psoralen analogs with modified structures have been synthesized and studied. Some of them showed good therapeutic properties with fewer adverse effects.<sup>36</sup> For example, 4,4'-dimethylthieno-8-azacoumarin displayed antiproliferative activity in HL-60 cells without inducing erythematous reactions, which are the common side effects of methoxsalen (8-MOP) in therapy (Figure 1-7).<sup>37</sup>



4,4'-dimethylthieno-8-azacoumarin

**Figure 1-7.** Structure of psoralen analog.

UV-irradiation is also highly efficient for generating ortho-quinone methide (*o*-QM) intermediates capable of cross-linking DNA.<sup>38-40</sup> Various aromatic compounds have been developed as QM precursors. For example, Zhou's group designed and synthesized a class of phenol biquaternary ammonium salts **13** and **14**, which can form *o*-QM by photo-activation in

aqueous solution and then cross-link DNA (Figure 1-8).<sup>41</sup> The biphenol biquaternary ammonium **14** induced a much higher cross-linking yield with at pH=7.7 a low concentration (10  $\mu$ M).

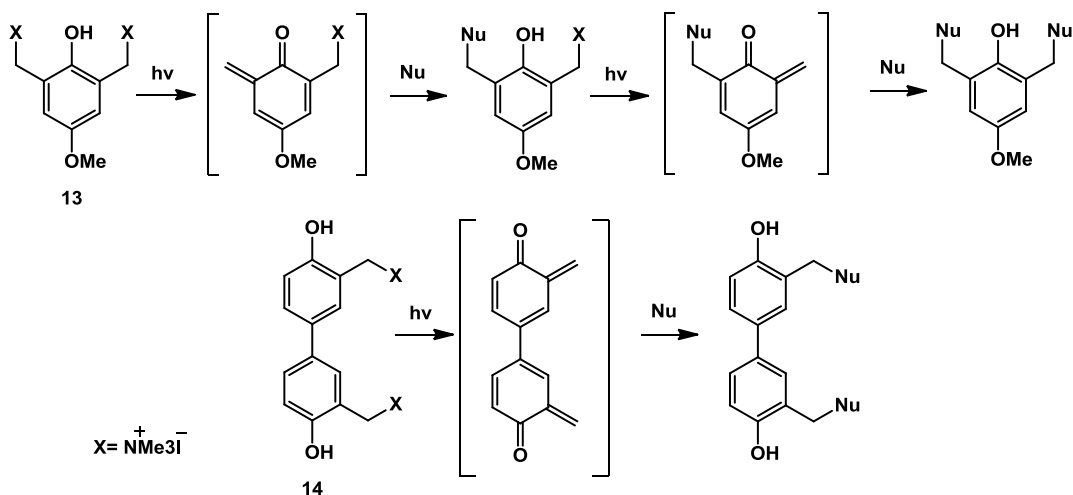


**Figure 1-8.** ICL formation by biquaternary ammonium salts.

Freccero's group has developed a class of binol quaternary ammonium salts, which act as photo-activated precursors to binolquinone methides (Figure 1-9).<sup>42</sup> Compounds **15** and **16** can induce efficient ICL formation upon irradiation at  $\lambda \geq 360$  nm.

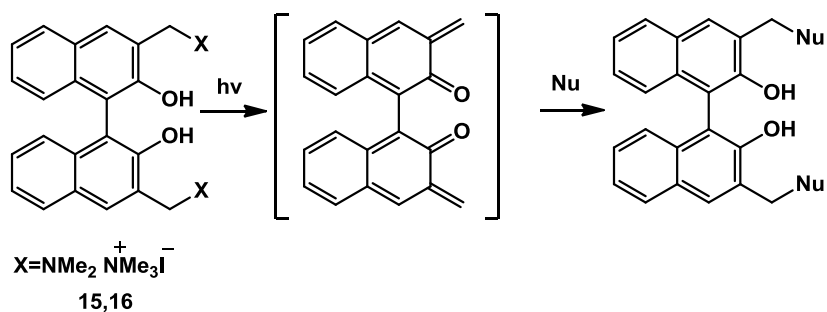


**Figure 1-9.** ICL formation by binol quaternary ammonium salts.

#### 1.2.2.2. DNA ICL agents activated by reduction



Rather than photo-activation, some ICL agents, such as mitomycin C, can undergo a reduction process to produce reactive intermediates that can cross-link DNA. This kind of agent is particularly suitable for the hypoxic cells existing in some solid tumors.

For example, aziridinylbenzoquinones **17** and **18**,<sup>43,44</sup> which constitute two aziridine rings in a quinone scaffold, can go through a two electron reduction under hypoxic condition. The lone pair of electrons is released from vinylogous amide conjugation with the quinone.<sup>45-47</sup> The increased electron density on the nitrogen atom of **19** facilitated the protonation of the aziridine ring and the subsequent ring-opening alkylation reaction of the aziridine (Figure 1-10). Among different aziridinylbenzoquinone compounds, diaziridinylquinone (DZQ) **17** and 2,5-bis(1-aziridinyl)-3,6-bis(carbethoxyamino)-1,4-benzoquinone (AZQ) **18** are the mostly studied therapeutic agents.<sup>46,47</sup>

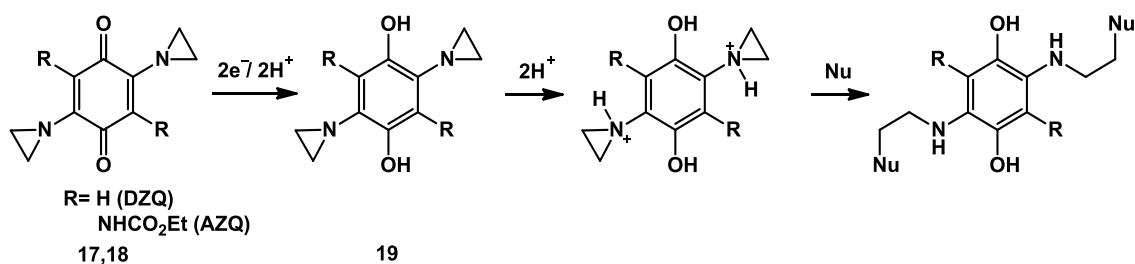


**Figure 1-10.** ICL formation by aziridinylbenzoquinones.

Some nitroaromatic alkylating prodrugs have been developed, which usually undergo a reductive conversion of an electron-withdrawing nitro group to an electron-donating amine substitution.

For example, the nitrobenzyl halides **20** showed hypoxic selectivity in cell culture by generating iminoquinone methide intermediate **21** under hypoxic condition (Figure 1-11).<sup>48</sup> The electron-withdrawing character of the nitro group greatly decreases the electron density of the mustard nitrogen, thereby masking the activity of nitrogen mustards. A number of nitroaniline chloro nitrogen mustards such as **22** had been synthesized and examined. The conjugation of the nitro

group with the long pair electrons on nitrogen prevent aziridinium formation but can be released and alkylate DNA after bio-reduction (Figure 1-12).<sup>49,50</sup>

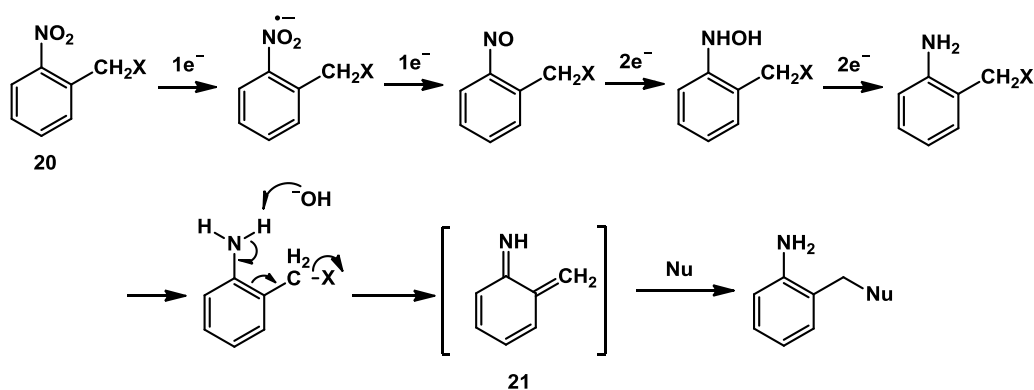


**Figure 1-11.** Mechanism of activation of *o*-nitrobenzyl compounds.

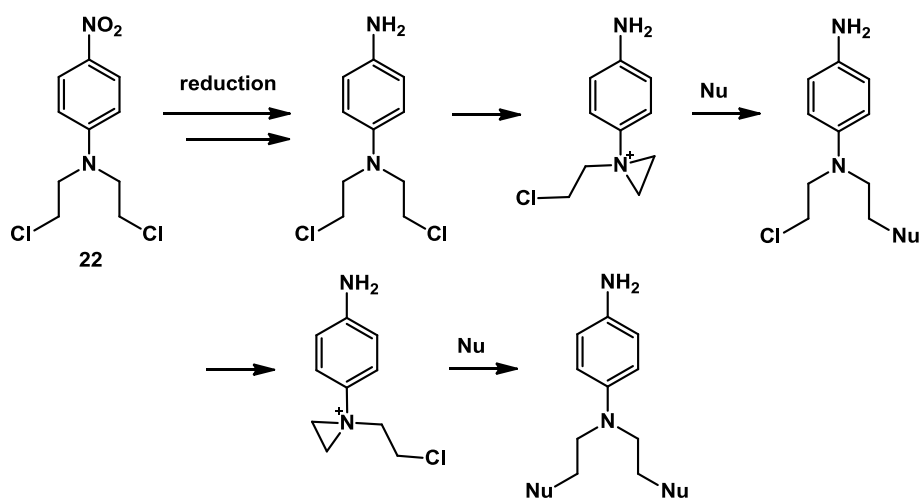


**Figure 1-12.** Reductive activation of nitrophenyl mustard.

### 1.2.2.3. DNA ICL agents activated by oxidation

Several clinically useful anticancer agents are oxidation-induced DNA cross-linking agents that are activated by cytochrome P-450 (CYPs). The P-450 enzymes belong to the superfamily of proteins containing a heme cofactor. They are the terminal oxidase enzymes in enzymatic reactions by using a variety of small molecules as substrates. The most common reaction of

CYPs is monooxygenation, including carbon hydroxylation, heteroatom hydroxylation, heteroatom dealkylations (via aldehyde generation), oxidations of  $\pi$ systems, and conversion of aldehydes or alcohols to the corresponding acids.<sup>51,52</sup>

Cyclophosphamide (CP) **23** was the first metabolically activated ICL agents. It undergoes oxidation at the C4 position to yield the corresponding 4-hydroxycyclophosphamide, **24**, which spontaneously goes through reversible ring opening to afford the biologically active aldophosphamide **25**.<sup>53,54</sup> The intermediate 4-hydroxycyclophosphamide can also be oxidized to stable amide **26** which is considered to be the deactivation of CP. The activated aldophosphamide further undergoes  $\beta$ -elimination of the phosphoryl to produce phosphoramidate mustard **27**. The hydrolysis of the phosphoramidate mustard generate the secondary mechlorethamine **28** (Figure 1-13).<sup>10,54</sup>

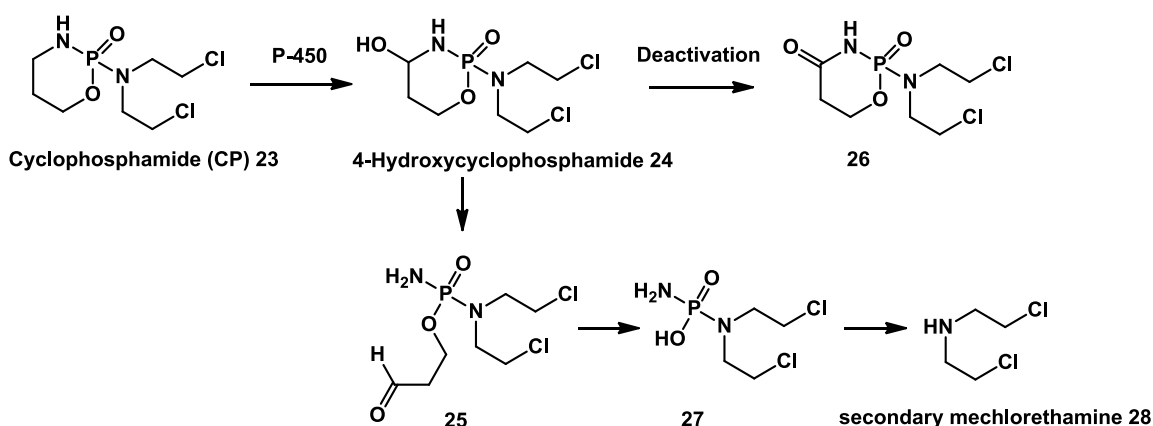


**Figure 1-13.** Oxidative activation of cyclophosphamide.

Hexamethylmelamine (HMM or Altretamine) **29** is also an antitumor agent that is activated by CYPs. It undergoes hydroxylation followed by dehydration upon oxidation by CYPs.<sup>55</sup> The resulting iminium **30** can alkylate nucleophiles in DNA (Figure 1-14). HMM is effective against a number of different human tumor cell lines, such as metastatic breast cancer, lymphoma,

cervical cancer, and bladder cancers.<sup>56</sup> It was approved by the FDA in 1990 and is widely used for treatment of ovarian cancer.

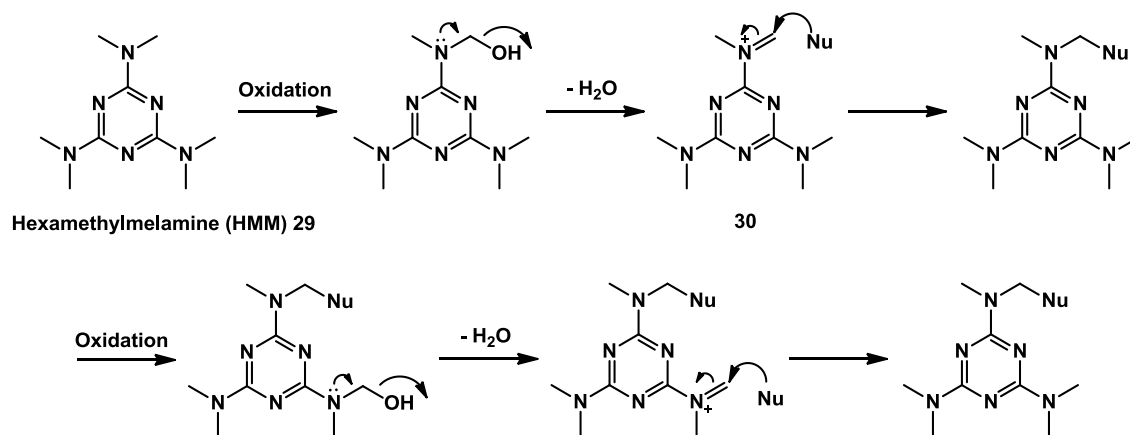


**Figure 1-14.** Oxidative activation of hexamethylmelamine.

Agents that induce DNA cross-links selectively in cancer cells are very limited. Few of them specifically target tumor-specific conditions and are usually limited to a narrow range of tumor cells. In order to design and develop more effective and highly selective antitumor agents, we explored the microenvironments that are unique to cancer cells to identify chemical methods and precursors for inducing DNA cross-link formation selectively in cancer cells.

### 1.3. Reactive Oxygen Species

#### 1.3.1. High levels of reactive oxygen species in cancer cell

Compared with the normal cells, the major distinguishing property of cancer cells is their diminished or unrestrained control of growth. The faster growth of cancer cells leads to increased metabolism, which alters the biochemical properties of cancer cells. Most cancer cells exhibit various genetic alterations and increased aerobic glycolysis and oxidative stress.<sup>57-59</sup> Higher levels of reactive oxygen species (ROS) have been observed in many kinds of cancer cells, such as chronic lymphocytic leukemia or hairy-cell leukemia cells.<sup>60,61</sup> Increased levels of oxidative

DNA damage products were detected in clinical solid tumor specimens and cancer cell lines.<sup>62,63</sup>

The increased generation of ROS is a unique property of cancer cells, which could be exploited to develop new strategies for cancer treatment.

Reactive oxygen species are defined as reactive chemical species containing oxygen. ROS are formed as by-products of normal aerobic metabolism.<sup>44</sup> There are two types of ROS, free radical ROS and non-radical ROS. The free radical ROS usually contain one or more unpaired electrons in their outer molecular orbitals, such as superoxide anion ( $O_2^-$ ), nitric oxide (NO), and hydroxyl radicals ( $OH^\cdot$ ). The non-radical ROS do not have unpaired electrons but can be converted to free radical ROS by chemical reaction. In biological systems, hydrogen peroxide ( $H_2O_2$ ), ozone ( $O_3$ ), peroxyxynitrate ( $NO_4^-$ ) and hydroxide ( $OH^-$ ) are common non-radical ROS.

ROS are essential for biological functions. They are linked to various physiological processes and essential protective mechanisms in living organisms. ROS regulate many signal transduction pathways by directly reacting with proteins, transcription factors, and genes thus modulating their functions. ROS are also involved in immune defense, antibacterial action and vascular tone. However, high levels of ROS are implicated in several harmful effects to cells, such as the oxygen free radicals that are highly reactive towards biological molecules. They can oxidize polyunsaturated fatty acids in lipids and amino acids in proteins. They can also oxidize the co-factors of some specific enzymes. The oxidative modification of these biomolecules can alter or impair their functions. A mild ROS level may result in transient cellular alteration, whereas a severe increase of ROS level in cells could cause irreversible oxidative damage, leading to cell death.

ROS can be produced from either endogenous or exogenous sources. Some exogenous factors, including industrial pollutants, pathogens and ionizing radiation can also induce ROS formation.

Inside the cells, mitochondria, peroxisomes, and inflammatory cell activation can generate ROS through multiple mechanisms. During oxidative metabolism in mitochondria, the majority of oxygen is reduced to water, however some may react with the electrons that leak from the mitochondrial respiratory chain to form superoxide anion, which can be converted to other ROS.<sup>64</sup> The superoxide anion can also be generated through enzymatic reaction by NADPH oxidase complexes, xanthine oxidase and cylooxygenases.<sup>65</sup> ROS are also produced as a byproduct through  $\beta$ -oxidation reactions of peroxisomal oxidases in peroxisomes<sup>66</sup> and detoxification reactions by cytochrome P450.

### 1.3.2. Hydrogen peroxide and its detection

Among different kinds of ROS, hydrogen peroxide ( $H_2O_2$ ) is particularly important because it is relatively stable. Hydrogen peroxide can be generated through dismutation of the superoxide anion by superoxide dismutase (SOD).<sup>67</sup> It can also be converted to hydroxyl free radicals via the metal-catalyzed Fenton reaction (Figure 1-15).<sup>68</sup> Compared to other ROS,  $H_2O_2$  has a lower reduction potential, which means it is more electronegative and less reactive. It also shows higher stability with a longer half-life and higher intracellular concentration (Table 1-1).<sup>69</sup> All these properties make  $H_2O_2$  an ideal signal molecule for evaluation of the cellular ROS level. In the past decades, a variety of  $H_2O_2$ -specific probes have been developed for detection and quantitation of  $H_2O_2$  in living cells.

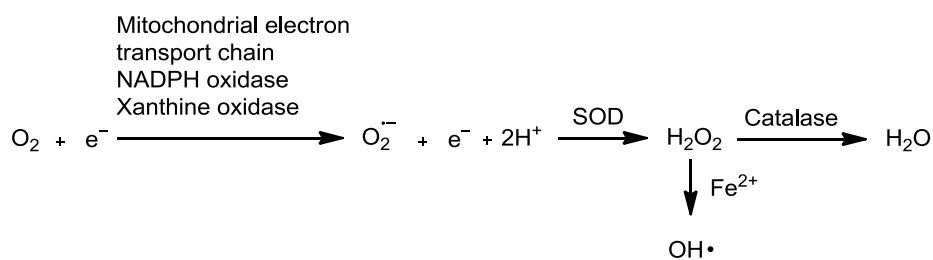


**Figure 1-15.** Generation of reactive oxygen species.

**Table 1-1.** Chemical properties of different ROS.

	$O_2^{\cdot-}$	$H_2O_2$	$OH\cdot$
Reduction potential (V)	0.94	0.32	2.31
$T_{1/2}$ (sec)	$10^{-6}$	$10^{-5}$	$10^{-9}$
in vivo concentration (M)	$10^{-10}$	$10^{-7}$	$10^{-15}$

For example, Chang's group took the advantage of selective cleavage of boronates by  $H_2O_2$  to design fluorescent probes for  $H_2O_2$  detection. They first focused on fluorescein analogues due to their high fluorescence intensity and synthesized boronate-masked fluorescein peroxyfluor-1 (PF1) **31** (Figure 1-16).<sup>70</sup> PF1 is a non-fluorescent compound but the addition of  $H_2O_2$  leads to formation of product **32** with strong green fluorescence. The fluorescence responses of PF1 platforms are highly  $H_2O_2$  selective (Figure 1-17). About 10 to 100 fold selectivity was achieved towards other ROS, such as superoxide, due to the deboronation and activation of PF1 was selective for  $H_2O_2$ . However, this probe can't detect endogenous  $H_2O_2$  because of its relatively low sensitivity to  $H_2O_2$ . In order to address this problem, the fluorophores masked with monoboronate were developed as they only need one equivalent of  $H_2O_2$  to release the highly fluorescent products. For example, peroxy green 1 (PG1) **33** and peroxy crimson 1 (PC1) **35** showed high selectivity and sensitivity for  $H_2O_2$  and also good membrane permeability. PG1 features an absorption band at 460 nm with weak emission at 510 nm ( $\Phi = 0.075$ ), while the reaction of PG1 with  $H_2O_2$  leads to a 10-fold increase in fluorescence due to formation of 2-Methyl-4-O-methyl Tokyo Green **34**. As PC1 has an even weaker emission band (584 nm,  $\Phi = 0.006$ ), the reaction of PC1 with  $H_2O_2$  leads to a greater increase of red fluorescence (40-fold) (Figure 1-18).<sup>71</sup> In addition, the boronic esters do not have intrinsic toxicity and the final product

boric acid is also non-toxic to humans, which made the arylboronates more attractive for  $H_2O_2$  detection.

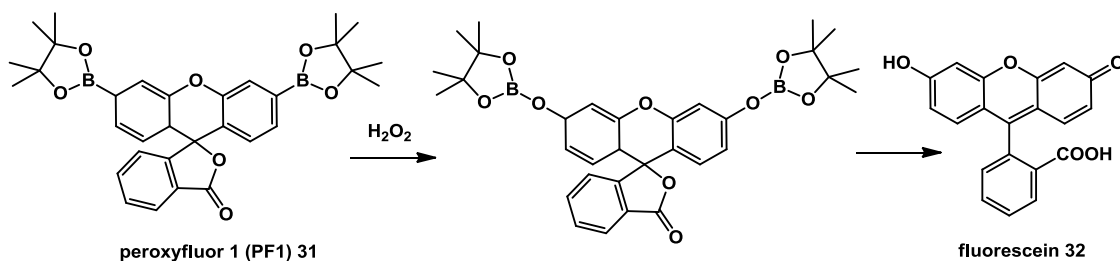


**Figure 1-16.** Activation of  $H_2O_2$  probes PF1.

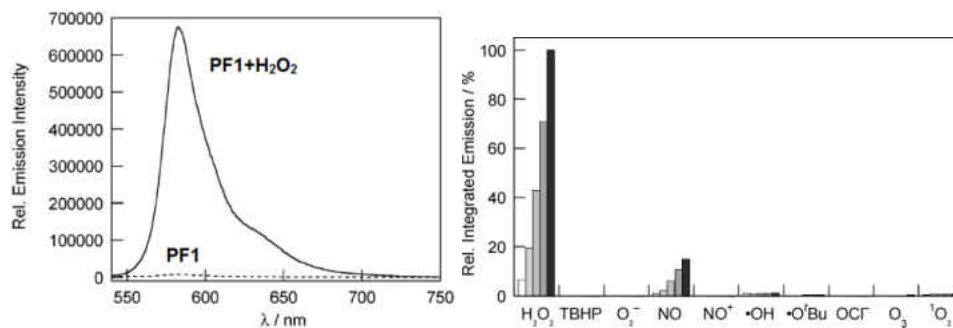


**Figure 1-17.** Spectroscopic response and selectivity of  $H_2O_2$  probes PF1.

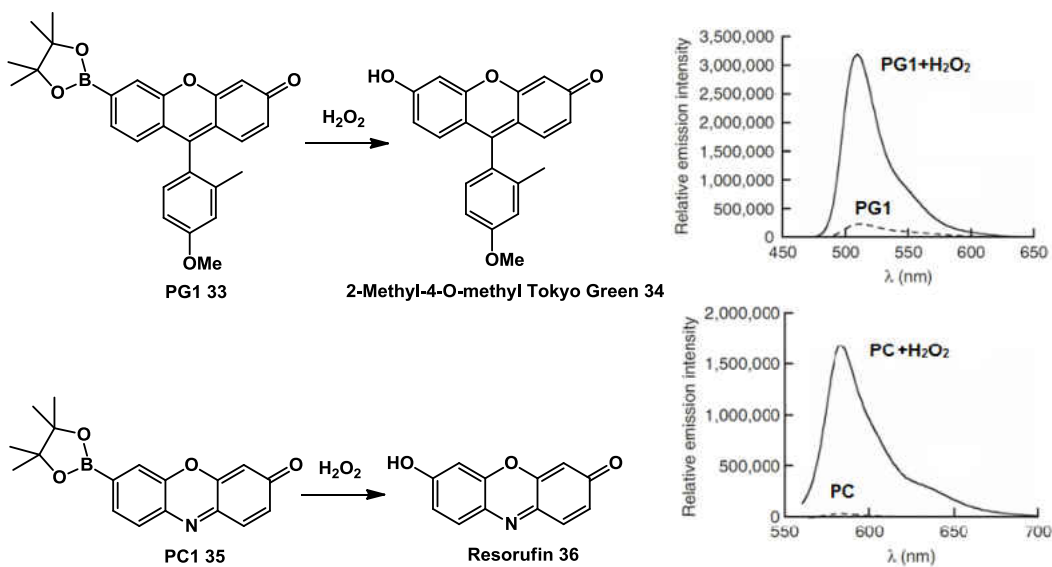


**Figure 1-18.** Activation and spectroscopic responses of  $H_2O_2$  probes PG1 and PC1.



The boronate analogue has been used for detection of H<sub>2</sub>O<sub>2</sub> in mitochondria. For example, mitochondria peroxy yellow 1 **36** (MitoPY1) has been developed for imaging mitochondrial H<sub>2</sub>O<sub>2</sub> in living cells by adding a phosphonium head that can deliver antioxidants and electrophiles to mitochondria. MitoPY1 shows a weak emission at 540 nm ( $\Phi = 0.019$ ) but can be oxidized by H<sub>2</sub>O<sub>2</sub> to form MitoPY1ox **37** resulting in strong fluorescence at 528 nm ( $\Phi = 0.405$ ) (Figure 1-19).<sup>72</sup>

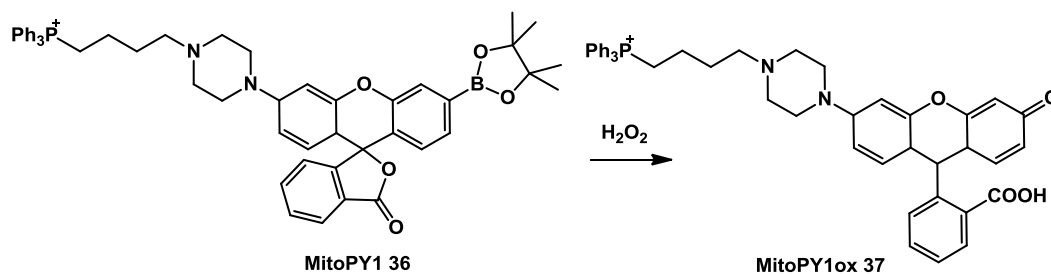


**Figure 1-19.** Activation of H<sub>2</sub>O<sub>2</sub> probe MitoPY1.

Guo's group has developed a fluorescent probe **38** which is not fluorescent but can be activated in the presence of both H<sub>2</sub>O<sub>2</sub> and Cu<sup>2+</sup> or Fe<sup>3+</sup>. The activation mechanism involves H<sub>2</sub>O<sub>2</sub>-induced oxidative deprotection of the boronate group to produce **39** followed by a metal-coordination-induced fluorescence enhancement to generate **40** (Figure 1-20).<sup>73</sup>

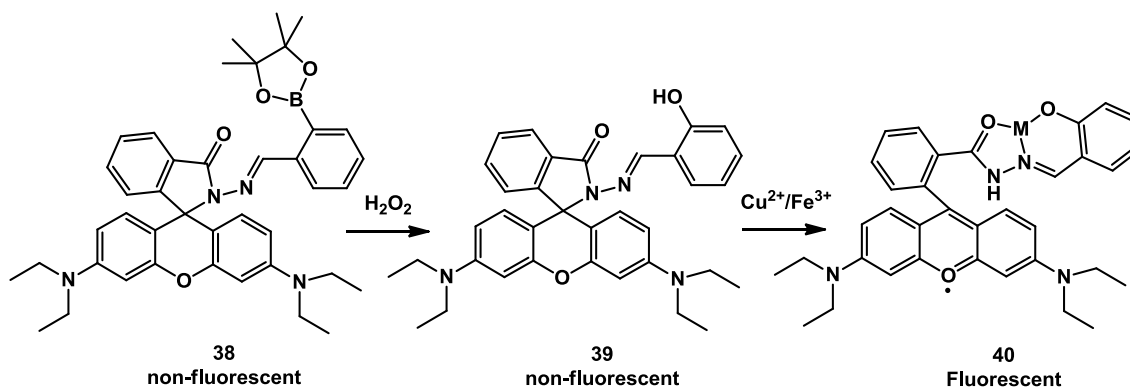


**Figure 1-20.** Activation of H<sub>2</sub>O<sub>2</sub> probe **38**.

Most probes for H<sub>2</sub>O<sub>2</sub> detection contain a boronate group that serves as a H<sub>2</sub>O<sub>2</sub>-responsive unit because the arylboronic ester selectively reacts with H<sub>2</sub>O<sub>2</sub> under physiological condition to produce the corresponding phenol. Conversion of an electron-withdrawing boronate group to a donating hydroxyl group alters the conjugation properties of the aromatic ring, which is expected to be suitable for developing H<sub>2</sub>O<sub>2</sub>-activated DNA cross-linking agents, such as prodrugs of nitrogen mustard or quinone methide (QM). My research goal is to design, synthesize, and characterize arylboronate analogues that do not cross-link DNA in the absence H<sub>2</sub>O<sub>2</sub>, but can be selectively activated by H<sub>2</sub>O<sub>2</sub> to release QM that directly bonds to DNA (Figure 1-21).

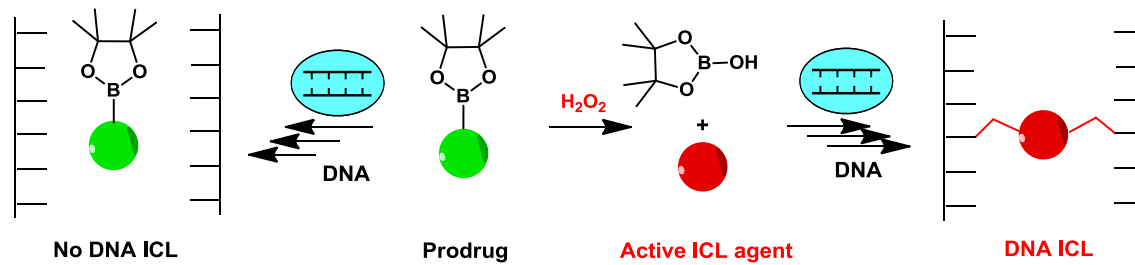


**Figure 1-21.** Design arylboronic ester H<sub>2</sub>O<sub>2</sub>-selective ICL agent.

## 1.4. Quinone Methide

### 1.4.1. The characterization and reactivity of quinone methide

Among the different kinds of ICL agents, quinone methide is an important electrophilic and transient intermediate that is widely implicated in alkylation processes. Quinone methides are a class of conjugated organic compounds that contain a cyclohexadiene core with a carbonyl and an exocyclic methylene unit. The carbonyl and methylene groups are oriented ortho, meta or para to each other leading to three types of QMs: *o*-QM, *m*-QM and *p*-QM (Figure 1-22). *o*-QM and *p*-QM are the most common isomers, due to the direct orbital interaction between the oxygen and methylene carbon. Such interaction does not exist in *m*-QM.

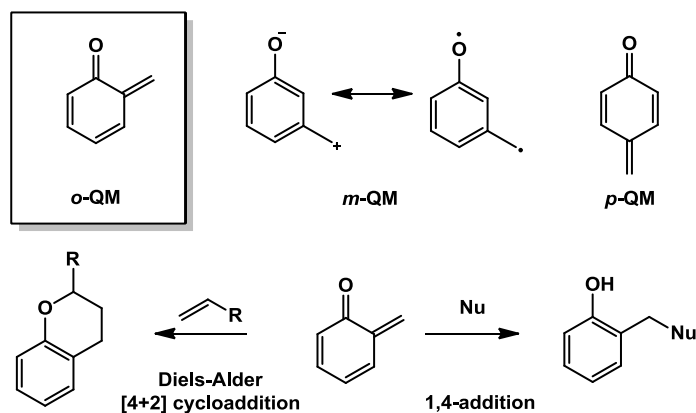


**Figure 1-22.** *o*-, *m*- and *p*-quinone methide and nucleophilic addition.

*o*-QM is a highly polarized intermediate in which the exocyclic methylene shows strong positive charge density. Thus the exocyclic methylene of *o*-QM acts as a good electrophilic center which readily reacts with nucleophiles. *o*-QM usually undergoes two kinds of reaction: 1,4-conjugate addition with nucleophiles to produce benzylic adducts and Diels-Alder [4+2] cycloaddition reactions with electron-rich dienophiles to form chromane adducts (Figure 1-22). The highly reactive *o*-QMs have been widely used in organic synthesis and biological system for preparation of a variety of important precursors such as 2H-chromene.<sup>74</sup> It has been demonstrated that QM can react with amino acids<sup>39</sup> and proteins<sup>75</sup> and inhibit the function of some enzymes. *o*-QMs have also been applied as alkylating functional groups in antitumor drugs or antibiotics. For example, QMs can react with the base moieties of 2'-deoxycytidine (dC), 2'-deoxyguanosine (dG), and 2'-deoxyadenine (dA) forming alkylated adducts. The cyclic nitrogens, exocyclic amino groups, and carbonyl groups in the base moieties act as nucleophiles (Figure 1-23). Among these, dG N7, dCN3, and dA N1 are strong nucleophiles that usually generate unstable adducts,<sup>76</sup> while dG N1, dG N2, and dA N6 are relatively weak nucleophiles that form stable adducts with QM (Figure 1-24).<sup>77</sup> The alkylation can take place with single stranded DNA, as

well as with duplex DNA. In duplex DNA, guanine is commonly the predominant target due to its strong nucleophiles, followed by cytosine and adenine. Thymine is inert to QMs.

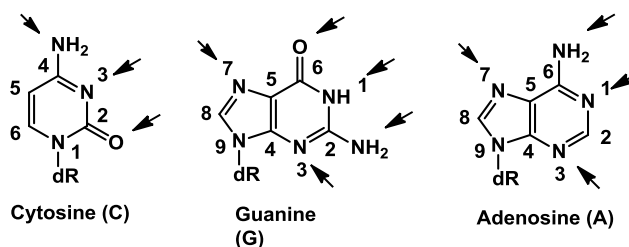


**Figure 1-23.** Nucleophiles in dC, dG and dA.

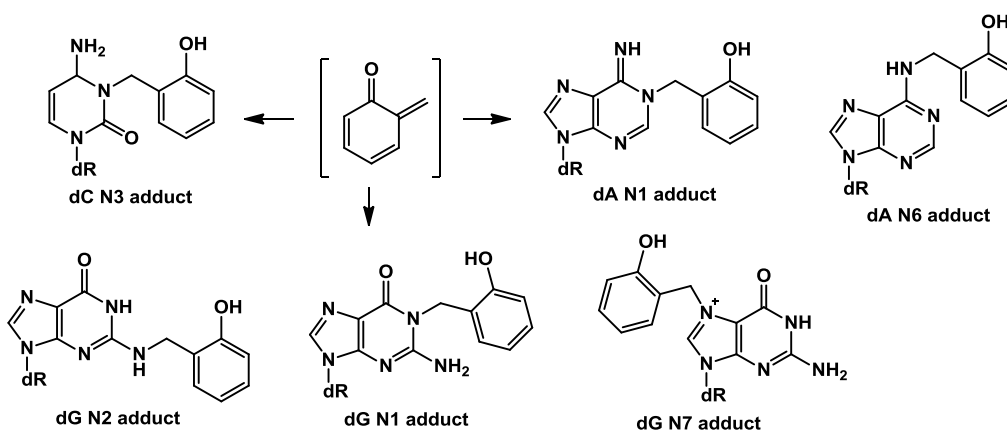


**Figure 1-24.** Nucleoside adducts formed by *o*-QM.

#### 1.4.2. Chemical methods to produce quinone methides

The transient intermediate QM can be generated through activation of stable quinone methide precursors such as benzyl substituted phenols. During the past decade, several chemical methods have been developed for generating QMs, such as heating,<sup>39</sup> UV-irradiation,<sup>41,42</sup> oxidation<sup>78,79</sup> (Figure 1-25) and various biological process.<sup>80-82</sup> For example, the groups of Zhou<sup>41</sup> and Freccero<sup>39,42</sup> have developed a series of photo-inducible DNA cross-linking agents that released QMs upon UV-irradiation. The QMs can also be generated in water from (2-hydroxybenzyl)

trimethylammonium iodide by heating at 80 °C under neutral conditions while the weak basic conditions can facilitate the QM generation.<sup>76</sup>

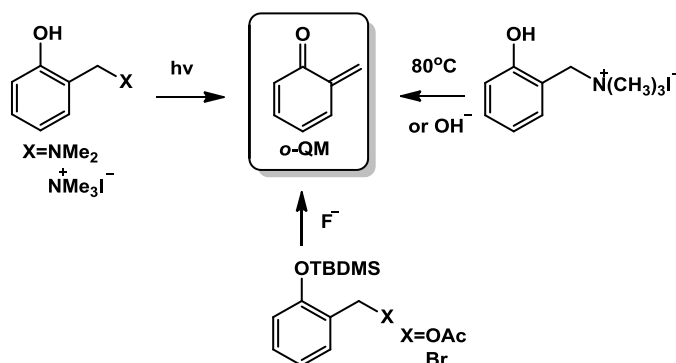


**Figure 1-25.** Photochemical, base catalyzed and fluoride induced QM generation.

Rokita's lab developed a series of silyl-protected quinone methide precursors **40** and **41**, which usually contain a bromide or an acetate group as the leaving group (Figure 1-26).<sup>83,84</sup> These compounds can be activated in the presence of fluoride ion to generate QM intermediates **42**, **43** that react with the nucleophilic N7 group of guanine to form a labile adduct or the 2-amino group of guanine to form a stable adduct.

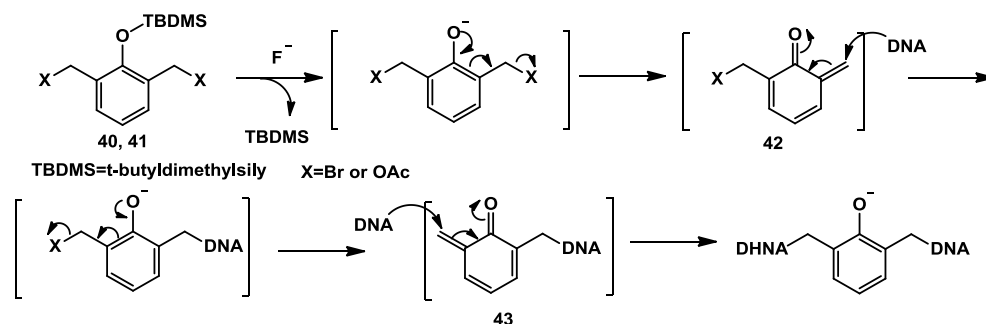


**Figure 1-26.** ICL formation by silyl-protected bis(acetoxymethyl)phenol.

QMs can also be produced from different biological enzymatic oxidation by oxidative enzymes including CYPs,<sup>78,79</sup> tyrosinase<sup>81</sup> and laccase.<sup>81,82</sup> For example, tamoxifen **44**, an antagonist of the estrogen receptor in breast tissue, is metabolized to the reactive species 4-hydroxytamoxifen

quinone methide **45** capable of cross-linking DNA. The metabolic pathway of tamoxifen is a two-step oxidation catalyzed by P450 followed by P450-mediated proton abstraction to generate **45** (Figure 1-27).<sup>78,79</sup>

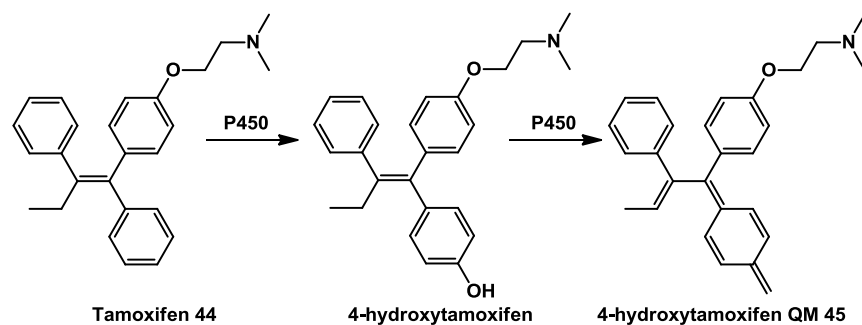


**Figure 1-27.** Formation of QM by oxidation of tamoxifen.

Acolbifene **46** is also a QM prodrug, which belongs to the fourth-generation selective estrogen receptor modulator (SERM) class. It is the most potent antiestrogen in terms of inhibition of estrogen receptor 1 (ER $\alpha$ ) and estrogen receptor 2 (ER $\beta$ ). Acolbifene can form two kinds of quinone methide intermediates through enzymatic oxidation by tyrosinase.<sup>80</sup> Oxidation of the methyl group leads to formation of the classic acolbifene quinone methide **48**. Another metabolic pathway involves stepwise oxidation of two phenol groups yielding a diquinone methide **47** (Figure 1-28).

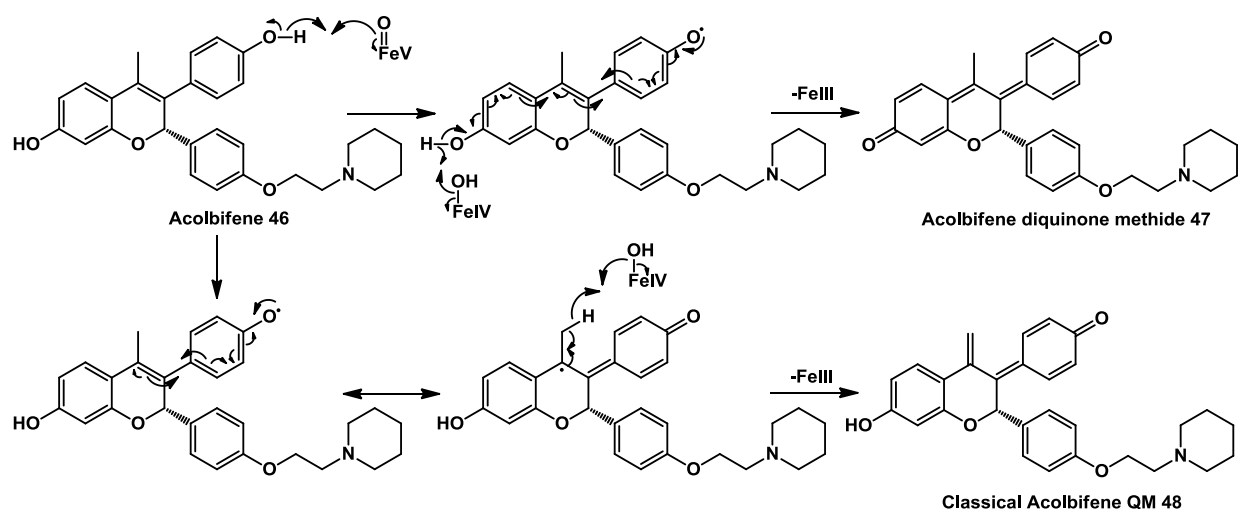


**Figure 1-28.** Formation of diquinone methide and classical acolbifene quinone methide by enzymatic oxidation.<sup>80</sup>

More recently, Greenberg's lab observed that the phenyl selenide derivatives of thymidine and 2'-deoxycidine can be activated by sodium periodate ( $\text{NaIO}_4$ ) to form methide derivatives that efficiently alkylate DNA.<sup>85-87</sup> Encouraged by this work, Zhou and coworkers designed and synthesized biphenyl selenide precursor **49**, which induced efficient DNA ICL formation via QM upon treatment with sodium periodate ( $\text{NaIO}_4$ ) (Figure 1-29).<sup>88</sup> Compound **49** produced 80% of DNA cross-linking at  $10 \mu\text{M}$ , which is more efficient than other phenyl selenides.<sup>88</sup> Similar trends in ICL formation were observed when using Rose Bengal as a singlet oxygen sensitizer.<sup>86</sup> However, most of the reported fluoride or redox generation protocols require chemical additives for the *in situ* activation of the QM. This feature increases the complexity of the application of QMs directly *in vivo*. The  $\text{H}_2\text{O}_2$ -induced QM precursors have the advantage that  $\text{H}_2\text{O}_2$  oxidation is bioorthogonal and  $\text{H}_2\text{O}_2$  is bio available. These properties make it more attractive for *in vivo* application.

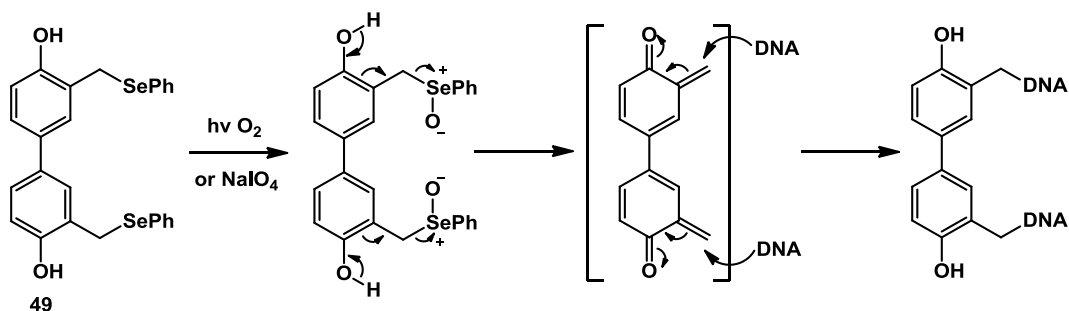


**Figure 1-29.** Formation of biquinone methide by oxidation of biphenyl selenide.

### 1.5. References

1. Watson, J. D., Crick, F. H. C. Molecular structure of nucleic acid. A structure for deoxyribosenucleic acid. *Nature* **1953**, *171*, 737-738.
2. Todd, A. R. Chemical structure of the nucleic acids. *Proc. Natl. Acad. Sci. U.S.A.* **1954**, *40*, 748-755.
3. Venter, J. C. The sequence of the human genome. *Science* **2001**, *291*, 1304-1351.
4. Pennisi, E. DNA's cast of thousands. *Science* **2003**, *300*, 282-285.
5. Alberts, B., Johnson, A., Lewis, J., Raff, M., Roberts, K., Walter, P. *Molecular Biology of the Cell*, 4th ed., Garland Science, New York. **2002**.
6. Alberts, B. DNA replication and recombination. *Nature* **2003**, *421*, 431-435.
7. Campbell, J. L. Eukaryotic DNA replication. *Ann. Rev. Biochem.* **1986**, *55*, 733-771.
8. Kornberg, A. DNA replication. *J. Biol. Chem.* **1988**, *263*, 1-4.
9. Gniazdowski, M. C., Cera, C., The effects of DNA covalent adducts on in vitro transcription. *Chem. Rev.* **1996**, *96*, 619-634.
10. Noll, D. M., Mason, T. M., Miller, P. S. Formation and repair of interstrand cross-links in DNA. *Chem. Rev.* **2006**, *106*, 277-301.



11. Dronkert, M. L. G., Kanaar, R. Repair of DNA interstrand cross-links. *Mutat. Res.* **2001**, *486*, 217-247.
12. Rajski, S. R., Williams, R. M., DNA cross-linking agents as antitumor drugs. *Chem. Rev.* **1998**, *98*, 2723-2795.
13. Gargiulo, D., Kumar, G. S., Musser, S. S., Tomasz, M. Structural and function modification of DNA by mitomycin C. Mechanism of the DNA sequence specificity of mitomycins. *Nucleic acids symp. ser.* **1994**, *34*, 169-170.
14. Tomasz M. Mitomycin C: small, fast and deadly (but very selective). *Chem. Biol.* **1995**, *2*, 575-579.
15. Das, A., Tang, K. S., Gopalakrishnan, S., Waring, M. J., Tomasz, M. Reactivity of guanine at m<sup>5</sup>CpG steps in DNA: evidence for electronic effects transmitted through the base pairs. *Chem. Biol.* **1999**, *6*, 461-471.
16. Cimino, G. D., Gamper, H. B., Isaacs, S. T., Hearst, J. E. Psoralens as photoactive probes of nucleic acid structure and function: organic chemistry, photochemistry, and biochemistry. *Ann. Rev. Biochem.* **1985**, *54*, 1151-1193.
17. Piette, J., Gamper, H. B., Van de Vorst, A., Hearst, J. E. Mutagenesis induced by site specifically placed 4'-hydroxymethyl-4, 5', 8-trimethylpsoralen adducts. *Nucleic acids Res.* **1988**, *16*, 9961-9977.
18. Averbeck, D. Recent advances in psoralen phototoxicity mechanism. *Photochem. Photobiol.* **1989**, *50*, 859-882.
19. Edelson, R., Berger, C., Gasparro, F., Jegasothy, B., Heald, P., Wintroub, B., Vonderheid, E., Knobler, R., Wolff, K., Plewig, G., McKiernan, G., Christiansen, I., Oster, M., Honigsmann, H., Wilford, H., Kokoschka, E., Rehle, T., Perez, M., Stingl, G., Laroche, L. Treatment of

- cutaneous T-cell lymphoma by extracorporeal photochemotherapy. *N. Engl. J. Med.* **1987**, *316*, 297-303.
20. Gasparro, F. P. Psoralen photobiology: recent advances. *Photochem. Photobiol.* **1996**, *63*, 553-557.
21. Lawley, P. D. Alkylation of DNA and its aftermath. *BioEssays* **1995**, *17*, 561-568.
22. Gilman, A., Philips, F. S. The biological actions and therapeutic applications of the  $\beta$ -chloroethyl amines and sulfides. *Science* **1946**, *103*, 409-436.
23. Rink, S. M., Solomon, M. S., Taylor, M. J., Rajur, S. B., Mclaughlin, L. W., Hopkins, P. B. Covalent structure of a nitrogen mustard-induced DNA interstrand cross-link: an N7-to-N7 linkage of deoxyguanosine residues at the duplex sequence 5'-d(GNC). *J. Am. Chem. Soc.* **1993**, *115*, 2551-2557.
24. Rink, S. M., Hopkins, P. B. A mechlorethamine-induced DNA interstrand cross-link bends duplex DNA. *Biochemistry* **1995**, *34*, 1439-1445.
25. Facon, T., Mary, J. Y., Hulin, C., Benboubker, L., Attal, M., Pegourie, B., ...& Intergroupe Francophone du Myélome. Melphalan and prednisone plus thalidomide versus melphalan and prednisone alone or reduced-intensity autologous stem cell transplantation in elderly patients with multiple myeloma (IFM 99-06): a randomised trial. *The Lancet* **2007**, *370*, 1209-1218.
26. Fuertes, M. A., Castilla, J., Alonso, C., Perez, J. M. Cisplatin biochemical mechanism of action: from cytotoxicity to induction of cell death through interconnections between apoptotic and necrotic pathways. *Curr. Med. Chem.* **2003**, *10*, 257-266.
27. Murray, V., Motyka, H., England, P. R., Wickham, G., Lee, H. H., Denny, W. A., McFadyen, W. D. The use of Taq DNA polymerase to determine the sequence specificity of DNA

- damage Caused by cis-diamminedichloroplatinum(II), Acridine-tethered Platinum(II) diammine complexes of two analogues. *J. Biol. Chem.* **1992**, 267, 18805-18809.
28. Pinto, A. L., Lippard, S. J. Sequence-dependent termination of in vitro DNA synthesis by cis- and trans- diamminedichloroplatinum(II). *Proc. Natl. Acad. Sci, U.S.A.* **1985**, 82, 4616-4619.
29. Ponti, M., Forrow, S. M., Souhami, R. L., D'Incalci, M., Hartley, J. A. Measurement of the sequence specificity of covalent DNA modification by antineoplastic agents using Taq DNA polymerase. *Nucleic Acids Res.* **1991**, 19, 2929-2933.
30. Royer-Pokora, B., Gordon, L. K., Haseltine, W. A. Use of exonuclease III to determine the site of stable lesions in defined sequences of DNA: the cyclobutane pyrimidine dimer and cis and trans dichlorodiammine platinum II examples. *Nucleic Acids Res.* **1981**, 9, 4595-4609.
31. Jamieson, E. R., Lippard, S. J. Structure, recognition, and processing of cisplatin-DNA adducts. *Chem. Rev.* **1999**, 99, 2467-2498.
32. Lebwohl, D., Canetta, R. Clinical development of platinum complexes in cancer therapy: an historical perspective and an update. *Eur. J. Cancer* **1998**, 34, 1522-1534.
33. Jakobs, A. E., Christiaens, L. E., Renson, M. J. Synthesis of monosulphur and monoselenium analogues of psoralen. *Tetrahedron* **1994**, 50, 9315-9324.
34. Rapoport, H., VanSickle, A. P. Azapsoralens. Synthesis of 8-azapsoralens. *J. Org. Chem.* **1990**, 55, 895.
35. Han, G. S., Shim, S. C. Photocycloaddition reactions of pyrazinopsoralen with simple olefins. *Photochem. Photobiol.* **1998**, 67, 84-89.
36. Kitamura, N., Kohtani, S., Nakagaki, R. Molecular aspects of furocoumarin reactions: Photophysics, photochemistry, photobiology, and structural analysis. *J. Photochem. Photobiol. C: Photochem. Rev.* **2005**, 6, 168-185.

37. Dalla Via, L., Magno, S. M., Rodighiero, P., Gia, O. Synthesis, photobiological activity and photoreactivity of methyl-thieno-8-azacoumarins, novel bioisosters of psoralen. *Bioorg. Med. Chem. Lett.* **2002**, *12*, 1253-1257.
38. Brousmiche, D. Photogeneration of an *o*-quinone methide from pyridoxine (vitamin B 6) in aqueous solution. *Chem. Commun.* **1998**, 491-492.
39. Modica, E., Zanaletti, R., Freccero, M., Mella, M. Alkylation of amino acids and glutathione in water by *o*-quinone methide. Reactivity and selectivity. *J. Org. Chem.* **2001**, *66*, 41-52.
40. Chiang, Y., Kresge, A. J., Zhu, Y. Flash photolytic generation of ortho-quinone methide in aqueous solution and study of its chemistry in that medium. *J. Am. Chem. Soc.* **2001**, *123*, 8089-8094.
41. Wang, P., Liu, R., Wu, X., Ma, H., Cao, X., Zhou, P., Zhang, J., Weng, X., Zhang, X., Qi, J., Zhou, X., Weng, L. A potent, water-soluble and photoinducible DNA cross-linking agent. *J. Am. Chem. Soc.* **2003**, *125*, 1116-1117.
42. Richter, S. N., Maggi, S., Mels, S. C., Palumbo, M., Freccero, M. Binol quinone methides as bisalkylating and DNA cross-linking agents. *J. Am. Chem. Soc.* **2004**, *126*, 13973-13979.
43. Khan, A. H., Driscoll, J. S. Potential central nervous system antitumor agents. Aziridinybenzoquinones. 1. *J. Med. Chem.* **1976**, *19*, 313-317.
44. Chou, F. T., Khan, A. H., Driscoll, J. S. Potential central nervous system antitumor agents. Aziridinybenzoquinones. 2. *J. Med. Chem.* **1976**, *19*, 1302-1308.
45. Lee, C. S., Hartley, J. A., Berardini, M. D., Butler, J., Siegel, D., Ross, D., Gibson, N. W. Alteration in DNA cross-linking and sequence selectivity of a series of aziridinybenzoquinones after enzymic reduction by DT-diaphorase. *Biochemistry* **1992**, *31*, 3019-3025.

46. Berardini, M. D., Souhami, R. L., Lee, C. S., Gibson, N. W., Butler, J., Hartley, J. A. Two structurally related diaziridinylbenzoquinones preferentially cross-link DNA at different sites upon reduction with DT-diaphorase. *Biochemistry*, **1993**, *32*, 3306-3312.
47. Lee, C. S., Pfeifer, G. P., Gibson, N. W. Mapping of DNA alkylation sites induced by aziridinylbenzoquinones in human cells by ligation-mediated polymerase chain reaction. *Cancer research* **1994**, *54*, 1622-1626.
48. Teicher, B. A., Sartorelli, A. C. Nitrobenzyl halides and carbamates as prototype bioreductive alkylating agents. *J. Med. Chem.* **1980**, *23*, 955-960.
49. Denny, W. A., Wilson, W. R. Considerations for the design of nitrophenyl mustards as agents with selective toxicity for hypoxic tumor cells. *J. Med. Chem.* **1986**, *29*, 879-887.
50. Palmer, B. D., Wilson, W. R., Pullen, S. M., Denny, W. A. Hypoxia-selective antitumor agents. 3. Relationships between structure and cytotoxicity against cultured tumor cells for substituted N, N-bis (2-chloroethyl) anilines. *J. Med. Chem.* **1990**, *33*, 112-121.
51. Gonzalez, F. J., Nebert, D. W. Evolution of the P450 gene superfamily: animal-plant 'warfare', molecular drive and human genetic differences in drug oxidation. *Trends in Genetics* **1990**, *6*, 182-186.
52. Borne, R. F., Foye, W. O., Lemke, T. L., Williams, D. A. *Principles of medicinal chemistry*. Williams & Wilkins, Baltimore, **1995**, pp 104-111.
53. Borch, R. F., Hoye, T. R., Swanson, T. A. In situ preparation and fate of cis-4-hydroxycyclophosphamide and aldophosphamide: proton and phosphorus-31 NMR evidence for equilibration of cis- and trans-4-hydroxycyclophosphamide with aldophosphamide and its hydrate in aqueous solution. *J. Med. Chem.* **1984**, *27*, 490-494.

54. Borch, R. F., Millard, J. A. The mechanism of activation of 4-hydroxycyclophosphamide. *J. Med. Chem.* **1987**, *30*, 427-431.
55. Legha, S. S., Slavik, M., Carter, S. K. Hexamethylmelamine. An evaluation of its role in the therapy of cancer. *Cancer* **1976**, *38*, 27-35.
56. Jackson, C., Crabb, T. A., Gibson, M., Godfrey, R., Saunders, R., Thurston, D. E. Studies on the stability of trimelamol, a carbinolamine-containing antitumor drug. *J. Pharm. Sci.* **1991**, *80*, 245-251.
57. Szatrowski, T. P., Nathan, C. F. Production of large amounts of hydrogen peroxide by human tumor cells. *Cancer Rev.* **1991**, *51*, 794-798.
58. Toyokuni, S., Okamoto, K., Yodoi, J., Hiai, H. Persistent oxidative stress in cancer. *FEBS letters*, **1995**, *358*, 1-3.
59. Trachootham, D., Alexandre, J., Huang, P. Targeting cancer cells by ROS-mediated mechanisms: a radical therapeutic approach? *Nature Rev. Drug Discov.* **2009**, *8*, 579-591.
60. Zhou, Y., Hileman, E. O., Plunkett, W., Keating, M. J., Huang, P. Free radical stress in chronic lymphocytic leukemia cells and its role in cellular sensitivity to ROS-generating anticancer agents. *Blood* **2003**, *101*, 4098-4104.
61. Kamiguti, A. S., Serrander, L., Lin, K., Harris, R. J., Cawley, J. C., Allsup, D. J., Slupsky, J. R., Krause, K., Zuzel, M. Expression and activity of NOX5 in the circulating malignant B cells of hairy cell leukemia. *J. Immunol.* **2005**, *175*, 8424-8430.
62. Martinez-Sanchez, G., Giuliani, A. Cellular redox status regulates hypoxia inducible factor-1 activity. Role in tumour development. *J. Exp. Clin. Cancer Res.* **2007**, *26*, 39.
63. Tsao, S. M., Yin, M. C., Liu, W. H. Oxidant stress and B vitamins status in patients with non-small cell lung cancer. *Nutr. Cancer* **2007**, *59*, 8-13.

64. St-Pierre, J., Buckingham, J. A., Roebuck, S. J., Brand, M. D. Topology of superoxide production from different sites in the mitochondrial electron transport chain. *J. Biol. Chem.* **2002**, *277*, 44784-44790.
65. Curtin, J. F., Donovan, M., Cotter, T. G. Regulation and measurement of oxidative stress in apoptosis. *J. Immunol. Methods* **2002**, *265*, 49-72.
66. Schrader, M., Fahimi, H. D. Peroxisomes and oxidative stress. *Biochimica et Biophysica Acta* **2006**, *1763*, 1755-1766.
67. Juarez, J. C., Manuia, M., Burnett, M. E., Betancourt, O., Boivin, B., Shaw, D. E., Tonks, N. K., Mazar, A. P., Doñate, F. Superoxide dismutase 1 (SOD1) is essential for H<sub>2</sub>O<sub>2</sub>-mediated oxidation and inactivation of phosphatases in growth factor signaling. *Proc. Natl. Acad. Sci. U.S.A.* **2008**, *105*, 7147-7152.
68. Winterbourn, C. C. Toxicity of iron and hydrogen peroxide: the Fenton reaction. *Toxicology letters*, **1995**, *82*, 969-974.
69. Giorgio, M., Trinei, M., Migliaccio, E., Pelicci, P. G. Hydrogen peroxide: a metabolic by-product or a common mediator of ageing signals? *Nature reviews Molecular cell biology*, **2007**, *8*, 722-728.
70. Miller, E. W., Albers, A. E., Pralle, A., Isacoff, E. Y., Chang, C. J. Boronate-based fluorescent probes for imaging cellular hydrogen peroxide. *J. Am. Chem. Soc.* **2005**, *127*, 16652-16659.
71. Miller, E.W., Tulyanthan, O., Ehud, Y.I., Chang, C.J. Molecular imaging of hydrogen peroxide produced for cell signaling. *Nat. Chem. Biol.* **2007**, *3*, 263–267.
72. Dickinson, B. C., Chang, C. J. A targetable fluorescent probe for imaging hydrogen peroxide in the mitochondria of living cells. *J. Am. Chem. Soc.* **2008**, *130*, 9638-9639.

73. Wei, Y., Zhang, Y., Liu, Z., Guo, M. A novel profluorescent probe for detecting oxidative stress induced by metal and H<sub>2</sub>O<sub>2</sub> in living cells. *Chem. Comm.* **2010**, *46*, 4472-4474.
74. Ferreira, S. B., da Silva, F. D. C., Pinto, A. C., Gonzaga, D. T. G., Ferreira, V.F. Syntheses of chromenes and chromanes *via* o-quinone methide intermediates. *J. Heterocyclic Chem.* **2009**, *46*, 1080-1097.
75. Zhang, D., Ogan, M., Gedamke, R., Roongta, V., Dai, R., Zhu, M., Rinehart, J. K., Klunk, L., Mitroka, J. Protein covalent binding of maxipost through a cytochrome P450-mediated ortho-quinone methide intermediate in rats. *Drug Metab. Dispos.* **2003**, *31*, 837-845.
76. Pande, P., Shearer, J., Yang, J., Greenberg, W. A. Rokita, S. E., Alkylation of nucleic acids by a model quinone methide. *J. Am. Chem. Soc.* **1999**, *121*, 6773-6779.
77. Weinert, E. E., Frankenfield, K. N., Rokita, S. E. Time-dependent evolution of adducts formed between deoxynucleosides and a model quinone methide. *Chem. Res. Toxicol.* **2005**, *18*, 1364-1370.
78. Dehal, S. S., Kupfer, D. Cytochrome P-450 3A and 2D6 catalyze *ortho*hydroxylation of 4-hydroxytamoxifen and 3-hydroxytamoxifen (droloxifene) yielding tamoxifen catechol: involvement of catechols in covalent binding to hepatic proteins. *Drug Metab. Dispos.* **1999**, *27*, 681-688.
79. Fan, P. W., Bolton, J. L. Bioactivation of tamoxifen to metabolite E quinone methide: reaction with glutathione and DNA. *Drug Metab. Dispos.* **2001**, *29*, 891-896.
80. Liu, J., Liu, H., van Breemen, R. B., Thatcher, G. R., Bolton, J. L. Bioactivation of the selective estrogen receptor modulator acolbifene to quinone methides. *Chemical research in toxicology*, **2005**, *18*, 174-182.



81. Clarkson, C., Musonda, C. C., Chibale, K., Campbell, W. E., Smith, P. Synthesis of totarol amino alcohol derivatives and their antiplasmodial activity and cytotoxicity. *Bioorg. Med. Chem.* **2003**, *11*, 4417-4422.
82. Ncanana, S., Baratto, L., Roncaglia, L., Riva, S., Burton, S. G. Laccase-mediated oxidation of totarol. *Adv Synth Catal.* **2007**, *349*, 1507-1513.
83. Veldhuyzen, W. F., Shallop, A. J., Jones, R. A., Rokita, S. E. Thermodynamic versus kinetic products of DNA alkylation as modeled by reaction of deoxyadenosine. *J. Am. Chem. Soc.* **2001**, *123*, 11126-11132.
84. Freccero, M. Quinone methides as alkylating and cross-linking agents. *Mini-Reviews in Organic Chemistry*, **2004**, *1*, 403-415.
85. Hong, I. S., Greenberg, M. M. Efficient DNA interstrand cross-link formation from a nucleotide radical. *J. Am. Chem. Soc.* **2005**, *127*, 3692-3693;
86. Hong, I. S., Greenberg, M. M. DNA interstrand cross-link formation initiated by reaction between singlet oxygen and a modified nucleotide. *J. Am. Chem. Soc.* **2005**, *127*, 10510-10511.
87. Hong, I. S., Ding, H., Greenberg, M. M. Oxygen independent DNA interstrand cross-link formation by a nucleotide radical. *J. Am. Chem. Soc.* **2006**, *128*, 485-491.
88. Weng, X., Ren, L.; Weng, L., Huang, J., Zhu, S.; Zhou, X., Weng, L. Synthesis and biological studies of inducible DNA cross-linking agents. *Angew. Chem. Int. Ed.*, **2007**, *119*, 8166-8169.

## Chapter 2. Synthesis and Biological Investigation of H<sub>2</sub>O<sub>2</sub>-Inducible DNA Cross-Linking Agents

### 2.1. Introduction

DNA cross-linking agents lead to covalent binding between two complementary strands, which prevents separation of DNA double strands, thus inhibiting DNA transcription and replication.<sup>1</sup>

Some ICL agents, such as nitrogen mustard derivatives, have been widely used in cancer treatment.<sup>2</sup> However, most existing cross-linking agents showed severe host toxicity due to the poor selectivity towards cancer cells. One novel approach to improve the selectivity of ICL agents toward cancer cells would be development of chemical agents that can be activated only under tumor-specific condition to cross-link DNA. Several chemical methods have been developed to generate DNA cross-linking or alkylating functional groups from a series of non-toxic precursors, such as photo irradiation, fluoride induction, and oxidation induction.<sup>2-9</sup>

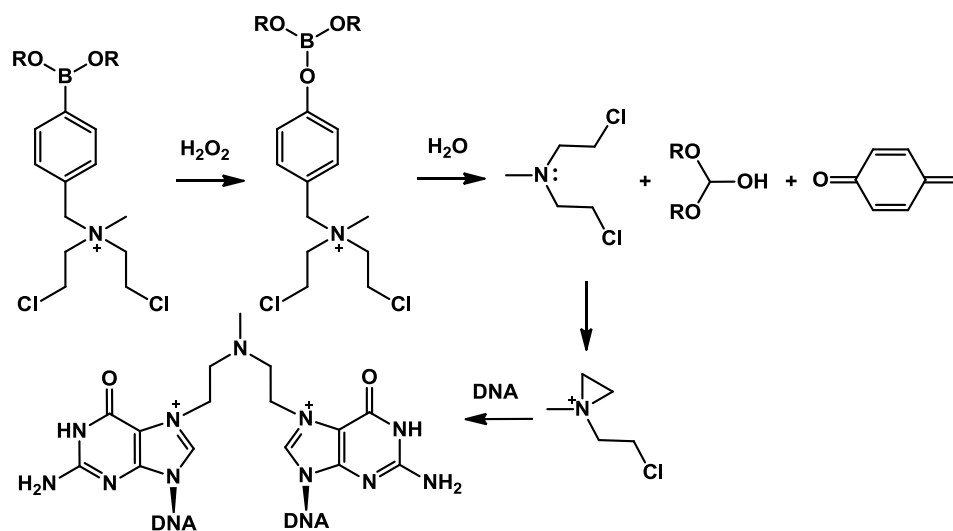
However, few of them can induce DNA cross-links selectively under tumor-specific conditions. Our group focuses on exploiting the differences between tumor and normal cells for developing inducible DNA cross-linking agents that are only toxic to tumor cells.

Comparing with normal cells, cancer cells contain higher level of reactive oxygen species (ROS), such as hydroxyl radical (OH·), superoxide radical anions (O<sub>2</sub><sup>·-</sup>), and hydrogen peroxide, which is one of the exclusive features of cancer cells caused by the increased active metabolism.<sup>10-11</sup>

Among different ROS, H<sub>2</sub>O<sub>2</sub> is relatively stable with a longer half-life and higher intracellular concentration.<sup>12</sup> It can serve as an ideal candidate for developing H<sub>2</sub>O<sub>2</sub>-inducible ICL agents. Such agents should contain a H<sub>2</sub>O<sub>2</sub>-responsive trigger that can react selectively with H<sub>2</sub>O<sub>2</sub> to release ICL agents. It is well-known that reaction of arylboronic esters with H<sub>2</sub>O<sub>2</sub> generates

phenols.<sup>13</sup> Such a reaction has been used to develop probes for H<sub>2</sub>O<sub>2</sub> detection. Thus, the arylboronic ester or acid is an ideal trigger unit for developing H<sub>2</sub>O<sub>2</sub>-inducible ICL agents.

Recently, our group has developed a series of H<sub>2</sub>O<sub>2</sub>-inducible nitrogen mustard prodrugs by using arylboronates or boronic acids as a trigger unit.<sup>14</sup> These prodrugs can be activated in the presence of H<sub>2</sub>O<sub>2</sub> to release nitrogen mustards which directly cross-link DNA at the *N7* of guanine (Scheme 2-1). DNA ICL assay indicated that these novel prodrugs showed good activity and selectivity toward H<sub>2</sub>O<sub>2</sub> (Figure 2-1 A). Furthermore, they selectively inhibit cancer cell growth but normal cells were less affected (Figure 2-1 B). These results demonstrated that the arylboronates can effectively mask the cytotoxicity of nitrogen mustards and be activated selectively by H<sub>2</sub>O<sub>2</sub>.<sup>14</sup>



**Scheme 2-1.** ICL formation induced by arylboronates upon H<sub>2</sub>O<sub>2</sub> activation.

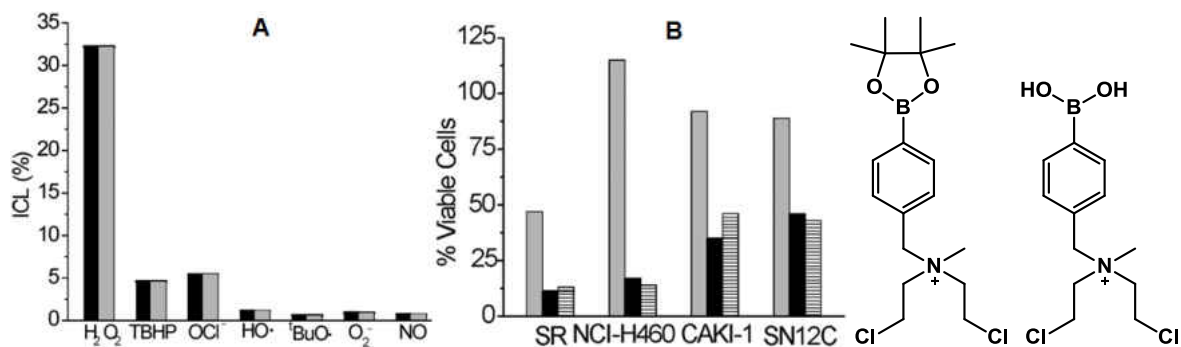


**Figure 2-1.** A. H<sub>2</sub>O<sub>2</sub> selectivity of ICL formation. B. Cytotoxicity toward different cancer cell lines (gray bar: control).

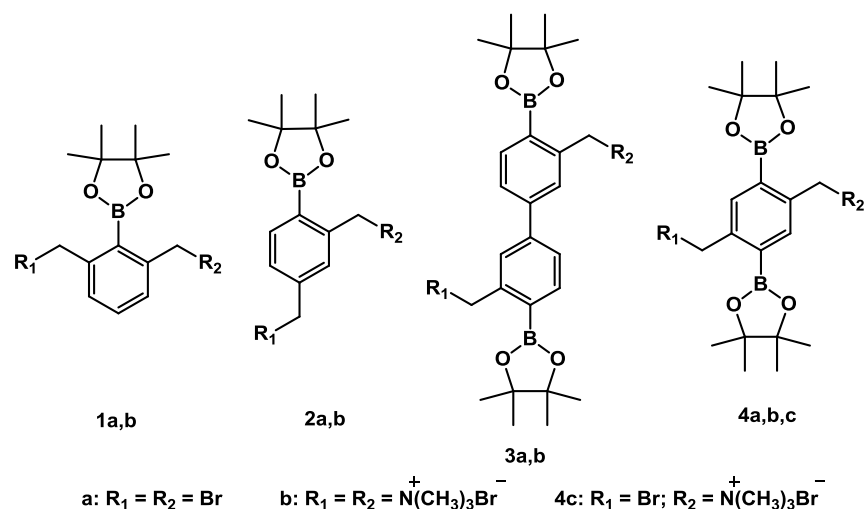
However, therapeutic utility of H<sub>2</sub>O<sub>2</sub>-activated prodrugs would require an efficient trigger that can be coupled with multiple potent effectors to maximize the ROS-inducible cytotoxicity.

Therefore, my first research topic is to design and synthesize arylboronic ester derivatives that can be activated selectively and efficiently by H<sub>2</sub>O<sub>2</sub> to release bisquinone methides directly cross-linking DNA.

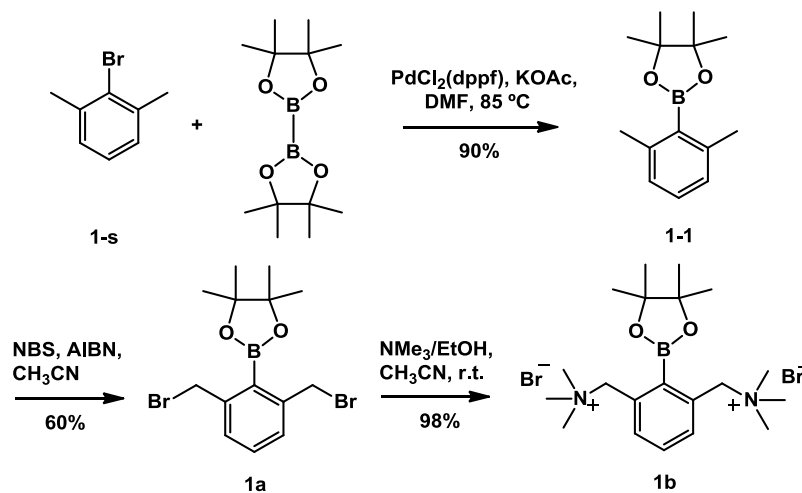
## 2.2. Arylboronic esters as H<sub>2</sub>O<sub>2</sub>-inducible ICL agents

### 2.2.1. Synthesis of **1a,b**

The arylboronic ester **2a,b** and **4a,b** and the biarylboronic ester **3a,b** were synthesized as previously described (Scheme 2-2).<sup>15</sup> Compound **1a** was synthesized starting from 2-bromo-m-xylene (**1-s**) (Scheme 2-3). Palladium-catalyzed borylation of **1-s** form the boronated intermediate **1-1**, which reacted with N-bromosuccinimide (NBS) through a radical pathway by using azobisisobutyronitrile (AIBN) as catalyst to provide the brominated analogue **1a**. **1a** was converted to quaternization product **1b** by using trimethylamine in acetonitrile (CH<sub>3</sub>CN) in nearly quantitative yield (Scheme 2-3).



**Scheme 2-2.** The structures of **1-4**.



**Scheme 2-3.** Synthesis of **1a,b**.

### 2.2.2. The reactivity of **1-4** toward DNA

Having successfully synthesized compounds **1-4**, their DNA cross-linking ability was investigated by allowing them to react with 49-mer DNA duplex **5** (Scheme 2-4) in a phosphate buffer (pH 8.0) at 37 °C. Duplex **5** is part of a p53 gene which is often mutated in more than 50% human cancers such as breast cancer. It was  $^{32}\text{P}$ -labeled at 5'-end in **5a** strand by using Gamma  $^{32}\text{P}$  ATP ( $[\gamma\text{-}^{32}\text{P}]$  ATP) and T4 Polynucleotide Kinase (T4 PNK). (Figure 2-2)

5'-dGCCTAGTTCTTTTAATTACTTGC AATGCAAGTAATTAAAGCTTGATCTG (**5a**)  
 3'-dCGGATCAAGAAAATTAATGAACGTTACGTTCAATTAATTTTCGAACTAGAC (**5b**)

**5**

**Scheme 2-4.** DNA duplex **5**.

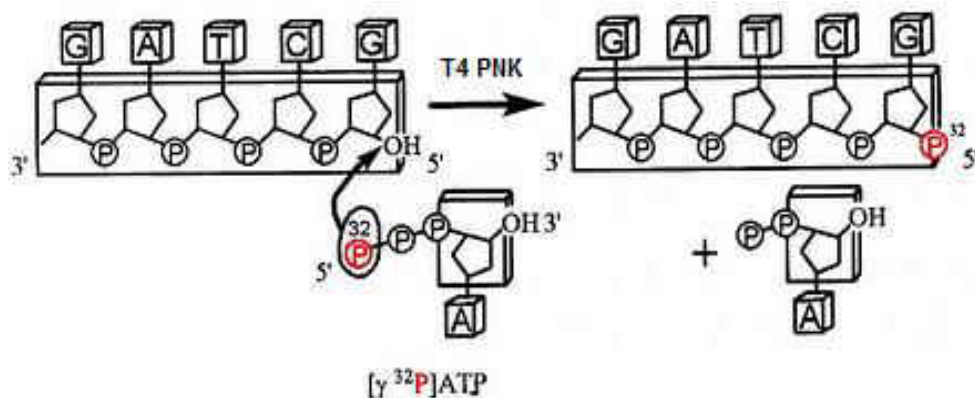


**Figure 2-2.** 5'-end oligonucleotide labeling reaction.

The ICL formation and yields were analyzed via denaturing polyacrylamide gel electrophoresis (PAGE). The cross-linking product and single strand DNA can be distinguished by the PAGE in which the cross-linked DNA migrates slower due to the higher molecular weight. Using phosphorimage analysis (Image Quant 5.2), the <sup>32</sup>P-labeled single stranded oligodeoxyribonucleotides (ODN) and the ICL product show different bands on the image plate. When compounds **1a,b** and DNA duplex **5** were incubated at 37 °C in the presence of H<sub>2</sub>O<sub>2</sub> for 24 hours, efficient ICL formation was observed with bromide **1a** (cross-linking yield 25% with 2 mM **1a**) but not with the corresponding quaternary ammonia salt **1b** (0%) (Figure 2-3).

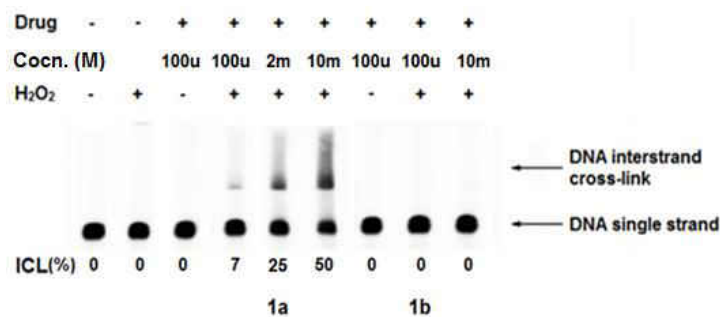


**Figure 2-3.** H<sub>2</sub>O<sub>2</sub>-induced DNA ICL formation by **1a**. Compound **1a,b** was incubated with duplex **5** at 37 °C for 24 h in the presence of H<sub>2</sub>O<sub>2</sub>.

Having confirmed H<sub>2</sub>O<sub>2</sub>-induced ICL formation by **1a**, we optimized the ICL reaction conditions for further investigation. The cross-linking efficiency of **1a** depended on its concentrations, the compound/H<sub>2</sub>O<sub>2</sub> ratios, and the pH of the buffer solution. The best compound/H<sub>2</sub>O<sub>2</sub> ratios were 1:1. The cross-linking yield increased as the concentration of **1a** increasing (Figure 2-4).

However, **1a** could not dissolve completely in the reaction mixture if the concentration is higher than 2 mM and the resulting ICL yield did not increase obviously. So 2 mM of drug was used for further study. In addition, cross-linking yields for **1a** were higher under basic conditions than acidic conditions (Figure 2-5), because the weak basic condition facilitated the reaction between arylboronic ester with hydrogen peroxide.<sup>13,14,16</sup> Thus, we chose weak basic buffer solution (pH 8) for further investigation.

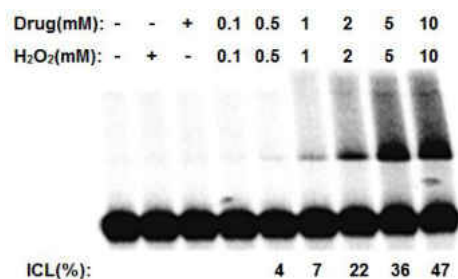


**Figure 2-4.** Concentration dependence of ICL formation by **1a**. Compound **1a** was incubated with duplex **5** at 37 °C for 24 h in the presence of H<sub>2</sub>O<sub>2</sub>.

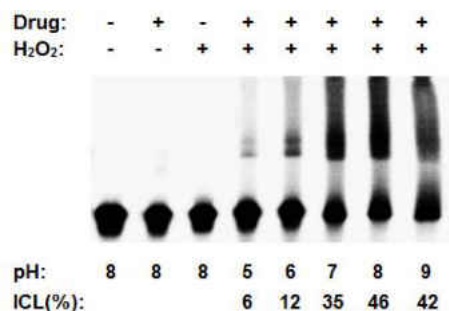


**Figure 2-5.** pH dependence of ICL formation by **1a**. Compound **1a** was incubated with duplex **5** at 24 °C for 48 h in the presence of H<sub>2</sub>O<sub>2</sub>.

Using the optimized ICL reaction conditions, the cross-linking abilities of **2a,b,3a,b**, and **4a,b** were investigated to further determine the structure and leaving group effect on the ICL formation. Similar to **1a** which generated 25% cross-linking yield at 2 mM concentration, the bromides **2a** (cross-linking yield 24%) and **3a** (9%) (Figure 2-6, lanes 4 and 5) led to efficient DNA ICL formation. However, DNA cross-linking was not observed with the quaternary ammonia salts **2b** and **3b** (Figure 2-6, lanes 8 and 9). These results demonstrated that bromine is a better leaving group for DNA cross-linking than the trimethylamine.

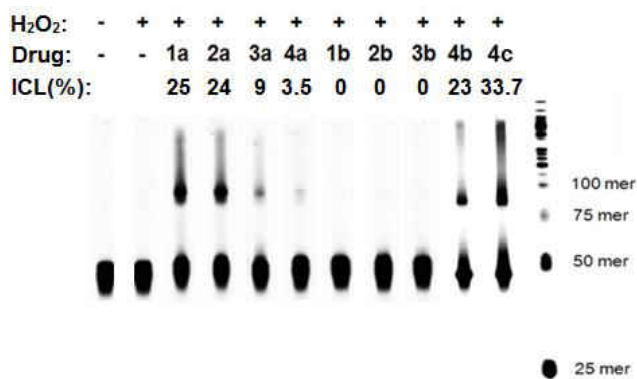
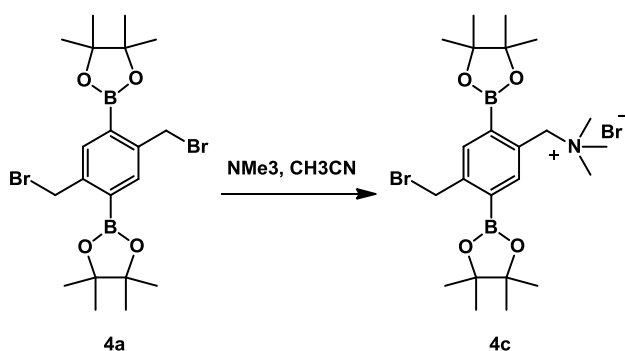


**Figure 2-6.** H<sub>2</sub>O<sub>2</sub>-induced DNA ICL formation by compounds **1-4**. Lane 1: DNA only (cross-linking yield 0%); lane 2: DNA with 100 μM H<sub>2</sub>O<sub>2</sub> (0%); lane 3: 2 mM **1a** (25%); lane 4: 2 mM **2a** (24%); lane 5: 2 mM **3a** (9%); lane 6: 2 mM **4a** (3.5%); lane 7: 2 mM **1b** (0%); lane 8: 2 mM



**2b** (0%); lane 9: 2 mM **3b** (0%); lane 10: 2 mM **4b** (23%); lane 11: 2 mM **4c** (33.7%); lane 12: DNA marker;  $[H_2O_2] = 2$  mM for **1-2** and 4 mM for **3-4**. Reaction mixture was incubated at 37 °C for 48 h.

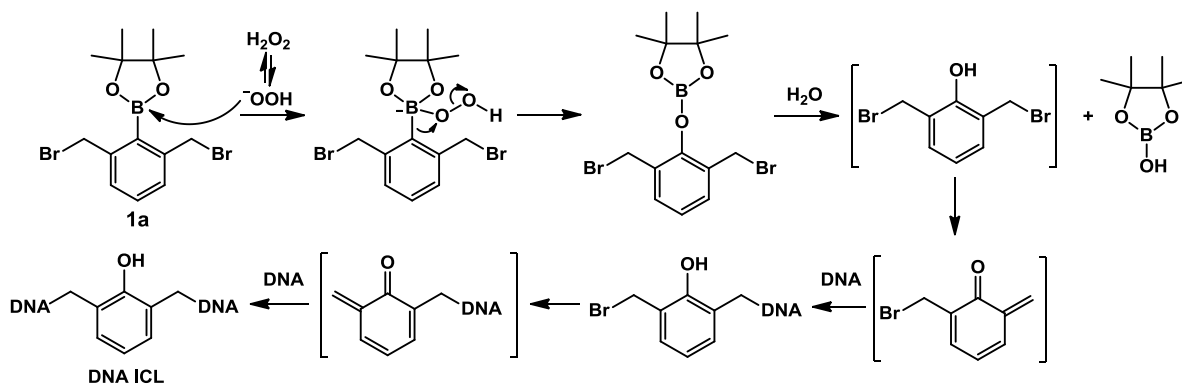
Different from **1-3**, the quaternary ammonia salt **4b** showed a higher cross-linking yield (23%) (Figure 2-6, lanes 10) than the corresponding bromide **4a** (3.5%) (Figure 2-5, lanes 6). Two factors are involved for this unusual phenomenon: the solubility issue and the presence of two boronate functional groups. First, compound **4b** is more water soluble than **4a**. We observed that **4a** precipitated out from the reaction mixture when being mixed with DNA solution. In order to solve the solubility issue, we synthesized compound **4c** containing a mixed leaving group: Br and  $NMe_3$  (Scheme 2-5) and investigated its cross-linking ability. Compound **4c** was able to dissolve in water or a mixture of  $H_2O/CH_3CN$ . Precipitation was not observed during the cross-linking reaction. As we expected, compound **4c** resulted in a much higher cross-linking yield (33.7%; Figure 2-6, lane 11) than the bromide **4a** (3.5%) and the quaternary ammonia salt **4b** (23.0%) under the same incubation conditions. These results suggested that in addition to the leaving groups, the water solubility also affected the cross-linking efficiency of **4a-c**. Second, conversion of two boronate esters to two hydroxyl groups in **4b** favors departure of trimethylamine (details are discussed in section 3.2.3).



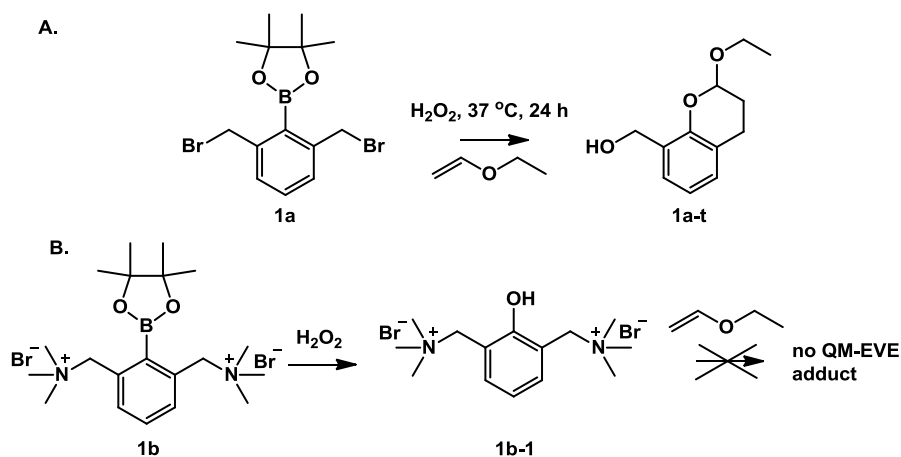
**Scheme 2-5.** Synthesis of **4c** that contains mixed leaving groups.

### 2.2.3. The mechanism of ICL formation

Having confirmed that compounds **1-4** can induce ICL formation in the presence of  $H_2O_2$ , we investigated the reaction mechanism of ICL formation. We proposed that the arylboronic esters underwent oxidative cleavage by  $H_2O_2$  to produce phenol intermediates, which spontaneously release quinone methide (QM) cross-linking DNA (Scheme 2-6).<sup>15</sup> To confirm QM formation from **1a**, we performed a QM-trapping reaction by using a large excess of ethyl vinyl ether (EVE) which is widely used as a trapping agent for QM. When **1a** and excess EVE were incubated at 37 °C for 24 h in the presence of  $H_2O_2$ , the QM trapping adduct **1a-t** was produced (Scheme 2-7 A). However, no trapping product was detected without  $H_2O_2$ . In the case of **1b**, the phenol product **1b-1** was isolated in quantitative yield (Scheme 2-7 B), which was not converted to QM due to the poor leaving group. These results supported that QM formation is critical for DNA cross-linking induced by **1a**.

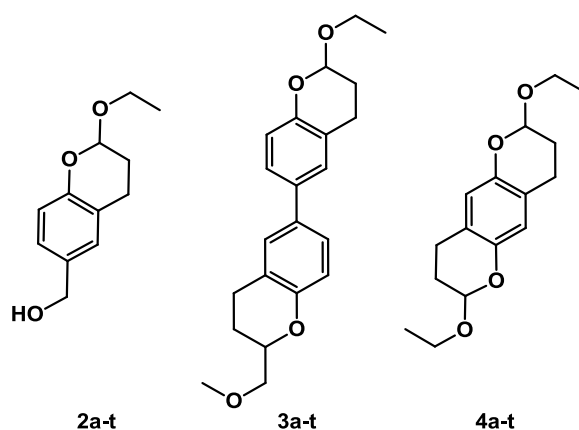


**Scheme 2-6.** Proposed mechanism of  $H_2O_2$ -induced ICL formation.

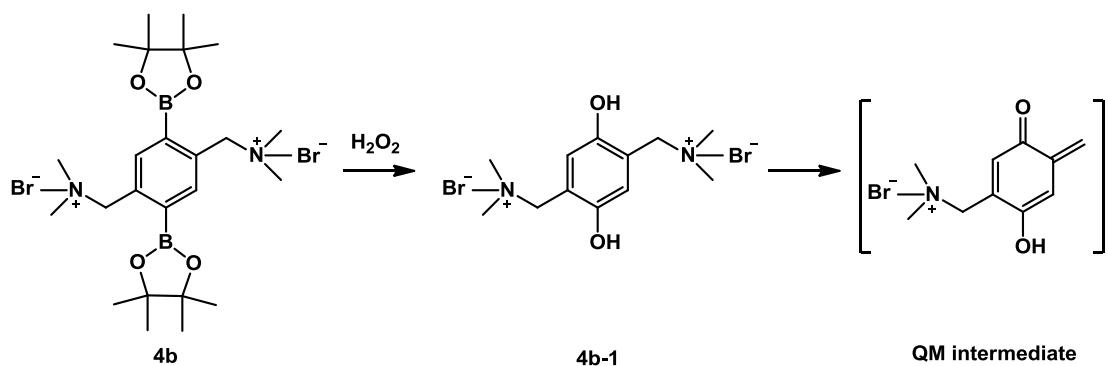


**Scheme 2-7.** QM-trapping reaction of **1a,b**. (A) QM-trapping product was generated by reaction of **1a**,  $\text{H}_2\text{O}_2$ , and EVE; (B) no QM-EVE adduct was generated from quaternary ammonia salt **1b**.

Similarly, QM trapping products were obtained from the reaction of **2a-4a**, **4b** and **4c** with EVE (Scheme 2-8). However, the reaction of **4b** and **4c** with EVE was not finished in 48 h, which is much slower than that of **4a** (3 h). This result supported that a better leaving group (e.g. bromine) facilitated QM formation. Among all quaternary ammonia salts **1b-4b**, only **4b** induced QM generation. This is due to that the oxidation product biphenol derivative **4b-1** contains two hydroxyl groups in the aromatic ring. The additional hydroxyl group is strongly donating, which favors QM formation (Scheme 2-9).



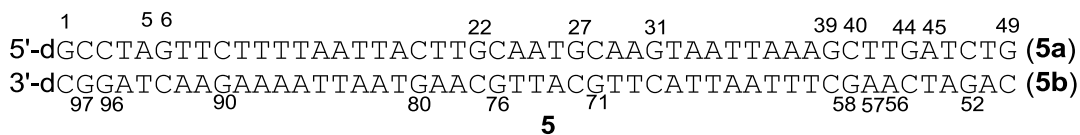
**Scheme 2-8.** QM-trapping product was generated by **2-4**.



**Scheme 2-9.** Proposed mechanism of H<sub>2</sub>O<sub>2</sub>-induced QM formation by **4b**.

#### 2.2.4. Determination of cross-linking site

In order to determine the cross-linking site, we evaluated the heating stability of purified cross-linked products and monoalkylated single-stranded DNA. There were about 55–62% of the ICLs formed from **1a-4a** that were stable to heating in phosphate buffer. When the isolated single stranded ODN and ICL products were treated with 1.0 M piperidine under heating, strong cleavage bands were observed with all dGs (Figure 2-7 lane 3 and 5). It is well-known that alkaline hydrolysis of N-7-alkylated purines occurs upon heating in piperidine (Scheme 2-10).<sup>17,18</sup> Clearly, the cross-linking reactions occurred mainly with dGs. There were around 50% of the ICL products that were stable upon the piperidine treatment. We proposed that the alkylation may also have occurred at the exocyclic amines of dG or other bases to form heat-stable ICL adducts. In addition, similar cleavage patterns were observed with single-stranded DNA as the ICL products, indicating that monoalkylation or intrastrand cross-linking occurred (Figure 2-7 lane 5).



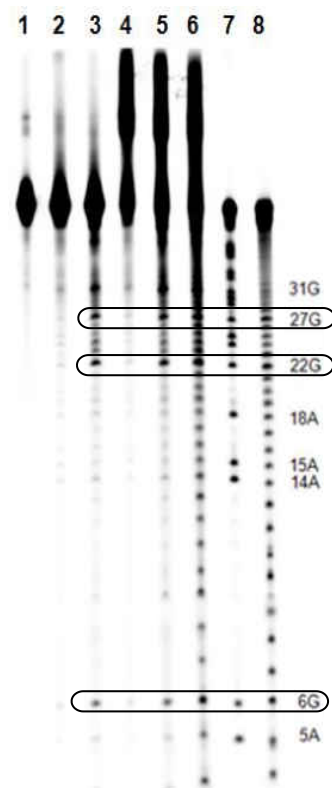
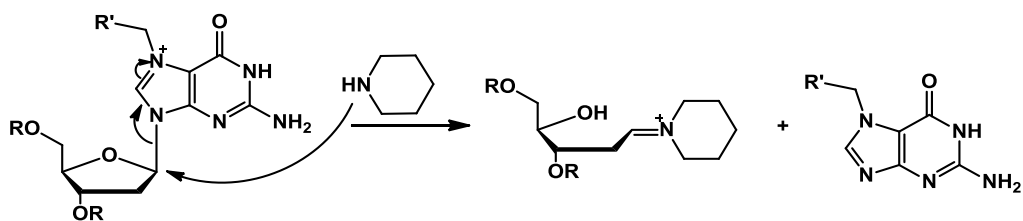
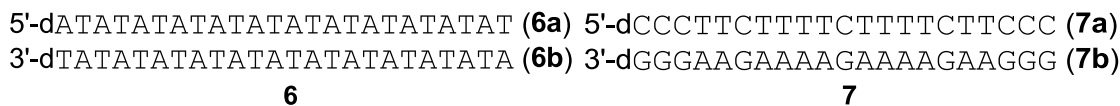


**Figure 2-7.** Determination of the reaction sites of **1a**. Phosphorimage autoradiogram of 20% denaturing PAGE analysis of the isolated ICL products and monoalkylated single stranded DNA (**5a'**) upon heating in piperidine or phosphate buffer. The ICL product and **5a'** were produced by incubation of duplex **5** with 1 mM **1a** and 1 mM H<sub>2</sub>O<sub>2</sub>. **5a** was radiolabeled at 5'-terminus. lane 1: isolated monoalkylated single stranded DNA (**5a'**); lane 2: **5a'** was heated in phosphate buffer at 90 °C for 30 min; lane 3: **5a'** was heated in 1.0 M piperidine at 90 °C for 30 min; lane 4: the ICL was heated in phosphate buffer at 90 °C for 30 min; lane 5: the ICL product was heated in 1.0 M piperidine at 90 °C for 30 min; lane 6: Fe·EDTA treatment of ICL; lane 7: G+A sequencing; lane 8: Fe·EDTA treatment of **5**.



**Scheme 2-10.** Cleavage of N-7-alkylated purines upon heating in piperidine.

To further confirm the cross-linking reaction sites, we designed and synthesized two DNA duplexes **6** and **7** with different sequences (Scheme 2-11). Duplex **6** is a self-complementary dAT strands, whereas duplex **7** contains only dCs/dTs in one strand and only dGs/dAs in the other. When **1a** was incubated with duplexes **6** and **7** in the presence of H<sub>2</sub>O<sub>2</sub>, no DNA cross-links were observed with duplex **6** (Figure 2-8 A), which suggests that cross-linking reactions did not take place with dT and dA. However, **1a** could induce ICL formation when treated with duplex **7** (Figure 2-7 B), which means the ICL can only occur between dG and dC in duplex **7**.



**Scheme 2-11.** DNA duplex **6** and **7**.

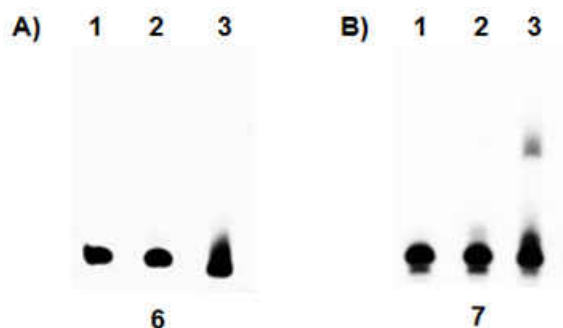


**Figure 2-8.** ICL formation from duplex **7** induced by **1a** upon H<sub>2</sub>O<sub>2</sub> activation. A) **1a** with duplex **6**; B) **1a** with duplex **7**. Lane 1: DNA with **1a** (2 mM) only; lane 2: DNA with H<sub>2</sub>O<sub>2</sub> (100 μM) only; lane 3: DNA with 2 mM and H<sub>2</sub>O<sub>2</sub>. Condition: incubation at 37 °C for 24 h.

In order to acquire more detailed information about the cross-linking sites, enzymatic digestion assay of both isolated ICL product and monoalkylated single stranded DNA has been performed with snake-venom phosphodiesterase and alkaline phosphatase. The enzyme-digested nucleotide mixtures were purified by HPLC (Figure 2-9). A new peak with a retention time of ~7.9 min was observed in both single stranded DNA and ICL product. The new peak was characterized by liquid chromatography-mass spectrometry (LC-MS), which showed an exact mass of guanine-dC adduct **8**. ( $[8+H]^+$  Calcd: 497.2, Measured:497.3) (Figure 2-10).

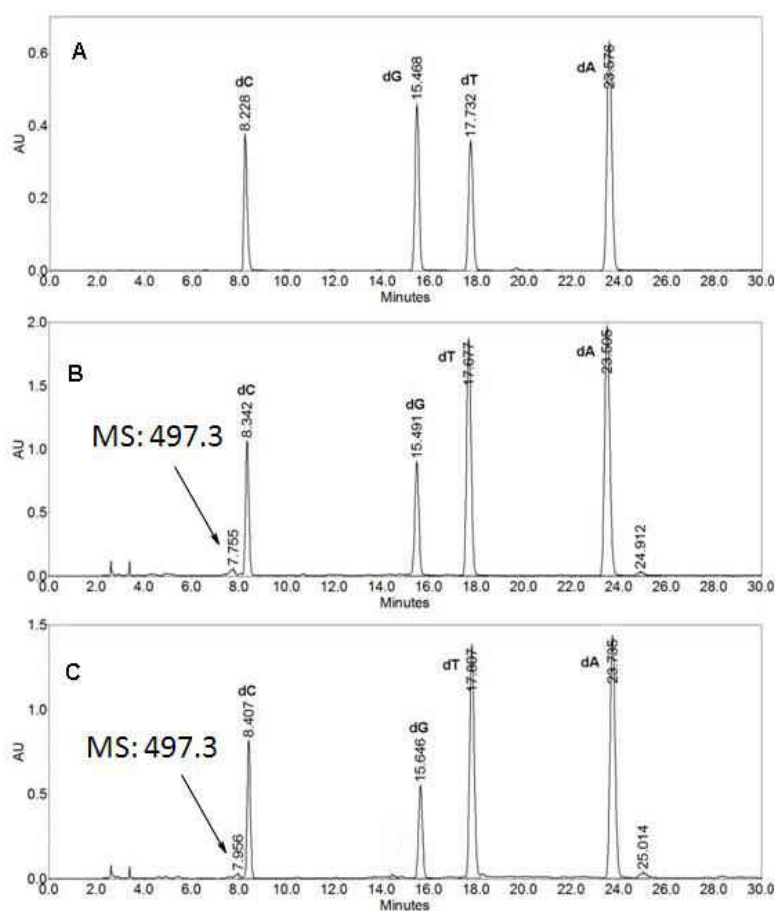


**Figure 2-9.** HPLC profiles of the enzymatic analysis. (A) DNA duplex **5** only as control; (B) **1a** treated single stranded **5a** and **5b**; (C) ICL products induced by **1a**, obtained by digestion with snake venom phosphodiesterase followed by alkaline phosphatase (analyzed by reverse-phase

HPLC (RP-18, at 260 nm) using gradient: 0-30 min 2-20% MeOH in water, 30-35 min 20-50% MeOH in water, 35-42 min 50-100% MeOH in water, 42-50 min 100% MeOH in water, at a flow rate 1.0 mL/min).

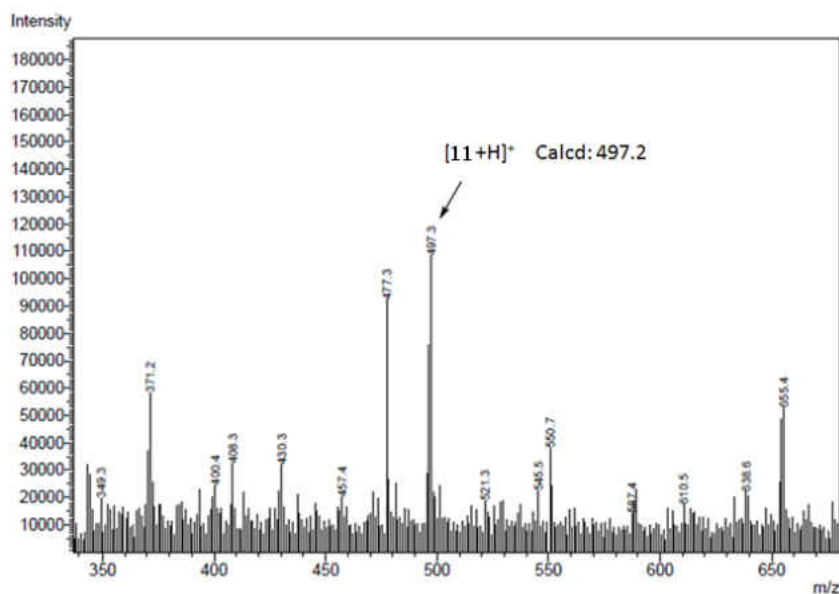
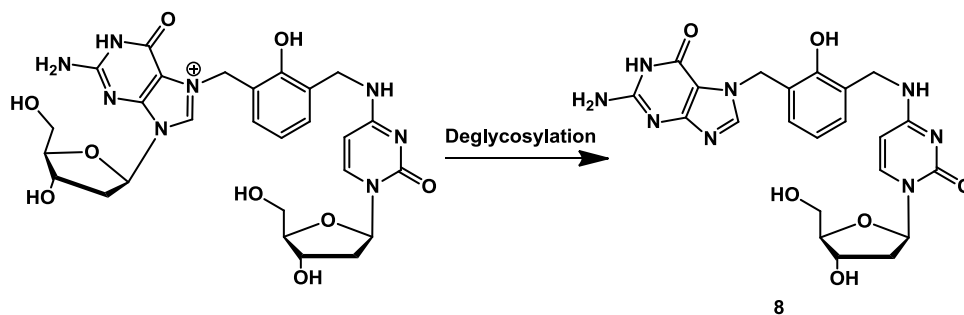


**Figure 2-10.** Mass spectrum of enzymatic digestion product corresponded to retention time about 7.9 min on HPLC chromatography.

Compound **8** was most likely resulted from deglycosylation of the corresponding N7 adduct of dG (Scheme 2-12), as glycosylic bond of positively charged N7-alkylated dG is labile to alkaline conditions. Several groups reported that deglycosylation occurred with the alkylated dGs formed by nitrogen mustards<sup>19,20</sup> or quinone methides,<sup>21</sup> which was confirmed by mass spectral analysis. Therefore, the cross-linking reactions induced by **1a** are likely to occur at dGs and dCs. Moreover, compound **8** was obtained from isolated **1a**-treated single stranded DNA, which indicated that there was also intrastrand cross-links formed between dGs and dCs.

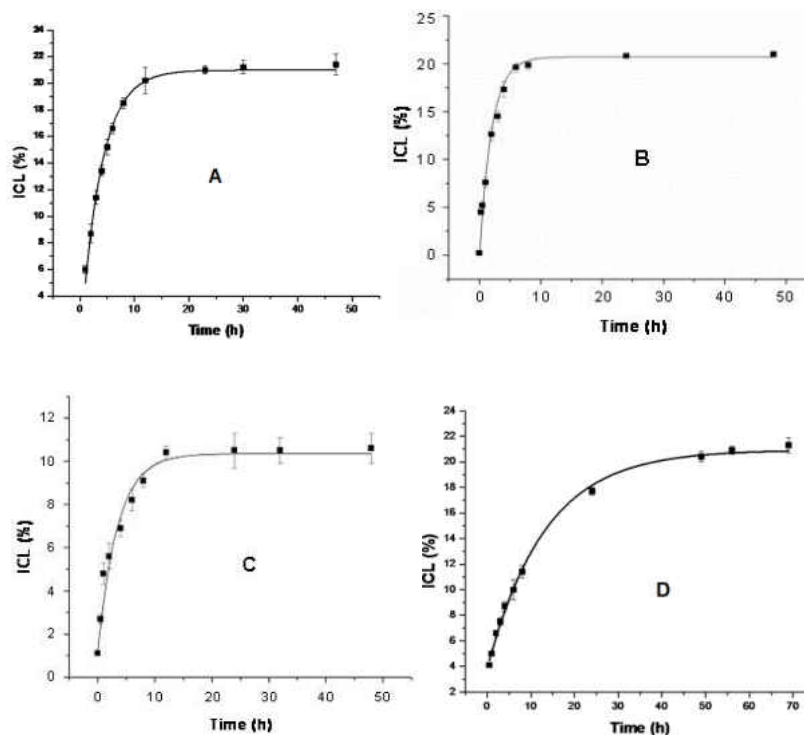




**Scheme 2-12.** Deglycosylation of N7 adduct of dG.

### 2.2.5. The kinetics of ICL formation

Having studied the reactivity of **1-4** with DNA, we further investigated the reaction kinetics. At first, we determined the rate constants for ICL formation induced by **1a-3a**, **4b**, and **4c** (Table 2-1) by time course study. ICL growth followed first-order kinetics (Figure 2-11). The rate constants for bromides **1a-3a** ( $k_{\text{obs}} = 8.8\text{-}14.1 \times 10^{-5} \text{ s}^{-1}$ ) were 2-3 times the rate constant for quaternary ammonium salt **4b** ( $k_{\text{obs}} = 4.9 \times 10^{-5} \text{ s}^{-1}$ ) (Table 2-1), which demonstrated that a better leaving group (e.g. Br) facilitate ICL formation.



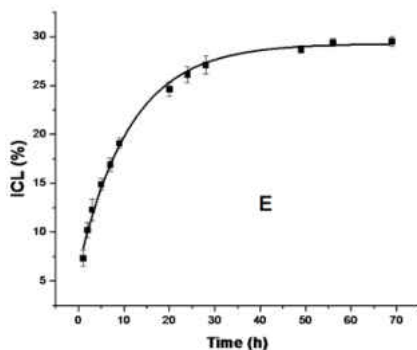
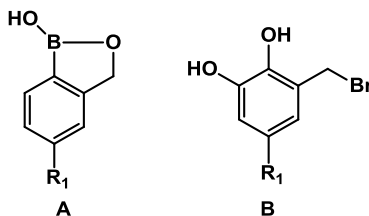


**Figure 2-11.** Kinetic rate of ICL formation from **5** upon treatment with bromides/ $\text{H}_2\text{O}_2$ . A. **1a** at time points 0, 1h, 2h, 3h, 4h, 5h, 6h, 8h, 12h, 23h, 30h, 47h. [**1a**] = 2 mM, and [ $\text{H}_2\text{O}_2$ ] = 1 mM. B. **2a** at time points 0, 15', 30', 1h, 2h, 4h, 6h, 8h, 24h, 48h. [**2a**] = 2 mM, and [ $\text{H}_2\text{O}_2$ ] = 1 mM. C. **3a** at time points 0, 30', 1h, 2h, 4h, 6h, 8h, 24h, 32h, 48h. [**3a**] = 1 mM, and [ $\text{H}_2\text{O}_2$ ] = 1 mM. D. **4b** at time points 0, 15', 30', 1h, 2h, 3h, 4h, 6h, 8h, 24h, 49h, 56h, 69h. [**4b**] = 2 mM, and [ $\text{H}_2\text{O}_2$ ] = 1 mM. E. **4c** at time points 0, 1h, 2h, 3h, 5h, 7h, 9h, 20h, 24h, 28h, 49h, 56h, 69h, 79h. [**4c**] = 2 mM, and [ $\text{H}_2\text{O}_2$ ] = 1 mM. Reaction mixtures were incubated in 37 °C.

**Table 2-1.** Rate of ICL formation from **5** upon treatment with bromide and salts.

compound	$k_{\text{obs}}, 10^{-5} \text{ s}^{-1}$	$t_{1/2}, \text{min}$	ICL yield %
<b>1a</b>	$8.8 \pm 1.3$	$130 \pm 13$	$21 \pm 1.4$
<b>2a</b>	$14.1 \pm 1.5$	$82 \pm 8$	$20 \pm 0.3$
<b>3a</b>	$13.8 \pm 1.2$	$84 \pm 9$	$10 \pm 0.9$
<b>4b</b>	$4.9 \pm 0.5$	$234 \pm 9$	$20 \pm 1.1$
<b>4c</b>	$3.7 \pm 0.3$	$312 \pm 10$	$28 \pm 0.5$

However, the cross-link yields do not correlate well with the kinetics. For example, the bromides **1a-3a** showed a larger  $k$  but a lower ICL yield than the salt **4b** or **4c**. One possible reason is that the better leaving property of  $-Br$  leads to nucleophilic substitution of bromides by water. In order to get more detailed information about the reaction, we used NMR spectroscopy to monitor the reaction. Because **1a-3a** can not dissolve in water, we chose a mixture of DMSO and deuterated phosphate buffer as solvent to better simulate cross-linking reaction condition. Different ratio of DMSO and buffer solution were tested without addition of  $H_2O_2$ . We observed that both boronate ester and benzylic bromo group were easily hydrolyzed (Figure 2-12 B). Bromide hydrolysis increased as the percentage of water increasing. To ensure all compounds soluble in a mixture of DMSO and phosphate buffer and minimize usage of water, a mixture of 10:1 DMSO/buffer was utilized for NMR measurement. Hydrolysis of compounds **1a-3a** can be seen from appearance of a variety of new peaks in the region between 4.0 and 6.0 ppm. However, this was not observed with **4b** (Figure 2-13). Meanwhile, recent studies performed by other group members showed that the boronate esters were easily hydrolyzed to generate (2-(hydroxymethyl)phenyl)boronic acid derivatives, which undergo intramolecular esterification to form benzo[*c*][1,2]oxaborol-1(3H)-ol derivatives (Scheme 2-12 A) without addition of  $H_2O_2$ .<sup>22</sup> In addition, bromides could also be oxidized by excess  $H_2O_2$  to form 1,2-dihydroxybenzene derivatives (Scheme 2-12 B). Both hydrolysis and oxidization reaction of bromide analogues might lead to a lower yield of ICL formation.



**Scheme 2-13.** Hydrolysis and oxidization product of bromide analogues.

In section 2.2.3, we proposed that mechanism of DNA cross-linking involved formation of the phenol intermediates followed by spontaneous release of QM, which directly cross-link DNA (Scheme 2-4). However, the phenol intermediates obtained from **1a-4a** were too reactive to be isolated from the reaction mixtures, while formation of QM trapping products provided evidence for generation of QMs from the phenol intermediates under physiological conditions. In order to determine whether formation of the phenol intermediates or QM generation is the rate-determining step for DNA cross-linking, we used NMR spectroscopy to monitor the reaction of these compounds with H<sub>2</sub>O<sub>2</sub> in a mixture of DMSO and D<sub>2</sub>O (Figure 2-12 to 2-17). Considering that the boronate esters are easily hydrolyzed to the corresponding boronic acids, which make the reaction more complicated for analysis, we allowed complete hydrolysis of **1a-4a** to the corresponding boronic acids in a DMSO/phosphate buffer (10:1) prior to the addition of H<sub>2</sub>O<sub>2</sub>. After that, more D<sub>2</sub>O was added to mimic the DNA cross-linking conditions. However, if the ratio of phosphate buffer to DMSO was more than 2:3, the boronic acids precipitated out. Finally, we used a mixture of phosphate buffer/DMSO (2:3) for NMR analysis.

From disappearance of the peaks at about 5.0 ppm (peak **d**), we were able to figure out the relative rate for the phenol intermediate formation. The relative reaction rates of these compounds with H<sub>2</sub>O<sub>2</sub> are in the order of **4a**  $\approx$  **4b**  $\approx$  **4c**  $\geq$  **3a**  $>$  **1a**  $>$  **2a** (Table 2-2). The reactions of diboronates **4a-4c** were too fast to determine the rate constant by NMR under these conditions (Figure 2-15 C-D, 2-16 D-E, and 2-17 D-E). The relative rates of QM formation were estimated by formation of the final products (peak **f**, its hydrolyzed compounds or peak **f'**, the formed free NMe<sub>3</sub>), which showed the following trend: **4a**  $>$  **3a**  $>$  **1a**  $>$  **2a**  $\geq$  **4b**  $\approx$  **4c** (Table 2-2, Figure 2-15). The kinetic data for DNA ICL formation (**2a**  $\approx$  **3a**  $>$  **1a**  $>$  **4b**  $\approx$  **4c**) (Table 2-1) showed a similar trend to those for QM formation but different from those for the phenol intermediates

formation, which suggested that QM formation is the rate-limiting step for DNA cross-linking. For **4c** with a mixed leaving group Br and NMe<sub>3</sub>, departure of NMe<sub>3</sub> was the rate-determining step which took about 40 hrs while departure of Br occurred within 3 min (Figure 2-17).

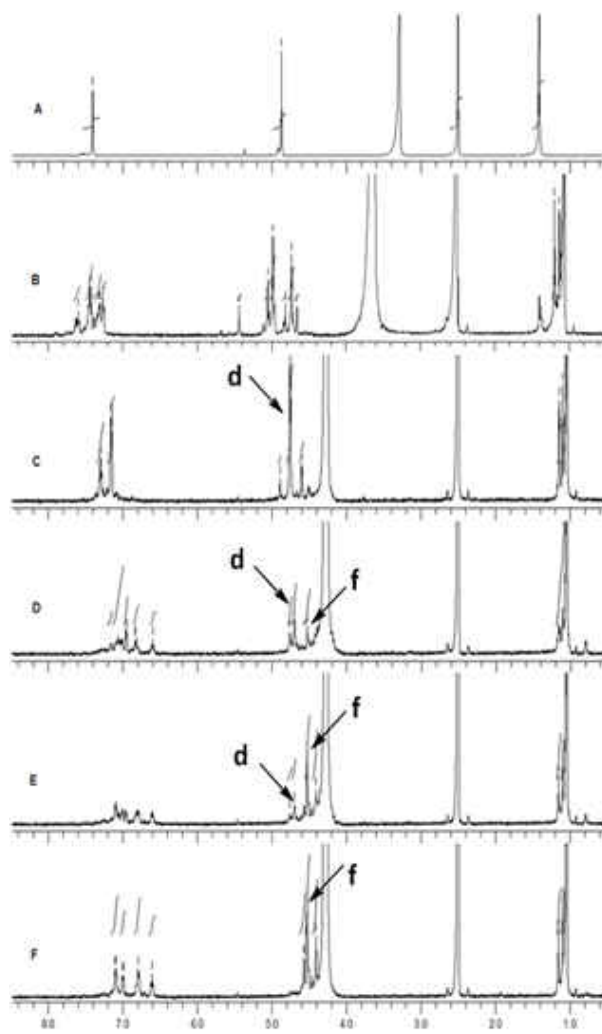


**Figure 2-12.** <sup>1</sup>H NMR analysis of **1a** in deuterated DMSO, D<sub>2</sub>O, and H<sub>2</sub>O<sub>2</sub>: (A) <sup>1</sup>H NMR of **1a** (0.003 mmol) in DMSO without addition of D<sub>2</sub>O and H<sub>2</sub>O<sub>2</sub>. (B) 41 h in mixture of DMSO (300 μL), D<sub>2</sub>O (20 μL), and pH8 buffer (10 μL); (C) additional 6 h after added additional DMSO (60 μL) and D<sub>2</sub>O (210 μL) in B; (D) 3 min after addition of H<sub>2</sub>O<sub>2</sub> (1.5 equiv.) in C; (E) 15 min after addition of H<sub>2</sub>O<sub>2</sub>; (F) 1.5 h after addition of H<sub>2</sub>O<sub>2</sub>.

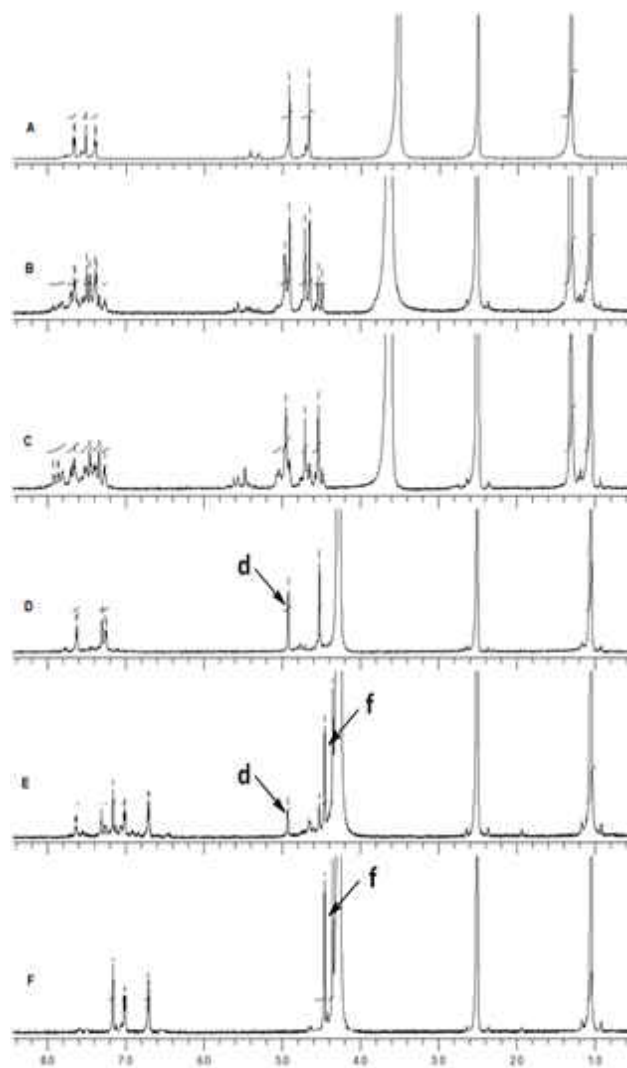


**Figure 2-13.**  $^1\text{H}$  NMR analysis of **2a** in deuterated DMSO,  $\text{D}_2\text{O}$ , and  $\text{H}_2\text{O}_2$ : **(A)**  $^1\text{H}$  NMR of **2a** (0.003 mmol) in DMSO without addition of  $\text{D}_2\text{O}$  and  $\text{H}_2\text{O}_2$ . **(B)** 3 h in mixture of DMSO (300  $\mu\text{L}$ ),  $\text{D}_2\text{O}$  (20  $\mu\text{L}$ ), and pH8 buffer (10  $\mu\text{L}$ ); **(C)** 17 h in mixture of DMSO (300  $\mu\text{L}$ ),  $\text{D}_2\text{O}$  (20  $\mu\text{L}$ ), and pH8 buffer (10  $\mu\text{L}$ ); **(D)** additional 1 h after added additional DMSO (60  $\mu\text{L}$ ) and  $\text{D}_2\text{O}$  (210  $\mu\text{L}$ ) in **C**; **(E)** 30 min after addition of  $\text{H}_2\text{O}_2$  (1.5 equiv.) in **D**; **(F)** 2.5 h after addition of  $\text{H}_2\text{O}_2$ .

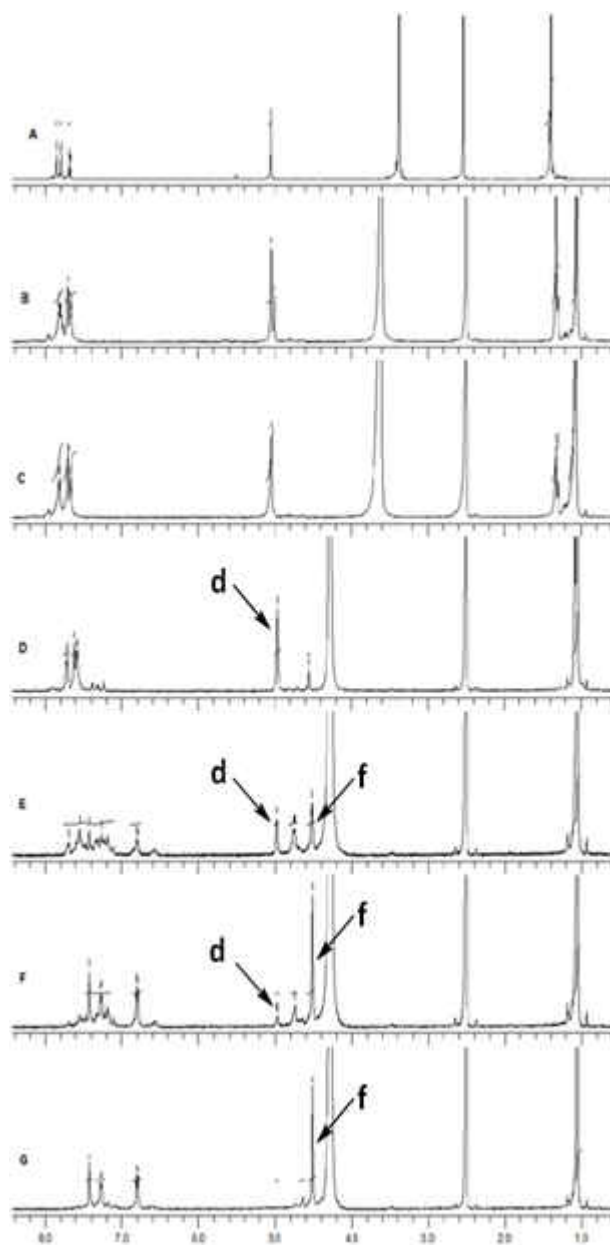


**Figure 2-14.**  $^1\text{H}$  NMR analysis of **3a** in deuterated DMSO,  $\text{D}_2\text{O}$ , and  $\text{H}_2\text{O}_2$ : (A)  $^1\text{H}$  NMR of **3a** (0.003 mmol) in DMSO only; (B) 3 h in mixture of DMSO (300  $\mu\text{L}$ ),  $\text{D}_2\text{O}$  (20  $\mu\text{L}$ ), and pH8 buffer (10  $\mu\text{L}$ ); (C) 16 h in mixture of DMSO (300  $\mu\text{L}$ ),  $\text{D}_2\text{O}$  (20  $\mu\text{L}$ ), and pH8 buffer (10  $\mu\text{L}$ ); (D) additional 30 min after added additional DMSO (60  $\mu\text{L}$ ) and  $\text{D}_2\text{O}$  (210  $\mu\text{L}$ ) in C; (E) 3 min after addition of  $\text{H}_2\text{O}_2$  (3 equiv.) in D; (F) 10 min after addition of  $\text{H}_2\text{O}_2$ ; (G) 30 min after addition of  $\text{H}_2\text{O}_2$ .

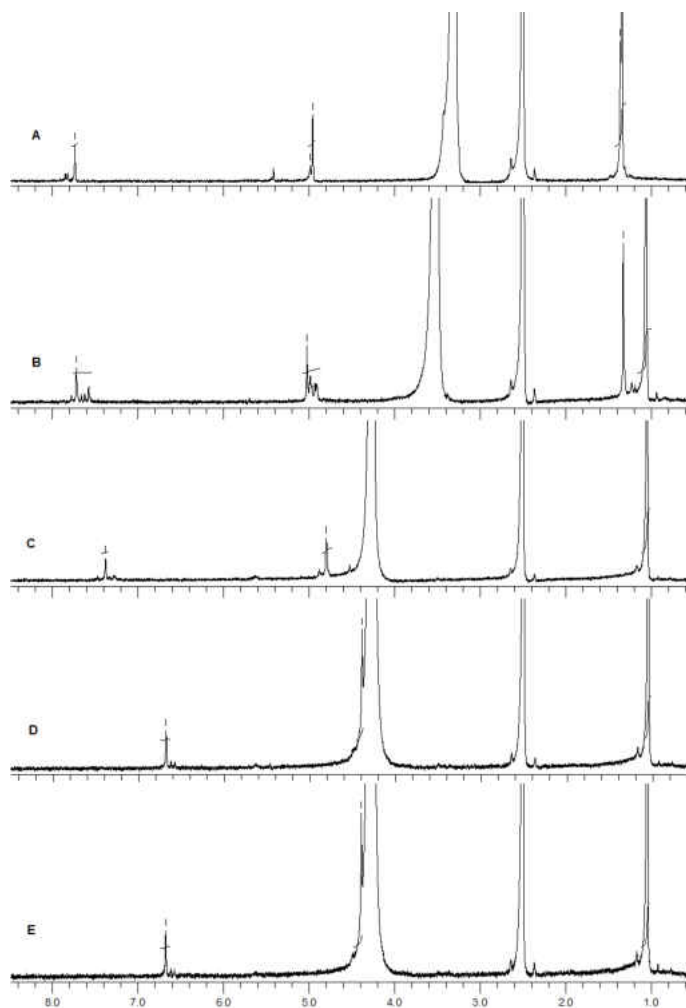


**Figure 2-15.**  $^1\text{H}$  NMR analysis of **4a** in deuterated DMSO,  $\text{D}_2\text{O}$ , and  $\text{H}_2\text{O}_2$ : **(A)**  $^1\text{H}$  NMR of **4a** (0.003 mmol) in DMSO only; **(B)** 3 h in mixture of DMSO (300  $\mu\text{L}$ ),  $\text{D}_2\text{O}$  (20  $\mu\text{L}$ ), and pH8 buffer (10  $\mu\text{L}$ ); **(C)** additional 3 h after added additional DMSO (60  $\mu\text{L}$ ) and  $\text{D}_2\text{O}$  (210  $\mu\text{L}$ ) in **B**; **(D)** 3 min after addition of  $\text{H}_2\text{O}_2$  (3 equiv.) in **C**; **(E)** 5 min after addition of  $\text{H}_2\text{O}_2$ .



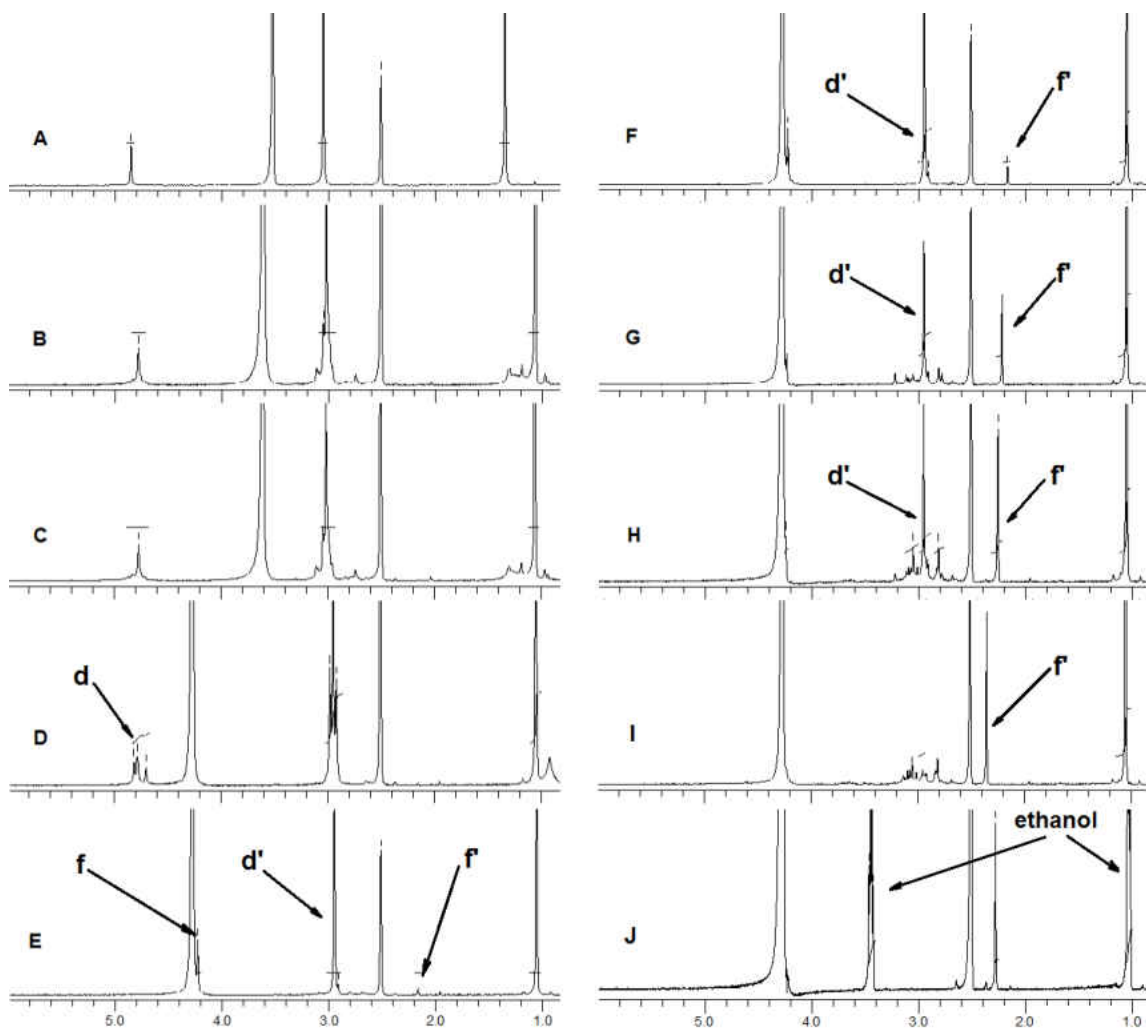


**Figure 2-16.**  $^1\text{H}$  NMR analysis of **4b** in deuterated DMSO,  $\text{D}_2\text{O}$ , and  $\text{H}_2\text{O}_2$ : (A)  $^1\text{H}$  NMR of **4b** (0.003 mmol) in DMSO only; (B) 10 min in mixture of DMSO (300  $\mu\text{L}$ ),  $\text{D}_2\text{O}$  (20  $\mu\text{L}$ ), and pH8 buffer (10  $\mu\text{L}$ ); (C) 2.5 h in mixture of DMSO (300  $\mu\text{L}$ ),  $\text{D}_2\text{O}$  (20  $\mu\text{L}$ ), and pH8 buffer (10  $\mu\text{L}$ ); (D) additional 12 h after added additional DMSO (60  $\mu\text{L}$ ) and  $\text{D}_2\text{O}$  (210  $\mu\text{L}$ ) in C; (E) 3 min after addition of  $\text{H}_2\text{O}_2$  (3 equiv.) in D; (F) 30 m after addition of  $\text{H}_2\text{O}_2$ ; (G) 4 h after addition of  $\text{H}_2\text{O}_2$ ; (H) 16 h after addition of  $\text{H}_2\text{O}_2$ ; (I) 40 h after addition of  $\text{H}_2\text{O}_2$ ; (J) Trimethyl amine ( $\text{NMe}_3$ ) in ethanol with addition of 1 M HCl (10  $\mu\text{L}$ ).



**Figure 2-17.**  $^1\text{H}$  NMR analysis of **4c** in deuterated DMSO,  $\text{D}_2\text{O}$ , and  $\text{H}_2\text{O}_2$ : (A)  $^1\text{H}$  NMR of **4c** (0.003 mmol) in DMSO only; (B) 30 min in mixture of DMSO (300  $\mu\text{L}$ ),  $\text{D}_2\text{O}$  (20  $\mu\text{L}$ ), and pH8 buffer (10  $\mu\text{L}$ ); (C) additional 30 min after added additional DMSO (60  $\mu\text{L}$ ) and  $\text{D}_2\text{O}$  (210  $\mu\text{L}$ ) in B; (D) additional 3 h after added additional DMSO (60  $\mu\text{L}$ ) and  $\text{D}_2\text{O}$  (210  $\mu\text{L}$ ) in C; (E) 3 min after addition of  $\text{H}_2\text{O}_2$  (3 equiv.) in D; (F) 30 min after addition of  $\text{H}_2\text{O}_2$ ; (G) 3 h after addition of  $\text{H}_2\text{O}_2$ ; (H) 18 h after addition of  $\text{H}_2\text{O}_2$ ; (I) 50 h after addition of  $\text{H}_2\text{O}_2$ ; (J) Trimethyl amine ( $\text{NMe}_3$ ) in ethanol with addition of 1 M HCl (10  $\mu\text{L}$ ).

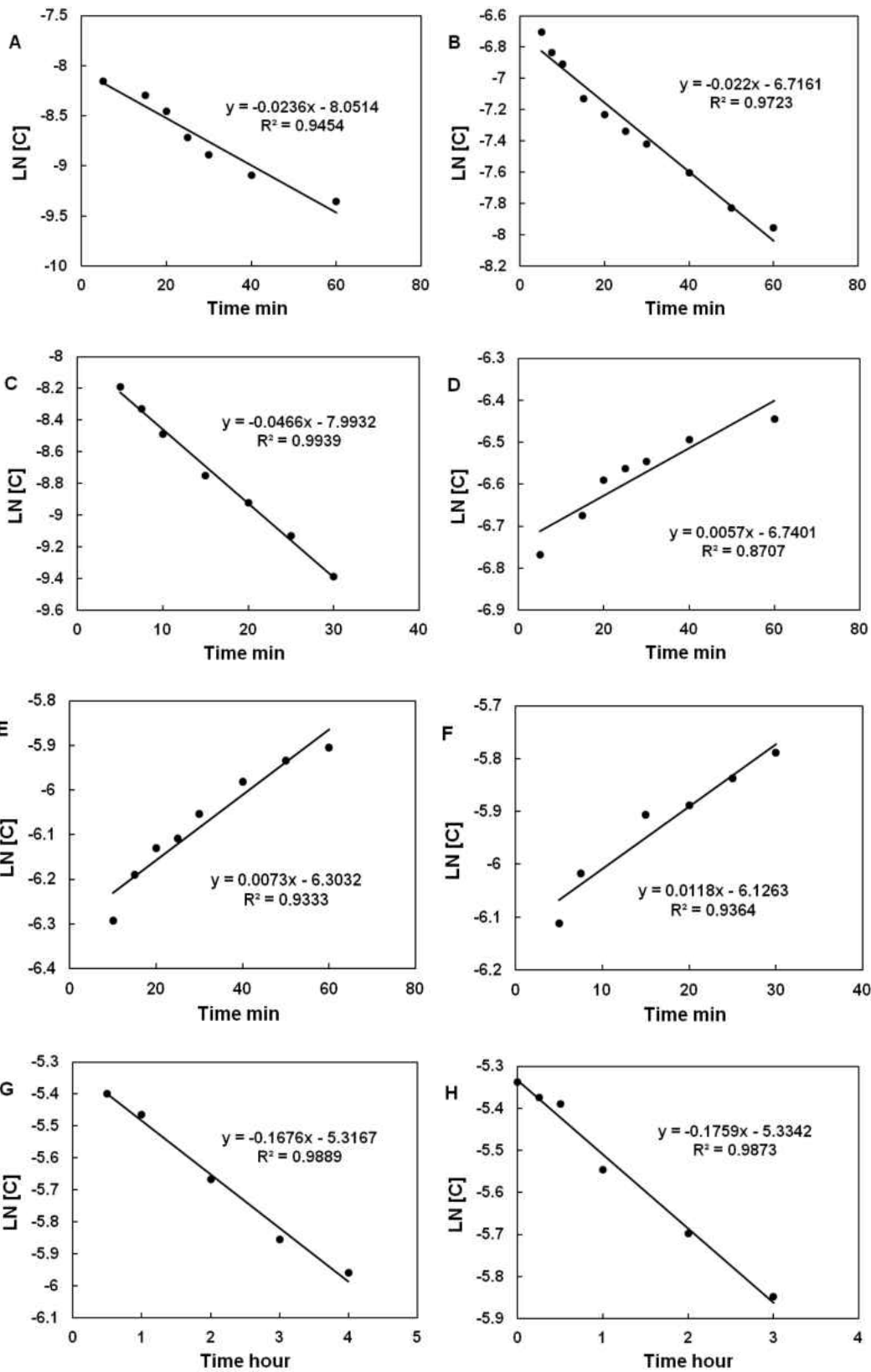


**Figure 2-18.** Rate constant for the disappearance of starting material (**A-C, G** and **H**) and the formation of hydrolyzed product (**D-F**) in NMR analysis with 360  $\mu\text{L}$  DMSO and 240  $\mu\text{L}$  pH 8 buffer: **A. 1a** (0.003 mmol) with  $\text{H}_2\text{O}_2$  (1.5 equiv) at time points 5', 15', 20', 25', 30', 40', 60'. **B. 2a** (0.003 mmol) with  $\text{H}_2\text{O}_2$  (1.5 equiv) at time points 5', 7.5', 10', 15', 20', 25', 30', 40', 50', 60'. **C. 3a** (0.003 mmol) with  $\text{H}_2\text{O}_2$  (3 equiv) at time points 5', 7.5', 10', 15', 20', 25', 30'. **D. 1a** (0.003 mmol) with  $\text{H}_2\text{O}_2$  (1.5 equiv) at time points 5', 15', 20', 25', 30', 40', 60'. **E. 2a** (0.003 mmol) with  $\text{H}_2\text{O}_2$  (1.5 equiv) at time points 10', 15', 20', 25', 30', 40', 50', 60'. **F. 3a** (0.003 mmol) with  $\text{H}_2\text{O}_2$  (3 equiv) at time points 5', 7.5', 15', 20', 25', 30'. **G. 4b** (0.003 mmol) with  $\text{H}_2\text{O}_2$  (1.5 equiv) at time points 0.5h, 1h, 2h, 3h, 4h. **H. 4c** (0.003 mmol) with  $\text{H}_2\text{O}_2$  (3 equiv) at time points 0 h, 0.25 h, 0.5 h, 1 h, 2 h, 3 h.

**Table 2-2.** Rate of starting material disappearance and QM formation.

Compounds	Disappearance of starting materials		QM formation	
	Time of completion (min)	$k_{\text{obs}}$ ( $10^{-5} \text{ s}^{-1}$ )	Time of completion (min)	$k_{\text{obs}}$ ( $10^{-5} \text{ s}^{-1}$ )
<b>1a</b>	60	$39.0 \pm 1.5$	60	$9.5 \pm 0.2$
<b>2a</b>	90	$36.7 \pm 3.8$	90	$12.2 \pm 1.1$
<b>3a</b>	30	$77.0 \pm 2.1$	30	$20.0 \pm 4.0$
<b>4a</b>	< 3	n.d.	< 3 min	n.d.
<b>4b</b>	< 3	n.d.	~3000	$4.6 \pm 0.3$
<b>4c</b>	< 3	n.d.	~2400	$4.8 \pm 0.5$
<sup>a</sup> n.d.: not determined				

Among four bromide analogues, **1a** and **2a** showed ICL yields that were 3 times the ICL yield from **3a** and 9 times that from **4a**. Compound **4c** with a mixed leaving group -Br and NMe<sub>3</sub> proved to be the most efficient for inducing ICL formation. We propose another two possible explanations for the greater cross-linking efficiency of **1a**, **2a**, and **4c**: (1) the better water solubility and (2) stepwise generation of bisQMs from the corresponding phenol derivatives. Compounds **1a**, **2a**, and **4c** were much more soluble than **3a** and **4a** under the reaction conditions. Furthermore, the two quinone methides were generated from **1a** or **2a** stepwise. Once the first QM reacted with one DNA strand, the stepwise formed second QM would have better interaction with the nucleophilic centers in the complementary DNA strand, which resulted in more efficient DNA ICL formation. For **4c**, fast formation of the first QM plays an important role for its higher ICL yield than compound **4b**. In contrast, the reaction of **3a** likely generated two methide groups simultaneously, in which case only molecules that were already well-positioned between two nucleophilic centers of two DNA strands would generate DNA ICLs, and the ICL yield would drop if either of the two methide groups reacted with H<sub>2</sub>O prior to addition of a nucleophile from the DNA duplex.<sup>23</sup> However, we cannot exclude other explanations for the greater cross-linking efficiency of **1a**, **2a**, and **4c**, such as DNA sequence, molecular structure, or distance between cross-linking sites.

### **2.3. Cytotoxicity towards cancer cells and future work**

Having established that **1a** could be activated by H<sub>2</sub>O<sub>2</sub> to release QM cross-linking DNA, the ability of these compounds to inhibit cancer cell growth was evaluated against 60 human cancer cells lines by National Cancer Institute DTP program. Single dose screening with 10 μM drugs showed that **1a** induced significant growth inhibition of specific cancer cell lines. For example, **1a** showed about 90% inhibition toward HL-60(TB) cells (Leukemia cells) and 67% inhibition

toward COLO 205 (Colon Cancer cells). However, the cytotoxicity of **1a** toward other cell lines **1a** is very limited. (Figure 2-19). This result encouraged us to use **1a** as a lead compound for designing new agents to improve cross-linking efficiency as well as cytotoxicity towards cancer cells.

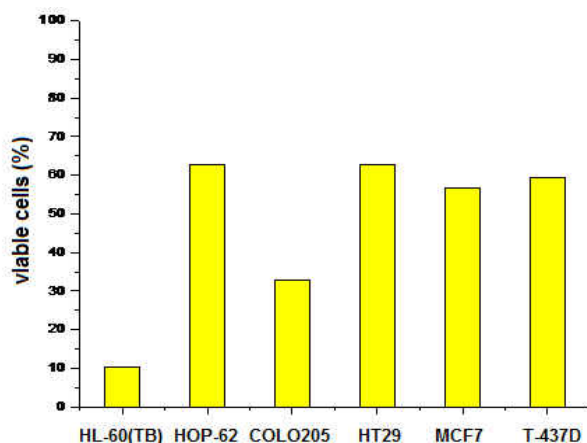


**Figure 2-19.** Effect of **1a** on cancer cells.

In conclusion, novel arylboronates (**1-4**) have been developed as H<sub>2</sub>O<sub>2</sub>-inducible DNA ICL agents, which provided an effective way to release DNA cross-linking functional group QM selectively in the presence of H<sub>2</sub>O<sub>2</sub>. The benzylic leaving group and the aromatic core structure significantly affected the DNA cross-linking ability of the arylboronates. The mechanism of ICL formation induced by these arylboronates involves generation of phenol intermediates that directly produce QMs capable of cross-linking DNA. The QM formation is the rate-determining step for DNA cross-linking. Bromine, the better of the two leaving groups, facilitates the efficient generation of QMs.

## 2.4. Experimental Section

**General Methods.** All chemicals were commercially purchased and used without further purification. Thin layer chromatography (TLC) was carried out on precoated silica gel plates and

visualized under UV light. Oligonucleotides were synthesized via standard automated DNA synthesis techniques. Deprotection of the synthesized DNA was carried out under mild deprotection conditions (28% aq. NH<sub>3</sub>, room temperature, overnight). Oligonucleotides were purified by 20% denaturing polyacrylamide gel electrophoresis. Radiolabeling was carried out according to the standard protocols.<sup>24</sup> Quantification of radiolabeled oligonucleotides was carried out using a Molecular Dynamics Phosphorimager equipped with ImageQuant Version 5.1 software. Enzymatic digestion products were purified with a HPLC, and mass spectra were available on an electron spray injection mass Spectrometer (ESI). <sup>1</sup>H, <sup>13</sup>C NMR spectra were collected on a 300 MHz and 500 MHz FT-NMR spectrometer. High resolution mass spectrometry was carried out on an atmospheric-pressure chemical ionization (APCI) TOF mass spectrometer.

**2-(2,6-Bismethylphenyl)-4,4,5,5-tetramethyl-[1,3,2]dioxaborolane (1-1).** 2-Bromo-1,3-dimethylbenzene (0.74 g, 4 mmol), bis(pinacolato)diboron (1.53 g, 6 mmol), KOAc (1.18 g, 12 mmol), and PdCl<sub>2</sub>(dppf) (98 mg, 0.12 mmol) were dissolved in DMF (40 mL) under argon atmosphere. The mixture was heated at 85 °C for 48 h and cooled to room temperature. Then, water (100 mL) was added and the mixture was extracted with CH<sub>2</sub>Cl<sub>2</sub> (3 x 50 mL). The combined organic layer was washed with water and brine dried over anhydrous Na<sub>2</sub>SO<sub>4</sub>, filtrated, and the solvent was evaporated. The crude product was purified through column chromatography with 0-50% EtOAc in hexane to provide **1-1** as colorless oil (0.74 g, 80%). <sup>1</sup>H NMR (300 MHz, CDCl<sub>3</sub>) δ 7.13 (t, *J* = 7.0 Hz, 1H), 6.95 (d, *J* = 7.0 Hz, 2H), 2.42 (s, 6H), 1.41 (s, 12H). <sup>13</sup>C NMR(500 MHz, CDCl<sub>3</sub>) δ 141.6, 129.1, 126.4, 83.4, 24.9, 22.2. The NMR spectra were consistent with literature value.<sup>25</sup>

**2-(2,6-Bisbromomethylphenyl)-4,4,5,5-tetramethyl-[1,3,2]dioxaborolane (1a).** Compound **1-**

**1** (0.83 g, 3.6 mmol) was dissolved in CH<sub>3</sub>CN (55 mL), and NBS (1.6 g, 9 mmol) and AIBN (62.9 mg) were added. The mixture was refluxed at 90 °C for 3 h. Then the mixture was concentrated and dissolved in DCM (100 mL). The organic phase was washed with H<sub>2</sub>O (3 x 50 mL) and dried with anhydrous Na<sub>2</sub>SO<sub>4</sub>. The solution was evaporated and the residue was subjected to column chromatography on silica gel with 0-50% DCM in hexane to give **1a** as a white solid (0.7 g, 50 %): mp 159-163 °C; <sup>1</sup>H NMR (300 MHz, CDCl<sub>3</sub>) δ 7.31 (m, 3H), 4.84 (s, 4H), 1.49 (s, 12H). <sup>13</sup>C NMR(500 MHz, CDCl<sub>3</sub>) δ 144.4, 130.8, 130.0, 84.4, 34.0, 25.2; HRMS(EI) *m/z* Calcd for C<sub>14</sub>H<sub>19</sub>BBr<sub>2</sub>O<sub>2</sub> [M]<sup>+</sup> 387.9845, found 387.9829. The NMR spectra were consistent with literature value.<sup>25</sup>

**1,1'-(2-(4,4,5,5-Tetramethyl-[1,3,2]dioxaborolan-2-yl)-1,3-henylene)bis(N,N,N-trimethylmethanaminium) bromide (1b)**. Compound **1a** (0.182 g, 0.47 mmol) was suspended in CH<sub>3</sub>CN (10 mL), and 4.2 M trimethylamine (0.34 mL, 1.41 mmol) in ethanol was added dropwise with stirring. The reaction mixture was stirred at r.t. for 12 h and concentrated resulting in **1b** as a white solid (0.22 g, 95%): mp 250-256 °C; <sup>1</sup>H NMR (300 MHz, D<sub>2</sub>O): δ 7.73-7.70 (m, 3H), 4.79 (s, 4H), 3.05 (s, 18H), 1.41 (s, 12H). <sup>13</sup>C NMR (500 MHz, DMSO): δ 136.3, 135.0, 131.3, 85.9, 68.1, 52.9, 25.3; HRMS(ESI): *m/z* Calcd for C<sub>20</sub>H<sub>37</sub>BBr<sub>2</sub>N<sub>2</sub>O<sub>2</sub> [(M-2Br)/2]<sup>+</sup> 174.1474, found 174.1460.

**1-(4-(bromomethyl)-2,5-bis(4,4,5,5-tetramethyl-1,3,2-dioxa-borolan-2-yl)phenyl)-N,N,N-trimethylmethanaminium bromide (4c)**. Bromide **4a** (50 mg, 0.1 mmol) was dissolved in CH<sub>3</sub>CN (2 mL), and 4.2 M trimethylamine (24 μL, 0.1 mmol) in ethanol was added dropwise while stirring. The reaction mixture was concentrated after 24 h at room temperature. The residue was purified by column chromatography with 0-15% methanol in DCM to afford the compound **4c** as white solid (7 mg, 12%): mp 216-220 °C; <sup>1</sup>H NMR (300 MHz, CDCl<sub>3</sub>) δ 8.02



(s, 1H), 7.87 (s, 1H), 4.99 (s, 2H), 4.91 (s, 2H), 3.46 (s, 9H), 1.39 (s, 24H);  $^{13}\text{C}$  NMR (500 MHz,  $\text{CDCl}_3$ )  $\delta$  146.3, 140.6, 139.2, 131.8, 85.1, 84.7, 68.3, 53.1, 32.3, 25.0, 24.9; HRMS (ESI)  $m/z$  Calcd for  $\text{C}_{23}\text{H}_{39}\text{B}_2\text{Br}_2\text{NO}_4$   $[\text{M}-\text{Br}]^+$  494.2243, found 494.2247.

**1,1'-(2-Hydroxy-1,3-phenylene)bis(*N,N,N*-trimethylmethan -aminium) bromide (1b-1).** A solution of **1b** (50 mg) in a mixture of  $\text{H}_2\text{O}$  (3 mL), 1 M potassium phosphate buffer (52  $\mu\text{L}$ , pH 8), and  $\text{H}_2\text{O}_2$  (1.9 equivalent of **1b**) was incubated at 37  $^\circ\text{C}$  for 3 h, then rinsed with ethyl acetate (3  $\times$  5 mL) and DCM (3  $\times$  5 mL). The aqueous phase was dried under vacuum yielding **10b** as white solid quantitatively: mp 214-218  $^\circ\text{C}$ ;  $^1\text{H}$  NMR (500 MHz,  $\text{D}_2\text{O}$ ):  $\delta$  7.32 (d,  $J = 7.5$  Hz, 2H), 6.56 (t,  $J = 7.5$  Hz, 1H), 4.36 (s, 4H), 2.96 (s, 18H).  $^{13}\text{C}$  NMR (500 MHz, DMSO):  $\delta$  137.3, 118.2, 112.8, 65.6, 52.2; HRMS(ESI):  $m/z$  Calcd for  $\text{C}_{14}\text{H}_{26}\text{Br}_2\text{N}_2\text{O}$   $[(\text{M}-2\text{Br})/2]^+$  119.1017, found 119.1022.

**QM Trapping Assay. General Procedure.** A solution of bromides **1a-4a** (50 mg) in a mixture of  $\text{CH}_3\text{CN}$  (3 mL) and 1 M potassium phosphate buffer (52  $\mu\text{L}$ , pH 8) was incubated at 37  $^\circ\text{C}$  for 30 min with excess ethyl vinyl ether (EVE). Then  $\text{H}_2\text{O}_2$  (1.9 equivalent of bromides) was added to initiate the reaction. The reaction mixture was stirred at 37  $^\circ\text{C}$  for 24 h, then evaporated. Water (2 mL) was added to the residue, and extracted with ethyl acetate (3  $\times$  5 mL). The organic phase was combined, dried over anhydrous  $\text{Na}_2\text{SO}_4$ , and evaporated. The crude product was purified through column chromatography with 0-50% EtOAc in hexane to provide QM-EVE adducts **1a-t** to **4a-t**.

**(2-Ethoxychroman-8-yl)methanol (1a-t).** Colorless oil, 16% yield (4.9 mg).  $^1\text{H}$  NMR (300 MHz,  $\text{CDCl}_3$ ):  $\delta$  7.20-6.82 (m, 3H), 5.35 (s, 1H), 4.78-4.58 (m, 2H), 3.98-3.84 (m, 1H), 3.72-3.58 (m, 1H), 3.05-2.88 (m, 1H), 2.68-2.56 (m, 1H), 2.28 (s, 1H), 2.12-1.92 (m, 2H), 1.21 (t,  $J = 7.2$  Hz, 3H).  $^{13}\text{C}$  NMR (500 MHz,  $\text{CDCl}_3$ ):  $\delta$  150.1, 128.9, 128.5, 126.5, 122.6, 120.4, 97.2, 63.9,

62.0, 26.5, 20.5, 15.1; HRMS (APCI):  $m/z$  Calcd for  $C_{12}H_{16}O_3$   $[M-H]^+$  207.1021, found 207.1025.

**(2-Ethoxychroman-6-yl)methanol (2a-t).** Colorless oil, 11% yield (3.4 mg).  $^1H$  NMR (300 MHz,  $CDCl_3$ ):  $\delta$  7.16-7.08 (m, 2H), 6.82 (d,  $J = 8.1$  Hz, 1H), 5.27 (s, 1H), 4.61 (s, 2H), 3.98-3.84 (m, 1H), 3.72-3.58 (m, 1H), 3.08-2.92 (m, 1H), 2.72-2.58 (m, 1H), 2.12-1.92 (m, 2H), 1.61 (br, 1H), 1.21 (t,  $J = 7.2$  Hz, 3H).  $^{13}C$  NMR (500 MHz,  $CDCl_3$ ):  $\delta$  151.9, 133.0, 128.5, 126.5, 122.7, 117.1, 97.0, 65.3, 63.7, 26.5, 20.5, 15.1; HRMS (APCI):  $m/z$  Calcd for  $C_{12}H_{16}O_3$   $[M-H]^+$  207.1021, found 207.1023.

**2,7-Diethoxy-2,3,4,7,8,9-hexahydropyrano[2,3-g]chromene (3a-t).** Colorless oil, 21% yield (8.8 mg).  $^1H$  NMR (300 MHz,  $CDCl_3$ ):  $\delta$  6.54 (s, 2H) 5.21 (s, 2H), 3.96-3.86 (m, 2H), 3.72-3.58 (m, 2H), 3.04-2.90 (m, 2H), 2.64-2.54 (m, 2H), 2.08-1.90 (m, 4H), 1.21 (t,  $J = 7.2$  Hz, 6H).  $^{13}C$  NMR (500 MHz,  $CDCl_3$ ):  $\delta$  145.8, 121.5, 116.5, 96.8, 63.5, 26.7, 20.5, 15.1; HRMS (APCI):  $m/z$  Calcd for  $C_{16}H_{22}O_4$   $[M+NH_4]^+$  296.1862, found 296.1861.

**2,2'-Diethoxy-6,6'-bichroman (4a-t).** Colorless oil, 26% yield (13.8 mg).  $^1H$  NMR (300 MHz,  $CDCl_3$ ):  $\delta$  7.34-7.24 (m, 4H), 6.87 (d, 2H,  $J = 8.1$  Hz), 5.30 (s, 2H), 3.98-3.88 (m, 2H), 3.72-3.62 (m, 2H), 3.08-2.96 (m, 2H), 2.74-2.62 (m, 2H), 2.08-1.92 (m, 4H), 1.21 (t,  $J = 7.2$  Hz, 6H).  $^{13}C$  NMR (500 MHz,  $CDCl_3$ ):  $\delta$  151.3, 133.7, 127.6, 125.7, 122.7, 117.2, 97.0, 63.7, 26.6, 20.7, 15.2; HRMS (APCI):  $m/z$  Calcd for  $C_{22}H_{26}O_4$   $[M+NH_4]^+$  372.2175, found 372.2178.

**Interstrand cross-link formation and kinetics study with duplex DNA.** The  $^{32}P$ -labelled oligonucleotide (0.5  $\mu M$ ) was annealed with 1.5 equiv of the complementary strand by heating to 65  $^\circ C$  for 3 min in a buffer of 10 mM potassium phosphate (pH 7) and 100 mM NaCl, followed by slow-cooling to room temperature overnight. The  $^{32}P$ -labeled oligonucleotide duplex (0.5  $\mu M$ ,

2  $\mu\text{L}$ ) was mixed with 1 M NaCl (2  $\mu\text{L}$ ), 100 mM potassium phosphate (2  $\mu\text{L}$ , pH 8.0), 10 mM  $\text{H}_2\text{O}_2$  (2  $\mu\text{L}$ ), and compounds **1b-4b** (concentration range: 10  $\mu\text{M}$  to 7 mM) and appropriate amount of autoclaved distilled water to give a final volume of 20  $\mu\text{L}$ . For Bromides **1a-4a**, 6  $\mu\text{L}$   $\text{CH}_3\text{CN}$  was added in reaction mixture to facilitate their dissolution. The reaction was incubated at 37  $^\circ\text{C}$  for 24 h and quenched by an equal volume of 90% formamide loading buffer, then subjected to 20% denaturing polyacrylamide gel analysis. For kinetics study, aliquots (final concentration: 50 nM  $^{32}\text{P}$ -labeled oligonucleotide duplex, 100 mM NaCl, 10 mM potassium phosphate, 1 mM  $\text{H}_2\text{O}_2$ , 2 mM of **1-4**) were taken at the prescribed times and immediately quenched by 90% formamide loading buffer, and stored at -20  $^\circ\text{C}$  until subjecting to 20% denaturing PAGE analysis.

**Enzyme digestion of cross-linked oligonucleotides.** Interstrand cross-linked oligonucleotide (38 nmol) was dissolved in 0.1 M Tris-HCl buffer, pH 8.0 (300  $\mu\text{L}$ ) and snake-venom phosphodiesterase (8.0  $\mu\text{L}$ , 0.34 U) in a buffer of 110 mM Tris-HCl, pH 8.9, 110 mM NaCl, 15 mM  $\text{MgCl}_2$ , and 50% glycerol was added. The mixture was incubated at 37  $^\circ\text{C}$  for 1 h. Then, alkaline phosphatase (8.0  $\mu\text{L}$ , 80 U) in 16  $\mu\text{L}$  alkaline phosphatase buffer (100 mM NaCl, 50 mM Tris-HCl, 10 mM  $\text{MgCl}_2$  and 1 mM dithiothreitol) was added. The reaction mixture was incubated at 37  $^\circ\text{C}$  for another hour. The digested products were passed through a Microcon cellulose filter (10,000 molecular cut off, Amicon Inc.) by centrifugation at 15,000 RPM. The filtrate was collected, lyophilized, redissolved in  $\text{H}_2\text{O}$  (500  $\mu\text{L}$ ), and analyzed by reversed-phase HPLC (RP-18, at 260 nm) using the following gradient: 0-30 min 2-20% MeOH in water, 30-35 min 20-50% MeOH in water, 35-42 min 50-0% MeOH in water, 42-50 min 0% MeOH in water, at a flow rate 1.0 mL/min.

**Stability study of ICL product formed with DNA Duplex.** After the cross-linking reaction, the reaction mixtures (0.35  $\mu\text{M}$  DNA duplex, 20  $\mu\text{L}$ ) were co-precipitated with calf thymus DNA (2.5 mg/mL, 5  $\mu\text{L}$ ) and NaOAc (3 M, 5  $\mu\text{L}$ ) in the presence of EtOH (90  $\mu\text{L}$ ) at  $-80\text{ }^\circ\text{C}$  for 30 min, followed by centrifuging for 5 min at 15000 rpm. The supernatant was removed, and the pellet was washed with cold 75% EtOH and lyophilized for 30 min in a Centrivap Concentrator of LABCONCO at  $37\text{ }^\circ\text{C}$ . The dried DNA fragments were dissolved in  $\text{H}_2\text{O}$  (30  $\mu\text{L}$ ) and divided into three portions. One portion (10  $\mu\text{L}$ ) was incubated with piperidine (2 M, 10  $\mu\text{L}$ ) at  $90\text{ }^\circ\text{C}$  for 30 min, and the second portion (10  $\mu\text{L}$ ) was incubated with 0.1 M NaCl and 10 mM potassium phosphate buffer (pH 8, 10  $\mu\text{L}$ ) under the same conditions, and the third portion was used as control sample. The samples were subjected to electrophoresis on a 20% denaturing polyacrylamide gel.

**Hydroxyl Radical Reaction (Fe·EDTA Reaction).** Fe(II)·EDTA cleavage reactions of  $^{32}\text{P}$ -labeled oligonucleotide (0.1  $\mu\text{M}$ ) were performed in a buffer containing 50  $\mu\text{M}$   $(\text{NH}_4)_2\text{Fe}(\text{SO}_4)_2$ , 100  $\mu\text{M}$  EDTA, 5 mM sodium ascorbate, 0.5 M NaCl, 50 mM sodium phosphate (pH 7.2), and 1 mM  $\text{H}_2\text{O}_2$  for 3 min at room temperature (total substrate volume 20  $\mu\text{L}$ ) and then quenched with 100 mM thiourea (10  $\mu\text{L}$ ). Samples were lyophilized and incubated with 1 M piperidine (20  $\mu\text{L}$ ) at  $90\text{ }^\circ\text{C}$  for 30 min. The mixture was lyophilized again, dissolved in 20  $\mu\text{L}$   $\text{H}_2\text{O}$ : 90% formamide loading buffer (1:1), and subjected to 20% denaturing PAGE analysis.

## 2.5. References

1. Noll, D. M., Mason, T. M., Miller, P. S. Formation and repair of interstrand cross-links in DNA. *Chem. Rev.* **2006**, *106*, 277–301.
2. Rajsiki, S. R., Williams, R. M., DNA cross-linking agents as antitumor drugs. *Chem. Rev.* **1998**, *98*, 2723-2795.

3. Hong, I. S., Greenberg, M. M. DNA interstrand cross-link formation initiated by reaction between singlet oxygen and a modified nucleotide. *J. Am. Chem. Soc.* **2005**, *127*, 10510-10511.
4. Hong, I. S., Ding, H., Greenberg, M. M. Oxygen independent DNA interstrand cross-link formation by a nucleotide radical. *J. Am. Chem. Soc.* **2006**, *128*, 485-491.
5. Veldhuyzen, W. F., Pande, P., Rokita, S. E. A transient product of DNA alkylation can be stabilized by binding localization. *J. Am. Chem. Soc.* **2003**, *125*, 14005-14013.
6. Richter, S. N., Maggi, S., Mels, S. C., Palumbo, M., Freccero, M. Binolquinonemethides as bisalkylating and DNA cross-linking agents. *J. Am. Chem. Soc.* **2004**, *126*, 13973-13979.
7. Wang, H., Rokita, S. E. Dynamic cross-linking is retained in duplex DNA after multiple exchange of strands. *Angew. Chem., Int. Ed.* **2010**, *122*, 6093-6096.
8. Wang, P., Liu, R., Wu, X., Ma, H., Cao, X., Zhou, P., Zhang, J., Weng, X., Zhang, X., Qi, J., Zhou, X., Weng, L. A potent, water-soluble and photoinducible DNA cross-linking agent. *J. Am. Chem. Soc.* **2003**, *125*, 1116-1117.
9. Weng, X., Ren, L., Weng, L., Huang, J., Zhu, S., Zhou, X., Weng, L. Synthesis and biological studies of inducible DNA cross-linking. *Angew. Chem., Int. Ed.* **2007**, *46*, 8020-8023.
10. Szatrowski, T. P., Nathan, C. F. Production of large amounts of hydrogen peroxide by human tumor cells. *Cancer Rev.* **1991**, *51*, 794-798.
11. Trachootham, D., Alexandre, J., Huang, P. Targeting cancer cells by ROS-mediated mechanisms: a radical therapeutic approach? *Nature Rev. Drug Discov.* **2009**, *8*, 579-591.

12. Giorgio, M., Trinei, M., Migliaccio, E., Pelicci, P. G. Hydrogen peroxide: a metabolic by-product or a common mediator of ageing signals? *Nature reviews Molecular cell biology*, **2007**, *8*, 722-728.
13. Kuivila, H. G., Armour, A. G. Electrophilic displacement reactions. IX. Effects of substituents on rates of reactions between hydrogen peroxide and benzenboronic Acid<sup>1-3</sup>. *J. Am. Chem. Soc.* **1975**, *79*, 5659-5662.
14. Kuang, Y., Balakrishnan, K., Gandhi, V., Peng, X. Hydrogen peroxide inducible DNA cross-linking agents: targeted anticancer prodrugs. *J. Am. Chem. Soc.* **2011**, *133*, 19278-19281.
15. Cao, S., Wang, Y., Peng, X. ROS-inducible DNA cross-linking agent as a new anticancer prodrug building block. *Chem. Eur. J.* **2012**, *18*, 3850-3854.
16. Kuivila, H. G. Electrophilic Displacement Reactions. III. Kinetics of the reaction between hydrogen peroxide and benzenboronic acid<sup>1</sup>. *J. Am. Chem. Soc.* **1954**, *76*, 870-874.
17. Haraguchi, K., Delaney, M. O., Wiederholt, C. J., Sambandam, A., Hantosi, Z., Greenberg, M. M. Synthesis and characterization of oligodeoxynucleotides containing formamidopyrimidine lesions and nonhydrolyzable analogues. *J. Am. Chem. Soc.* **2002**, *124*, 3263-3269.
18. Peng, X., Hong, I. S., Li, H., Seidman, M. M., Greenberg, M. M. Interstrand cross-link formation in duplex and triplex DNA by modified pyrimidines. *J. Am. Chem. Soc.* **2008**, *130*, 10299-10306.
19. Mattes, W. B., Hartley, J. A., Kohn, K. W. DNA sequence selectivity of guanine N-7 alkylation by nitrogen mustards. *Nucleic Acids Res.* **1986**, *14*, 2971-2987.
20. Maxam, A. M., Gilbert, W. Sequencing end-labeled DNA with base-specific chemical cleavages. *Methods Enzymol.* **1980**, *65*, 499-560.

21. Veldhuyzen, W. F., Lam, Y. F., Rokita, S. E. 2'-Deoxyguanosine reacts with a model quinone methide at multiple sites. *Chem. Res. Toxicol.* **2001**, *14*, 1345-1351.
22. Cao, S., Christiansen, R., Peng, X. Substituent effects on oxidation-induced formation of quinone methides from arylboronic ester precursors. *Chem. Eur. J.* **2013**, *19*, 9050-9058.
23. Wang, H., Wahi, M. S., Rokita, S. E. Immobilizing a transient electrophile for DNA cross-linking. *Angew. Chem., Int. Ed.* **2008**, *47*, 1291-1293.
24. Maniatis, T., Fritsch, E. F., Sambrook, J. *Molecular Cloning*, Cold Spring Harbor Laboratory, Cold Spring Harbor, NY. **1982**.
25. Lux, C. G., Joshi-Barr, S., Nguyen, T., Mahmoud, E., Schopf, E., Fomina, N., Almutairi, A. Biocompatible polymeric nanoparticles degrade and release cargo in response to biologically relevant levels of hydrogen peroxide. *J. Am. Chem. Soc.* **2012**, *134*, 15758-15764.

## 2.6. Appendices A: Characterization of Compounds:

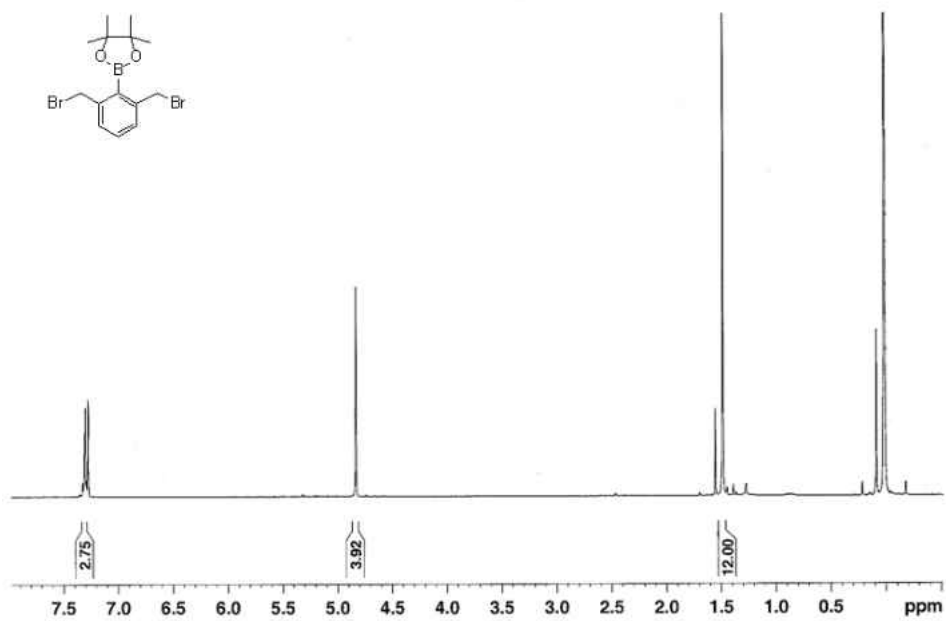


Figure 2-6-1.  $^1\text{H NMR}$  spectra of compound **1a**.

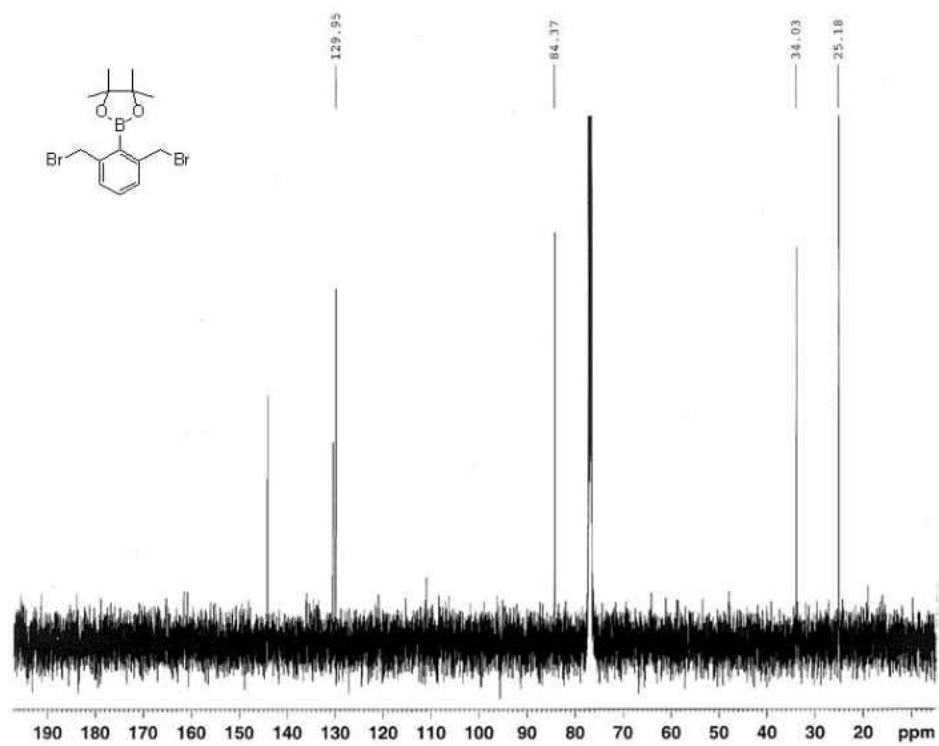


Figure 2-6-2.  $^{13}\text{C NMR}$  spectra of compound **1a**.



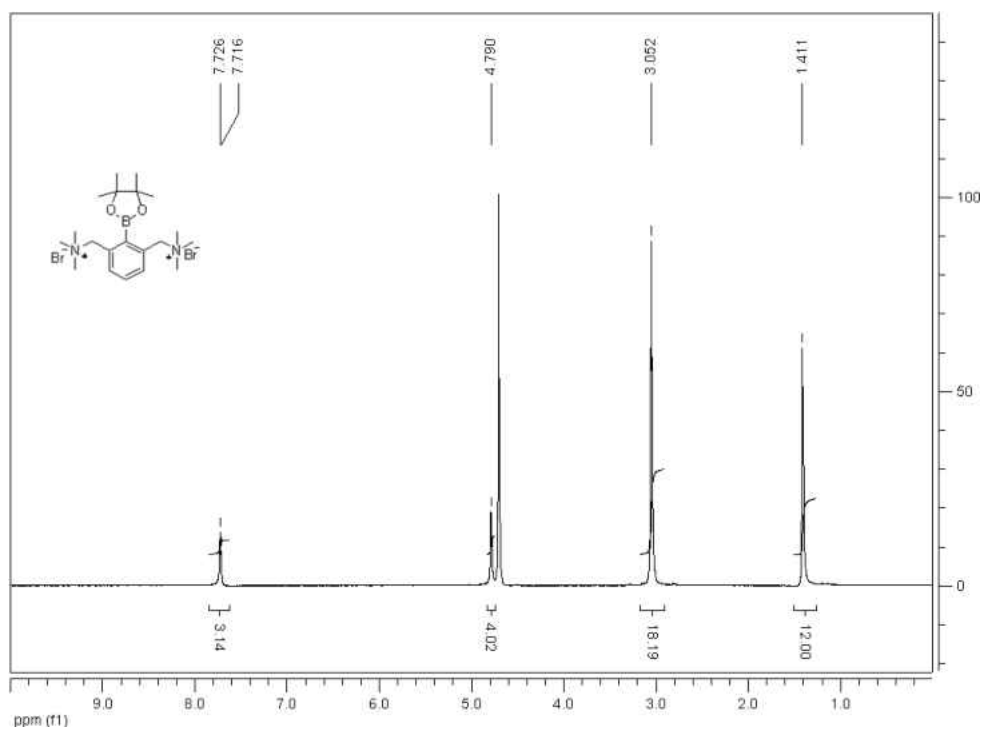


Figure 2-6-3.  $^1\text{H}$  NMR spectra of compound **1b**.

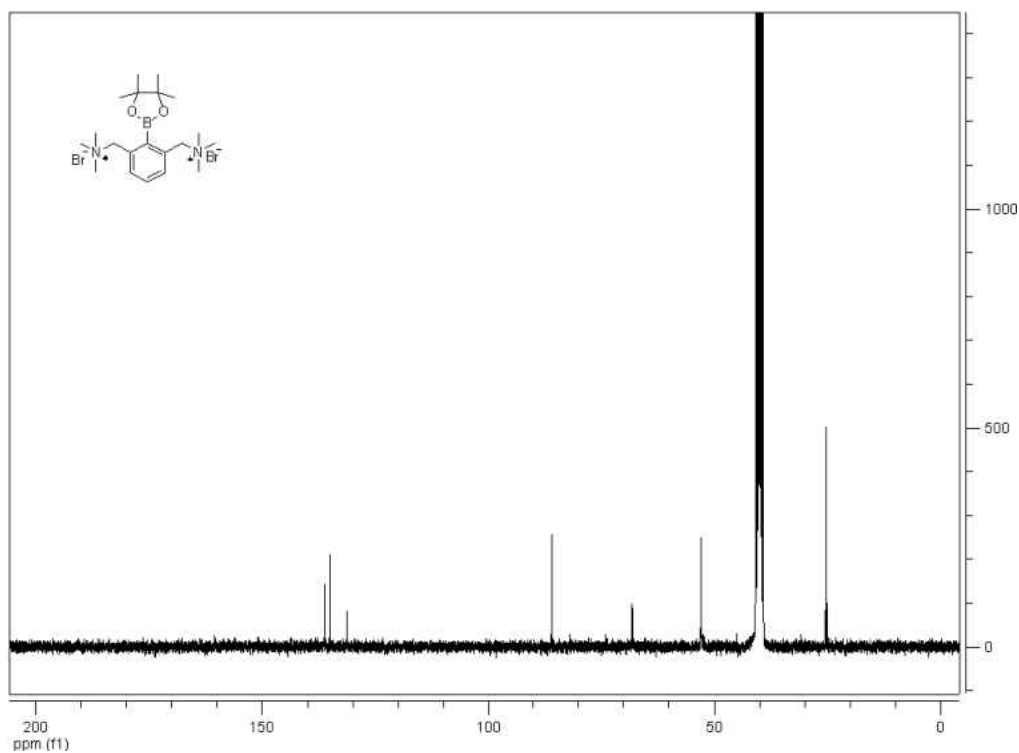


Figure 2-6-4.  $^{13}\text{C}$  NMR spectra of compound **1b**.

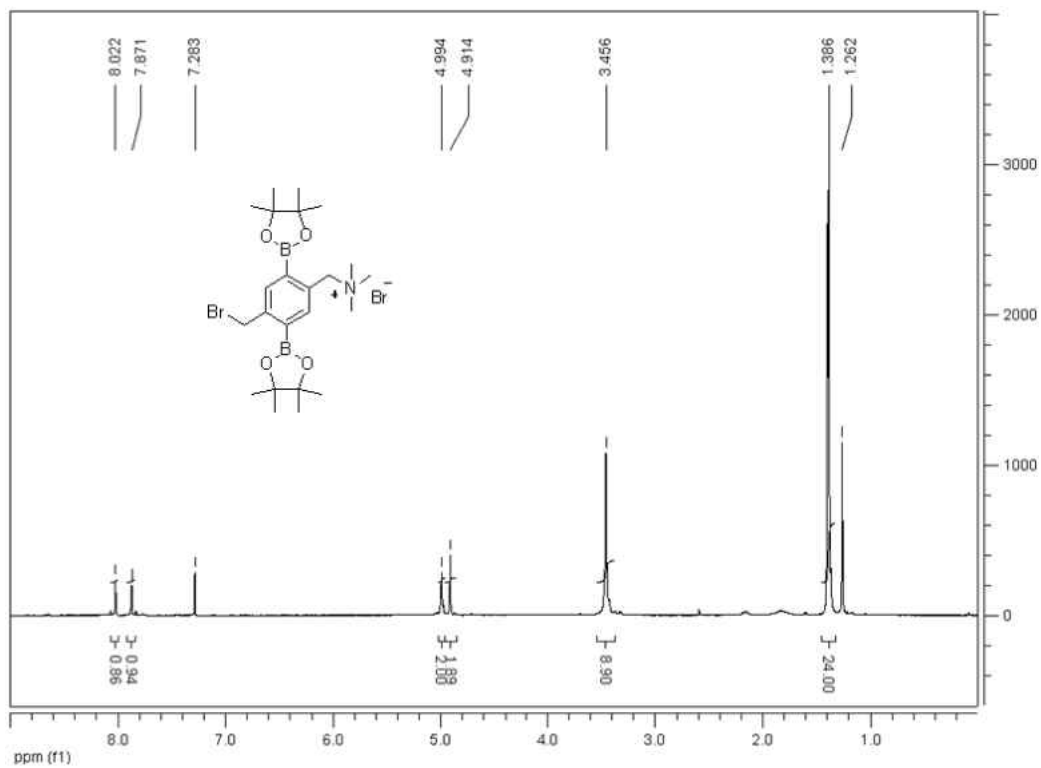


Figure 2-6-5.  $^1\text{H}$  NMR spectra of compound **4c**.

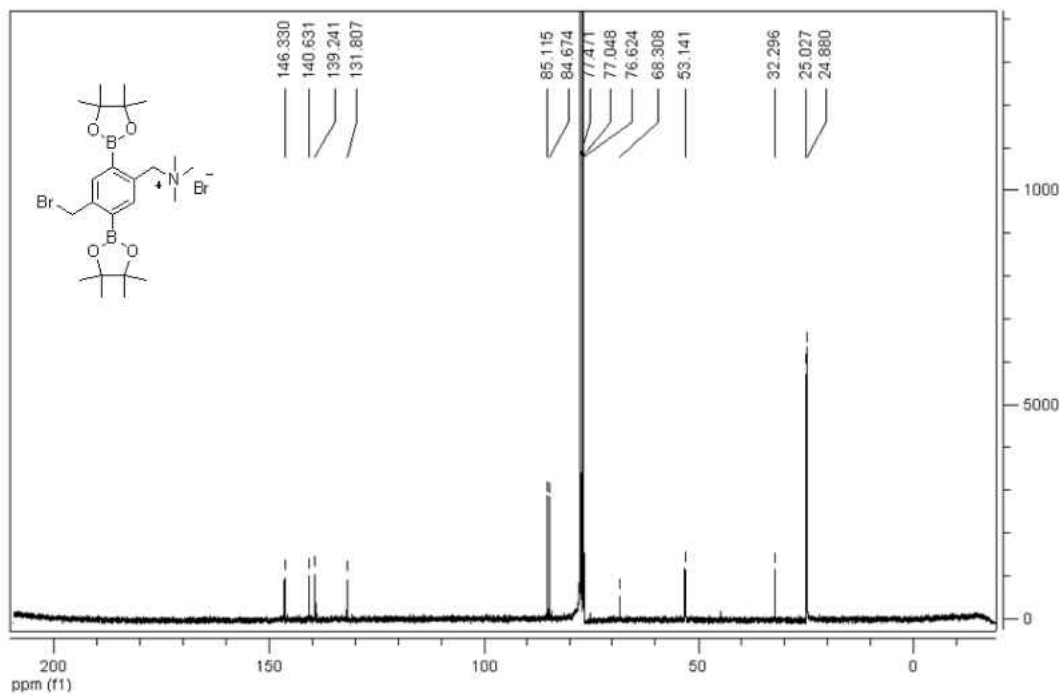


Figure 2-6-6.  $^{13}\text{C}$  NMR spectra of compound **4c**.

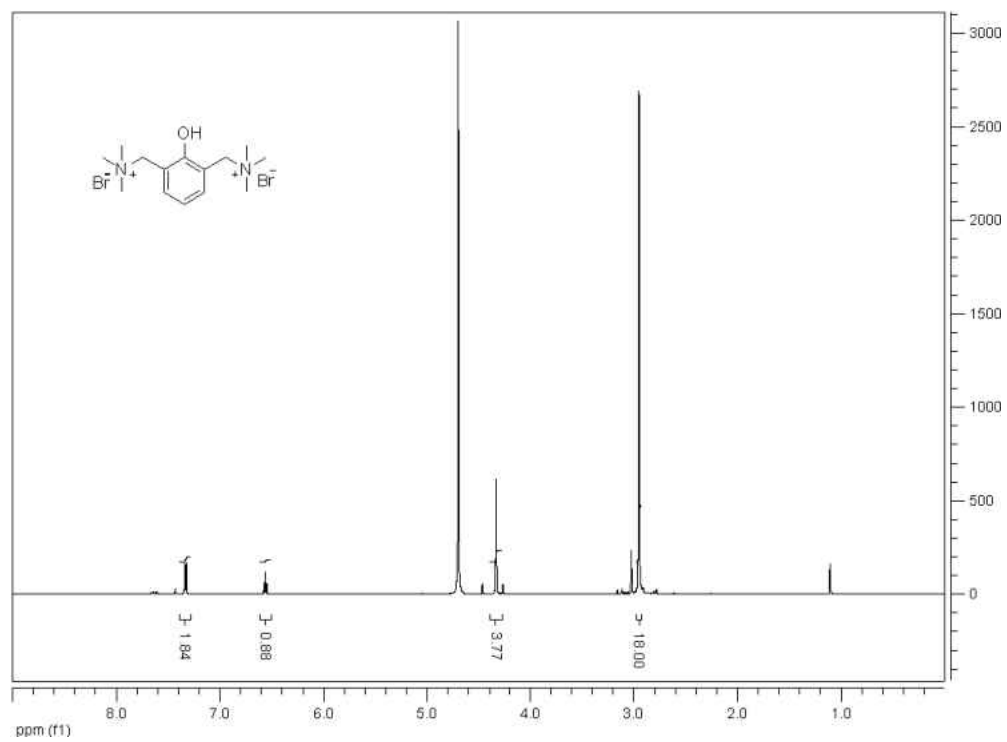


Figure 2-6-7.  $^1\text{H}$  NMR spectra of compound **1b-1**.

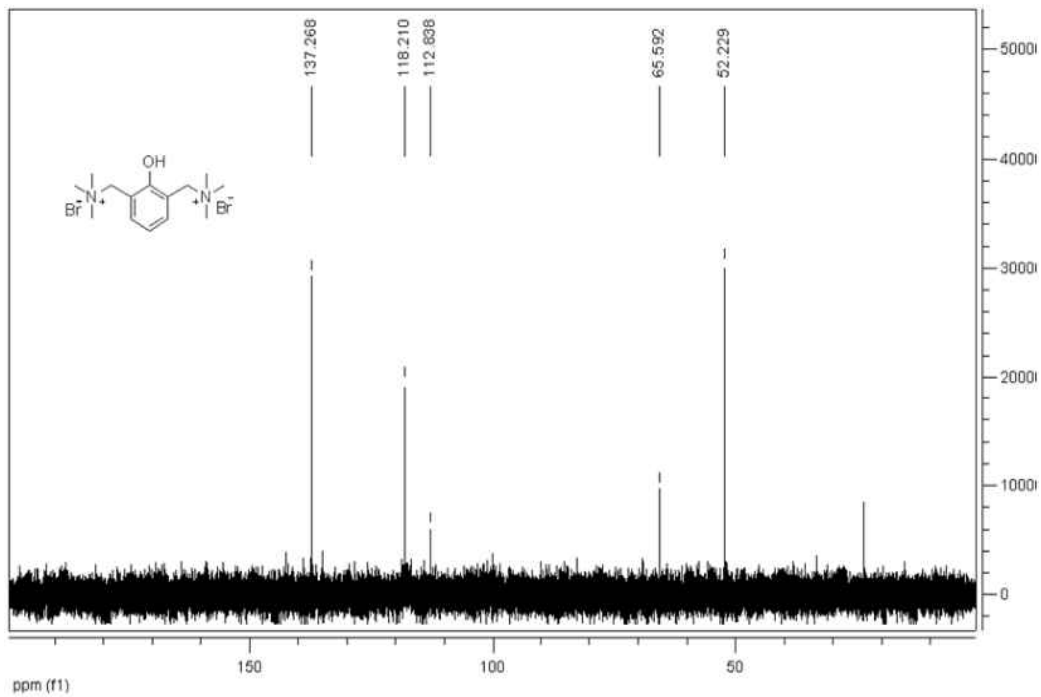


Figure 2-6-8.  $^{13}\text{C}$  NMR spectra of compound **1b-1**.

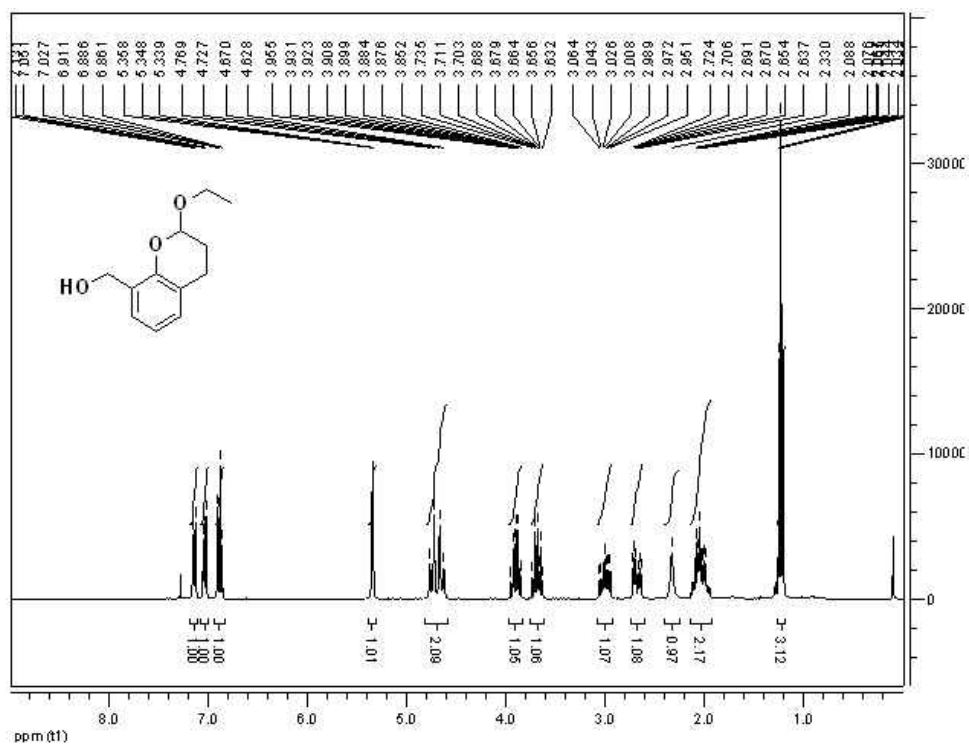


Figure 2-6-9.  $^1\text{H}$  NMR spectra of compound **1a-t**.

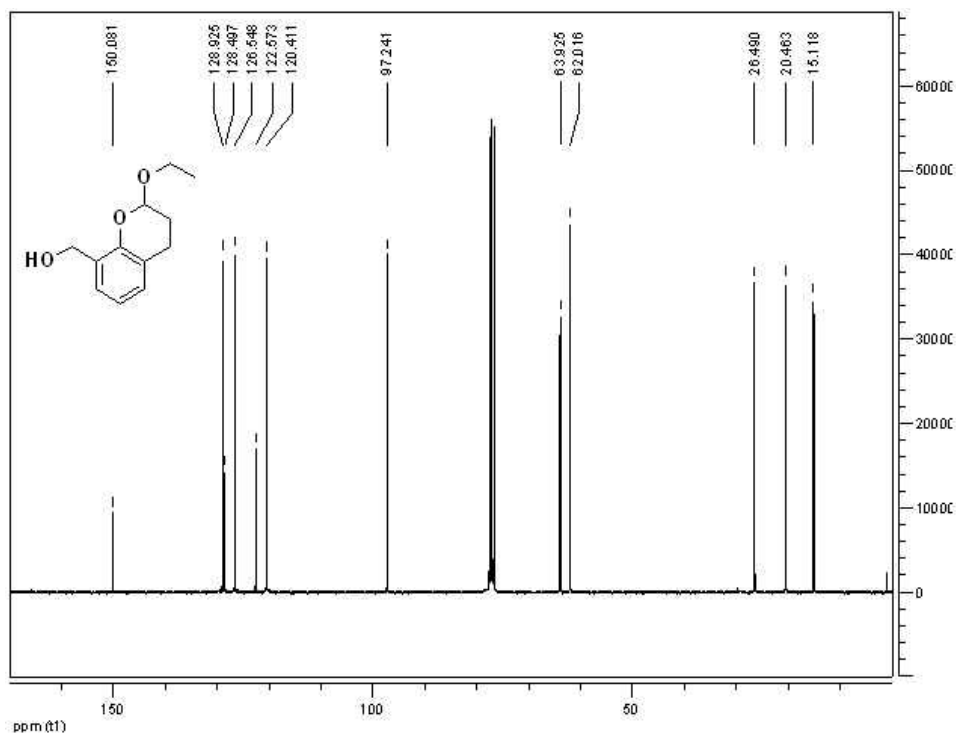
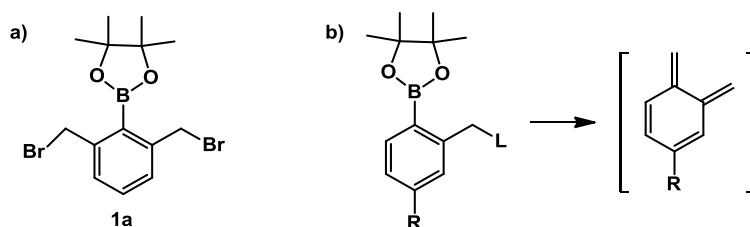


Figure 2-6-10.  $^{13}\text{C}$  NMR spectra of compound **1a-t**.

## Chapter 3. Optimization of H<sub>2</sub>O<sub>2</sub>-Activated Quinone Methide Prodrugs to Improve DNA Cross-Linking Efficiency and Cytotoxicity towards Cancer Cells

### 3.1. Introduction

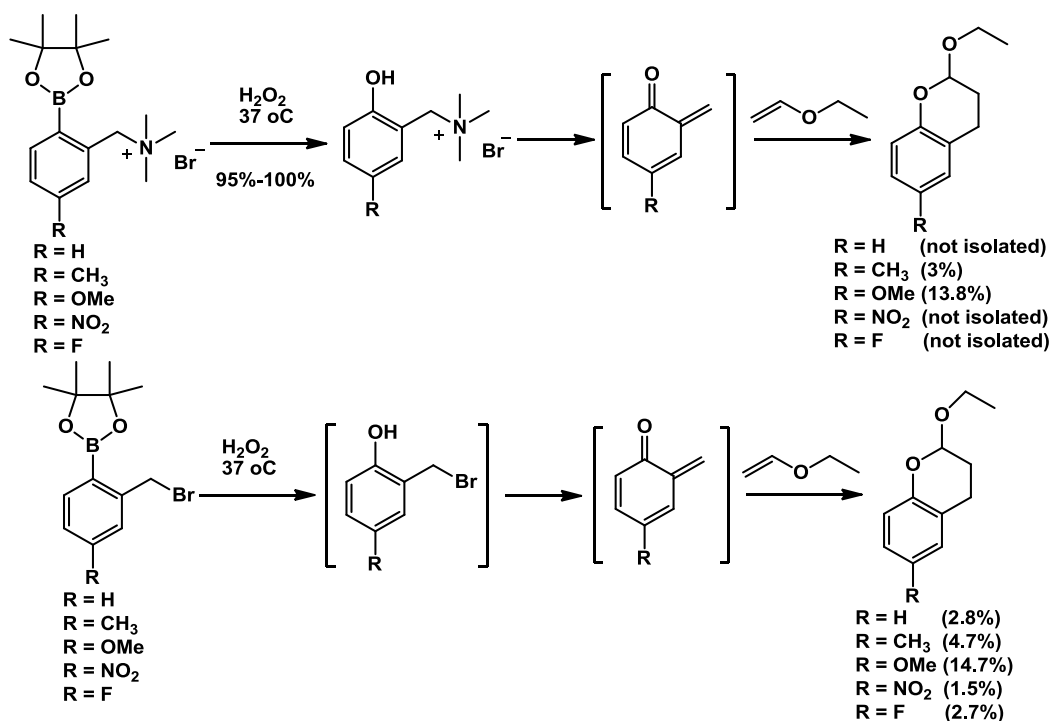
Previous results showed that the arylboronates selectively reacted with H<sub>2</sub>O<sub>2</sub> and generated the phenol intermediate which directly produced QM capable of cross-linking DNA. The benzylic leaving group and the aromatic structure significantly affected the DNA cross-linking efficiency of the arylboronates. Among the arylboronates that have been developed, compound **1a** (Scheme 3-1 a) effectively inhibited cancer cell growth.<sup>1,2</sup> In this work, we use **1a** as a lead compound for further optimization to improve the potency of the H<sub>2</sub>O<sub>2</sub>-activated quinone methide prodrugs.



**Scheme 3-1.** Structure of **1a** and the factors influence QM formation.

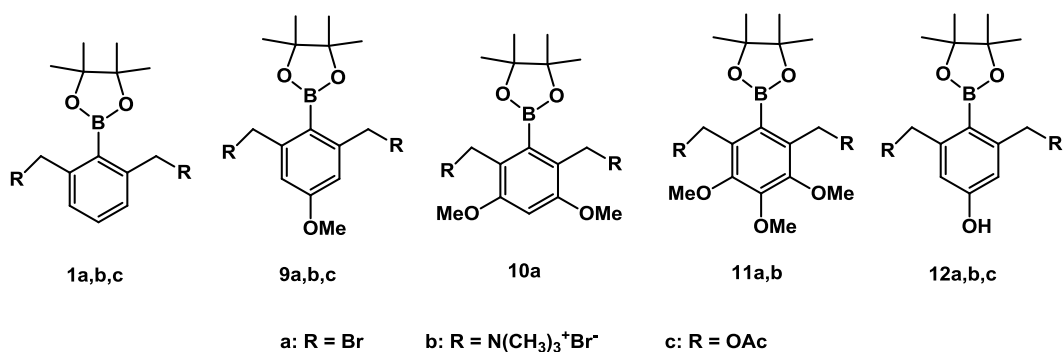
Rokita's group have shown that formation of QMs from fluoride-cleavable precursors are strongly dependent on the leaving groups attached to the benzylic position.<sup>3,4</sup> They have also studied the reversible generation of some substituted *o*-QMs from conventional precursors and their reactivities in conjugate addition reactions. The results indicated that electron-donating groups greatly facilitated QM generation and regeneration, whereas electron-withdrawing substituents strongly suppress this process.<sup>4</sup> Recently, Peng's group has found that several factors influenced the reactivity of the arylboronates with H<sub>2</sub>O<sub>2</sub> and subsequent QM formation, such as the leaving group L, the aromatic substituent R, and the core structure (Scheme 3-1 b). The electron-withdrawing groups at the aromatic ring facilitated formation of phenol products from

the aryboronates, whereas electron-donating groups slowed down this process. On the contrary, the electron-donating groups favor formation of QMs.<sup>5</sup> A combination of an electron-withdrawing aromatic group and a poor leaving group inhibited QM formation, while a good leaving group and/or a strong donating group are beneficial for QM generation (Scheme 3-2).



**Scheme 3-2.** Effect of substituents on QM formation.

Several leaving groups, such as Br, OAc,  $\text{NMe}_3^+$ ,  $\text{NMe}_2$ , OH and  $\text{SCH}_2\text{CH}_2\text{OH}$  have been introduced in different QM precursors. Among these well-studied leaving groups, the acetate group was successfully used in fluoride-induced or photo-induced QM formation.<sup>4,6,7</sup> Inspired by these findings, we modify **1a** with different leaving groups (e.g. Br, OAc) and different electron-donating groups (e.g. OMe and OH) at the benzene ring (Scheme 3-3). Thus, we designed and synthesized compounds **1c** and **9-12** and conducted a more detailed investigation on the effects of the electron-donating groups and benzylic leaving groups on the  $\text{H}_2\text{O}_2$ -induced DNA cross-linking ability and *in vitro* cytotoxicity of these aryboronic esters.



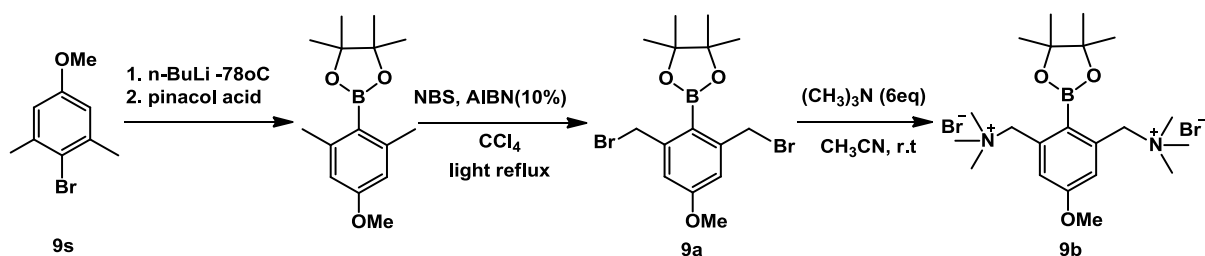
**Scheme 3-3.** The structures of **9-12**.

### 3.2. Modification of **1a** to improve DNA cross-linking efficiency

#### 3.2.1. Design and Synthesis of arylboronic ester **9-12**

The synthesis of compounds **9-12** involved two general steps: borylation and introduction of leaving groups. Compound **9a** was synthesized starting from commercially available 2-bromo-5-methoxy-1,3-dimethylbenzene **9s** via borylation by using *n*-butyllithium and isopropoxyboronic acid pinacol ester, and followed by bromination by using NBS and AIBN reflux under light.

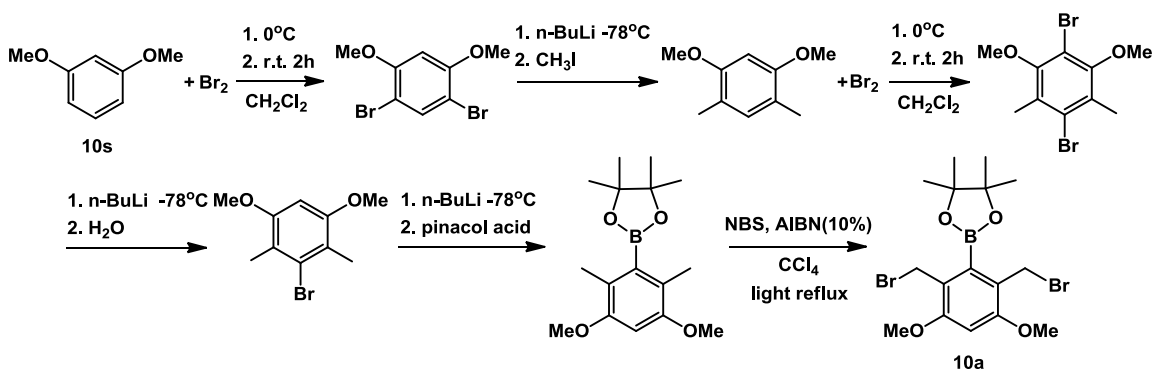
Quaternization of **9a** with trimethylamine provided **9b** in nearly quantitative yield (Scheme 3-4).



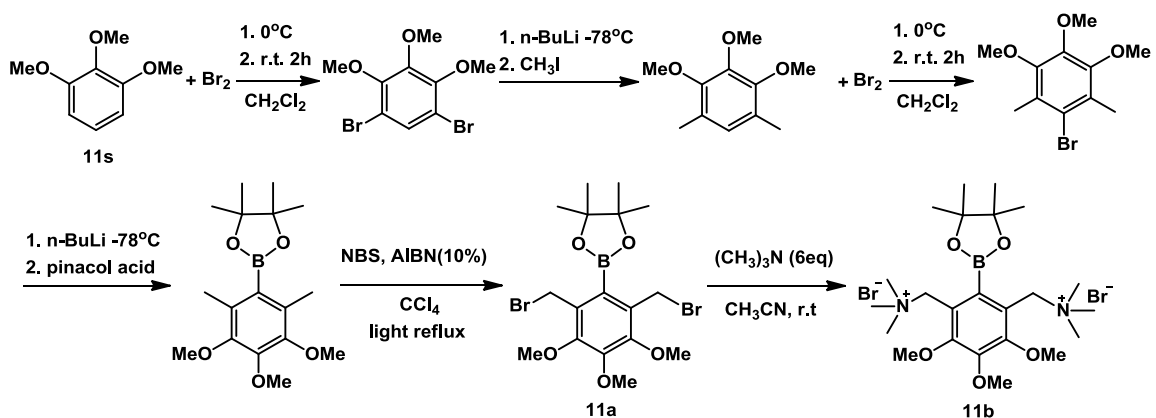
**Scheme 3-4.** Synthesis of **9a,b**.

Compounds **10a** and **11a** were synthesized from 3-bromo-1,5-dimethoxy-2,4-dimethylbenzene **10s** and 1-bromo-3,4,5-trimethoxy-2,6-dimethylbenzene **11s** that were prepared according to the synthetic route reported by Connell and co-workers.<sup>7</sup> The borylation and bromination were

carried out in a similar way to that used for compound **9a** (Scheme 3-5 and 3-6). Compound **10a** is too labile to be used as a precursor for synthesis of the corresponding trimethylamine salt.



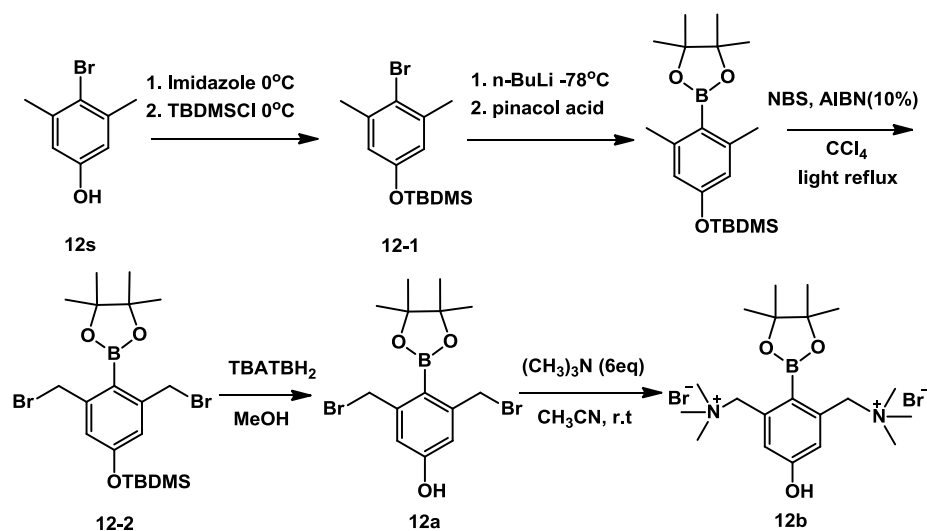
**Scheme 3-5.** Synthesis of **10a**.



**Scheme 3-6.** Synthesis of **11a,b**.

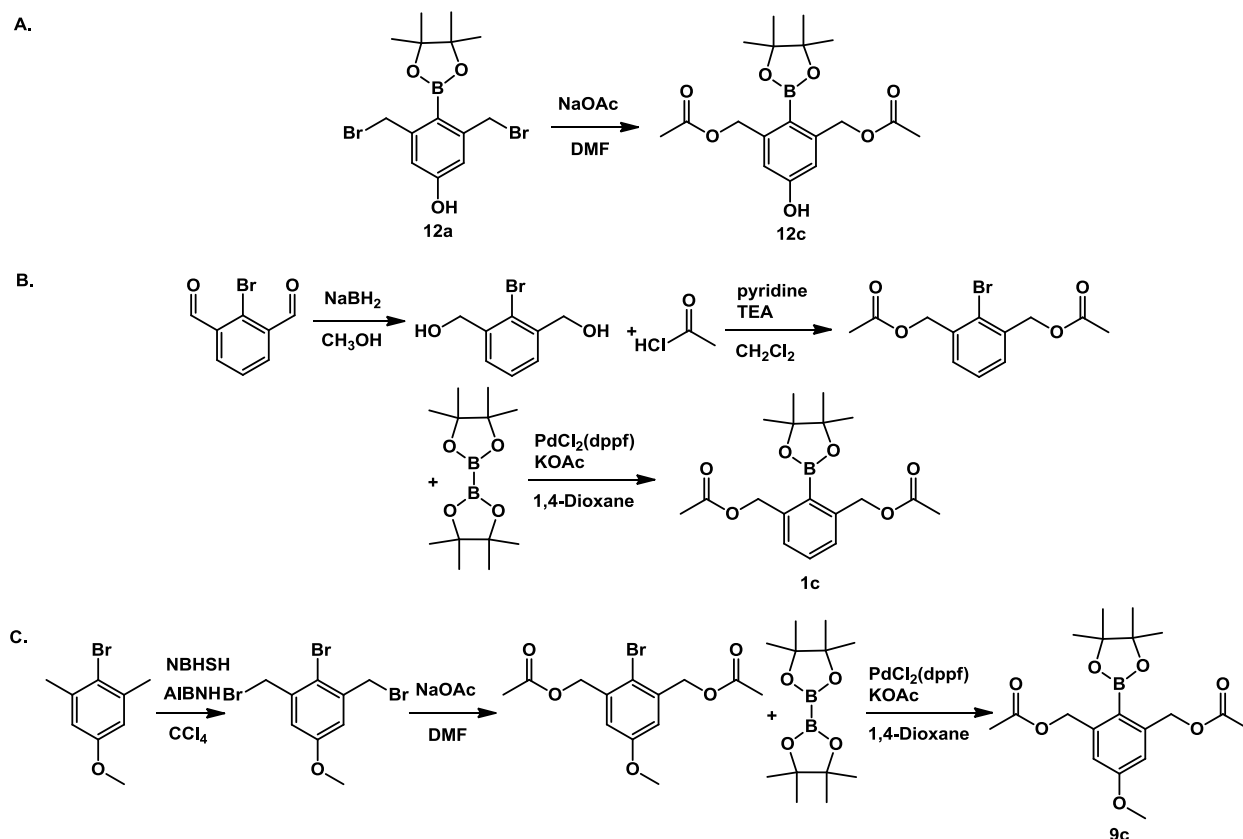
Compound **12a** was synthesized starting from 4-bromo-3,5-dimethylphenol **12s**. The phenol group of **12s** was protected with tert-butyldimethylsilane yielding **12-1**. Borylation of **12-1** followed by bromination resulted in **12-2**, which was deprotected with tetrabutylammonium tribromide (TBATB) to generate **12a**. Quaternization of **12a** with trimethylamine provided **12b** in nearly quantitative yield (Scheme 3-7).





**Scheme 3-7.** Synthesis of **12a,b**.

Compounds **1c**, **9c**, and **12c** containing OAc as leaving group were prepared via different precursors (Schemes 3-8). Compound **12a** was employed as starting material for **12c**. Direct replacement of Br with OAc using sodium acetate in DMF led to formation of **12c** (Scheme 3-8 A). However, compounds **1c** and **9c** cannot be directly synthesized from **1a** and **9a** because the arylboronic esters were easily to be hydrolyzed under the reaction conditions. Thus, introduction of the acetate group was performed prior to borylation. Compound **1c** was prepared from 2-bromoisophthalaldehyde via reduction using  $\text{NaBH}_4$  followed by acylation and then palladium-catalyzed borylation (Scheme 3-8 B), while **9c** was synthesized from 2-bromo-5-methoxy-1,3-dimethylbenzene via bromination followed by nucleophilic substitution by using  $\text{NaOAc}$  at last borylation (Scheme 3-8 C).



**Scheme 3-8.** Synthesis of **1c**, **9c**, and **12c**.

### 3.2.2. DNA cross-linking assay

The DNA cross-linking abilities of **9-12** were investigated by allowing them to react with 49-mer DNA duplex **5** in a phosphate buffer at 37 °C for 24 h. Initially, 2 mM drug with 2 mM H<sub>2</sub>O<sub>2</sub> were used for comparison of the reactivity. ICL formation and yields were analyzed via denaturing polyacrylamide gel electrophoresis (PAGE) with phosphorimage analysis (Image Quant 5.2). Apart from **10a**, most compounds (**9a**, **12a**, **12b**, **1c**, **9c** and **12c**) do not cross-link DNA in the absence of H<sub>2</sub>O<sub>2</sub>, but can be activated by H<sub>2</sub>O<sub>2</sub> inducing efficient ICL formation. DNA cross-linking products were not observed without H<sub>2</sub>O<sub>2</sub> but efficiently formed with H<sub>2</sub>O<sub>2</sub>, which indicated that these compounds can be selectively and efficiently activated by H<sub>2</sub>O<sub>2</sub> to induce DNA crosslinks.

5'-dGCCTAGTTCTTTTAATTACTTGCAATGCAAGTAATTAAAGCTTGATCTG (**5a**)  
 3'-dCGGATCAAGAAAATTAATGAACGTTACGTTTCATTAATTTGGAAGTAGAC (**5b**)

5

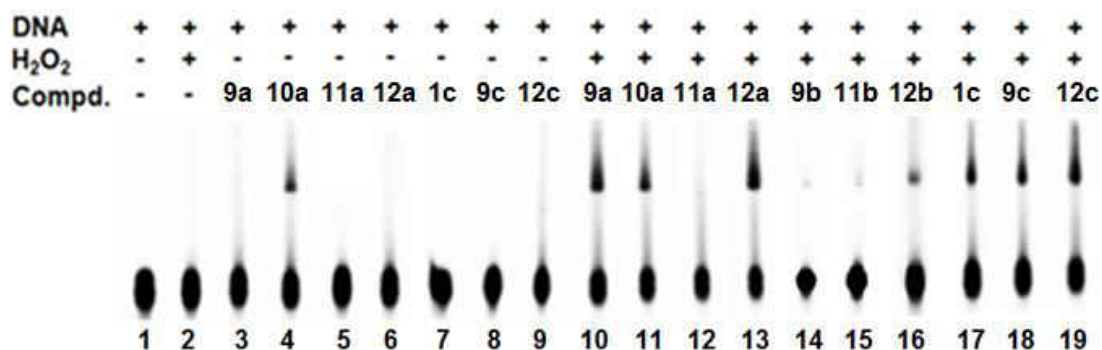


**Figure 3-1.** H<sub>2</sub>O<sub>2</sub>-induced DNA ICL formation by compounds **9-12**. Lane 1: DNA only (cross-linking yield 0%); lane 2: DNA with 100 μM H<sub>2</sub>O<sub>2</sub> (0%); lane 3: 2 mM **9a** (0%); lane 4: 2 mM **10a** (17%); lane 5: 2 mM **11a** (0%); lane 6: 2 mM **12a** (0%); lane 7: 2 mM **1c** (0%); lane 8: 2 mM **9c** (0%); lane 9: 2 mM **12c** (0%); lane 10-19 with H<sub>2</sub>O<sub>2</sub>: lane 10: 2 mM **9a** (34%); lane 11: 2 mM **10a** (20%); lane 12: 2 mM **11a** (0%); lane 13: 2 mM **12a** (42%); lane 14: 2 mM **9b** (0%); lane 15: 2 mM **11b** (0%); lane 16: 2 mM **12b** (5%); lane 17: 2 mM **1c** (21%); lane 18: 2 mM **9c** (26%); lane 19: 2 mM **12c** (32%). [H<sub>2</sub>O<sub>2</sub>] = 2 mM (Reaction mixture was incubated at 37 °C for 48 h in pH8 buffer).

### 3.2.3. The effect of substituents on the DNA cross-link formation

#### 3.2.3.1. The electron-donating group favors the ICL formation

In order to conduct a more detailed and systematic investigation about the substituent effects on ICL formation, we compared the stability and reactivity of **9a-11a** firstly. Comparing with **10a** (20%) and **11a** (0%), **9a** induced a much higher ICL yield (34%). 4,6-Dimethoxy compound **10a** is not stable and easily decomposed even at 0 °C, which might be one of the reasons for its low efficiency for DNA cross-linking. We did observe decomposition of **10a** during <sup>13</sup>C NMR

measurement though it was stable for  $^1\text{H}$  NMR measurement. In addition, compound **10a** did not show selectivity, which induced ICL formation even without  $\text{H}_2\text{O}_2$  (17%) (Figure 3-2), while the presence of  $\text{H}_2\text{O}_2$  only slightly increased the ICL yield of **10a** (20%). Obviously, the presence of two methoxy groups on the para position to methylene greatly enhanced the electrophilicity of  $\text{CH}_2\text{Br}$ . Although **11a** is more stable than **10a**, DNA cross-linking was not observed at pH 8 (Figure 3-3). However, we did observe that the ICL formation induced by **11a** strongly depended on the pH values. The acidic conditions resulted in higher ICL yields than neutral and basic conditions (Figure 3-6). Among these compounds, **9a** was the best  $\text{H}_2\text{O}_2$ -inducible ICL agent which is chemically stable. These results indicated that the position-4 that is *meta* to the QM methylene is an ideal site for further modification.

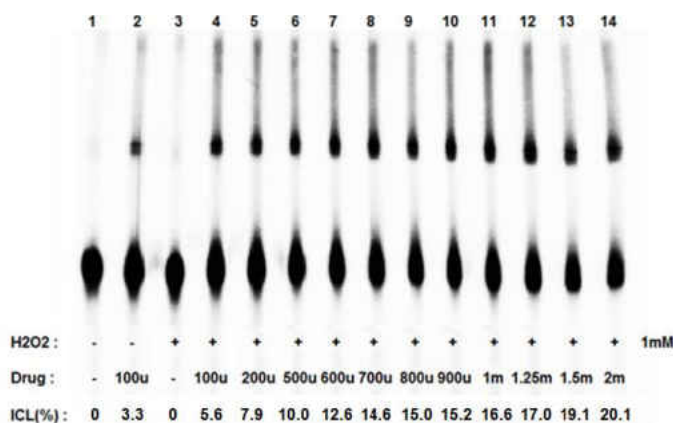


**Figure 3-2.** Compound/ $\text{H}_2\text{O}_2$  ratio dependence of ICL formation by **10a**. Phosphorimage autoradiogram of 20% denaturing PAGE analysis of **5** under varying concentration ratio of drug **10a** to  $\text{H}_2\text{O}_2$ . Condition: 37 °C incubation for 24 h at pH8.

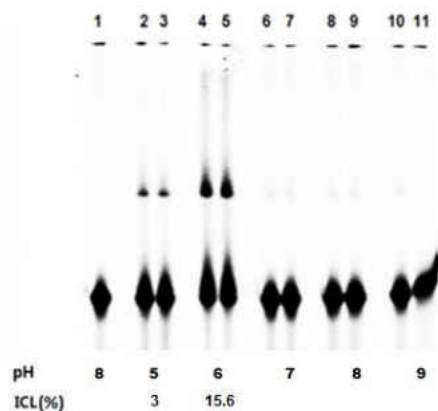


**Figure 3-3.** pH dependence of ICL formation by **11a**. Phosphorimage autoradiogram of 20% denaturing PAGE analysis of 2 mM **11a** with **5**. Condition: 37 °C incubation for 24 h.

Thus, we designed and synthesized **12a** with a hydroxyl group at the position-4 and investigated its reactivity toward DNA. As expected, **12a** is relatively stable and inert toward DNA, but can react with H<sub>2</sub>O<sub>2</sub> to form QMs that directly cross-link DNA (50 ± 5%). This provided another evidences that the electron-donating group on the position-4 favors the ICL formation. Further study showed that the cross-linking yield of **9a** and **12a** were affected by their concentrations, the compound/H<sub>2</sub>O<sub>2</sub> ratio, and the pH of the buffer solution. The best compound/H<sub>2</sub>O<sub>2</sub> ratio was 1:1 (Figure 3-4 and 3-7). The cross-linking yield increased as the concentration increasing (Figure 3-5 and 3-8). The cross-linking was more efficient under basic conditions than acidic conditions (Figure 3-6 and 3-9). All these results are consistent with previously study with other arylboronates (**1-4a** in Chapter 2).<sup>1,2</sup>

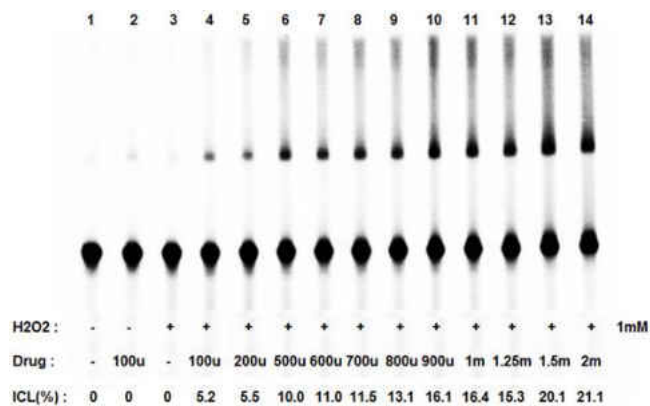


**Figure 3-4.** Compound/H<sub>2</sub>O<sub>2</sub> ratio dependence of ICL formation by **9a**. Phosphorimage autoradiogram of 20% denaturing PAGE analysis of **5** under varying concentration ratio of drug **9a** to H<sub>2</sub>O<sub>2</sub>. Condition: 37 °C incubation for 24 h at pH8.

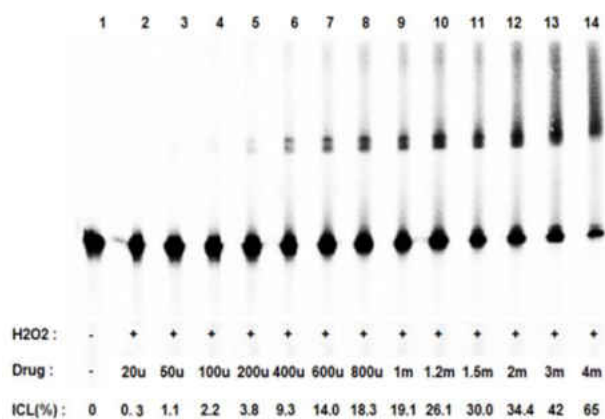


**Figure 3-5.** Concentration dependence of ICL formation by **9a**. Phosphorimage autoradiogram of 20% denaturing PAGE analysis of **5** with different concentration of **9a**. Condition: 37 °C incubation for 24 h at pH8.

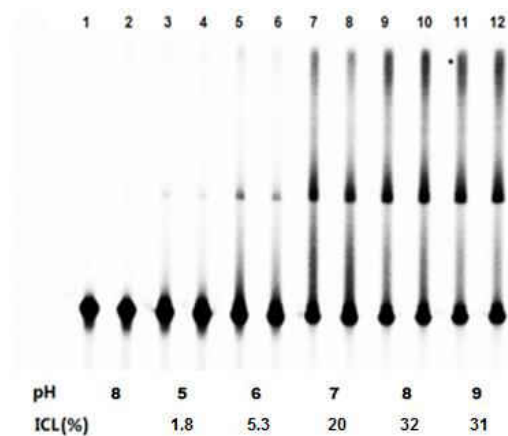


**Figure 3-6.** pH dependence of ICL formation by **9a**. Phosphorimage autoradiogram of 20% denaturing PAGE analysis of 2 mM **9a** with **5**. Condition: 37 °C incubation for 24 h.

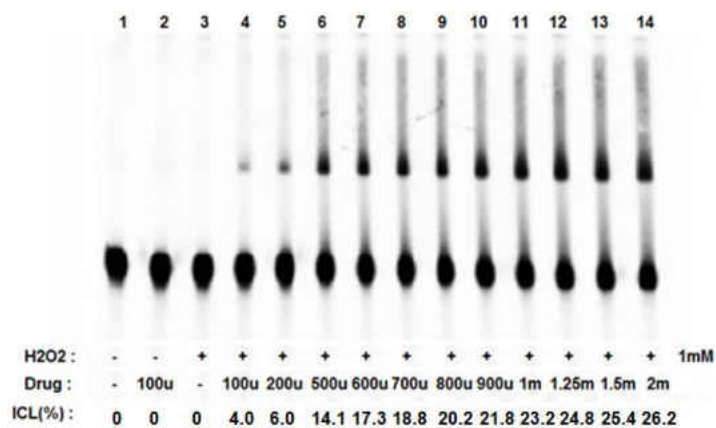


**Figure 3-7.** Compound/H<sub>2</sub>O<sub>2</sub> ratio dependence of ICL formation by **12a**. Phosphorimage autoradiogram of 20% denaturing PAGE analysis of **5** under varying concentration ratio of drug **12a** to H<sub>2</sub>O<sub>2</sub>. Condition: 37 °C incubation for 24 h at pH8.

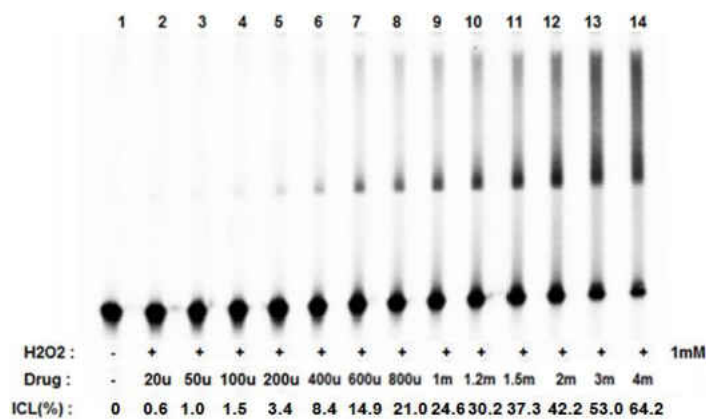


**Figure 3-8.** Concentration dependence of ICL formation by **12a**. Phosphorimage autoradiogram of 20% denaturing PAGE analysis of **5** with different concentration of **12a**. Condition: 37 °C incubation for 24 h at pH8.

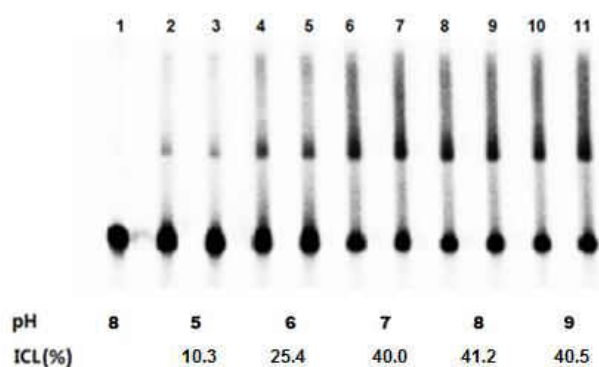


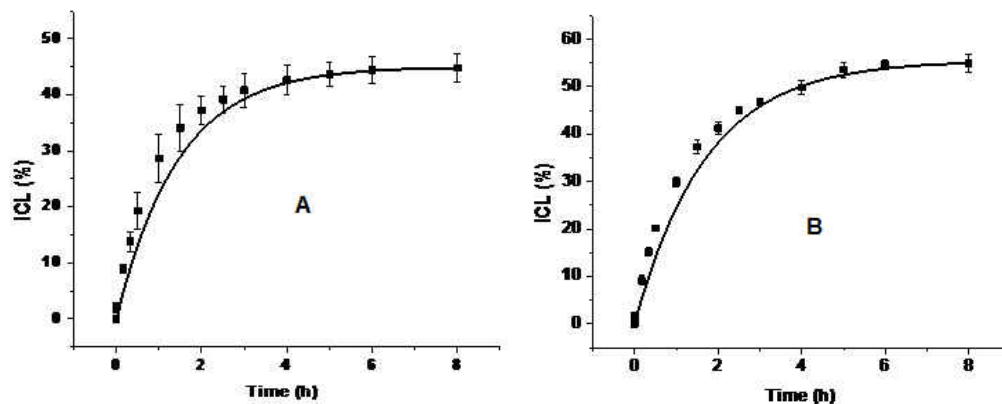
**Figure 3-9.** pH dependence of ICL formation by **12a**. Phosphorimage autoradiogram of 20% denaturing PAGE analysis of 2 mM **12a** with **5**. Condition: 37 °C incubation for 24 h.

### 3.2.3.2. The kinetics of ICL formation induced by **1a**, **9a** and **12a**

In order to fully investigate the effect of the aromatic substituents on DNA ICL formation, we studied the kinetics of DNA cross-linking and compared the rate constants for ICL formation induced by **1a**, **9a**, and **12a** (Table 3-1). The ICL growth induced by **9a** and **12a** followed first-order kinetics (Figure 3-10) which is similar to their parent compound **1a**. The rate constants for **9a** and **12a** with an electron-donating group were 2-3 times the rate constants for **1a**. This result



indicated that the electron-donating substituent greatly facilitated the ICL formation rate as well as enhanced the cross-linking yield.



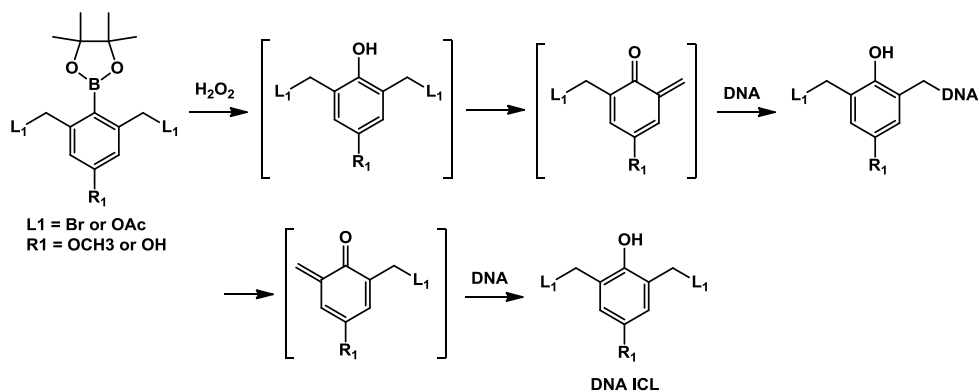
**Figure 3-10.** Kinetic rate of ICL formation from **5** upon treatment with bromides/ $\text{H}_2\text{O}_2$ . **A.** **9a** at time points 0, 5', 10', 20', 30', 1 h, 1.5 h, 2 h, 2.5 h, 3 h, 4 h, 5 h, 6 h, 8 h. [**9a**] = 2 mM, and [ $\text{H}_2\text{O}_2$ ] = 2 mM. **B.** **12a** at time points 0, 5', 10', 20', 30', 1 h, 1.5 h, 2 h, 2.5 h, 3 h, 4 h, 5 h, 6 h, 8 h. [**12a**] = 2 mM, and [ $\text{H}_2\text{O}_2$ ] = 2 mM. Reaction mixtures were incubated in 37 °C.

Table 3-1. Rate of ICL formation from **5** upon treatment with bromides.

compound	$k_{\text{obs}}, 10^{-5} \text{ s}^{-1}$	$t_{1/2}, \text{min}$	ICL(%)
<b>1a</b>	$8.8 \pm 1.3$	$130 \pm 13$	20
<b>9a</b>	$18.8 \pm 0.4$	$61 \pm 2$	40
<b>12a</b>	$25.1 \pm 0.5$	$46 \pm 1$	50

Previous studies showed that the mechanism of ICL formation induced by these arylboronates involved the generation of phenol intermediates followed by spontaneous release of QMs which is capable of cross-linking DNA. The QM formation is the rate-determining step for DNA cross-

linking (Scheme 3-9). A similar mechanism was proposed for compounds **9a** and **12a**, which was supported by QM-trapping reaction by using large excess of EVE.



**Scheme 3-9.** The mechanism of  $\text{H}_2\text{O}_2$ -induced ICL formation.

In order to investigate the effect of electron-donating group on both formation of the phenol intermediates and QM generation, we determined the rate constant of these compounds with  $\text{H}_2\text{O}_2$  by NMR analysis (Figure 3-11 and 3-12). We used a mixture of phosphate buffer (pH8 in  $\text{D}_2\text{O}$ ) and DMSO in a 2:3 ratio for the NMR kinetic study to ensure good solubility of the compounds and analogs in the DNA cross-linking reaction condition.

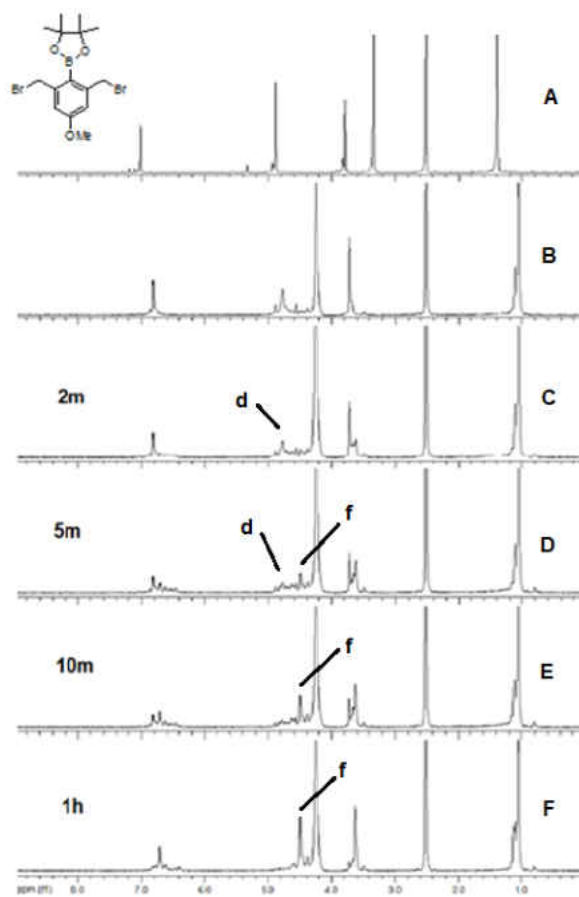


**Figure 3-11.**  $^1\text{H}$  NMR analysis of **9a** in deuterated DMSO,  $\text{D}_2\text{O}$ , and  $\text{H}_2\text{O}_2$ : (A)  $^1\text{H}$  NMR of **9a** (0.003 mmol) in DMSO without addition of  $\text{D}_2\text{O}$  and  $\text{H}_2\text{O}_2$ ; (B) After 4 h in a mixture of DMSO (300  $\mu\text{L}$ ),  $\text{D}_2\text{O}$  (20  $\mu\text{L}$ ), and pH8 buffer (10  $\mu\text{L}$ ); additional DMSO (60  $\mu\text{L}$ ) and  $\text{D}_2\text{O}$  (210  $\mu\text{L}$ ) were added into the reaction mixture. (C) 2 min after addition of  $\text{H}_2\text{O}_2$  (1.5 equiv.) in the reaction mixture from step (B); (D) 5 min after addition of  $\text{H}_2\text{O}_2$ ; (E) 10 min after addition of  $\text{H}_2\text{O}_2$ ; (F) 1 h after addition of  $\text{H}_2\text{O}_2$ . [**d** represents the benzylic methylene proton of the hydrolysis product (the corresponding boronic acid) of the boronate ester **9a**; **f** represents the benzylic methylene proton of the final product obtained from the hydrolysis of the QM.]

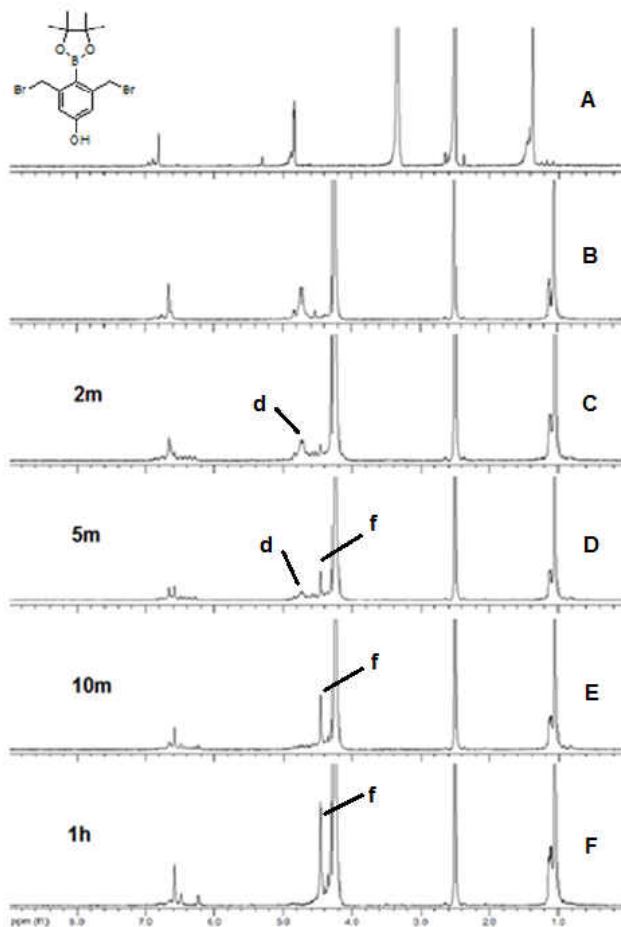


**Figure 3-12.** <sup>1</sup>H NMR analysis of **12a** in deuterated DMSO, D<sub>2</sub>O, and H<sub>2</sub>O<sub>2</sub>: (A) <sup>1</sup>H NMR of **12a** (0.003 mmol) in DMSO without addition of D<sub>2</sub>O and H<sub>2</sub>O<sub>2</sub>; (B) After 4 h in a mixture of DMSO (300 μL), D<sub>2</sub>O (20 μL), and pH8 buffer (10 μL); additional DMSO (60 μL) and D<sub>2</sub>O (210 μL) were added into the reaction mixture. (C) 2 min after addition of H<sub>2</sub>O<sub>2</sub> (1.5 equiv.) in the reaction mixture from step (B); (D) 5 min after addition of H<sub>2</sub>O<sub>2</sub>; (E) 10 min after addition of H<sub>2</sub>O<sub>2</sub>; (F) 1 h after addition of H<sub>2</sub>O<sub>2</sub>.

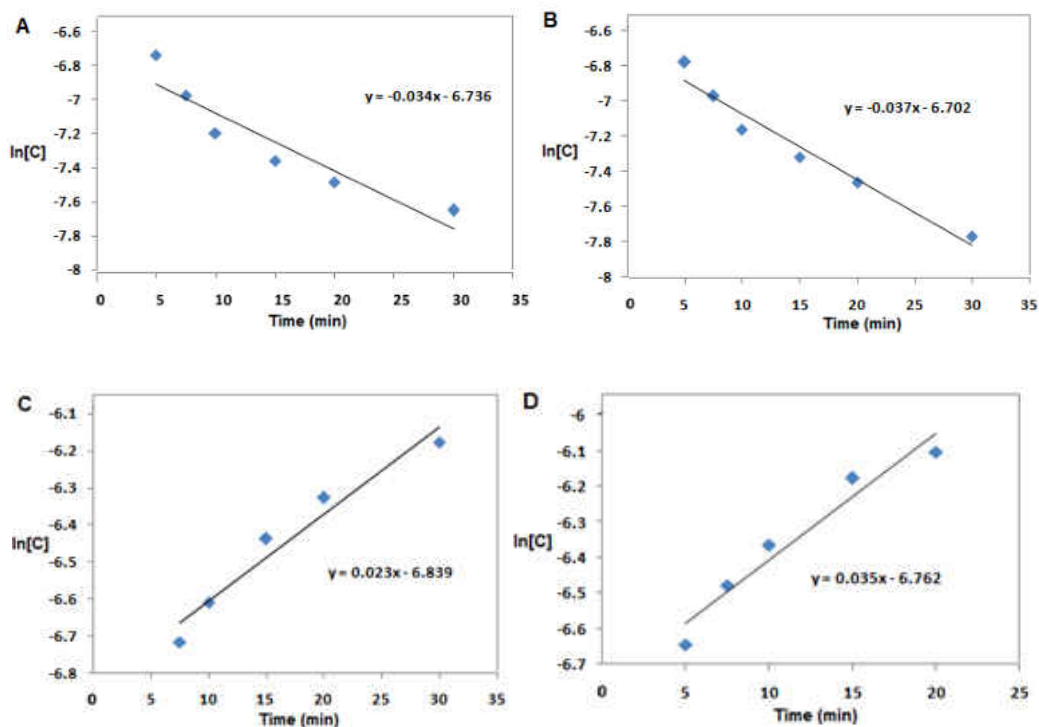


**Figure 3-13.** Rate constant for the disappearance of starting material (**A** and **B**) and the formation of hydrolyzed product (**C** and **D**) in NMR analysis with 360  $\mu\text{L}$  DMSO and 240  $\mu\text{L}$  pH 8 buffer: **A.** **9a** (0.003 mmol) with  $\text{H}_2\text{O}_2$  (1.5 equiv) at time points 5', 7.5', 10', 15', 20', 30'. **B.** **12a** (0.003 mmol) with  $\text{H}_2\text{O}_2$  (1.5 equiv) at time points 5', 7.5', 10', 15', 20', 30'. **C.** **9a** (0.003 mmol) with  $\text{H}_2\text{O}_2$  (1.5 equiv) at time points 7.5', 10', 15', 20', 30'. **D.** **12a** (0.003 mmol) with  $\text{H}_2\text{O}_2$  (1.5 equiv) at time points 5', 7.5', 10', 15', 20'.

The relative rate for the phenol intermediate formation was evaluated by the disappearance of the peaks at about 5.0 ppm (peak d) corresponding to  $-\text{CH}_2-$  of the precursors. The relative reaction rates of these compounds with  $\text{H}_2\text{O}_2$  were in the order of **12a**  $\geq$  **9a**  $>$  **1a** (Table 3-2). In comparison with **1a**, there was no obviously increase for the rate of phenol intermediate formation for **9a** and **12a**. The relative rates of QM formation were estimated by the formation of the final products (peak f, its hydrolyzed compounds), which showed a similar trend: **12a**  $>$  **9a**  $>$  **1a** (Table 3-2). The rate of QM formation for **4a** is around 6 times the rate of **1a** and **9a** is about

4 times of **1a**. However, the rate of QM formation is generally slower than that of generation of the corresponding phenol intermediates. All these results indicated that QM formation is still the rate-determining step for DNA cross-linking. The kinetic data for QM formation showed a similar trend to that of DNA ICL formation (**12a** > **9a** > **1a**) (Table 3-1), which provided further evidences for that the electron-donating groups greatly facilitate QM formation as well as DNA ICL formation.

**Table 3-2.** Rate of starting material disappearance and QM formation.

Compounds	Disappearance of starting materials		QM formation	
	Time of completion (min)	$k_{obs}$ ( $10^{-5} \text{ s}^{-1}$ )	Time of completion (min)	$k_{obs}$ ( $10^{-5} \text{ s}^{-1}$ )
<b>1a</b>	60	39.0	60	9.5
<b>9a</b>	60	56.7	60	38.3
<b>12a</b>	60	61.7	60	58.3

#### 3.2.4. The effect of leaving group on the DNA cross-link formation

Compounds **9b** and **12b** bearing  $\text{NMe}_3$  as leaving group were not good ICL agents. **9b** can only induced a little ICL formation if extend the incubation time to 3 d (Figure 3-14). A low ICL yield (5%) was observed for **12b** when it was incubated with DNA duplex **5** for 1 d at  $37^\circ\text{C}$  in the presence of  $\text{H}_2\text{O}_2$  (Figure 3-1 lane 16). The NMR analysis of **9b** showed that there was tiny amount trimethylamine formation after 1d (Figure 3-15 D) which indicated that the phenol intermediate could not further convert to QM. For **12b** only around 15% of the phenol products release trimethylamine leaving group to generate final product. These results demonstrated that

the NMe<sub>3</sub> is a poor leaving group for ICL formation even introduced the electron-donating substituent in it.

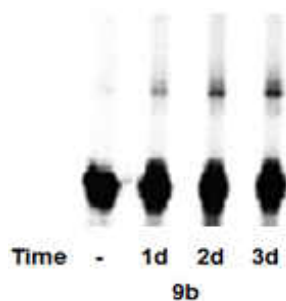


**Figure 3-14.** ICL formation induced by **9b** by extend the incubation time to 3 days.

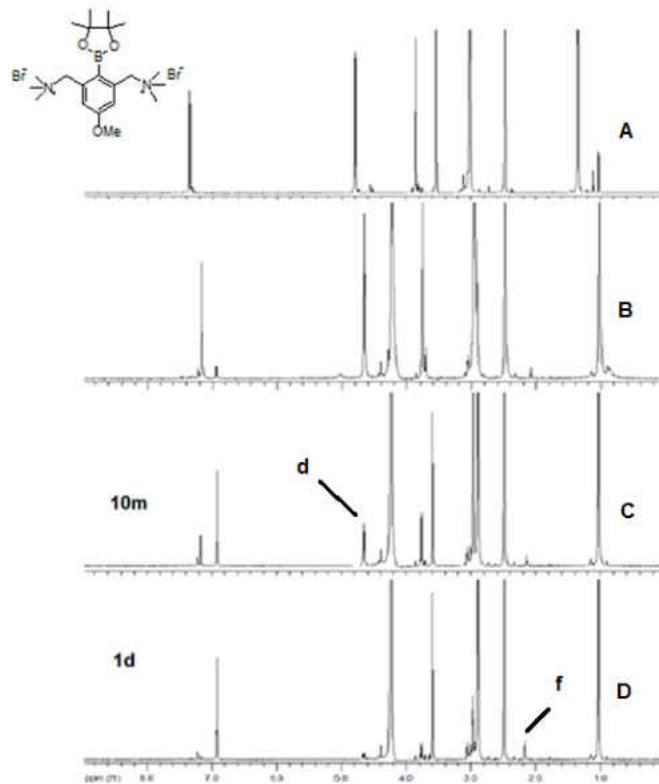


**Figure 3-15.** <sup>1</sup>H NMR analysis of **9b** in deuterated DMSO, D<sub>2</sub>O, and H<sub>2</sub>O<sub>2</sub>: (A) <sup>1</sup>H NMR of **9b** (0.003 mmol) in DMSO without addition of D<sub>2</sub>O and H<sub>2</sub>O<sub>2</sub>; (B) After 4 h in a mixture of DMSO (300 μL), D<sub>2</sub>O (20 μL), and pH8 buffer (10 μL); additional DMSO (60 μL) and D<sub>2</sub>O (210 μL)

were added into the reaction mixture. (C) 10 min after addition of H<sub>2</sub>O<sub>2</sub> (1.5 equiv.) in the reaction mixture from step (B); (D) 1 day after addition of H<sub>2</sub>O<sub>2</sub>.

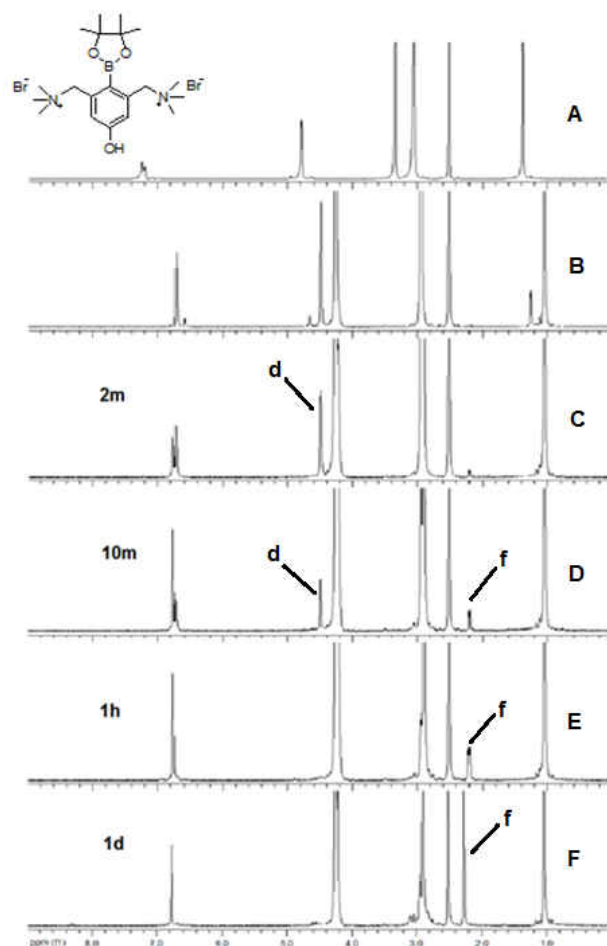


**Figure 3-16.** <sup>1</sup>H NMR analysis of **12b** in deuterated DMSO, D<sub>2</sub>O, and H<sub>2</sub>O<sub>2</sub>: (A) <sup>1</sup>H NMR of **12b** (0.003 mmol) in DMSO without addition of D<sub>2</sub>O and H<sub>2</sub>O<sub>2</sub>; (B) After 4 h in a mixture of DMSO (300 μL), D<sub>2</sub>O (20 μL), and pH8 buffer (10 μL); additional DMSO (60 μL) and D<sub>2</sub>O (210 μL) were added into the reaction mixture. (C) 2 min after addition of H<sub>2</sub>O<sub>2</sub> (1.5 equiv.) in the reaction mixture from step (B); (D) 10 min after addition of H<sub>2</sub>O<sub>2</sub>; (E) 1 h after addition of H<sub>2</sub>O<sub>2</sub>; (F) 1 d after addition of H<sub>2</sub>O<sub>2</sub>.

The acetate group was used as a good leaving group in a number of inducible DNA cross-linking agents developed in the research groups of Freccero, Rokita and Greenberg's. We expected that



the arylboronic esters with OAc as benzylic leaving group could be an efficient H<sub>2</sub>O<sub>2</sub>-inducible ICL agent. A series of arylboronic esters **1c**, **9c** and **12c** containing OAc as the leaving groups were successfully synthesized and their cross-linking ability was investigated. As expected, these compounds can be activated by H<sub>2</sub>O<sub>2</sub> to form DNA ICLs. However, the cross-linking yields of **1c**, **9c**, and **12c** (25%, 30% and 35%) are less than the corresponding bromides **1a**, **9a**, and **12a** (25%, 40%, and 50%). Further study showed that ICL formation induced by **1c**, **9c**, and **12c** did not follow the first order kinetics (Figure 3-17) and the cross-linking yield did not correlate well with the reaction rates (Table 3-3). One of the possible reasons is the hydrolysis of the acetate under the conditions used for DNA cross-linking study. In order to test our hypothesis, the NMR analysis was performed with **9c** and **12c** in a mixture of phosphate buffer (pH8 in D<sub>2</sub>O) and DMSO in a 2:3 ratio. The results showed that the acetate group was hydrolyzed prior to addition of H<sub>2</sub>O<sub>2</sub> (Figure 3-18 and 3-19 B), which should be one of the reasons leading to a low ICL yield for **9c** and **12c**. We also observed that the reactivity of **9c** and **12c** with H<sub>2</sub>O<sub>2</sub> was much slower than **9a** and **12a**. However, due to the complexity of the reactions, the rate constants could not be estimated. The reaction of **9a** and **12a** with H<sub>2</sub>O<sub>2</sub> was complete within 30 min for **9a** and 20 min for **12a**, while only 65% of **9c** and 50% of **12c** reacted with H<sub>2</sub>O<sub>2</sub> within 1 hour (Figure 3-11 and 3-12 E, F) (Figure 3-18 and 3-19 E). The possible reason for the slower reaction of **9c** and **12c** towards H<sub>2</sub>O<sub>2</sub> is formation of the hypercoordinated complexes (Scheme 3-10) caused by the interaction between the oxygen of OAc and the trigonal boron. All of the above observations suggested that the acetate group was not a good leaving group for designing novel arylboronic esters as efficient H<sub>2</sub>O<sub>2</sub>-inducible cross-linking agents.

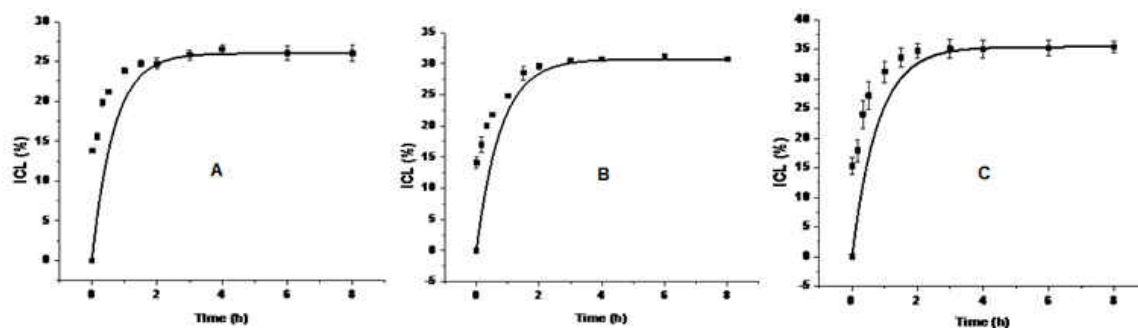


**Figure 3-17.** Kinetic rate of ICL formation from **5** upon treatment with bromides/ $\text{H}_2\text{O}_2$ . **A.** **1c** at time points 0, 5', 10', 20', 30', 1 h, 1.5 h, 2 h, 3 h, 4 h, 6 h, 8 h. [**1c**] = 2 mM, and [ $\text{H}_2\text{O}_2$ ] = 2 mM. **B.** **9c** at time points 0, 5', 10', 20', 30', 1 h, 1.5 h, 2 h, 3 h, 4 h, 6 h, 8 h. [**9c**] = 2 mM, and [ $\text{H}_2\text{O}_2$ ] = 2 mM. **C.** **12c** at time points 0, 5', 10', 20', 30', 1 h, 1.5 h, 2 h, 3 h, 4 h, 6 h, 8 h. [**12c**] = 2 mM, and [ $\text{H}_2\text{O}_2$ ] = 2 mM. Reaction mixtures were incubated in 37 °C.

**Table 3-3.** Kinetics of ICL formation and monomer reaction.

Comps	Kinetics of ICL formation			Kinetics of monomer reaction	
	Rate constant $k_{obs}(10^{-5} \text{ s}^{-1})$	$t_{1/2}, \text{min}$	ICL(%)	Disappearance of starting materials $k_{obs}(10^{-5} \text{ s}^{-1})$	QM formation $k_{obs}(10^{-5} \text{ s}^{-1})$
<b>1c</b>	$52.1 \pm 1.1$	$22 \pm 1$	$25 \pm 2$	19.4	n.d.
<b>9c</b>	$41.1 \pm 0.8$	$28 \pm 1$	$30 \pm 3$	9.1	n.d.
<b>12c</b>	$26.8 \pm 0.7$	$43 \pm 1$	$35 \pm 4$	8.3	n.d.

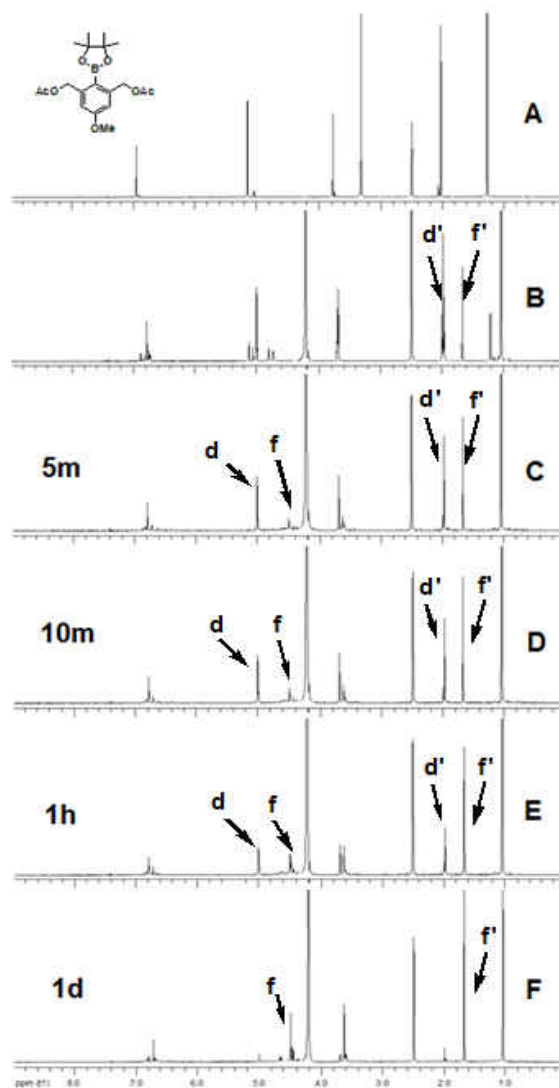


**Figure 3-18.**  $^1\text{H}$  NMR analysis of **9c** in deuterated DMSO,  $\text{D}_2\text{O}$ , and  $\text{H}_2\text{O}_2$ : (A)  $^1\text{H}$  NMR of **9c** (0.003 mmol) in DMSO without addition of  $\text{D}_2\text{O}$  and  $\text{H}_2\text{O}_2$ ; (B) After 4 h in a mixture of DMSO (300  $\mu\text{L}$ ),  $\text{D}_2\text{O}$  (20  $\mu\text{L}$ ), and pH8 buffer (10  $\mu\text{L}$ ); additional DMSO (60  $\mu\text{L}$ ) and  $\text{D}_2\text{O}$  (210  $\mu\text{L}$ ) were added into the reaction mixture. (C) 5 min after addition of  $\text{H}_2\text{O}_2$  (1.5 equiv.) in the reaction mixture from step (B); (D) 10 min after addition of  $\text{H}_2\text{O}_2$ ; (E) 1 h after addition of  $\text{H}_2\text{O}_2$ ; (F) 1 d after addition of  $\text{H}_2\text{O}_2$ .

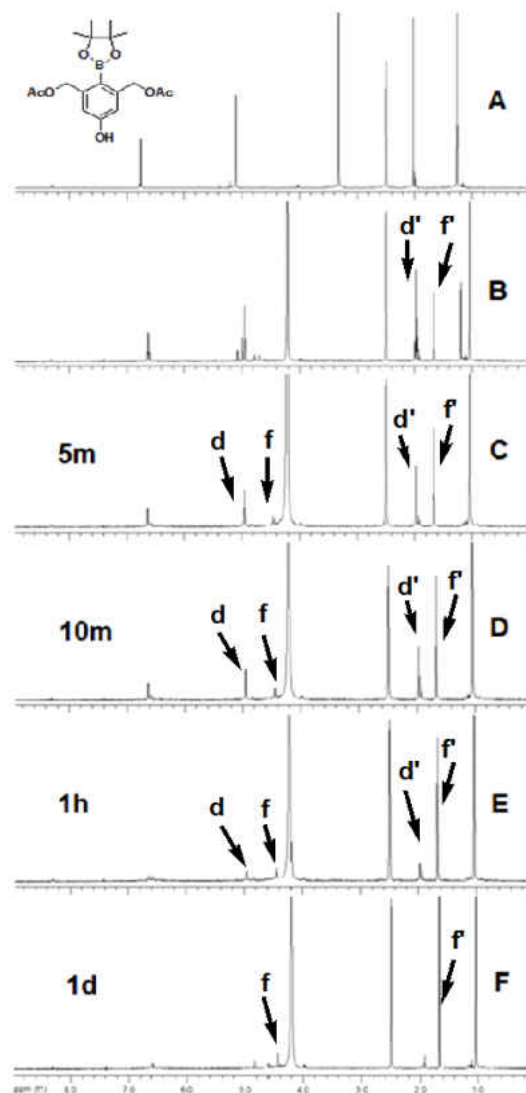
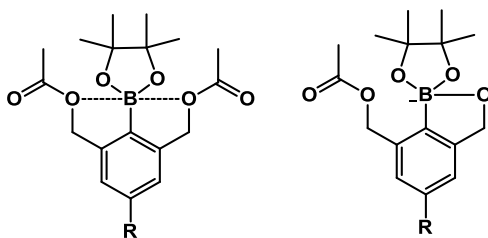


**Figure 3-19.** <sup>1</sup>H NMR analysis of **12c** in deuterated DMSO, D<sub>2</sub>O, and H<sub>2</sub>O<sub>2</sub>: (A) <sup>1</sup>H NMR of **12c** (0.003 mmol) in DMSO without addition of D<sub>2</sub>O and H<sub>2</sub>O<sub>2</sub>; (B) After 4 h in a mixture of DMSO (300 μL), D<sub>2</sub>O (20 μL), and pH8 buffer (10 μL); additional DMSO (60 μL) and D<sub>2</sub>O (210 μL) were added into the reaction mixture. (C) 5 min after addition of H<sub>2</sub>O<sub>2</sub> (1.5 equiv.) in the reaction mixture from step (B); (D) 10 min after addition of H<sub>2</sub>O<sub>2</sub>; (E) 1 h after addition of H<sub>2</sub>O<sub>2</sub>; (F) 1 d after addition of H<sub>2</sub>O<sub>2</sub>.



**Scheme 3-10.** Hypercoordination of arylboronic derivatives.

### 3.3. Cytotoxicity of **9a** and **12a** towards cancer cell lines

Having established that **9a** and **12a** could be effectively activated by  $H_2O_2$  to induce efficient ICL formation, their toxicity towards cancer cells was evaluated in biological systems. Initially, the ability of **1a** and **9a** for inhibiting cancer cell growth was determined with 60 human cancer cell lines by National Cancer Institute DTP program. Single dose screening with 10  $\mu M$  of **9a** induced significant growth inhibition of most cancer cell lines (Figure 3-21), which showed **9a** was more toxic than **1a** (Figure 3-20). The growth percentage of most cell lines treated with 10  $\mu M$  of **9a** was less than 50%. Thus, the GI50 of **9a** was further evaluated in 60 human cancer cell lines panel by five concentration levels. Compound **9a** showed a GI50 of 2  $\mu M$  in most cancer cells (Table 3-4). The result showed that **9a** is a potent anticancer prodrug that can be used as a lead compound for further development.

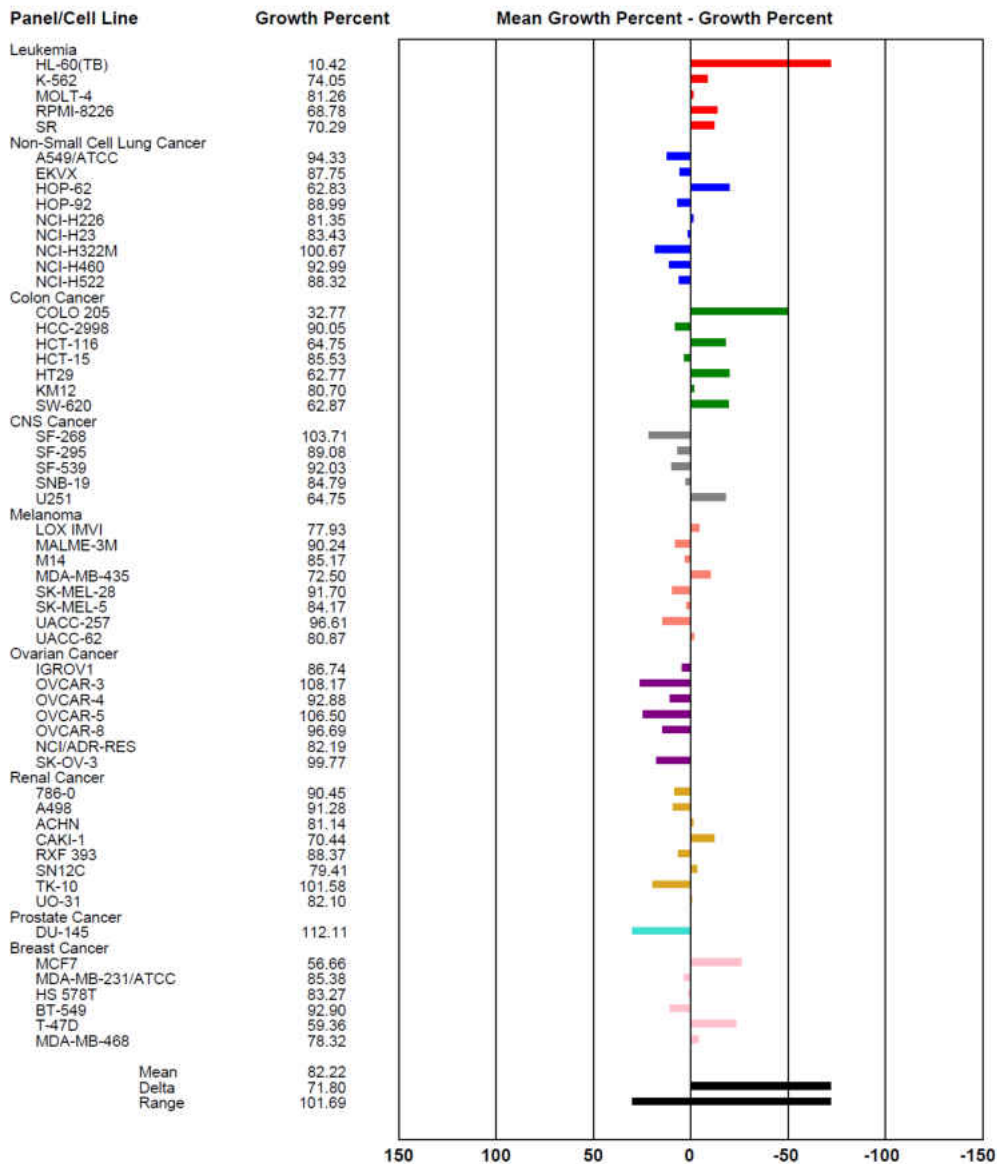


**Figure 3-20.** Cytotoxicity of compound **1a** towards 60 human tumor cell lines. Each cell line was grown in two plates and treated with drug (10  $\mu$ M) for 48 h at 37  $^{\circ}$ C, 5% CO<sub>2</sub>, 95% air, and 100% relative humidity. The growth percent was determined by NCI-60 DTP Human Tumor Cell Line Screen.

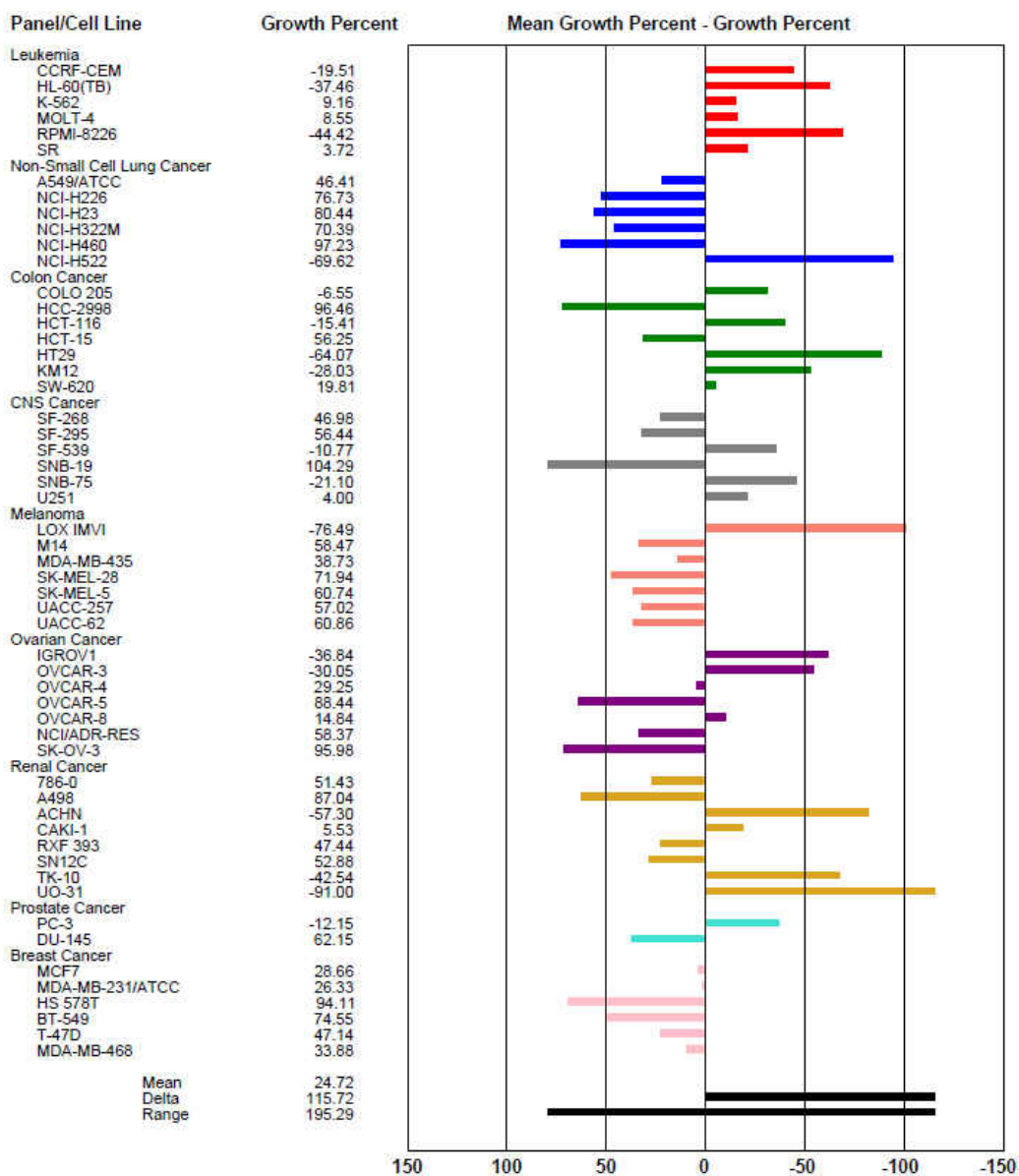


**Figure 3-21.** Cytotoxicity of compound **9a** towards 60 human tumor cell lines. Each cell line was grown in two plates and treated with drug (10  $\mu$ M) for 48 h at 37  $^{\circ}$ C, 5% CO<sub>2</sub>, 95% air, and 100% relative humidity. The growth percent was determined by NCI-60 DTP Human Tumor Cell Line Screen.

**Table 3-4.** The Cytotoxicity of **9a** in 60 cell lines.

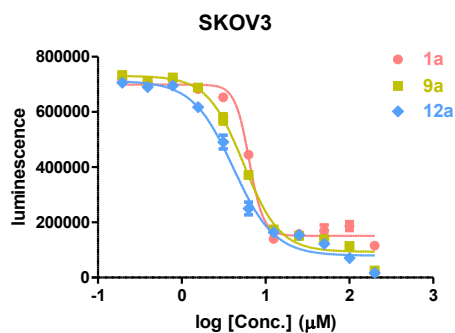
Tumor type	Cell line	GI <sub>50</sub> (μM)
leukemia	CCRF-CEM	2.12
	HL-60(TB)	2.01
	K-562	2.75
	MOLT-4	2.70
	RPMI-8226	2.23
	SR	2.27
Non-Small Cell Lung Cancer	A549/ATCC	3.10
	HOP-62	2.10
	HOP-92	1.52
	NCI-H226	3.09
	NCI-H23	2.14
	NCI-H322M	5.64
	NCI-H460	3.38
	NCI-H522	1.66
Colon Cancer	COLO 205	2.08
	HCC-2998	6.12
	HCT-116	1.80
	HCT-15	2.37
	HT29	2.13
	KM12	2.15
	SW-620	2.07
CNS Cancer	SF-268	2.31
	SF-295	1.82
	SF-539	1.70
	SNB-19	4.89
	SNB-75	1.64
	U251	2.68
Melanoma	LOX IMVI	1.81
	MALME-3M	1.99
	M14	1.97
	MDA-MB-435	1.89
	SK-MEL-2	2.18
	SK-MEL-28	1.82
	SK-MEL-5	2.29
	UACC-62	2.13
Ovarian Cancer	IGROV1	2.51



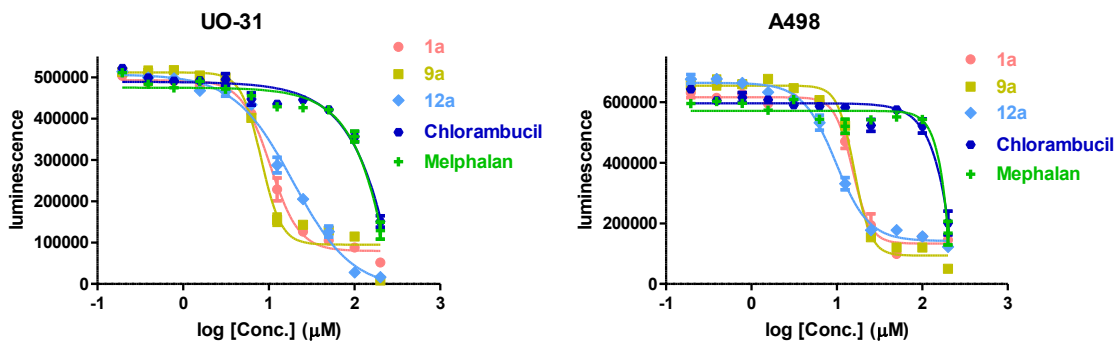
	OVCAR-3	1.96
	OVCAR-4	3.33
	OVCAR-5	2.08
	OVCAR-8	3.33
	NCI/ADR-RES	3.44
	SK-OV-3	4.97
Renal Cancer	786-0	2.08
	A498	12.0
	ACHN	1.82
	CAKI-1	1.85
	RXF 393	1.79
	SN12C	1.79
	TK-10	1.92
	UO-31	1.68
Prostate Cancer	PC-3	1.85
	DU-145	2.77
Breast Cancer	MCF7	2.45
	MDA-MB-231/ATCC	2.11
	HS 578T	2.85
	BT-549	1.92
	T-47D	2.03
	MDA-MB-468	1.80

Encouraged by the NCI results, we compared the cytotoxicity of these compounds in a few cancer cell lines, such as ovarian cancer SKOV3 cell, breast cancer MDA-MB-468 cell, and seven renal cancer cell lines. The initial test with SKOV3 cells showed that no cytotoxicity was observed with **1c**, **9c**, and **11a**, while compounds **1a**, **9a**, and **12a** led to cancer cell apoptosis with an IC<sub>50</sub> of 6.3  $\mu$ M for **1a**, 5.2  $\mu$ M for **9a**, 3.8  $\mu$ M for **12a** (Figure 3-22). Therefore, we focused on the active compounds **1a**, **9a**, and **12a** and compared their cytotoxicity with two clinically used alkylating agents: chlorambucil and melphalan. The breast cancer MDA-MB-468 cell and seven different renal cancer cell lines, UO-31, A498, SN12C, 786-0, TK-10, CAKI-1 and ACHN, have been tested. In general, **1a**, **9a**, and **12a** showed a higher cytotoxicity than

chlorambucil and melphalan in these cell lines. Additionally, **9a** is more toxic than **1a** and **12a** in most cell lines except for CAKI-1 cells which are more sensitive toward **12a** than toward **1a** and **9a** (Table 3-4). Among the cell lines tested, MDA-MB-468 cells are the most sensitive ones towards these H<sub>2</sub>O<sub>2</sub>-activated QM prodrugs. Among different renal cancer cell lines, compounds **1a**, **9a**, and **12a** are more cytotoxic to UO-31, A498, SN12C and 786-0 (IC<sub>50</sub> of 7.7 μM - 27.8 μM) than TK-10, CAKI-1 and ACHN (Figure 3-23 and Table 3-4). All these result demonstrated that **9a** and **12a** are the potent anticancer prodrugs which will be useful for future design. Further study to evaluate the *in vivo* activity and the mechanism of action are under-going.



**Figure 3-22.** Cytotoxicity of **1a**, **9a** and **12a** toward ovarian cell line SKOV3.



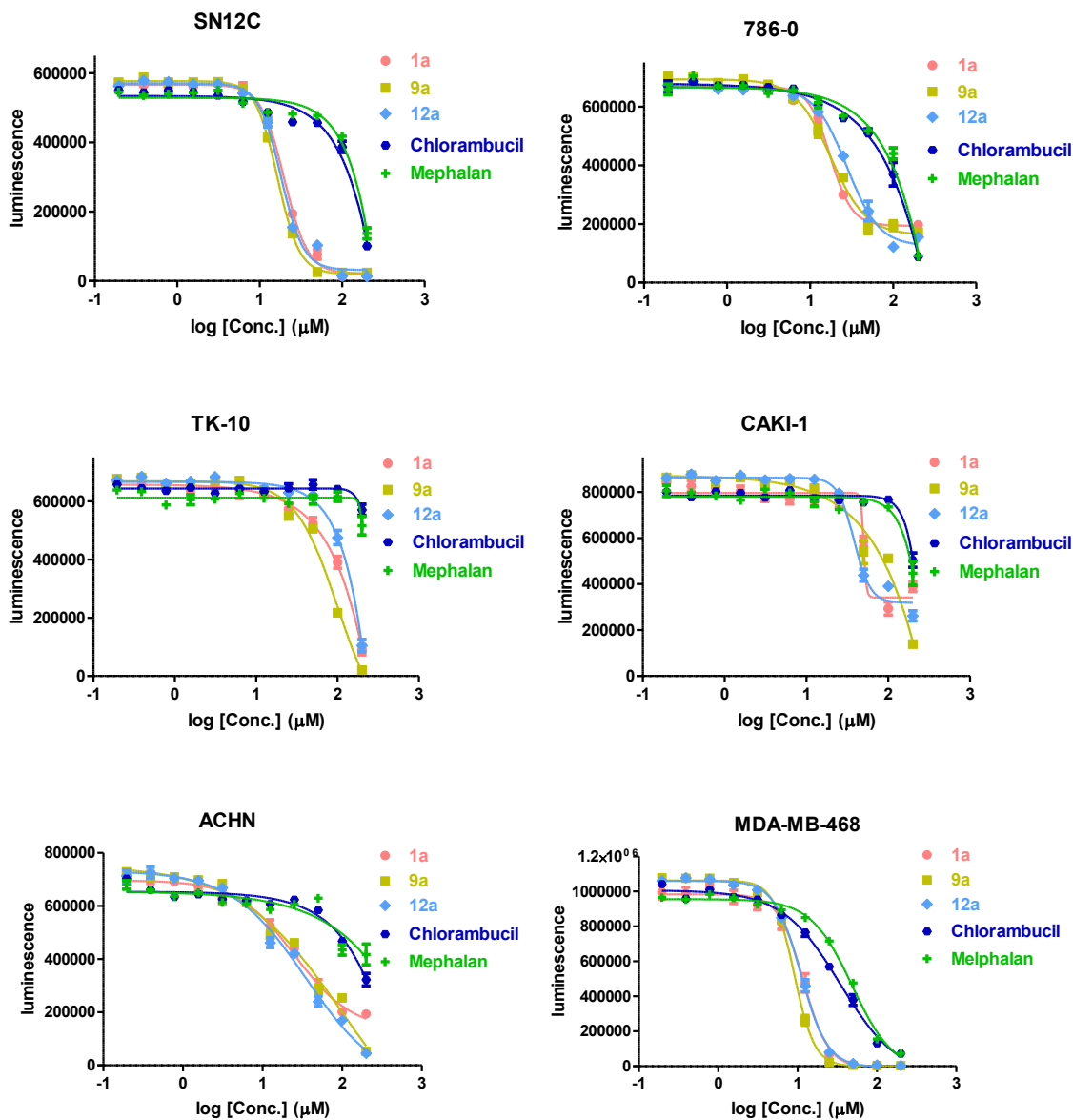


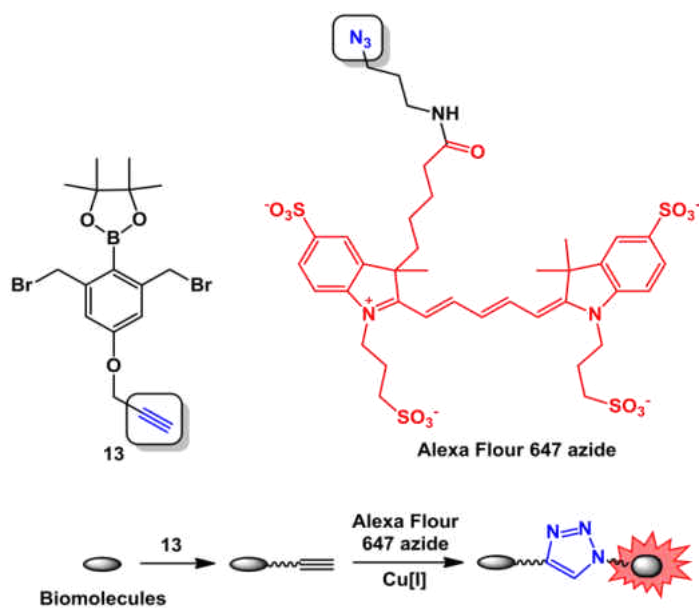
**Figure 3-23.** Cytotoxicity of **1a**, **9a** and **12a** toward renal cell lines and breast cell line MDA-MB-468.

**Table 3-5.** IC<sub>50</sub> of **1a**, **9a** and **12a** toward renal and breast cell lines.

Tumor type	Cell line	IC <sub>50</sub> ( $\mu$ M)				
		1a	9a	12a	Chlorambucil	Melphalan
renal cancer	UO-31	25.3	10.8	19.5	40.7	42.9
	A498	33.3	18.1	21	280	135
	SN12C	27.0	18.6	24.4	135	71
	786-0	20.3	10.8	27.8	55.5	19.2
	TK-10	21.4	16.2	35.4	n.d.	54.5
	ACHN	26.9	20.0	35.7	133	52.1
	CAKI-1	50.3	n.d.	38.3	n.d.	n.d.
breast cancer	MBA-MB-468	11.9	9.0	11.0	34.4	48.7

### 3.4. Identification of biological quinone methide prodrug targets

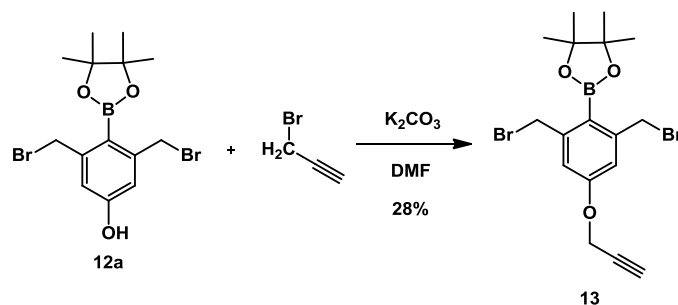
To identify the molecular targets of this class of produgs (such as DNA, RNA, or protein), we designed and synthesized an acetylene-modified quinone methide prodrug **13**. Biomolecules reactin with **13** can be modified with azide-modified fluorophores such as Alexa Flour 647 azide by a “click” reaction. (Scheme 3-11)



**Scheme 3-11.** Structure of **13** and Alexa Fluor 647 azide and a scheme of a pull-down reaction using Cu[I]-catalyzed azides-alkynes cycloaddition.

### 3.4.1. Synthesis and DNA cross-linking study with alkyne-modified arylboronic ester **13**

Compound **13** was directly synthesized from alkylation of **12a** using propargyl bromide (Scheme 3-12). The DNA cross-linking ability of **13** was investigated by using the 49-mer DNA duplex **5**. Similar to **12a**, compound **13** can be activated by H<sub>2</sub>O<sub>2</sub> to induce efficient ICL formation. The cross-linking yield was dependent on the compound/H<sub>2</sub>O<sub>2</sub> ratio, drug concentration, and the pH of the buffer solution (Figure 3-24 to 3-26). The ICL growth induced by **13** followed first-order kinetics (Figure 3-27) with a rate of  $k_{\text{obs}} = 18.9 \pm 0.3 \times 10^{-5} \text{ s}^{-1}$ , and  $t_{1/2} = 61 \pm 1 \text{ min}$ . The ICL yield was around  $55 \pm 5\%$  which was similar to compounds **9a** and **12a**. These results demonstrated that **13** is an efficient H<sub>2</sub>O<sub>2</sub>-activated DNA cross-linking agent, which can serve as a probe for identifying biological targets for these QM prodrugs.



**Scheme 3-12.** Synthesis of **13**.

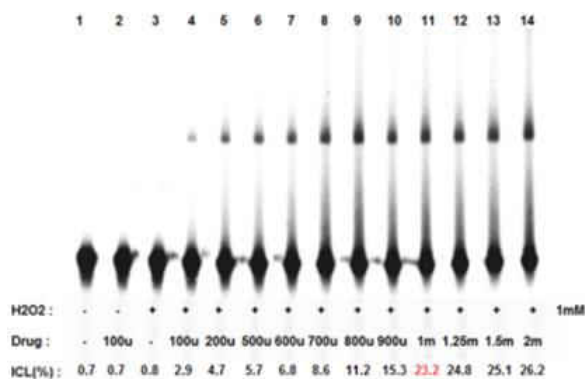


**Figure 3-24.** Compound/ $\text{H}_2\text{O}_2$  ratio dependence of ICL formation by **13**. Phosphorimage autoradiogram of 20% denaturing PAGE analysis of **5** under varying concentration ratio of drug **13** to  $\text{H}_2\text{O}_2$ . Condition: 37 °C incubation for 24 h at pH8.

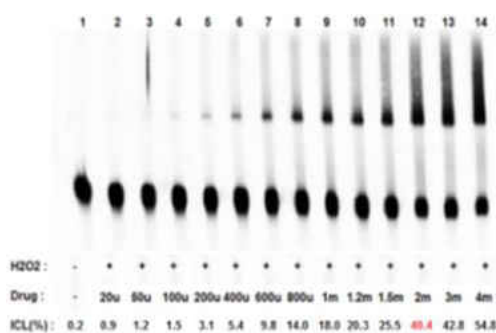


**Figure 3-25.** Concentration dependence of ICL formation by **13**. Phosphorimage autoradiogram of 20% denaturing PAGE analysis of **5** with different concentration of **13**. Condition: 37 °C incubation for 24 h at pH8.

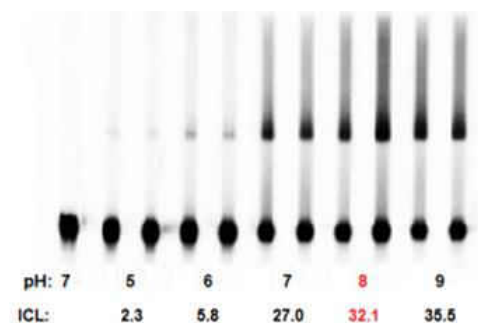


**Figure 3-26.** pH dependence of ICL formation by **13**. Phosphorimage autoradiogram of 20% denaturing PAGE analysis of 2 mM **13** with **5**. Condition: 37 °C incubation for 24 h.

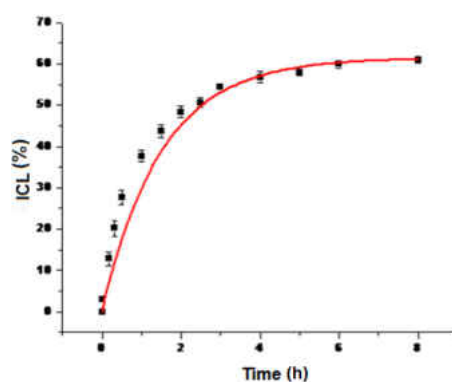


**Figure 3-27.** Kinetic rate of ICL formation from **5** upon treatment with **13**/ $\text{H}_2\text{O}_2$ . **13** at time points 0, 5', 10', 20', 30', 1 h, 1.5 h, 2 h, 2.5 h, 3 h, 4 h, 5 h, 6 h, 8 h. [**13**] = 2 mM, and [ $\text{H}_2\text{O}_2$ ] = 2 mM. Reaction mixtures were incubated in 37 °C.

### 3.4.2. Fluorescence detection of **13**-labelled DNA

Have successfully synthesized **13** containing an alkyne group and proved that it can efficiently induce ICL formation in the presence of  $\text{H}_2\text{O}_2$ , we used an Alexa Flour 647 picoly azide kit for fluorescence detection of **13**-labelled DNA. Initially, the reaction was performed with a 49-mer DNA duplex, which was incubated with **13** in the presence of  $\text{H}_2\text{O}_2$  followed by Alexa Flour 647 picoly azide with an excitation and emission maximum of 650/668 nm (Scheme 3-12). A strong band was detected in the bottom of the PAGE gel, which was the excess unreacted picoly azide

(Figure 3-28 A, lane 4). A cross-linking product band was observed if only the top part of the gel was scanned (Figure 3-28 B, lane 4), while this was not observed with the DNA not treated with **13** (lane 3). This result indicated that **13** covalently cross-linked with DNA duplex **5**, which further reacted with fluorophores-linked azide through Cu-catalyzed “click” reaction. Such a method can be used for detection of biological targets of QM prodrugs.

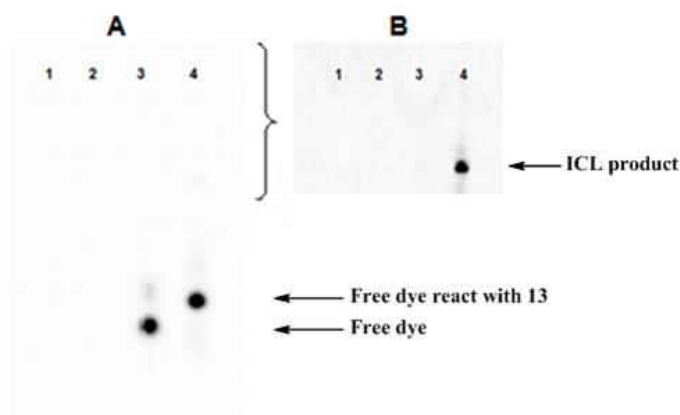


**Figure 3-28.** Fluorescence detected ICL formation by **13** using a 635 nm laser line. A. The full scan of the PAGE gel. B. Top part scan of the PAGE gel. Lane 1: DNA only; lane 2: DNA incubated with **13**; lane 3: DNA only treated with Fluor 647 azide; lane 4: DNA incubated with **13** first, then treated with Fluor 647 azide.

Encouraged by this result, we investigated the labeling of cellular targets by **13**. The  $IC_{50}$  of compound **13** for SKOV3 cells was 5.6  $\mu\text{M}$  (Figure 3-29). For the labeling study, we incubated SKOV3 cells with 2  $\mu\text{M}$  of **13** for 24 hours. After that incubation period, the cells were harvested and lysed followed by separation of DNA, RNA, and protein using an AllPrep kit (Qiagen). First the genomic DNA and total RNA were analyzed by using a 1.5 % agarose gel and stained with ethidium bromide (Figure 3-30). Both preparations had a significant amount of polynucleotides. Subsequently, these fractions were treated with Alexa Fluor 647 Picolyl Azide in the presence of a copper salt to covalently and fluorescently label quinone methide prodrug cross-linked



products. After gel separation, no fluorescent bands matching the corresponding polynucleotide bands were detected (Figure 3-31 C). The Alexa Fluor 647 Picolyl Azide however, produced two fluorescent bands at low molecular weight. One possible reason is that the alkylation sites are dispersed and the “click” reaction efficiency is low. In order to solve this problem, we will try to enrich the target by using a pull-down column. Importantly, the treated and non-treated protein fractions were reacted with Alexa Fluor 647 Picolyl Azide and separated by SDS gel chromatography. No labeling was observed for the protein fraction.

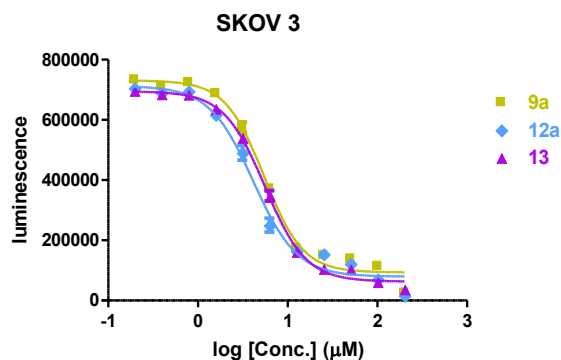


**Figure 3-29.** Cytotoxicity of **9a**, **12a** and **13** toward ovarian cancer cell line SKOV3.

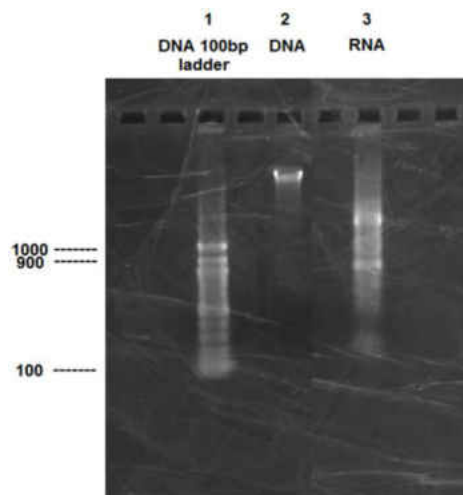


**Figure 3-30.** Purified genomic DNA and total RNA from **13** treated SKOV3 cell.

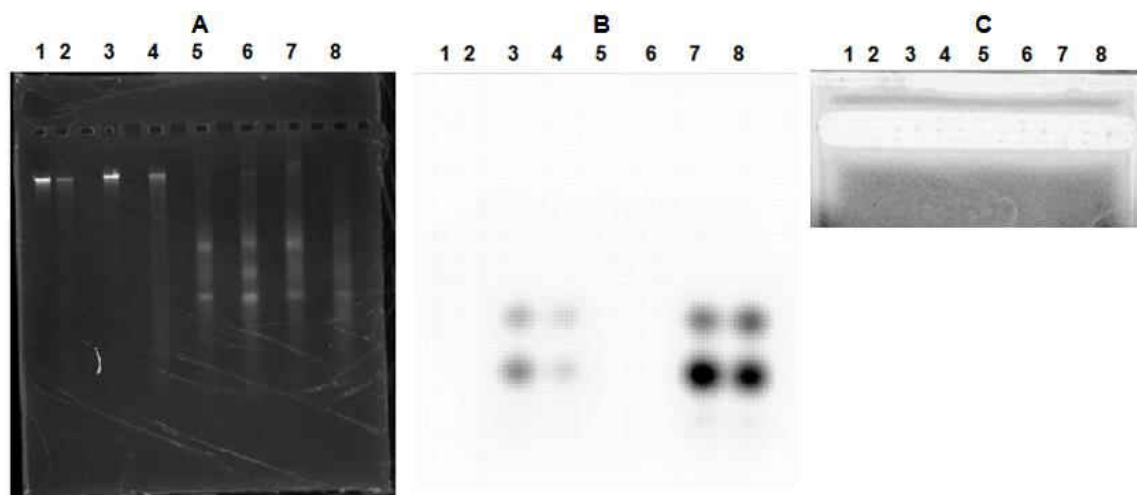


**Figure 3-31.** Fluorescence detection of genomic DNA and total RNA from **13** traded SKOV3 cell. A. Agarose gel stained with ethidium bromide. B. The full scan of the agarose gel. C. Top part scan of the agarose gel. Lane 1: genomic DNA from SKOV3; lane 2: genomic DNA from **13** traded SKOV3; lane 3: genomic DNA from SKOV3 traded with Fluor 647 azide; lane 4: genomic DNA from **13** traded SKOV3 traded with Fluor 647 azide. Line 5-8: the corresponding total RNA from the same cells.

### 3.5. Experimental Section

**General Methods.** Unless otherwise specified, chemicals were purchased from Aldrich or Fisher Scientific and were used as received without further purification. T4 polynucleotide kinase was obtained from New England Biolabs. Oligonucleotides were synthesized via standard automated DNA synthesis techniques using an Applied Biosystems model 394 instrument in a 1.0  $\mu$ M scale using commercial 1000Å CPG-succinyl-nucleoside supports. Deprotection of the nucleobases and phosphate moieties as well as cleavage of the linker were carried out under mild deprotection conditions using a mixture of 40% aq. MeNH<sub>2</sub> and 28% aq. NH<sub>3</sub> (1:1) at room temperature for 2 h. Radiolabeling was carried out according to the standard protocols.<sup>8</sup> [ $\gamma$ -<sup>32</sup>P]ATP was purchased from Perkin-Elmer Life Sciences. Quantification of radiolabeled

oligonucleotides was carried out using a Molecular Dynamics Phosphorimager equipped with ImageQuant Version 5.2 software.  $^1\text{H}$  NMR and  $^{13}\text{C}$  NMR spectra were taken on either a Bruker DRX 300 MHz and 500 MHz spectrophotometer. High resolution mass spectrometry was performed at University of California-Riverside and University of Wisconsin-Milwaukee Mass Spectrometry Lab.

**Interstrand cross-link formation with duplex DNA 5.** The  $^{32}\text{P}$ -labelled oligonucleotide (0.5  $\mu\text{M}$ ) was annealed with 1.5 equiv of the complementary strand by heating to 65  $^\circ\text{C}$  for 3 min in buffer 10 mM potassium phosphate (pH 7), and 100 mM NaCl, followed by slow-cooling to room temperature overnight. The  $^{32}\text{P}$ -labeled oligonucleotide duplex (2  $\mu\text{L}$ , 0.5  $\mu\text{M}$ ) was mixed with 1 M NaCl (2  $\mu\text{L}$ ), 100 mM potassium phosphate (2  $\mu\text{L}$ , pH 8), 10 mM  $\text{H}_2\text{O}_2$  (2  $\mu\text{L}$ ), and compound **9a** or **12a** (concentration range: 10  $\mu\text{M}$  to 2 mM in 6  $\mu\text{L}$   $\text{CH}_3\text{CN}$ ) and appropriate amount of autoclaved distilled water were added to give a final volume of 20  $\mu\text{L}$ . The reaction was incubated at room temperature for 24 h and quenched by an equal volume of 90% formamide loading buffer, then subjected to 20% denaturing polyacrylamide gel electrophoresis.

**Cell inhibition study of 1a and 9a towards tumor cells.** The *In vitro* cancer cell screen was performed at the National Cancer Institute (NCI Developmental Therapeutics Program). The procedure details can be found in NCI website: <http://dtp.nci.nih.gov/branches/btb/ivclsp.html>.

*Methodology of the In Vitro cancer screen.* The human tumor cell lines are grown in RPMI 1640 medium containing 5% fetal bovine serum and 2 mM L-glutamine. Cells are inoculated into 96 well microtiter plates in 100  $\mu\text{L}$  at plating densities ranging from 5,000 to 40,000 cells/well depending on the doubling time of individual cell lines. After cell inoculation, the microtiter plates are incubated at 37  $^\circ\text{C}$ , 5 %  $\text{CO}_2$ , 95% air, and 100% relative humidity for 24 h prior to addition of drugs.

After 24 h, two plates of each cell line are fixed *in situ* with TCA, to represent a measurement of the cell population for each cell line at the time of drug addition ( $T_z$ ). Drugs are solubilized in dimethyl sulfoxide at 4 mM concentration and stored frozen prior to use. At the time of drug addition, an aliquot of frozen concentrate is thawed and diluted to 20  $\mu$ M with complete medium containing 50  $\mu$ g/ml gentamicin. Aliquot of 100  $\mu$ l of the drug dilution is added to the microtiter wells already containing 100  $\mu$ l of medium, resulting in the required final drug concentration (10  $\mu$ M).

Following drug addition, the plates are incubated for an additional 48 h at 37 °C, 5% CO<sub>2</sub>, 95% air, and 100% relative humidity. For adherent cells, the assay is terminated by the addition of cold TCA. Cells are fixed *in situ* by the gentle addition of 50  $\mu$ l of cold 50% (w/v) TCA (final concentration, 10% TCA) and incubated for 60 minutes at 4 °C. The supernatant is discarded, and the plates are washed five times with tap water and air dried. Sulforhodamine B (SRB) solution (100  $\mu$ l) at 0.4% (w/v) in 1% acetic acid is added to each well, and plates are incubated for 10 minutes at room temperature. After staining, unbound dye is removed by washing five times with 1% acetic acid and the plates are air dried. Bound stain is subsequently solubilized with 10 mM trizma base, and the absorbance is read on an automated plate reader at a wavelength of 515 nm.

**Cell cytotoxicity study of 1a, 9a and 12a toward tumor cells.** The human tumor cell lines are grown in RPMI 1640 medium containing 5% fetal bovine serum and 2 mM L-glutamine. Cells are inoculated into 384-well microtiter plates in 20  $\mu$ L at plating densities ranging from 5,000 to 10,000 cells/well. After cell inoculation, the microtiter plates are incubated at 37 °C, 5 % CO<sub>2</sub>, 95% air, and 100% relative humidity for 2-3 h prior to addition of drugs.

Drugs are solubilized in dimethyl sulfoxide at 20 mM concentration and serially diluted ten times each time 50% decrease in DMSO in a 384-well plate. Then 200 nL of the serially diluted drug were added to the cell plate (1:100 dilution) by using Freedom EVOware two times 100 nL transfer. Following drug addition, the plates are incubated for an additional 48 h at 37 °C, 5% CO<sub>2</sub>, 95% air, and 100% relative humidity. After 48 hours, 20 µL celltiter-Glo Luminescent solution were added to the cell plate. The plate was then incubated at room temperature for 10 mins before the luminescent was measured with Infinite M1000.

**Fluorescence detection of 13-labelled ODN.** The complementary oligonucleotides **5a** and **5b** (50 µM) was annealed by heating to 65 °C for 3 min in a buffer of 10 mM potassium phosphate (pH 7) and 100 mM NaCl, followed by slow-cooling to room temperature overnight. The oligonucleotide duplex (50 µM, 20 µL) was mixed with 1 M NaCl (5 µL), 100 mM potassium phosphate (5 µL, pH 8.0), and compound **13** (100 µM, 20 µL). The reaction was incubated at 37 °C for 24 h. 4.35 µL of 10 X Click-iT reaction buffer (buffer B), 0.5 µL of 500 µM Alexa Fluor PCA solution, 1.00 µL CuSO<sub>4</sub>-copper protectant pre-mix which include 0.55 µL of CuSO<sub>4</sub> (Component C) and 0.45 µL of Copper protectant (Component D), and 5 µL of 1 X Click-iT buffer additive were mixed together to make the reaction cocktail for a single reaction volume of 50 µL. The reaction cocktail was added to 39.65 µL ODN reaction mixture and incubated for 30 mins at r.t. protected from light. The reaction quenched by an equal volume of 90% formamide loading buffer, then subjected to 20% denaturing polyacrylamide gel analysis and detected by using a 635 nm laser line.

**Purification of genomic DNA, total RNA, and total protein from same cell.** The SKOV3 cell line is grown in RPMI 1640 medium containing 5% fetal bovine serum and 2 mM L-glutamine into a 150 cm<sup>2</sup> cell culture flask. The flask was incubated at 37 °C, 5 % CO<sub>2</sub>, 95% air, and 100%

relative humidity for 2-3 h. After that 10  $\mu$ L 10 mM **13** (dissolved into DMSO) is added and incubated for 24 hours. The cell samples are first lysed in buffer RLT which is a highly denaturing guanidine-isothiocyanate-containing buffer and homogenized by directly passed through a QIAshredder spin column. The lysate is then passed through an AllPrep DNA spin column allows selective and efficient binding of genomic DNA, the AllPrep DNA spin column is washed with Buffer AW1 and Buffer AW2 and pure DNA is then eluted with 100  $\mu$ L Buffer EB (preheated to 70 °C). Ethanol is added to the flow-through from the AllPrep DNA spin column and mix well by pipetting to provide appropriate binding conditions for RNA. Transfer up to 700  $\mu$ L of sample (including any precipitate) to an RNeasy spin column, which allow total RNA binds to the membrane. The RNeasy spin column then wash with Buffer RW1 and Buffer RPE, and total RNA is eluted in 30-50  $\mu$ L RNase-free water. Buffer APP, a novel aqueous protein precipitation solution, is added to the flow-through of the RNeasy spin column, and the precipitated proteins are pelleted by centrifugation.

**Fluorescence detection of genomic DNA and total RNA from cell.** A 4.35  $\mu$ L of 10 X Click-iT reaction buffer (buffer B), 0.5  $\mu$ L of 500  $\mu$ M Alexa Fluor PCA solution, 1.00  $\mu$ L CuSO<sub>4</sub>-copper protectant pre-mix which include 0.55  $\mu$ L of CuSO<sub>4</sub> (Component C) and 0.45  $\mu$ L of Copper protectant (Component D), and 5  $\mu$ L of 1 X Click-iT buffer additive were mixed together to make the reaction cocktail for a single reaction volume of 50  $\mu$ L. The reaction cocktail was added to 39.65  $\mu$ L purified genomic DNA or total RNA and incubated for 30 mins at r.t. protected from light. The reaction quenched by 10  $\mu$ L 6 X DNA loading dye, then subjected to 1.5 % agrose gel and detected by using a 635 nm laser line or stained with ethidium bromide.

**2-(4-methoxy-2,6-dimethylphenyl)-4,4,5,5-tetramethyl-1,3,2-dioxaborolane.** To a stirred solution of 2-bromo-5-methoxy-1,3-dimethylbenzene (1.50 g, 7.0 mmol) in anhydried THF (40

mL) was added dropwise a 2.5 M solution of n-BuLi (3.36 mL, 8.4 mmol) at -78 °C via cannula over a 2 min period under argon. The cloudy solution was stirred at -78 °C for 30 min. Isopropoxyboronic acid pinacol ester (1.72 mL, 8.4 mmol) was added at once at -78 °C under argon via syringe. The mixture was allowed to stir at -78 °C for 30 min and then warm to room temperature slowly and stirred for 6 h. The mixture was quenched with aqueous 1 N HCl solution, extracted with 3 x 30 mL EtOAc, the organic layer was washed with water, and brine, dried with sodium sulfate, and concentrated under reduced pressure then purified through column chromatography (5% EtOAc/Hexane) to give 1.38 g (75%) of pure 2-(4-methoxy-2,6-dimethylphenyl)-4,4,5,5-tetramethyl-1,3,2-dioxaborolane as white solid. <sup>1</sup>H NMR (300 MHz, CDCl<sub>3</sub>) δ 6.53 (s, 2H), 3.78 (s, 3H), 2.42 (s, 6H), 1.39 (s, 12H).

**2-(2,6-bis(bromomethyl)-4-methoxyphenyl)-4,4,5,5-tetramethyl-1,3,2-dioxaborolane (9a).**

To a stirred solution of 2-(4-methoxy-2,6-dimethylphenyl)-4,4,5,5-tetramethyl-1,3,2-dioxaborolane (1.31 g, 5 mmol), NBS (1.87 g, 10.5 mmol) and AIBN (82.1 mg, 0.5 mmol) in anhydrous CCl<sub>4</sub> (30 mL) was stirred to reflux under a light for 2 h. The mixture was allowed to cool to room temperature. Evaporated the solvent and added 50 mL CH<sub>2</sub>Cl<sub>2</sub>, the organic layer was washed with water, and brine, dried with sodium sulfate, and concentrated under reduced pressure then purified through column chromatography (30% DCM/Hexane) to give **9a** (0.63 g 30%) as white solid. <sup>1</sup>H NMR (300 MHz, CDCl<sub>3</sub>): δ 6.85 (s, 2H), 4.84 (s, 4H), 3.84 (s, 3H), 1.46 (s, 12H). <sup>13</sup>C NMR (125 MHz, CDCl<sub>3</sub>): δ 160.7, 146.4, 115.7, 84.0, 55.3, 34.1, 25.1. HRMS (APCI): m/z calcd. for C<sub>15</sub>H<sub>21</sub>O<sub>3</sub>BBr<sub>2</sub> [M+H]<sup>+</sup> 419.0026, found 419.0022.

**1,1'-(5-methoxy-2-(4,4,5,5-tetramethyl-1,3,2-dioxaborolan-2-yl)-1,3-phenylene)bis(N,N,N-trimethylmethanaminium) bromide (9b).**

A mixture of CH<sub>3</sub>CN (10 mL), 4.2 M trimethylamine (0.72 ml, 3 mmol) in ethanol and **9a** (419.9 mg, 1 mmol) was stirred at r.t. over

night. The reaction mixture was concentrated to give **9b** (530 mg, 99%) as white solid.  $^1\text{H}$  NMR (300 MHz, DMSO-*d*6):  $\delta$  8.43 (d,  $J = 4.2$  Hz, 2H), 7.71-7.67 (m, 4H), 7.49 (t,  $J = 6.9$  Hz, 2H), 7.38 (s, 2H), 4.83 (s, 4H), 3.91 (s, 3H), 3.08 (s, 18H), 1.40 (s, 12H).  $^{13}\text{C}$  NMR (125 MHz, DMSO-*d*6):  $\delta$  160.8, 136.5, 137.5, 122.2, 85.4, 67.8, 52.9, 25.2. HRMS (ESI):  $m/z$  calcd. for  $\text{C}_{21}\text{H}_{39}\text{N}_2\text{O}_3\text{BBr}_2$  [ $\text{M}-2\text{Br}$ ] $^{2+}$  189.1523, found 189.1522.

**1,5-dibromo-2,4-dimethoxybenzene.** To a stirred solution of 1,3-dimethoxybenzene (2.76 g, 20 mmol) in  $\text{CH}_2\text{Cl}_2$  (25 mL) was added dropwise a solution of bromine in  $\text{CH}_2\text{Cl}_2$  (2.16 mL, 42 mmol) at 0 °C via cannula over a 2 min period under argon. The reaction was stirred for 2 h at room temperature. The product was washed with saturated sodium thiosulfate until the organic phase became colorless, dried with sodium sulfate and concentrated under reduced pressure then purified through column chromatography (5% EtOAc/Hexane) to give 1,5-dibromo-2,4-dimethoxybenzene (5.88 g, 99%) as a white solid.  $^1\text{H}$  NMR (300 MHz,  $\text{CDCl}_3$ ):  $\delta$  7.68 (s, 1H), 6.52 (s, 1H), 3.93 (s, 6H). The NMR spectra were consistent with literature values.<sup>9</sup>

**1,5-dimethoxy-2,4-dimethylbenzene.** A 2.5 M solution of *n*-BuLi (18.4 mL, 46 mmol) was added to a solution of 1,5-dibromo-2,4-dimethoxybenzene (5.88 g, 20 mmol) in 125 mL of ether at -78 °C under argon, and the cloudy solution was stirred at -78 °C for 30 min. Iodomethane (5.48 mL, 88 mmol) was added slowly at -78 °C under argon via syringe. The mixture was allowed to warm to room temperature and stirred for 1 h. A second addition of *n*-BuLi (18.4 mL, 46 mmol) was added at -78 °C under argon and stirred at -78 °C for 30 min. Iodomethane (5.48 mL, 88 mmol) was added again slowly at -78 °C under argon via syringe. The mixture was allowed to warm to room temperature and stirred for 1 h. The mixture was diluted with ether, quenched with aqueous  $\text{NH}_4\text{Cl}$ , washed with 1 N NaOH, water, and brine, dried with sodium sulfate, and concentrated under reduced pressure then purified through column chromatography



(2.5% EtOAc/Hexane) to give 1,5-dimethoxy-2,4-dimethylbenzene (1.68 g, 51%) as white solid.  $^1\text{H}$  NMR (300 MHz,  $\text{CDCl}_3$ ):  $\delta$  6.90 (s, 1H), 6.44 (s, 1H), 3.85 (s, 6H), 2.15 (s, 6H). The NMR spectra were consistent with literature values.<sup>9</sup>

**1,4-dibromo-2,6-dimethoxy-3,5-dimethylbenzene.** To a stirred solution of 1,5-dimethoxy-2,4-dimethylbenzene (1.68 g, 10 mmol) in  $\text{CH}_2\text{Cl}_2$  (40 mL) was added dropwise a solution of bromine (1.29 mL, 25 mmol) in  $\text{CH}_2\text{Cl}_2$  (2 mL) at 0 °C via cannula over a 2 min period under argon. The reaction was stirred for 16 h at room temperature. The product was washed with saturated sodium thiosulfate until the organic phase became colorless, dried with sodium sulfate and concentrated under reduced pressure then purified through column chromatography (10%  $\text{CH}_2\text{Cl}_2$ /Hexane) to give 1,4-dibromo-2,6-dimethoxy-3,5-dimethylbenzene (2.7 g, 83%) as white solid.  $^1\text{H}$  NMR (300 MHz,  $\text{CDCl}_3$ ):  $\delta$  3.80 (s, 6H), 2.41 (s, 6H). The NMR spectra were consistent with literature values.<sup>9</sup>

**3-bromo-1,5-dimethoxy-2,4-dimethylbenzene.** A 2.5 M solution of n-BuLi (3.36 mL, 8.4 mmol) solution was added to a solution of 1,4-dibromo-2,6-dimethoxy-3,5-dimethylbenzene (2.7 g, 8.4 mmol) in 100 mL of ether at -78 °C under argon, and the colorless solution was stirred at -78 °C for 1 h.  $\text{H}_2\text{O}$  (300 mg, 16.78 mmol) in 3 mL of THF was added slowly at -78 °C under argon. The mixture was allowed to warm to room temperature and stirred for 1 h. The mixture was quenched with saturated  $\text{NH}_4\text{Cl}$ , washed with  $\text{NH}_4\text{OH}$ , water, and brine, dried with sodium sulfate, and concentrated under reduced pressure then purified through column chromatography (10%  $\text{CH}_2\text{Cl}_2$ /Hexane) to give 3-bromo-1,5-dimethoxy-2,4-dimethylbenzene (1.88 g, 92%) as white solid.  $^1\text{H}$  NMR (300 MHz,  $\text{CDCl}_3$ ):  $\delta$  6.45 (s, 1H), 3.84 (s, 6H), 2.29 (s, 6H). The NMR spectra were consistent with literature values.<sup>9</sup>

**2-(3,5-dimethoxy-2,6-dimethylphenyl)-4,4,5,5-tetramethyl-1,3,2-dioxaborolane.** To a stirred

solution of 3-bromo-1,5-dimethoxy-2,4-dimethylbenzene (1.88 g, 7.7 mmol) in anhydried THF (40 mL) was added dropwise a 2.5 M solution of n-BuLi (3.7 mL, 9.25 mmol) at -78 °C via cannula over a 2 min period under argon. The cloudy solution was stirred at -78 °C for 30 min. Isopropoxyboronic acid pinacol ester (1.89 mL, 9.25 mmol) was added at once at -78 °C under argon via syringe. The mixture was allowed to stir at -78 °C for 30 min and then warm to room temperature slowly and stirred for 6 h. The mixture was quenched with aqueous 1 N HCl solution, extracted with 3 x 30 mL EtOAc, the organic layer was washed with water, and brine, dried with sodium sulfate, and concentrated under reduced pressure then purified through column chromatography (5% EtOAc/Hexane) to give 2-(3,5-dimethoxy-2,6-dimethylphenyl)-4,4,5,5-tetramethyl-1,3,2-dioxaborolane (3.32 g, 73%) as white solid. <sup>1</sup>H NMR (300 MHz, CDCl<sub>3</sub>): δ 6.46 (s, 1H), 3.81 (s, 6H), 2.21 (s, 6H), 1.42 (s, 12H). <sup>13</sup>C NMR (75 MHz, CDCl<sub>3</sub>): δ 156.1, 121.2, 97.2, 83.9, 56.0, 25.1, 14.7. HRMS (ESI): m/z calcd. for C<sub>16</sub>H<sub>25</sub>O<sub>4</sub>B [M]<sup>+</sup> 291.1877, found 291.1872.

**2-(2,6-bis(bromomethyl)-3,5-dimethoxyphenyl)-4,4,5,5-tetramethyl-1,3,2-dioxaborolane (10a).** To a stirred solution of 2-(3,5-dimethoxy-2,6-dimethylphenyl)-4,4,5,5-tetramethyl-1,3,2-dioxaborolane (584 mg, 2 mmol), NBS (854 mg, 4.8 mmol) and AIBN (32.8 mg, 0.2 mmol) in anhydried CCl<sub>4</sub> (10 mL) was stirred to reflux under a light for 2 h. The mixture was allowed to cool to room temperature. Evaporated the solvent and added 20 mL CH<sub>2</sub>Cl<sub>2</sub>, the organic layer was washed with water, and brine, dried with sodium sulfate, and concentrated under reduced pressure to give **10a** (300 mg, 28%). <sup>1</sup>H NMR (300 MHz, CDCl<sub>3</sub>): δ 6.47 (s, 1H), 4.9 (s, 4H), 3.92 (s, 6H), 1.49 (s, 12H). **10a** is not stable for <sup>13</sup>C NMR and MS.

**1,5-dibromo-2,3,4-trimethoxybenzene.** To a stirred solution of 1,2,3-trimethoxybenzene (4.21 g, 25 mmol) in CH<sub>2</sub>Cl<sub>2</sub> (40 mL) was added dropwise a solution of bromine in CH<sub>2</sub>Cl<sub>2</sub> (2.83 mL,

55 mmol) at 0 °C via cannula over a 2 min period under argon. The reaction was stirred for 2 h at room temperature. The product was washed with saturated sodium thiosulfate until the organic phase became colorless, dried with sodium sulfate and concentrated under reduced pressure then purified through column chromatography (20% CH<sub>2</sub>Cl<sub>2</sub>/Hexane) to give 1,5-dibromo-2,3,4-trimethoxy-benzene (6.72 g, 83%) as a colorless liquid. <sup>1</sup>H NMR (300 MHz, CDCl<sub>3</sub>): δ 7.49 (s, 1H), 3.94 (s, 3H), 3.90 (s, 6H). The NMR spectra were consistent with literature values.<sup>9</sup>

**2,3,4-trimethoxy-1,5-dimethylbenzene.** A 2.2 M solution of n-BuLi (11.45 mL, 25.2 mmol) was added to a solution of 1,5-dibromo-2,3,4-trimethoxybenzene (6.76 g, 20.9 mmol) in 100 mL of ether at -78 °C under argon, and the cloudy solution was stirred at -78 °C for 30 min. Iodomethane (3.14 mL, 50.4 mmol) was added slowly at -78 °C under argon via syringe. The mixture was allowed to warm to room temperature and stirred for 1 h; the mixture became clear. A second addition of n-BuLi (11.45 mL, 25.2 mmol) was added at -78 °C under argon and stirred at -78 °C for 30 min. Iodomethane (3.14 mL, 50.4 mmol) was added again slowly at -78 °C under argon via syringe. The mixture was allowed to warm to room temperature and stirred for 1 h. The mixture was diluted with ether, quenched with aqueous NH<sub>4</sub>Cl, washed with 1 N NaOH, water, and brine, dried with sodium sulfate, and concentrated under reduced pressure then purified through column chromatography (2.5% EtOAc/Hexane) to give 2,3,4-trimethoxy-1,5-dimethylbenzene (3.18 g, 78%) as colorless liquid. <sup>1</sup>H NMR (300 MHz, CDCl<sub>3</sub>): δ 6.71 (s, 1H), 3.94 (s, 3H), 3.85 (s, 6H), 2.21 (s, 6H). The NMR spectra were consistent with literature values.<sup>9</sup>

**1-bromo-3,4,5-trimethoxy-2,6-dimethylbenzene.** To a stirred solution of 2,3,4-trimethoxy-1,5-dimethylbenzene (3.18 g, 16.2 mmol) in CH<sub>2</sub>Cl<sub>2</sub> (40 mL) was added dropwise a solution of bromine (1 mL, 19.4 mmol) in CH<sub>2</sub>Cl<sub>2</sub> (2 mL) at 0 °C via cannula over a 2 min period under

argon. The reaction was stirred for 4 h at room temperature. The product was washed with saturated sodium thiosulfate until the organic phase became colorless, dried with sodium sulfate and concentrated under reduced pressure then purified through column chromatography (20% CH<sub>2</sub>Cl<sub>2</sub>/Hexane) to give 1-bromo-3,4,5-trimethoxy-2,6-dimethylbenzene (3.88 g, 87%) as colorless liquid. <sup>1</sup>H NMR (300 MHz, CDCl<sub>3</sub>): δ 3.92 (s, 3H), 3.83 (s, 6H), 2.34 (s, 6H). The NMR spectra were consistent with literature values.<sup>9</sup>

**4,4,5,5-tetramethyl-2-(3,4,5-trimethoxy-2,6-dimethylphenyl)-1,3,2-dioxaborolane.** To a stirred solution of 1-bromo-3,4,5-trimethoxy-2,6-dimethylbenzene (3.88 g, 14.2 mmol) in anhydried THF (40 mL) was added dropwise a 2.2 M solution of n-BuLi (7.7 mL, 17 mmol) at -78 °C via cannula over a 2 min period under argon. The cloudy solution was stirred at -78 °C for 30 min. Isopropoxyboronic acid pinacol ester (3.47 mL, 17 mmol) was added at once at -78 °C under argon via syringe. The mixture was allowed to stir at -78 °C for 30 min and then warm to room temperature slowly and stirred for 6 h. The mixture was quenched with aqueous 1 N HCl solution, extracted with 3 x 30 mL EtOAc, the organic layer was washed with water, and brine, dried with sodium sulfate, and concentrated under reduced pressure then purified through column chromatography (5% EtOAc/Hexane) to give 4,4,5,5-tetramethyl-2-(3,4,5-trimethoxy-2,6-dimethylphenyl)-1,3,2-dioxaborolane (3.32 g, 73%) as white solid. <sup>1</sup>H NMR (300 MHz, CDCl<sub>3</sub>): δ 3.91 (s, 3H), 3.79 (s, 6H), 2.28 (s, 6H), 1.41 (s, 12H). <sup>13</sup>C NMR (75 MHz, CDCl<sub>3</sub>): δ 149.7, 147.2, 130.3, 83.9, 60.7, 60.5, 25.0, 15.1. HRMS (ESI): m/z calcd. for C<sub>17</sub>H<sub>27</sub>O<sub>5</sub>B [M]<sup>+</sup> 321.1982, found 321.1983.

**2-(2,6-bis(bromomethyl)-3,4,5-trimethoxyphenyl)-4,4,5,5-tetramethyl-1,3,2-dioxaborolane (11a):** A solution of 4,4,5,5-tetramethyl-2-(3,4,5-trimethoxy-2,6-dimethylphenyl)-1,3,2-dioxaborolane (1.28 g, 4 mmol), NBS (1.71 g, 9.6 mmol) and AIBN (65.6 mg, 0.4 mmol) in

anhydrous  $\text{CCl}_4$  (30 mL) was stirred to reflux under a light for 2 h. The mixture was allowed to cool to room temperature. Evaporated the solvent and added 20 mL  $\text{CH}_2\text{Cl}_2$ , the organic layer was washed with water, and brine, dried with sodium sulfate, and concentrated under reduced pressure then purified through column chromatography (2.5% EtOAc/Hexane) to give **11a** (0.53 g, 28%) as white solid.  $^1\text{H}$  NMR (300 MHz,  $\text{CDCl}_3$ )  $\delta$  4.90 (s, 4H), 3.99 (s, 6H), 3.91 (s, 3H), 1.48 (s, 12H).  $^{13}\text{C}$  NMR (75 MHz,  $\text{CDCl}_3$ ):  $\delta$  152.7, 147.4, 132.8, 84.5, 61.2, 60.6, 27.6, 25.1. HRMS (ESI):  $m/z$  calcd. for  $\text{C}_{17}\text{H}_{25}\text{O}_5\text{BBr}$   $[\text{M}]^+$  477.0193, found 477.0179.

**1,1'-(4,5,6-trimethoxy-2-(4,4,5,5-tetramethyl-1,3,2-dioxaborolan-2-yl)-1,3-phenylene)bis(N,N,N-trimethylmethanaminium) bromide (11b)**. A mixture of  $\text{CH}_3\text{CN}$  (10 mL), 4.2 M trimethylamine (0.72 mL, 3 mmol) in ethanol and **11a** (478.0 mg, 1 mmol) was stirred at r.t. over night. The reaction mixture was concentrated to give **11b** (536 mg, 90%) as white solid.  $^1\text{H}$  NMR (300 MHz,  $\text{DMSO}-d_6$ ):  $\delta$  8.43 (d,  $J = 4.2$  Hz, 2H), 4.66 (s, 4H), 3.93 (s, 6H), 3.89 (s, 3H), 3.05 (s, 18H), 1.41 (s, 12H).  $^{13}\text{C}$  NMR (75 MHz,  $\text{DMSO}-d_6$ ):  $\delta$  156.6, 148.2, 123.3, 86.0, 62.9, 61.9, 61.1, 53.3, 25.2. HRMS (ESI):  $m/z$  calcd. for  $\text{C}_{21}\text{H}_{39}\text{N}_2\text{O}_3\text{BBr}_2$   $[\text{M}-2\text{Br}]^{2+}$  219.1629, found 219.1631.

**(4-bromo-3,5-dimethylphenoxy)(tert-butyl)dimethylsilane**. A solution of 4-bromo-3,5-dimethylphenol (3.0 g, 15 mmol) and imidazole (2.25 g, 33 mmol) in DMF (20 mL) was cooled to 0 °C then TBDMSCl (2.49 g, 16.5 mmol) was added in one portion at 0 °C. The solution was warmed up to room temperature slowly and stirred for 30 min. The solution was cooled down to 0 °C again and the reaction was quenched with water. The aqueous layer was extracted with  $\text{Et}_2\text{O}$  and the organic layer was washed with water, brine, dried with  $\text{Na}_2\text{SO}_4$  and filtered. The solvent was removed under reduced pressure and the residue was purified by flash chromatography using hexane to give (4-bromo-3,5-dimethylphenoxy)-tert-butyl-dimethylsilane

(4.41 g, 92%) as colorless liquid.  $^1\text{H}$  NMR (300 MHz,  $\text{CDCl}_3$ ):  $\delta$  6.60 (s, 2H), 2.37 (s, 6H), 0.99 (s, 9H), 0.20 (s, 6H). The NMR spectra were consistent with literature values.<sup>10</sup>

**tert-butyl(3,5-dimethyl-4-(4,4,5,5-tetramethyl-1,3,2-dioxaborolan-2-yl)phenoxy)dimethylsilane.** To a stirred solution of (4-bromo-3,5-dimethylphenoxy)-tert-butyl-dimethylsilane (4.41 g, 14.0 mmol) in anhydried THF (30 mL) was added dropwise a 2.2 M solution of n-BuLi (8.43 mL, 21.1 mmol) at  $-78\text{ }^\circ\text{C}$  via cannula over a 10 min period under argon. The cloudy solution was stirred at  $-78\text{ }^\circ\text{C}$  for 30 min. Isopropoxyboronic acid pinacol ester (4.30 mL, 21.1 mmol) was added at once at  $-78\text{ }^\circ\text{C}$  under argon via syringe. The mixture was allowed to stir at  $-78\text{ }^\circ\text{C}$  for 30 min and then warm to room temperature slowly and stirred for 4 h. The mixture was quenched with aqueous 1 N HCl solution, extracted with 3 x 30 mL EtOAc, the organic layer was washed with water, and brine, dried with sodium sulfate, and concentrated under reduced pressure then purified through column chromatography (20% DCM/Hexane) to give tert-butyl [3,5-dimethyl-4-(4,4,5,5-tetramethyl-1,3,2-dioxaborolan-2-yl)phenoxy]dimethylsilane (4.1 g, 85%) as white solid.  $^1\text{H}$  NMR (300 MHz,  $\text{CDCl}_3$ ):  $\delta$  6.47 (s, 3H), 2.37 (s, 6H), 1.39 (s, 12H), 0.98 (s, 9H), 0.18 (s, 6H).  $^{13}\text{C}$  NMR (125 MHz,  $\text{CDCl}_3$ ):  $\delta$  156.5, 144.1, 118.6, 83.4, 25.7, 25.0, 22.4, 18.2.

**(3,5-bis(bromomethyl)-4-(4,4,5,5-tetramethyl-1,3,2-dioxaborolan-2-yl)phenoxy)(tert-butyl)dimethylsilane.** A solution of tert-butyl(3,5-dimethyl-4-(4,4,5,5-tetramethyl-1,3,2-dioxaborolan-2-yl)phenoxy)dimethylsilane (4.1 g, 11.8 mmol), NBS (5.11 g, 28.4 mmol) and AIBN (194 mg, 0.118 mmol) in anhydried  $\text{CCl}_4$  (100 mL) was stirred to reflux under a light for 2 h. The mixture was allowed to cool to room temperature. Evaporated the solvent and added 100 mL  $\text{CH}_2\text{Cl}_2$ , the organic layer was washed with water, and brine, dried with sodium sulfate, and concentrated under reduced pressure then purified through column chromatography (20%

DCM/Hexane) to give tert-butyl [3,5- bis(bromomethyl)-4-(4,4,5,5-tetramethyl-1,3,2-dioxaborolan-2-yl)phenoxy]dimethylsilane (2.67 g, 44%) as white solid.  $^1\text{H}$  NMR (300 MHz,  $\text{CDCl}_3$ ):  $\delta$  6.79 (s, 2H), 4.80 (s, 4H), 1.47 (s, 12H), 1.00 (s, 9H), 0.23 (s, 6H).  $^{13}\text{C}$  NMR (125 MHz,  $\text{CDCl}_3$ ):  $\delta$  157.1, 146.3, 121.9, 84.0, 34.0, 25.7, 25.1, 18.2. HRMS (APCI): m/z calcd. for  $\text{C}_{20}\text{H}_{33}\text{O}_3\text{BSiBr}_2$   $[\text{M}+\text{H}]^+$  519.0736, found 519.0736.

**3,5-bis(bromomethyl)-4-(4,4,5,5-tetramethyl-1,3,2-dioxaborolan-2-yl)phenol (12a).** A solution of (3,5-bis(bromomethyl)-4-(4,4,5,5-tetramethyl-1,3,2-dioxaborolan-2-yl)phenoxy)(tert-butyl) dimethylsilane (2.6 g, 5.0 mmol) and TBATB (0.24 g, 0.5 mmol) in MeOH (50 mL) was stirred for one day, and another TBATB (0.24 g, 0.5 mmol) was added to the solution. The mixture was allowed to stirred one more day. Evaporated the solvent and purified through column chromatography (20% DCM/Hexane) to give **12a** (0.72 g, 36%) as white solid.  $^1\text{H}$  NMR (300 MHz,  $\text{CDCl}_3$ ):  $\delta$  6.78 (s, 2H), 4.79 (s, 4H), 1.46 (s, 12H).  $^{13}\text{C}$  NMR (125 MHz,  $\text{CDCl}_3$ ):  $\delta$  156.8, 146.7, 117.1, 84.1, 33.7, 25.1. HRMS (ESI): m/z calcd. for  $\text{C}_{14}\text{H}_{19}\text{O}_3\text{BBr}_2$   $[\text{M}]^+$  402.9825, found 402.9814.

**1,1'-(5-hydroxy-2-(4,4,5,5-tetramethyl-1,3,2-dioxaborolan-2-yl)-1,3-phenylene)bis(N,N,N-trimethylmethanaminium) bromide (12b).** A mixture of  $\text{CH}_3\text{CN}$  (10 mL), 4.2 M trimethylamine (0.72 ml, 3 mmol) in ethanol and **12a** (406.0 mg, 1 mmol) was stirred at r.t. over night. The reaction mixture was concentrated to give **12b** (519 mg, 99%) as white solid.  $^1\text{H}$  NMR (300 MHz,  $\text{DMSO}-d_6$ ):  $\delta$  10.9 (s, 12H), 7.22 (s, 2H), 4.79 (s, 4H), 3.05 (s, 18H), 1.39 (s, 12H).  $^{13}\text{C}$  NMR (75 MHz,  $\text{DMSO}-d_6$ ):  $\delta$  159.8, 137.5, 123.7, 85.2, 67.8, 52.8, 25.2. HRMS (ESI): m/z calcd. for  $\text{C}_{20}\text{H}_{37}\text{N}_2\text{O}_3\text{BBr}_2$   $[\text{M}-2\text{Br}]^{2+}$  182.1445, found 182.1446.

**(2-bromo-1,3-phenylene)dimethanol.** A solution of 2-bromoisophthalaldehyde (2.12 g, 10 mmol) and  $\text{NaBH}_4$  (1.91 g, 24 mmol) in MeOH (25 mL) was stirred for 12 h at room temperature.

The reaction mixture was concentrated. Water was added to the residue and the product was extracted with EtOAc, organic layer was dried over Na<sub>2</sub>SO<sub>4</sub>, and evaporated. The (2-bromo-1,3-phenylene)dimethanol was obtained as white solid (1.77 g, 82%) and was used without any further purification. <sup>1</sup>H NMR (300 MHz, DMSO-*d*<sub>6</sub>): δ 7.45-7.39 (m, 3H), 5.41 (t, *J* = 5.4 Hz 2H), 4.53 (d, *J* = 2.7 Hz 4H).

**(2-bromo-1,3-phenylene)bis(methylene) diacetate.** To solution of (2-bromo-1,3-phenylene)dimethanol (1.08 g, 5 mmol) in CH<sub>2</sub>Cl<sub>2</sub> (25 mL) was added TEA (2.02 g, 20 mmol), pyridine (1.58 g, 20 mmol) and acetyl chloride (1.56 g, 20 mmol) at 0 °C. The solution was stirred over night. The reaction mixture were washed with water and brine, dried over Na<sub>2</sub>SO<sub>4</sub>, and concentrated under reduced pressure then purified through column chromatography (2.5% EtOAc/Hexane) to give (2-bromo-1,3-phenylene)bis(methylene) diacetate (1.13 g, 75%) as white solid. <sup>1</sup>H NMR (300 MHz, CDCl<sub>3</sub>) δ 7.43-7.36 (m, 3H), 5.25 (s, 4H), 2.17 (s, 6H). <sup>13</sup>C NMR (75 MHz, CDCl<sub>3</sub>): δ 170.6, 136.1, 129.4, 127.4, 124.3, 66.0, 20.9.

**(2-(4,4,5,5-tetramethyl-1,3,2-dioxaborolan-2-yl)-1,3-phenylene)bis(methylene) diacetate (1c).** A mixture of (2-bromo-1,3-phenylene)bis(methylene) diacetate (301 mg, 1 mmol), bis(pinacolato)diboron (508 mg, 2 mmol), KOAc (589 mg, 6 mmol), and PdCl<sub>2</sub>(dppf) (49 mg, 0.06 mmol) in 1,4-dioxane (20 mL) was refluxed under argon over night and cooled to room temperature. Then water was added, and the mixture was extracted with EtOAc. The combined organic layer was washed with water and brine, dried over anhydrous Na<sub>2</sub>SO<sub>4</sub>, and concentrated under reduced pressure then purified through column chromatography (50% DCM/Hexane) to provide **c** (121.9 mg, 35%) as colorless oil. <sup>1</sup>H NMR (300 MHz, CDCl<sub>3</sub>): δ 7.36-7.39 (m, 3H), 5.28 (s, 4H), 2.08 (s, 6H), 1.39 (s, 12H). <sup>13</sup>C NMR (75 MHz, CDCl<sub>3</sub>): δ 170.6, 141.0, 130.0,



129.2, 84.1, 66.6, 24.9, 21.1. HRMS (ESI):  $m/z$  calcd. for  $C_{18}H_{25}O_6B [M+NH_4]^+$  366.2086, found 366.2084.

**2-bromo-1,3-bis(bromomethyl)-5-methoxybenzene.** A mixture of 2-bromo-5-methoxy-1,3-dimethylbenzene (1.15 g, 5.4 mmol), NBS (2.12 g, 11.9 mmol) and AIBN (88.8 mg, 0.54 mmol) in  $CCl_4$  (50 mL) was refluxed under argon for 4 h. The mixture was allowed to cool to room temperature. Evaporated the solvent and added 50 mL  $CH_2Cl_2$ , the organic layer was washed with water, brine, and dried over  $Na_2SO_4$ , and concentrated under reduced pressure then purified through column chromatography (10% DCM/Hexane) to give 2-bromo-1,3-bis(bromomethyl)-5-methoxybenzene (0.71 g, 35%) as white solid.  $^1H$  NMR (300 MHz,  $CDCl_3$ ):  $\delta$  7.00 (s, 2H), 4.62 (s, 4H), 3.84 (s, 3H).

**(2-bromo-5-methoxy-1,3-phenylene)bis(methylene) diacetate.** A mixture of 2-bromo-1,3-bis(bromomethyl)-5-methoxybenzene (0.71 g, 1.9 mmol) and NaOAc (0.79 g, 9.6 mmol) were suspended in DMF (20 mL) and heated for 8 h at 80 °C. The mixture was allowed to cool to room temperature and diluted with EtOAc and washed with water, brine, and dried over  $Na_2SO_4$ , and concentrated under reduced pressure then purified through column chromatography (10% DCM/Hexane) to give (2-bromo-5-methoxy-1,3-phenylene)bis(methylene) diacetate (0.51 g, 81%) as white solid.  $^1H$  NMR (300 MHz,  $CDCl_3$ ):  $\delta$  6.96 (s, 2H), 5.21 (s, 4H), 3.84 (s, 3H), 2.18 (s, 6H).  $^{13}C$  NMR (75 MHz,  $CDCl_3$ ):  $\delta$  170.5, 158.9, 137.0, 114.9, 114.2, 65.9, 55.6, 20.9.

**(5-methoxy-2-(4,4,5,5-tetramethyl-1,3,2-dioxaborolan-2-yl)-1,3-phenylene)bis(methylene) diacetate (9c).** A mixture of (2-bromo-5-methoxy-1,3-phenylene)bis(methylene) diacetate (331 mg, 1 mmol), bis(pinacolato)diboron (508 mg, 2 mmol), KOAc (589 mg, 6 mmol), and  $PdCl_2(dppf)$  (49 mg, 0.06 mmol) in 1,4-dioxane (20 mL) was refluxed under argon over night and cooled to room temperature. Then water was added, and the mixture was extracted with

EtOAc. The combined organic layer was washed with water and brine, dried over anhydrous  $\text{Na}_2\text{SO}_4$ , and concentrated under reduced pressure then purified through column chromatography (50% DCM/Hexane) to provide **1c** (147.5 mg, 39%) as white solid.  $^1\text{H}$  NMR (300 MHz,  $\text{CDCl}_3$ ):  $\delta$  6.91 (s, 2H), 5.29 (s, 4H), 3.85 (s, 4H), 2.10 (s, 6H), 1.37 (s, 12H).  $^{13}\text{C}$  NMR (75 MHz,  $\text{CDCl}_3$ ):  $\delta$  170.7, 160.9, 143.6, 114.5, 83.8, 66.6, 24.8, 21.1. HRMS (ESI):  $m/z$  calcd. for  $\text{C}_{19}\text{H}_{27}\text{O}_7\text{B}$   $[\text{M}+\text{NH}_4]^+$  396.2192, found 396.2186.

**(5-hydroxy-2-(4,4,5,5-tetramethyl-1,3,2-dioxaborolan-2-yl)-1,3-phenylene)bis(methylene) diacetate (12c)**. A mixture of **12a** (100 mg, 0.248 mmol) and NaOAc (101.5 mg, 1.238 mmol) were suspended in DMF (10 mL) and heated for 8 h at 80 °C. The mixture was allowed to cool to room temperature and diluted with EtOAc and washed with water, brine, and dried over  $\text{Na}_2\text{SO}_4$ , and concentrated under reduced pressure then purified through column chromatography (5% EtOAc/DCM) to give **1** (27 mg, 31%) as white solid.  $^1\text{H}$  NMR (300 MHz,  $\text{CDCl}_3$ ):  $\delta$  6.86 (s, 2H), 5.28 (s, 4H), 2.10 (s, 6H), 1.37 (s, 12H).  $^{13}\text{C}$  NMR (75 MHz,  $\text{CDCl}_3$ ):  $\delta$  171.9, 157.1, 144.0, 115.7, 83.8, 66.3, 24.8, 21.1. HRMS (ESI):  $m/z$  calcd. for  $\text{C}_{18}\text{H}_{25}\text{O}_7\text{B}$   $[\text{M}+\text{NH}_4]^+$  382.2035, found 382.2035.

**2-(2,6-Bis(bromomethyl)-4-(prop-2-ynyloxy)phenyl)-4,4,5,5-tetramethyl-1,3,2-dioxaborolane (13)**. To a stirred solution of **12a** (100 mg, 0.25 mmol), and  $\text{K}_2\text{CO}_3$  (68.4 mg, 0.50 mmol) in anhydrous DMF (2 mL) was stirred at room temperature for 30 min. Propargyl bromide (0.033 mL, 0.30 mmol) was added at room temperature. The mixture was stirred for 2 h at room temperature. The mixture was extracted with  $3 \times 10$  mL EtOAc, the organic layer was washed with water, and brine, dried with sodium sulfate, and concentrated under reduced pressure then purified through column chromatography (50% DCM/Hexane) to give of 2-(2,6-bis(bromomethyl)-4-(prop-2-ynyloxy)phenyl)-4,4,5,5-tetramethyl-1,3,2-dioxaborolane **13** (20

mg, 28%) as colorless oil.  $^1\text{H}$  NMR (300 MHz,  $\text{CDCl}_3$ )  $\delta$  6.92 (s, 2H), 4.84 (s, 4H), 4.73 (d,  $J = 1.5$  Hz, 2H), 2.56 (t,  $J = 2.0$  Hz, 1H), 1.46 (s, 12H).  $^{13}\text{C}$  NMR (300 MHz,  $\text{CDCl}_3$ ): 158.6, 146.4, 116.5, 84.1, 76.1, 55.7, 33.9, 25.1. HRMS (ESI):  $m/z$  calcd. for  $\text{C}_{17}\text{H}_{21}\text{BO}_3\text{Br}_2$   $[\text{M}]^+$  440.9981, found 440.9991.

### 3.6. References

1. Cao, S., Wang, Y., Peng, X. ROS-inducible DNA cross-linking agent as a new anticancer prodrug building block. *Chem. Eur. J.* **2012**, *18*, 3850-3854.
2. Cao, S., Wang, Y., Peng, X. The leaving group strongly affects  $\text{H}_2\text{O}_2$ -induced DNA cross-linking by arylboronates. *J. Org. Chem.* **2014**, *79*, 501-508.
3. Weinert, E. E., Frankenfield, K. N., Rokita, S. E. Time-dependent evolution of adducts formed between deoxynucleosides and a model quinone methide. *Chem. Res. Toxicol.* **2005**, *18*, 1364-1370.
4. Weinert, E. E., Dondi, R., Colloredo-Melz, S., Frankenfield, K. N., Mitchell, C. H., Freccero, M., Rokita, S. E. Substituents on quinone methides strongly modulate formation and stability of their nucleophilic adducts. *J. Am. Chem. Soc.* **2006**, *128*, 11940-11947.
5. Cao, S., Christiansen, R., Peng, X. Substituent effects on oxidation-induced formation of quinone methides from arylboronic ester precursors. *Chem. Eur. J.* **2013**, *19*, 9050-9058.
6. Veldhuyzen, W. F., Shallop, A. J., Jones, R. A., Rokita, S. E. Thermodynamic versus kinetic products of DNA alkylation as modeled by reaction of deoxyadenosine. *J. Am. Chem. Soc.* **2001**, *123*, 11126-11132.
7. Verga, D., Nadai, M., Doria, F., Percivalle, C., Di Antonio, M., Palumbo, M., Richter, S. N., Freccero, M. Photogeneration and reactivity of naphthoquinone methides as purine selective DNA alkylating agents. *J. Am. Chem. Soc.* **2010**, *132*, 14625-14637.

8. Maniatis, T., Fritsch, E. F., Sambrook, J. *Molecular Cloning*, Cold Spring Harbor Laboratory, Cold Spring Harbor, NY. **1982**.
9. Bugarin, A., Connell, B.T. Chiral nickel (II) and palladium (II) NCN-pincer complexes based on substituted benzene: synthesis, structure, and lewis acidity. *Organometallics*, **2008**, *27*, 4357-4369.
10. Bos, M. E., Loncaric, C., Chunrui, W., Wuiff, W. D. Studies on the synthesis of richardianidin-1 via the tautomer-arrested annulation of fischer carbene complexes. *Synthesis*, **2006**, *21*, 3679-3705.

### 3.7. Appendices B: Characterization of Compounds

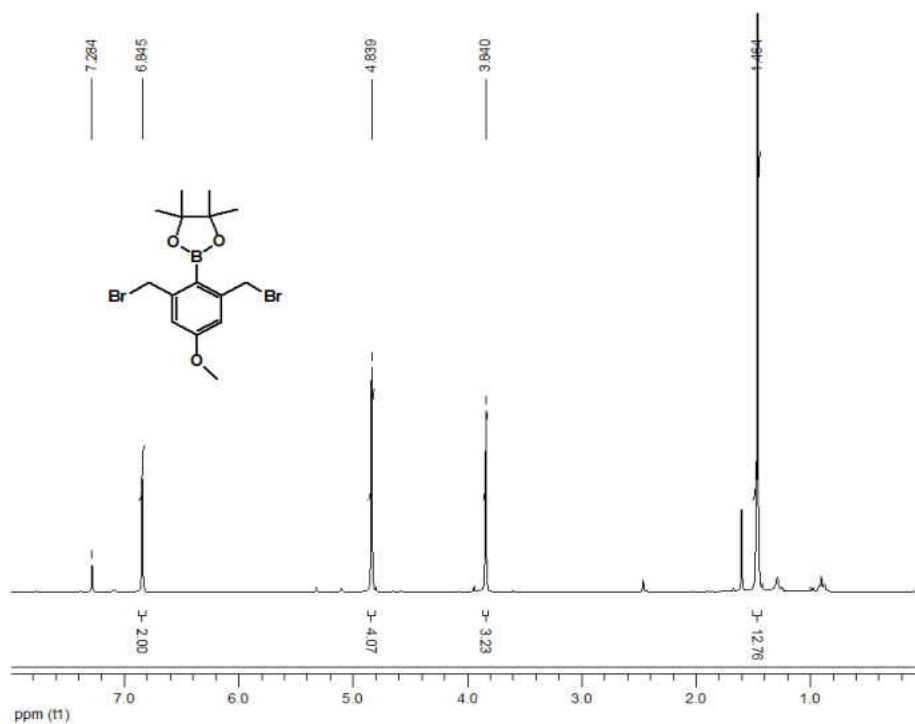


Figure 3-6-1.  $^1\text{H}$  NMR spectra of **9a**.

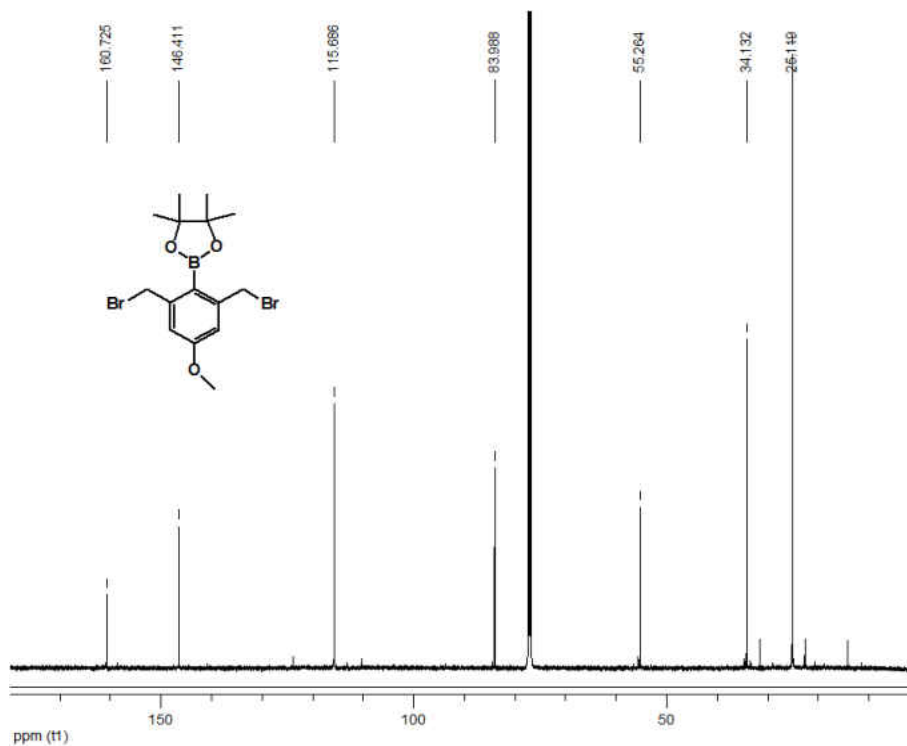


Figure 3-6-2.  $^{13}\text{C}$  NMR spectra of **9a**.

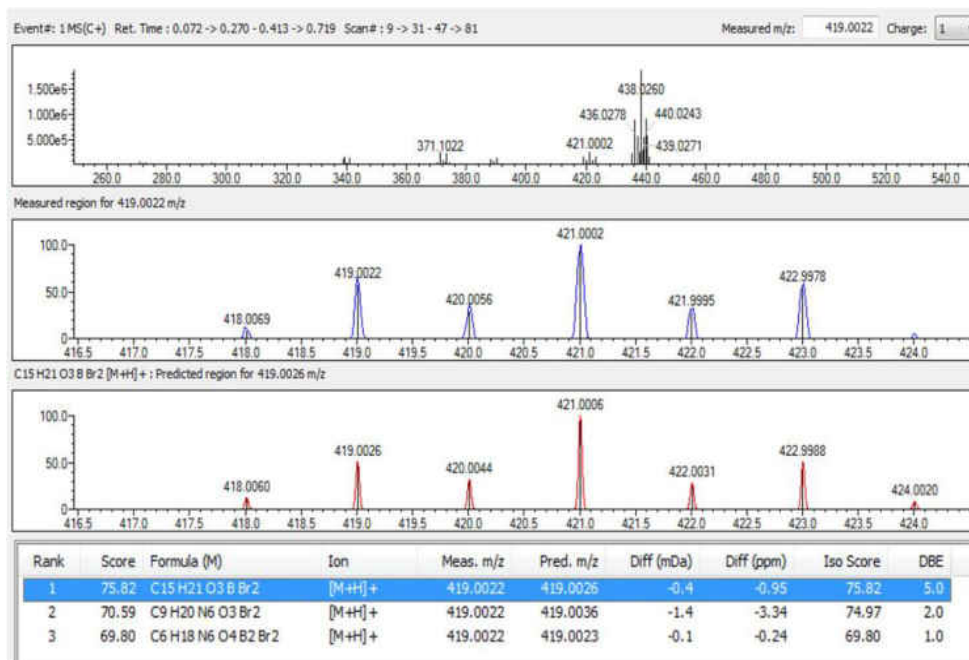


Figure 3-6-3. IT-TOF-MS (APCI) of **9a**.

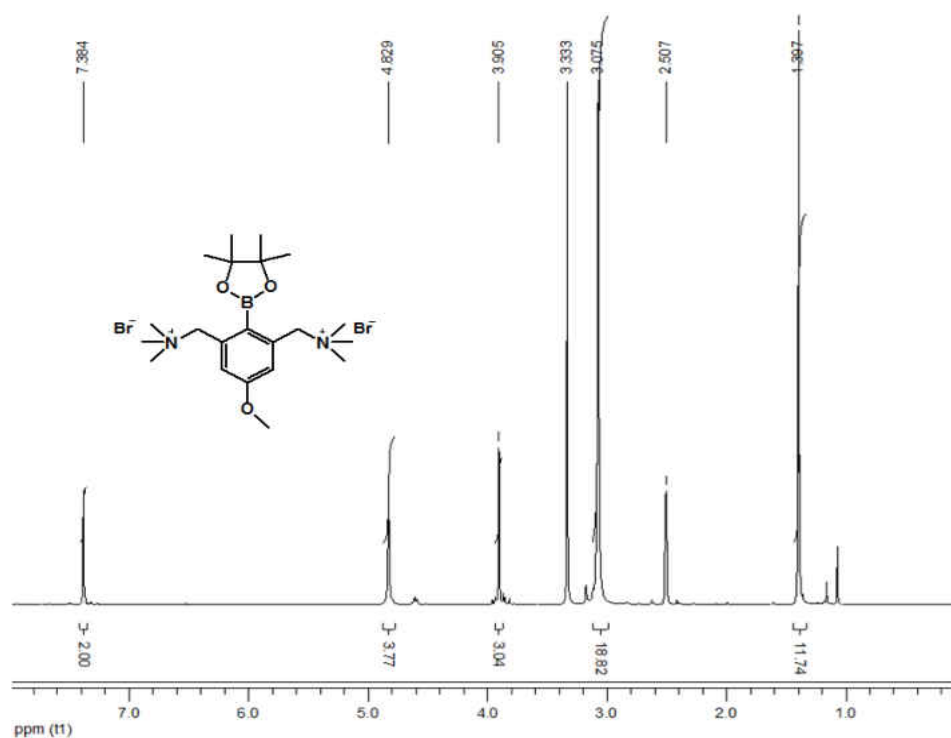


Figure 3-6-4. <sup>1</sup>H NMR spectra of **9b**.

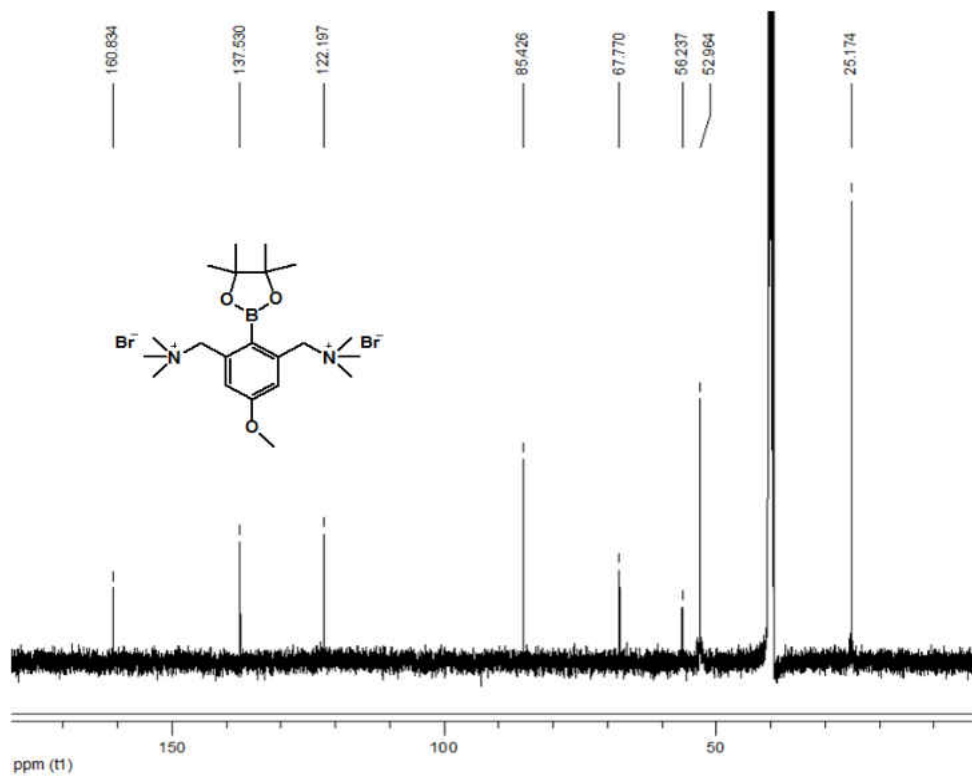


Figure 3-6-5.  $^{13}\text{C}$  NMR spectra of **9b**.

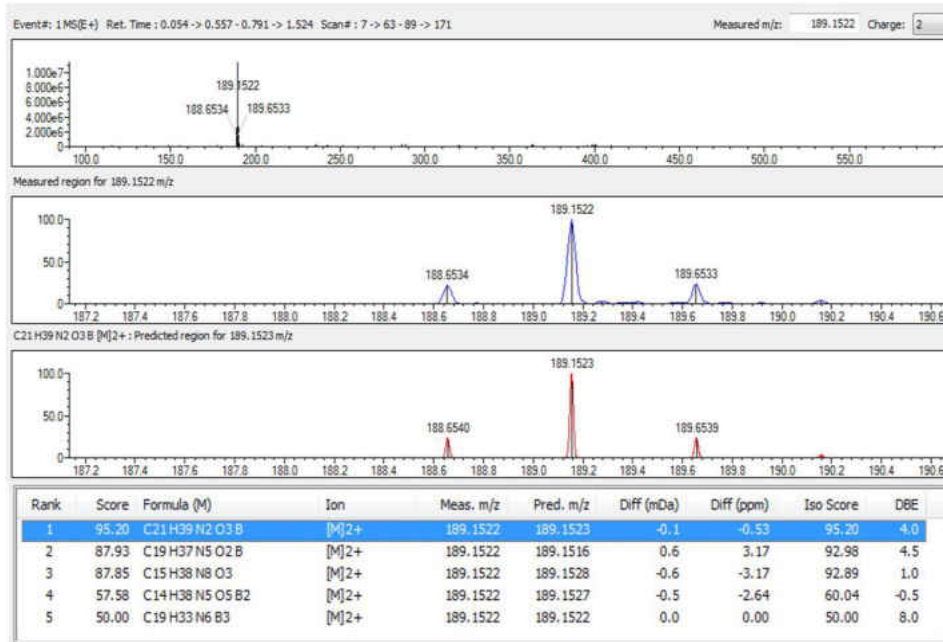


Figure 3-6-6. IT-TOF-MS (ESI) of **9b**.

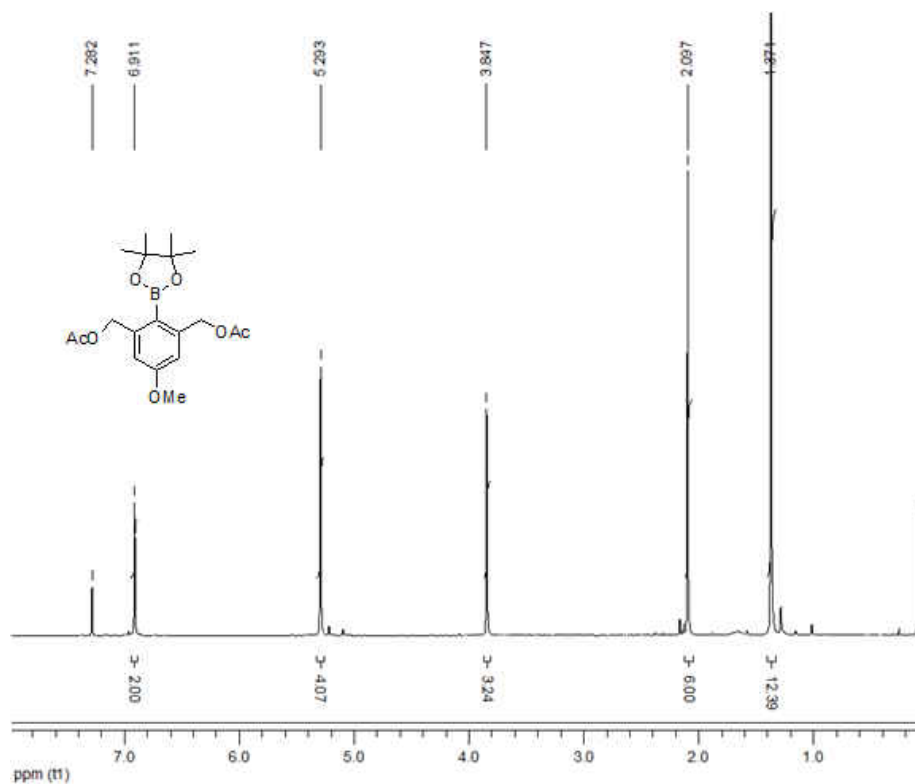


Figure 3-6-7.  $^1\text{H}$  NMR spectra of **9c**.

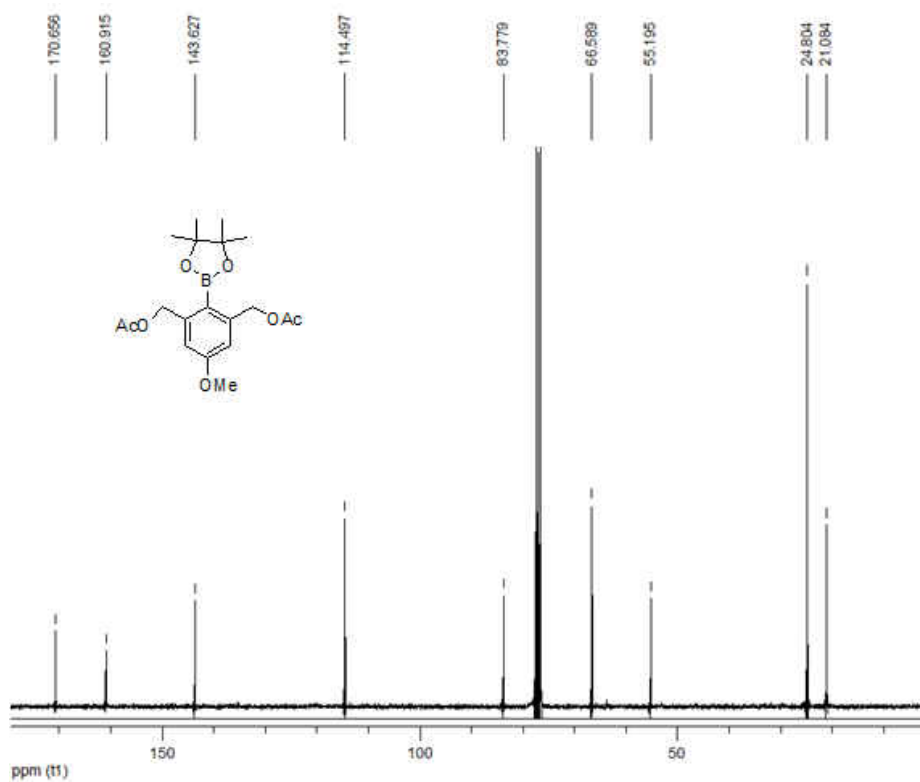


Figure 3-6-8.  $^{13}\text{C}$  NMR spectra of **9c**.



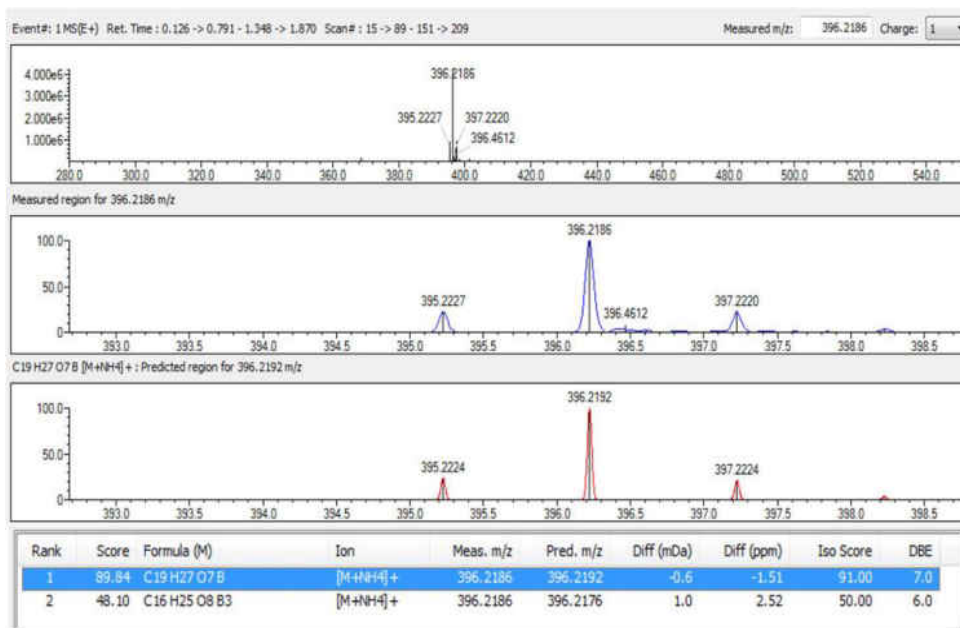


Figure 3-6-9. IT-TOF-MS (ESI) of **9c**.

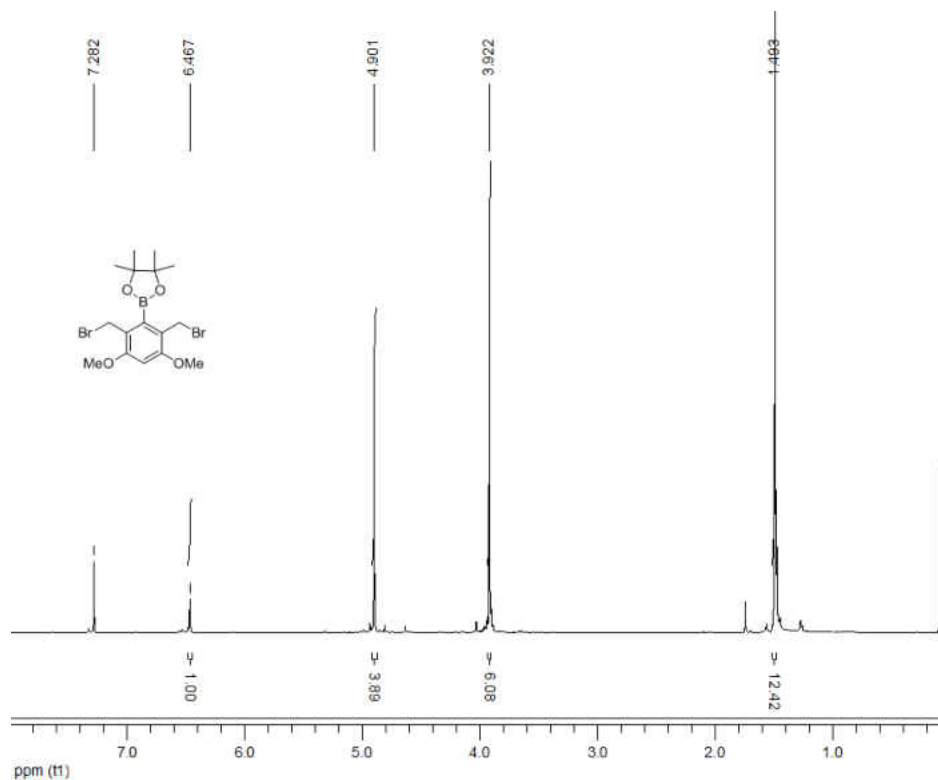


Figure 3-6-10. <sup>1</sup>H NMR spectra of **10a**.

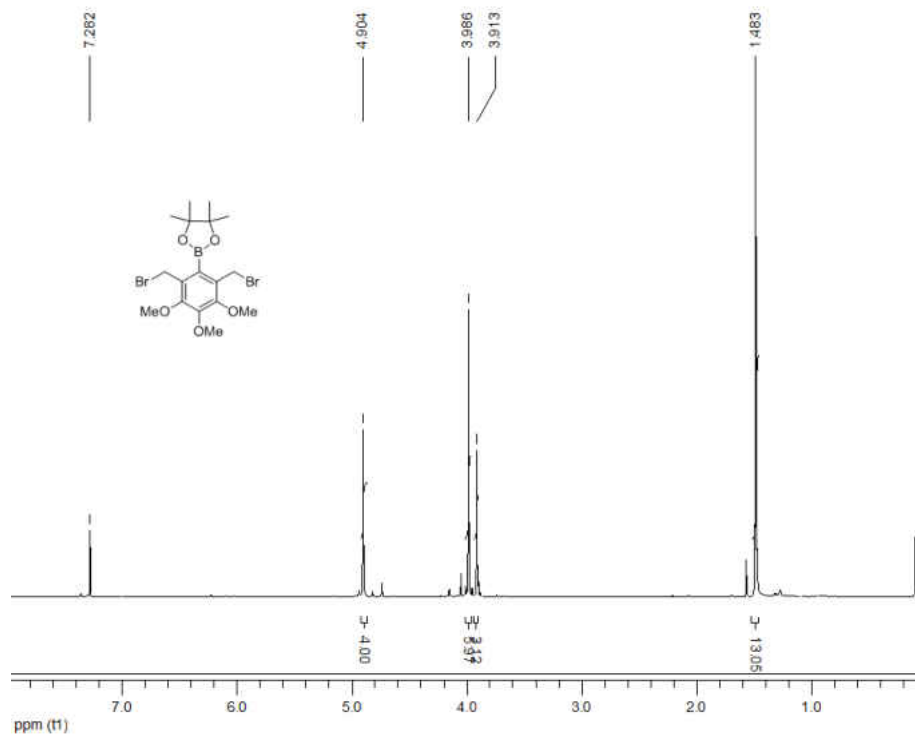


Figure 3-6-11. <sup>1</sup>H NMR spectra of **11a**.

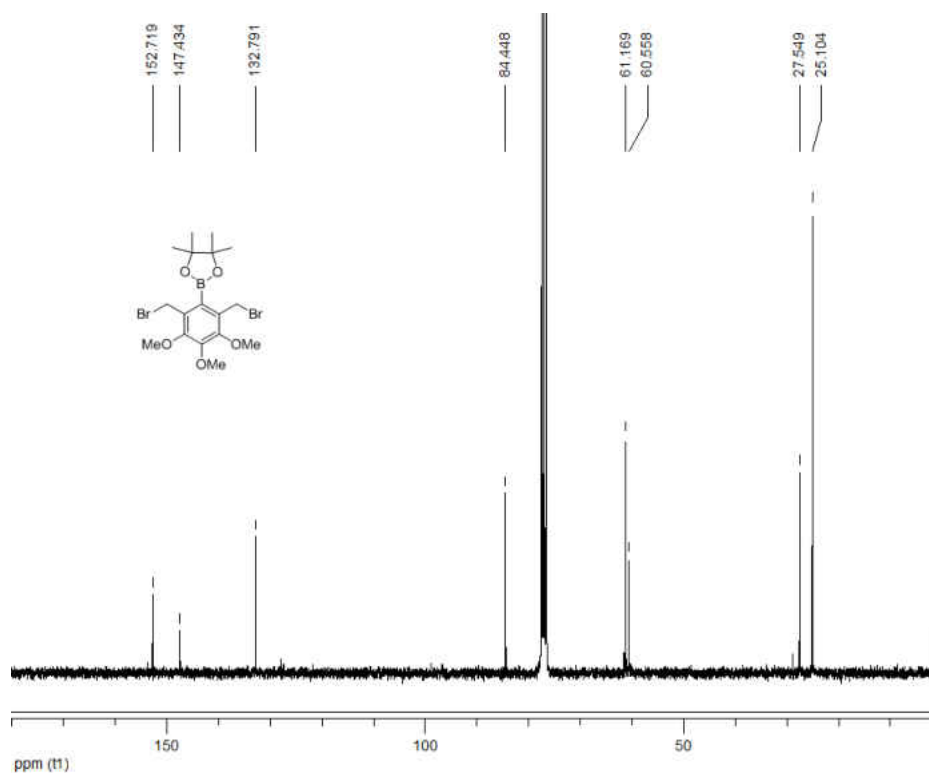


Figure 3-6-12. <sup>13</sup>C NMR spectra of **11a**.

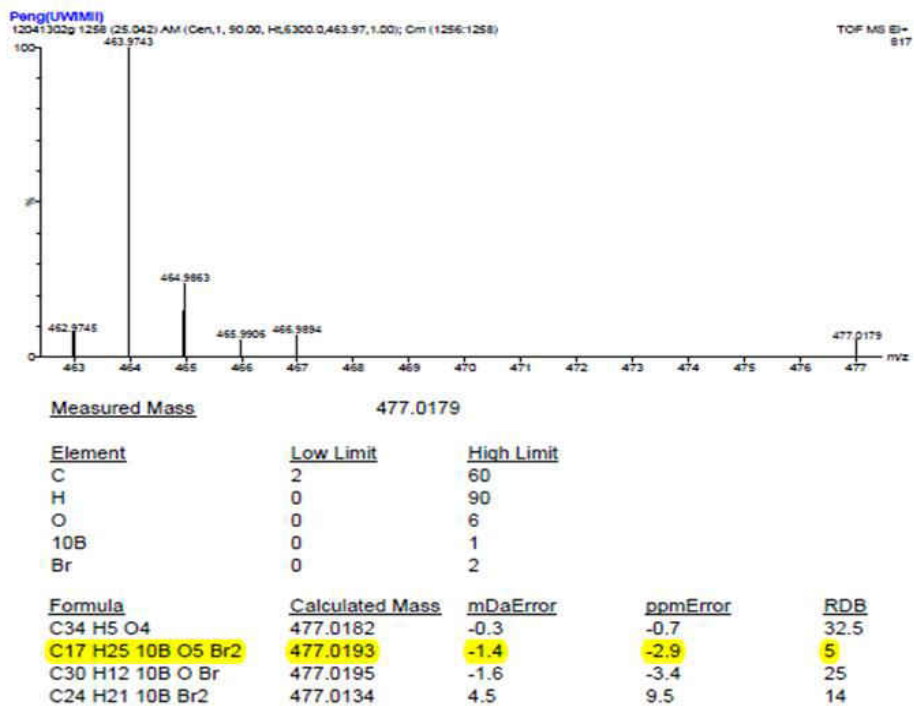


Figure 3-6-13. IT-TOF-MS (ESI) of **11a**.

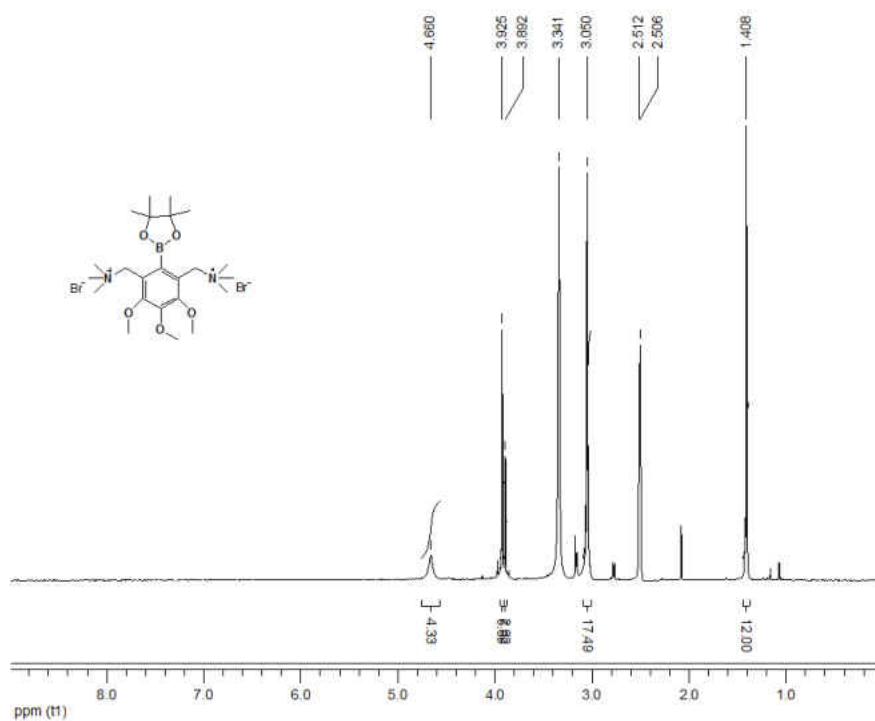


Figure 3-6-14. <sup>1</sup>H NMR spectra of **11b**.

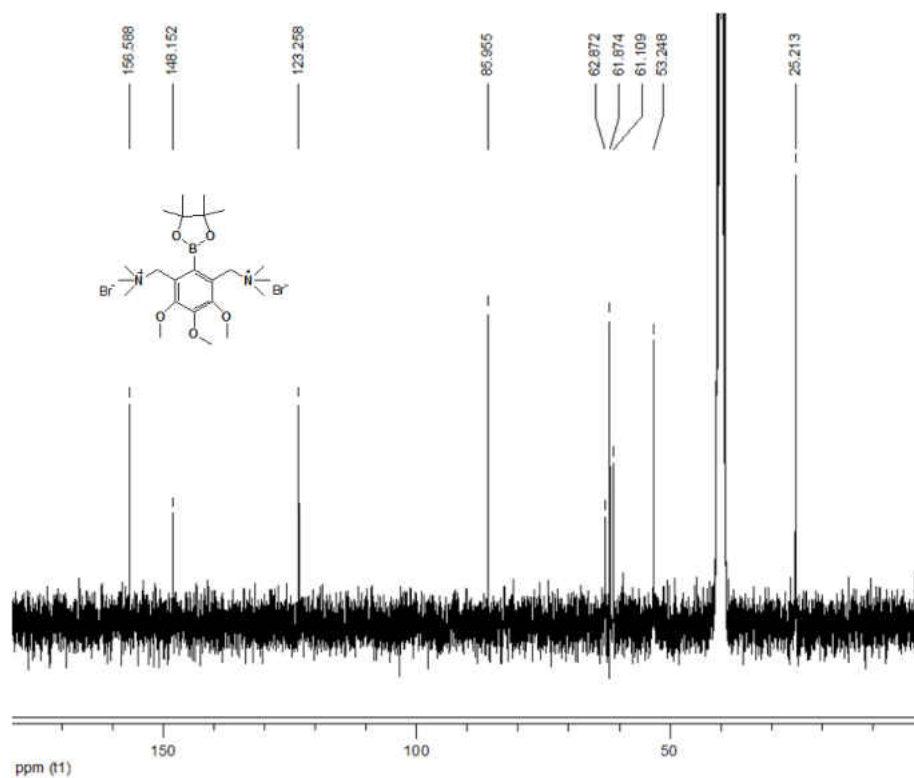


Figure 3-6-15.  $^{13}\text{C}$  NMR spectra of **11b**.

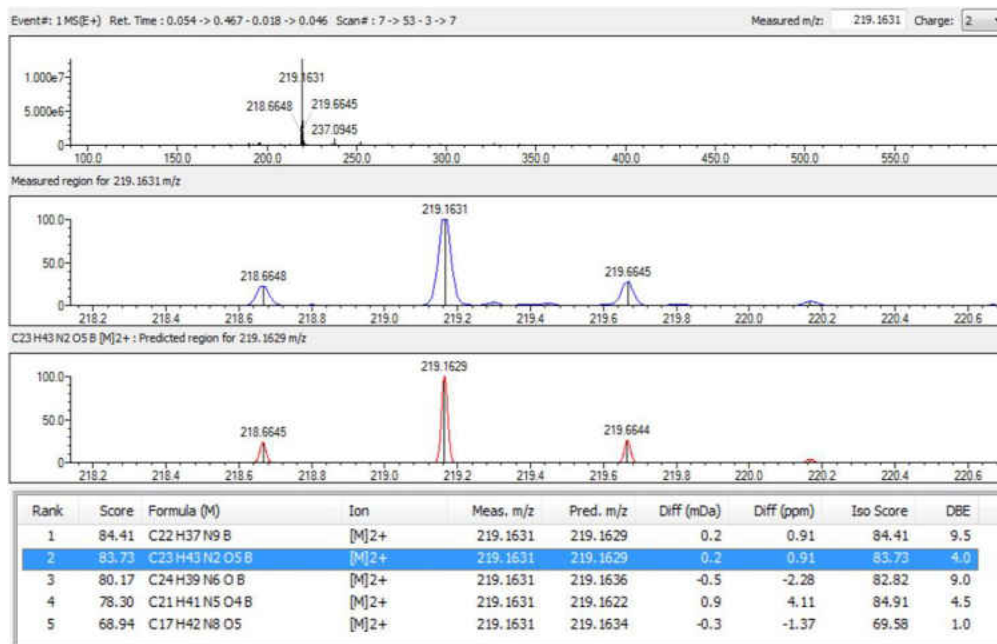


Figure 3-6-16. IT-TOF-MS (ESI) of **11b**.

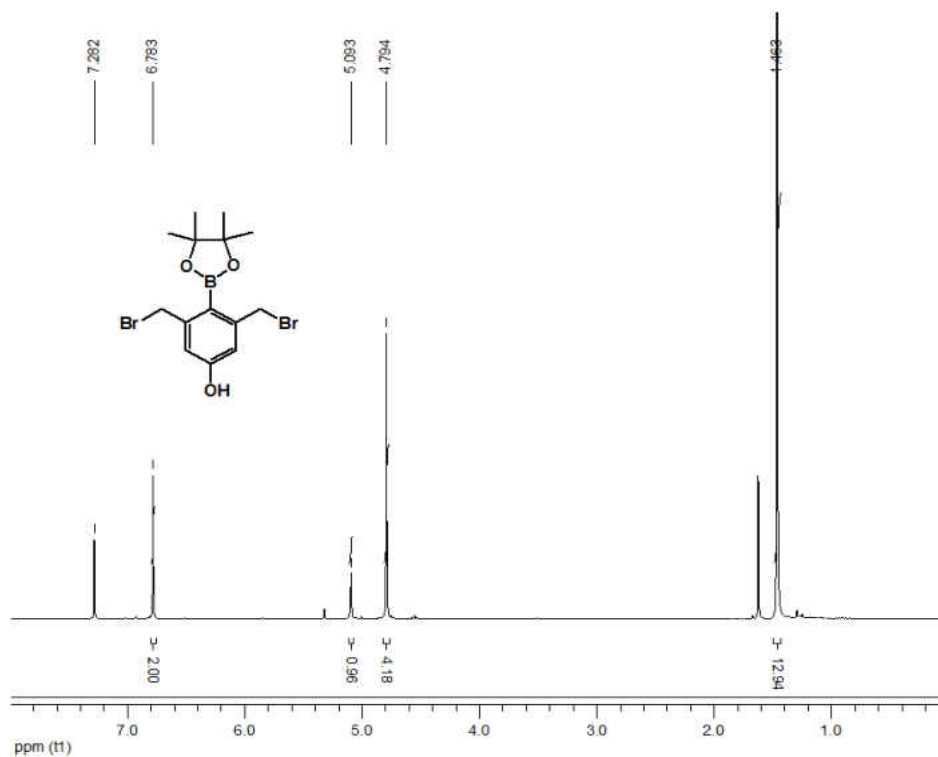


Figure 3-6-17.  $^1\text{H}$  NMR spectra of **12a**.

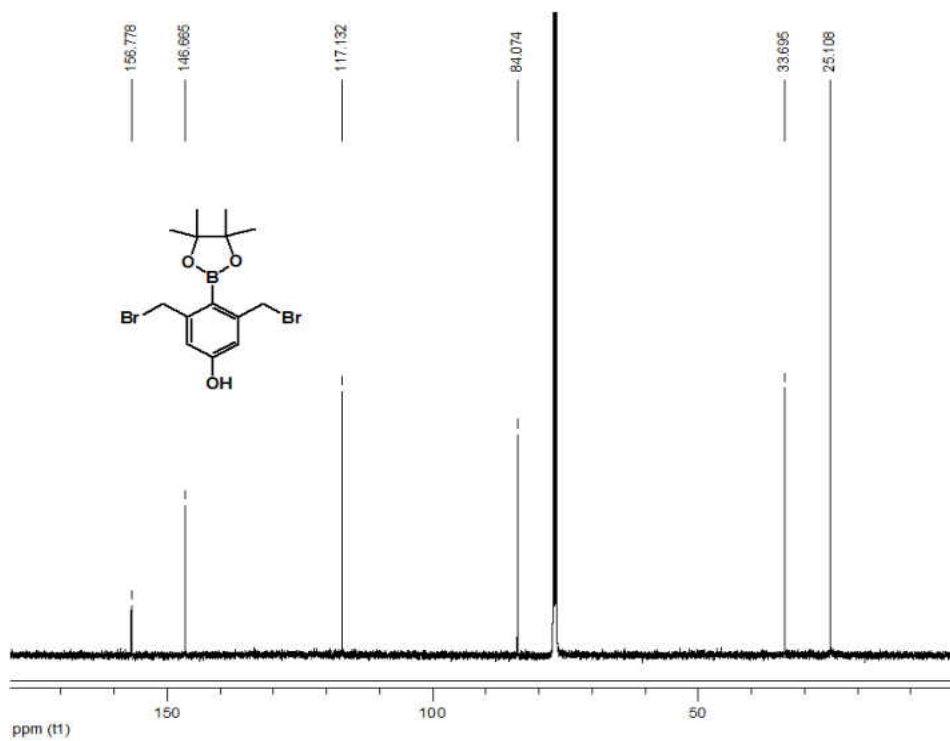


Figure 3-6-18.  $^{13}\text{C}$  NMR spectra of **12a**.

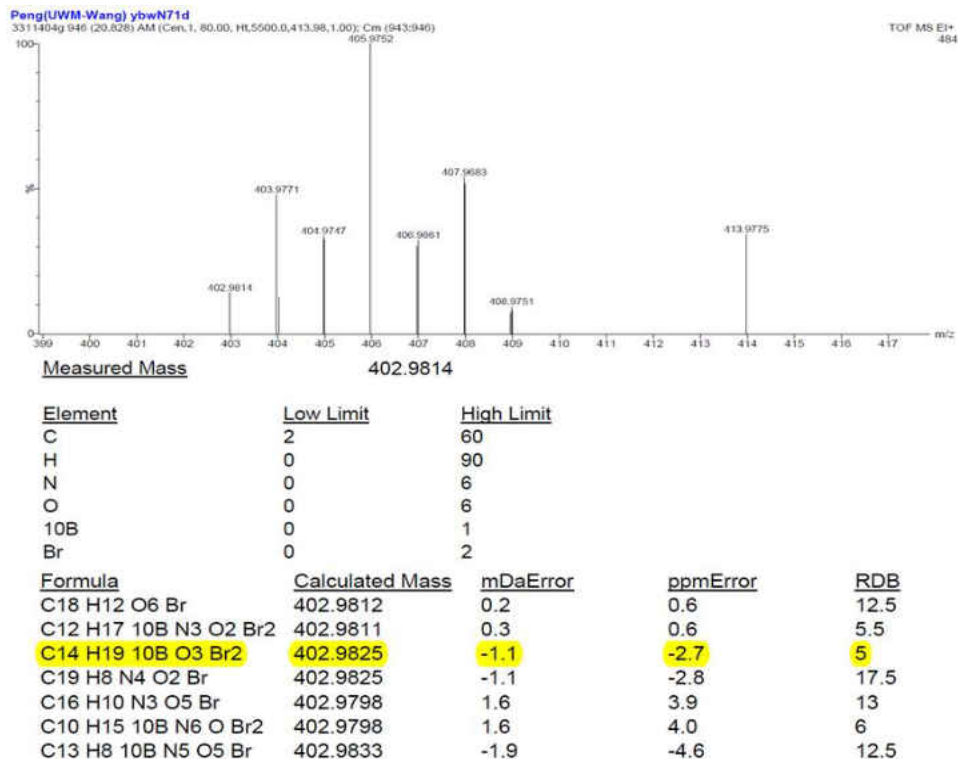


Figure 3-6-19. IT-TOF-MS (ESI) of **12a**.

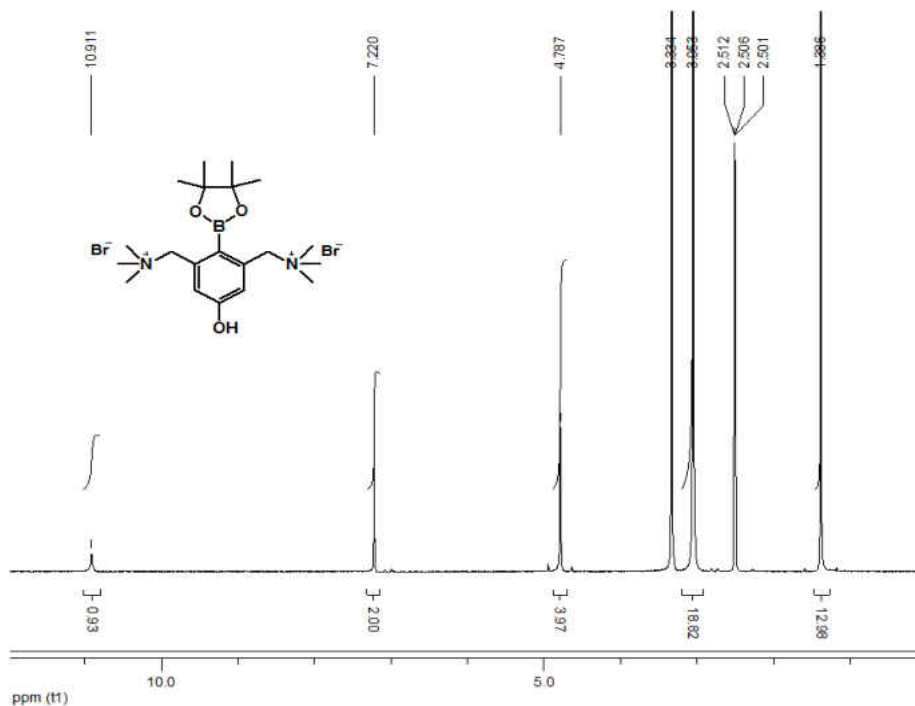


Figure 3-6-20. <sup>1</sup>H NMR spectra of **12b**.

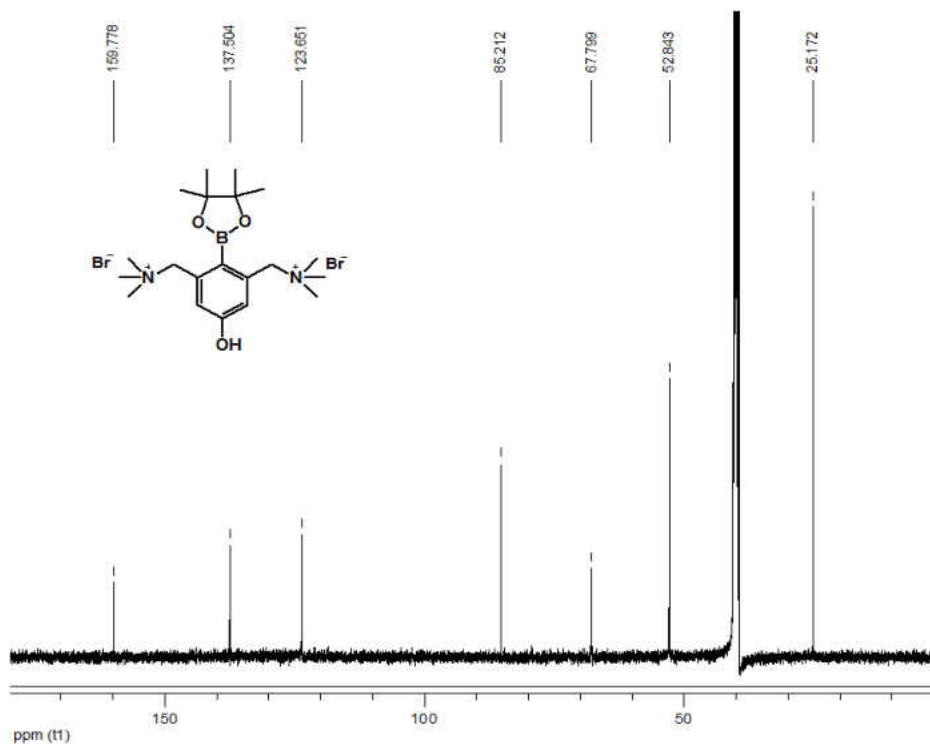


Figure 3-6-21.  $^{13}\text{C}$  NMR spectra of **12b**.

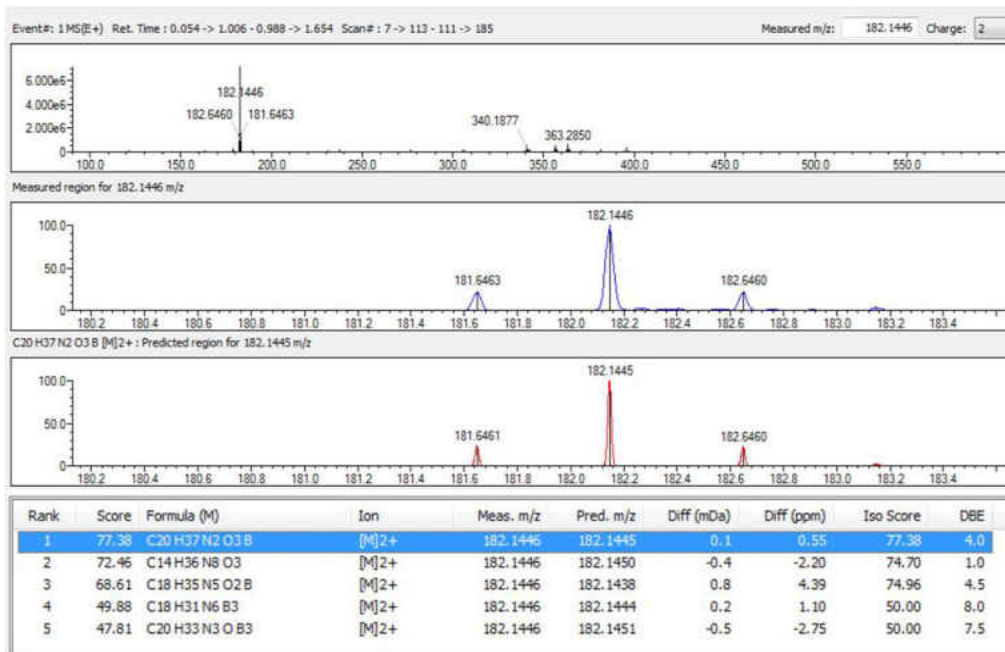


Figure 3-6-22. IT-TOF-MS (ESI) of **12b**.

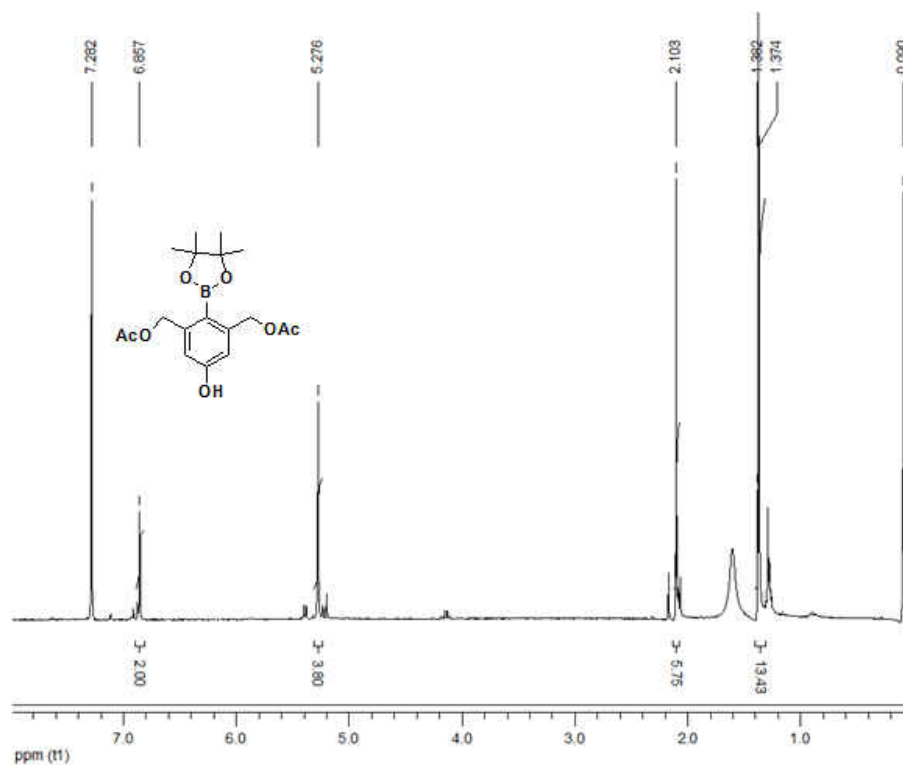


Figure 3-6-23. <sup>1</sup>H NMR spectra of **12c**.

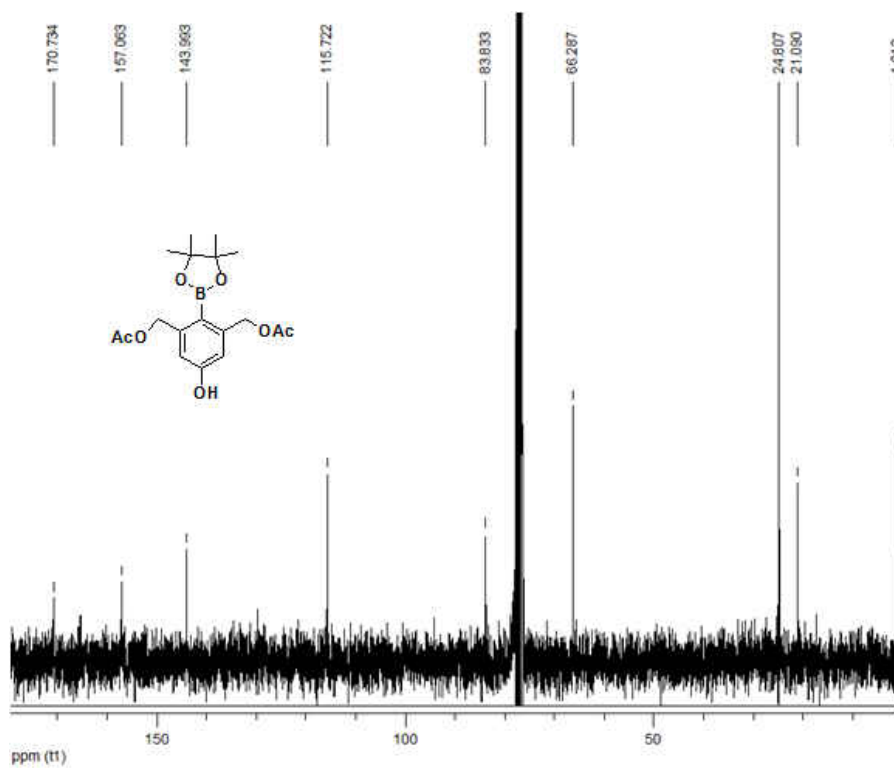


Figure 3-6-24. <sup>13</sup>C NMR spectra of **12c**.



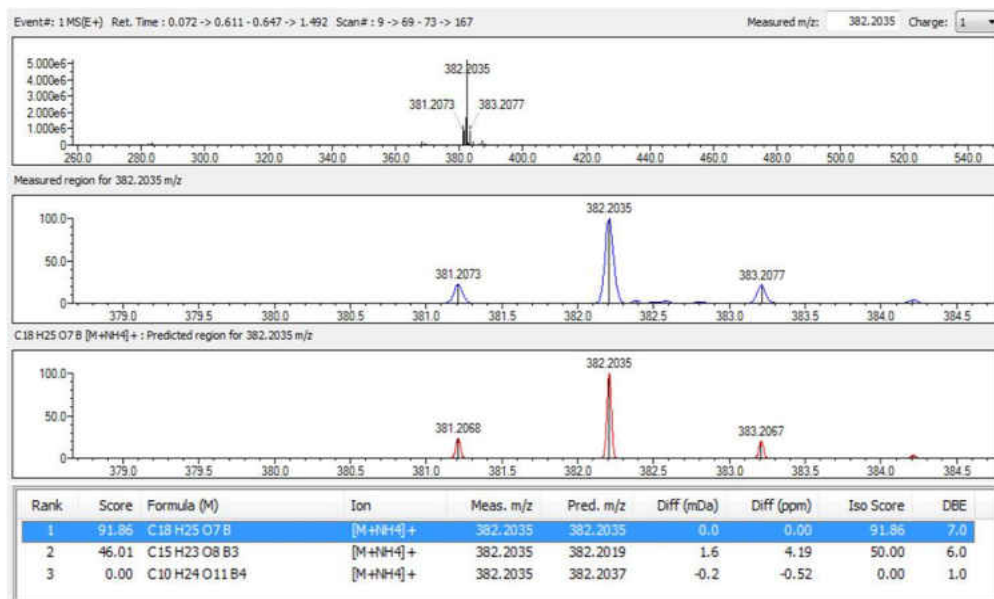


Figure 3-6-25. IT-TOF-MS (ESI) of **12c**.

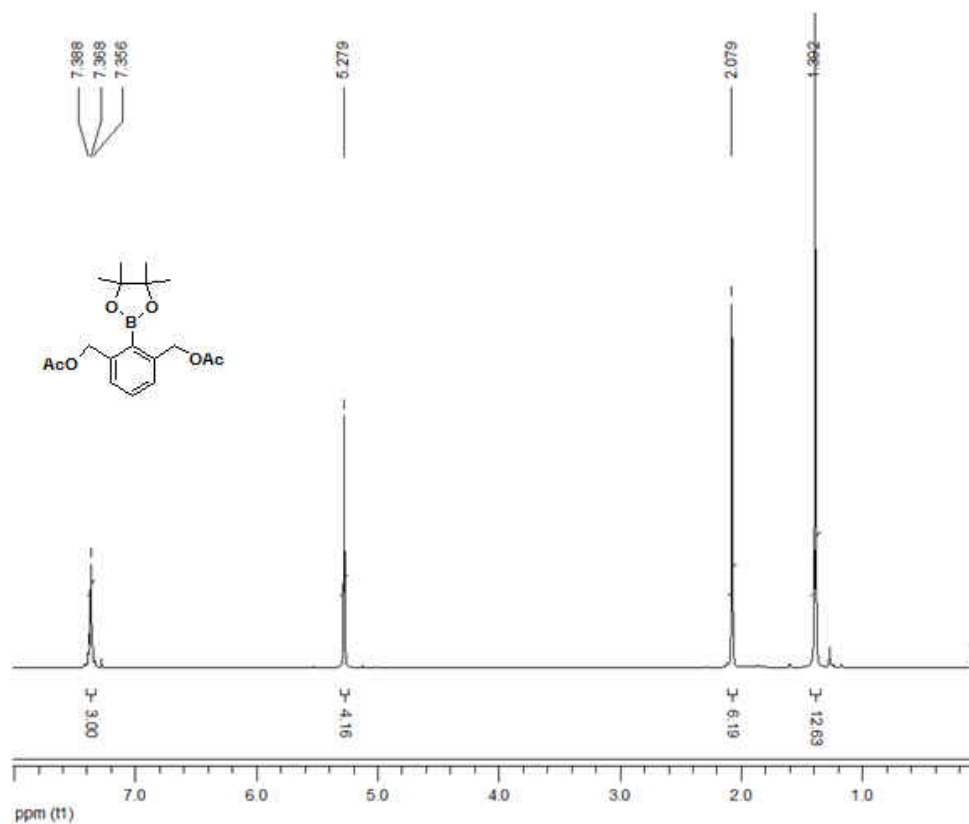


Figure 3-6-26. <sup>1</sup>H NMR spectra of **1c**.

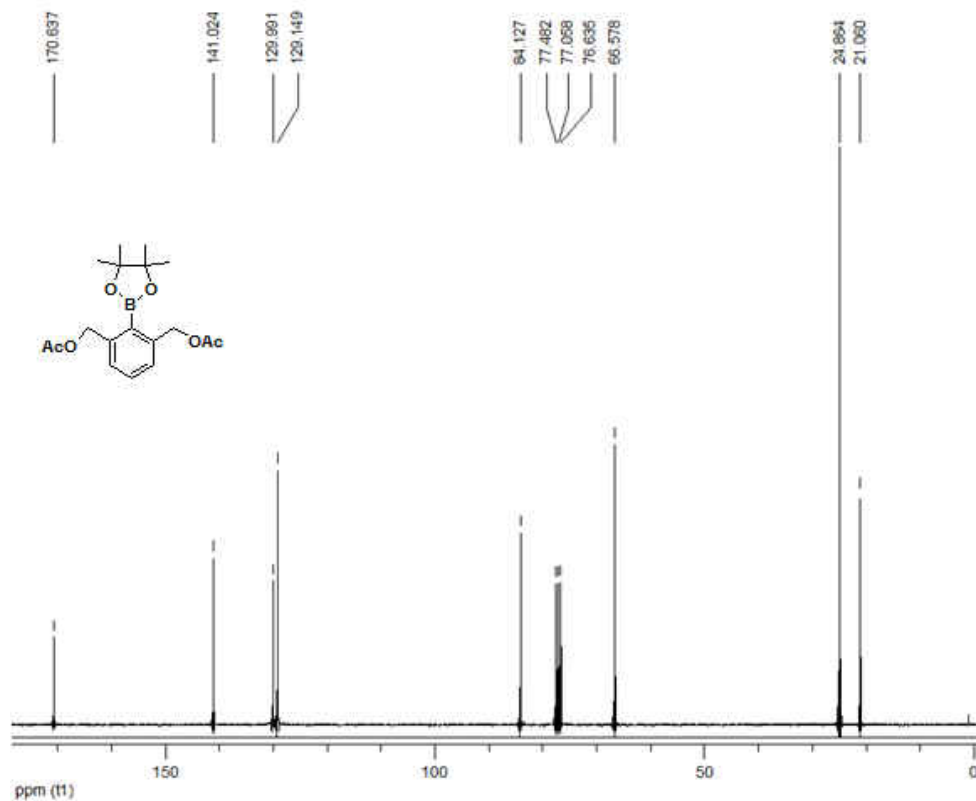


Figure 3-6-27.  $^{13}\text{C}$  NMR spectra of **1c**.

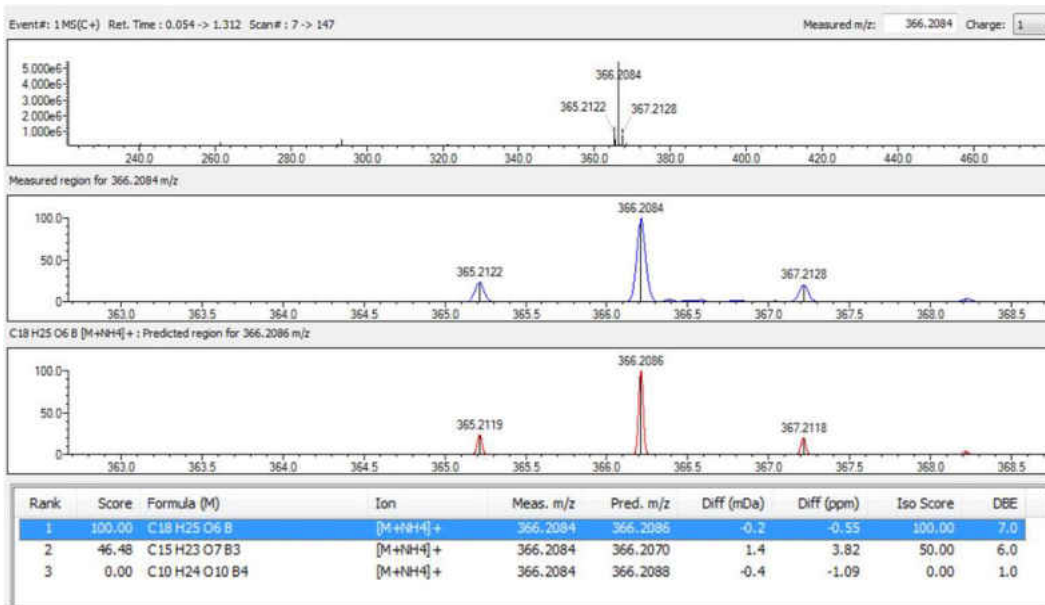


Figure 3-6-28. IT-TOF-MS (ESI) of **1c**.

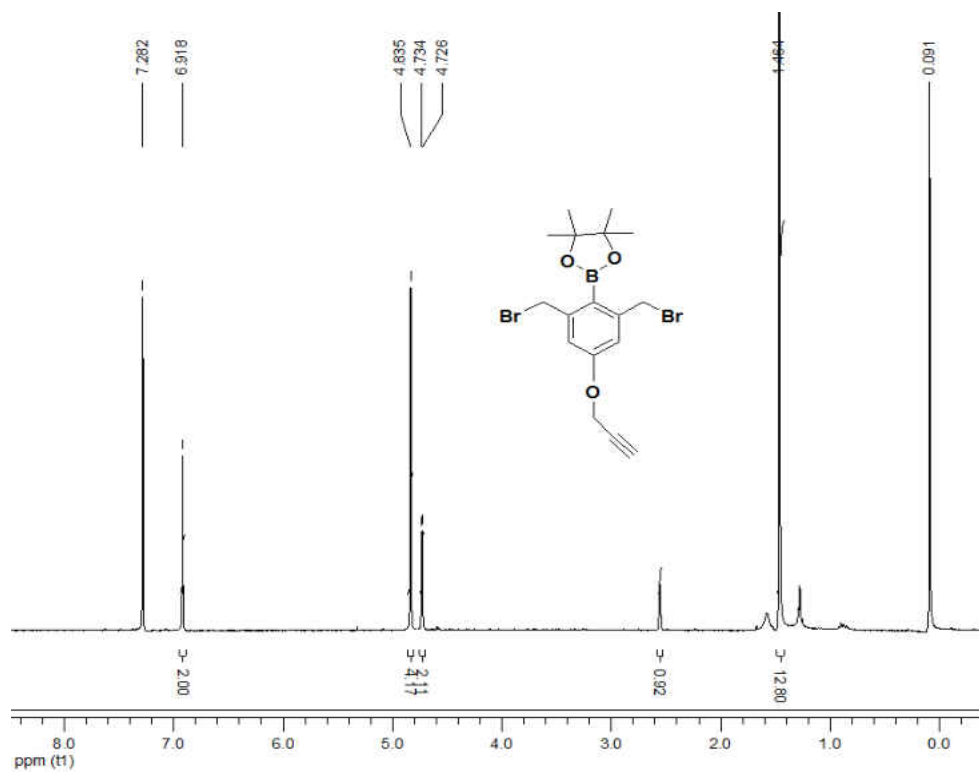


Figure 3-6-29.  $^1\text{H}$  NMR spectra of **13**.

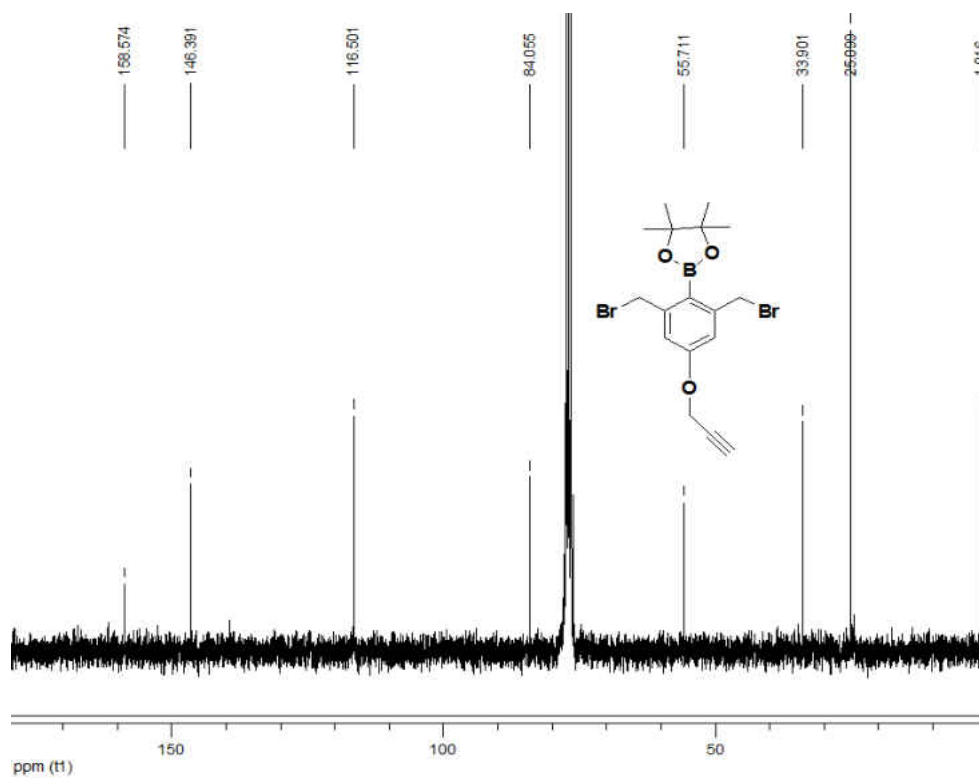
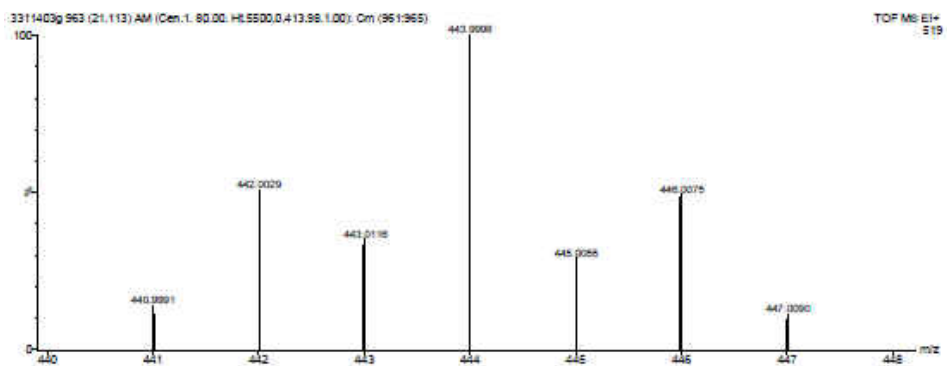


Figure 3-6-30.  $^{13}\text{C}$  NMR spectra of **13**.



Formula	Calculated Mass	mDaError	ppmError	RDB
C16 H10 10B N5 O5 Br	440.9989	0.2	0.4	14.5
C24 H12 N O3 Br	440.9995	-0.4	-0.9	19
C22 H10 N4 O2 Br	440.9982	0.9	2.1	19.5
<b>C17 H21 10B O3 Br2</b>	<b>440.9981</b>	<b>1.0</b>	<b>2.2</b>	<b>7</b>
C18 H12 10B N2 O6 Br	441.0003	-1.2	-2.6	14
C23 H N6 O5	441.0003	-1.2	-2.7	26.5
C9 H23 N4 O6 Br2	440.9979	1.2	2.8	-0.5
C28 H 10B N O5	440.9979	1.2	2.8	29.5
C12 H21 N5 O3 Br2	441.0006	-1.5	-3.3	4
C20 H19 10B N Br2	441.0008	-1.7	-3.9	11.5
C34 H O2	440.9971	2.0	4.5	34.5

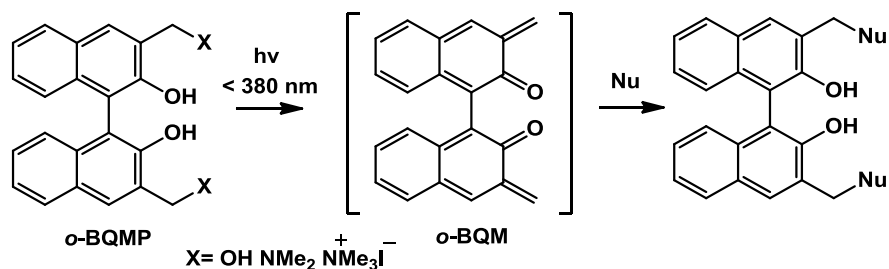
Figure 3-6-31. IT-TOF-MS (ESI) of **13**.

## Chapter 4. Photo-Induced Interstrand Cross-Link Formation by Naphthalene Boronates and its Mechanism Study

### 4.1. Introduction

Previous study showed that quinone methides (QMs) is an important intermediate in DNA cross-linking and alkylating process. More recently, several methods have been developed to activate bisaryl derivatives to cross-link DNA via bisquinone methides (bisQMs), such as fluoride-induction,<sup>1,2</sup> oxidation,<sup>3,4</sup> photo-irradiation,<sup>5</sup> and H<sub>2</sub>O<sub>2</sub>-induction.<sup>6,7</sup> Apart from QMs, some other active species such as radical and carbocation could also be involved in DNA alkylating process. Very recently, Dr. Greenberg and Li's group reported that photo-irradiation of modified thymidines yielded both 5-(2'-deoxyuridinyl)methyl cation and radical but only the cation produces ICLs in duplex DNA.<sup>8,9</sup> However, DNA ICL formation via a radical or a carbocation generated from a bisaryl derivative is probably least investigated.

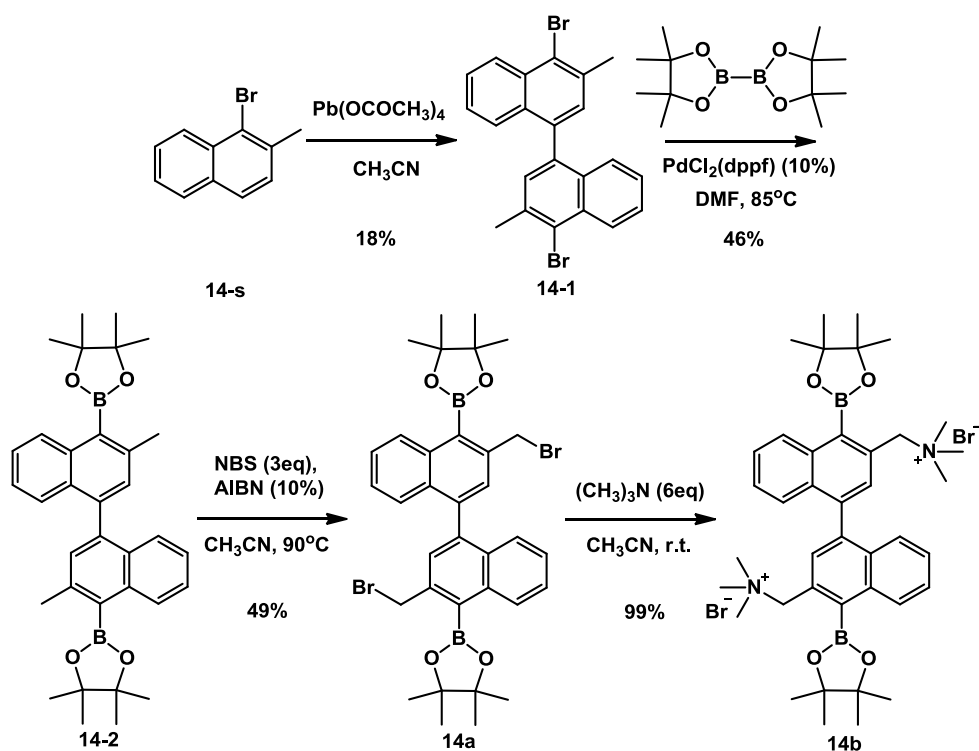
Our previous work showed that the phenylboronate derivatives, such as **1a**, **9a** and **12a** can be activated by H<sub>2</sub>O<sub>2</sub> to release QMs cross-linking DNA. Freccero's group reported a class of binaphthol derivatives, which can be activated by photo-irradiation to induce ICL formation via QMs. These *ortho*-binaphthalene quinone methide precursors (*o*-BQMP) have a strong absorbance above 310 nm and exhibit excellent solubility under physiological conditions (Scheme 4-1).<sup>10,11</sup> In this work, we designed and synthesized a few novel naphthalene boronate esters **14a,b** (Scheme 4-2) and studied their reactivity towards DNA upon H<sub>2</sub>O<sub>2</sub>-induction or photo-irradiation. We discovered that the naphthalene boronate esters were not good H<sub>2</sub>O<sub>2</sub>-inducible DNA cross-linking agents but can be activated by photo-irradiation to induce DNA ICL formation. The mechanism involves formation of free radicals which undergo oxidation to a methyl cation capable of alkylating DNA.



**Scheme 4-1.** QM generation by binolquinone methide precursors.

## 4.2. DNA cross-linking ability of binaphthalene boronate esters **14a** and **14b**

### 4.2.1. Synthesis of **14a** and **14b**



**Scheme 4-2.** Synthesis of compounds **14a** and **14b**.

Compounds **14a** and **14b** were synthesized starting from commercially available 1-bromo-2-methylnaphthalene (**14-s**) (Scheme 4-3). Treatment of **14-s** with lead tetraacetate in acetonitrile resulted in regiospecific oxidative dehydrodimerization to provide binaphthalene analogue **14-1**.

Palladium-catalyzed borylation of **14-1** yielded the boronated product **14-2**, which was converted to the brominated analogue **14a** by using NBS and AIBN in acetonitrile. Quaternization of **14a** with trimethylamine provided **14b** in a nearly quantitative yield.

#### 4.2.2. DNA cross-linking ability of **14a** and **14b**

Initially, the activity of **14a** and **14b** towards DNA was investigated by measuring DNA ICL formation with H<sub>2</sub>O<sub>2</sub> or photo induction. The reaction of **14a** or **14b** with duplex **5** was carried out in phosphate buffer (pH = 8.0) at 37 °C. ICL formation and cross-linking yields were analyzed via denaturing polyacrylamide gel electrophoresis (PAGE) with phosphorimager analysis (Image Quant 5.2). Without H<sub>2</sub>O<sub>2</sub> or UV irradiation, there was no ICLs formation by **14a** and **14b** (Figure 4-1, lanes 2, 5, 10 and 13). However, in the presence of H<sub>2</sub>O<sub>2</sub> or UV-irradiation (350 nm), both **14a** and **14b** induced DNA interstrand cross-link formation while higher ICL yield was observed with **14a** (Figure 4-1, lanes 4 and 12). For the same compound, UV-irradiation resulted in more efficient DNA cross-linking than H<sub>2</sub>O<sub>2</sub> induction. For example, when 200 μM of drugs were used, UV-irradiation led to 11% ICLs for **14a** and 7.1% for **14b** (Figure 4-1, lanes 4 and 7), while H<sub>2</sub>O<sub>2</sub> induced only 4.1% ICLs for **14a** and 2.9% for **14b** (Figure 4-1, lanes 12 and 15).

5'-dGCCTAGTTCTTTTAATTACTTGCAATGCAAGTAATTAAAGCTTGATCTG (**5a**)

3'-dCGGATCAAGAAAATTAATGAACGTTACGTTTCATTAATTTTCGAACTAGAC (**5b**)

**5**

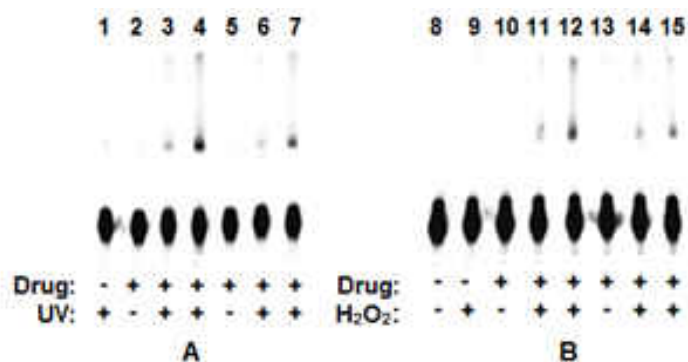


**Figure 4-1.** H<sub>2</sub>O<sub>2</sub> and UV induced ICL formation by **14a,b**. A. UV-induced DNA cross-link formation by compounds **14a** and **14b** at 37 °C for 4 h. Lane 1: DNA only; lane 2: 200 μM **14a** without UV; lane 3: 50 μM **14a** (cross-linking yield 4.2%); lane 4: 200 μM **14a** (10.9%); lane 5: 200 μM **14b** without UV; lane 6: 50 μM **14b** (3.2%); lane 7: 200 μM **14b** (7.1%). B. H<sub>2</sub>O<sub>2</sub>-induced DNA cross-link formation by compounds **14a** and **14b** at 37 °C for 24 h. Lane 8: DNA only; lane 9: H<sub>2</sub>O<sub>2</sub> only; lane 10: 200 μM **14a** without H<sub>2</sub>O<sub>2</sub>; lane 11: 50 μM **14a** and 100 μM H<sub>2</sub>O<sub>2</sub> (2.1%); lane 12: 200 μM **14a** and 400 μM H<sub>2</sub>O<sub>2</sub> (4.1%); lane 13: 200 μM **14b** without H<sub>2</sub>O<sub>2</sub>; lane 14: 50 μM **14b** and 100 μM H<sub>2</sub>O<sub>2</sub> (1.1%); lane 15: 200 μM **14b** and 400 μM H<sub>2</sub>O<sub>2</sub> (2.9%).

In order to optimize the ICL formation condition for later study, different concentration of drug were tested and we found that higher concentration of drugs led to increased ICL yields (Figures 4-2 to 4-5). However, the DNAs could not enter the gel completely if more than 200 μM of **14b** was used. That is possibly because of the presence of large amount positive charges when **14b** monoalkylated DNA strands (Figure 4-4 lane 9-11 and Figure 4-6 lane 8-9). It will lead to inaccurate estimation of the ICL yields. Thus, 200 μM of drugs were used for all further study. And also, the ICL formation was time-dependent. Extension of UV irradiation time increased the ICL yields (Figure 4-7 and 4-8). But longer irradiation time also induced DNA strands break (Figure 4-7 lane 9-11). So we chose 4 h UV irradiation for further investigation.



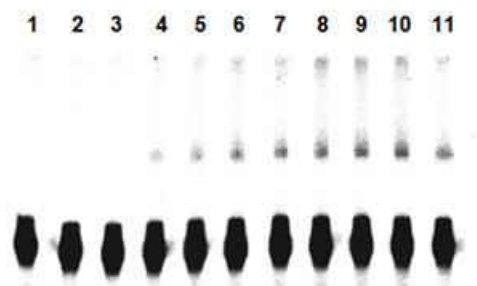


**Figure 4-2.** Concentration dependence of ICL formation by **14a** upon H<sub>2</sub>O<sub>2</sub> activation. The ratio of **14a**/H<sub>2</sub>O<sub>2</sub> is 1:2. Lane 1: with DNA only; lane 2: DNA with H<sub>2</sub>O<sub>2</sub> only; lane 3: DNA with **14a** only; lane 4: 10 μM **14a** (cross-linking yield 1.1%); lane 5: 20 μM **14a** (1.3%); lane 6: 50 μM **14a** (2.5%); lane 7: 100 μM **14a** (3.1%); lane 8: 200 μM **14a** (3.6%); lane 9: 500 μM **14a** (4.3%); lane 10: 1 mM **14a** (4.5%); lane 11: 2 mM **14a** (4.1%). Condition: 37 °C incubation at pH8 for 1 d.

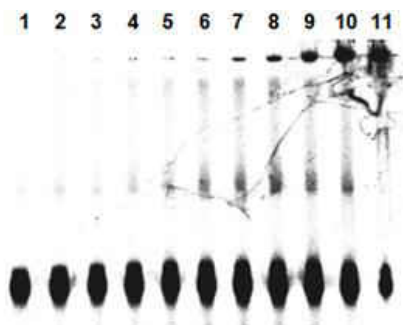


**Figure 4-3.** Concentration dependence of ICL formation by **14b** upon H<sub>2</sub>O<sub>2</sub> activation. The ratio of **14b**/H<sub>2</sub>O<sub>2</sub> is 1:2. Lane 1: with DNA only; lane 2: DNA with H<sub>2</sub>O<sub>2</sub> only; lane 3: DNA with **14b** only; lane 4: 10 μM **14b** (cross-linking yield 0.9%); lane 5: 20 μM **14b** (1.3%); lane 6: 50 μM **14b** (2.3%); lane 7: 100 μM **14b** (2.4%); lane 8: 200 μM **14b** (2.8%); lane 9: 500 μM **14b** (2.3%); lane 10: 1 mM **14b** (not quantified); lane 11: 2 mM **14b** (not quantified). Condition: 37 °C incubation at pH8 for 1 d.

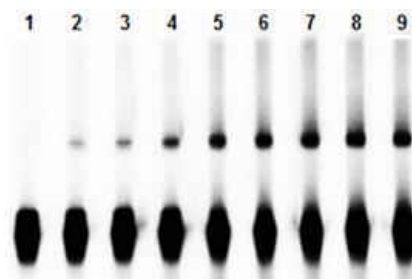


**Figure 4-4.** Concentration dependence of ICL formation by **14a** upon UV irradiation. Lane 1: with DNA only; lane 2: 10  $\mu\text{M}$  **14a** (cross-linking yield 1.4%); lane 3: 20  $\mu\text{M}$  **14a** (1.9%); lane 4: 50  $\mu\text{M}$  **14a** (3.6%); lane 5: 100  $\mu\text{M}$  **14a** (6.8%); lane 6: 200  $\mu\text{M}$  **14a** (11.1%); lane 7: 500  $\mu\text{M}$  **14a** (13.8%); lane 8: 1 mM **14a** (13.8%); lane 9: 2 mM **14a** (13.0%). Condition: UV irradiation at pH8 for 4h.

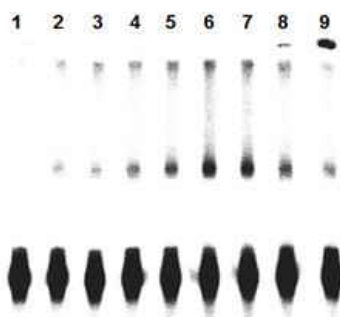


**Figure 4-5.** Concentration dependence of ICL formation by **14b** upon UV irradiation. Lane 1: with DNA only; lane 2: 10  $\mu\text{M}$  **14b** (cross-linking yield 2.2%); lane 3: 20  $\mu\text{M}$  **14b** (2.8%); lane 4: 50  $\mu\text{M}$  **14b** (3.8%); lane 5: 100  $\mu\text{M}$  **14b** (4.8%); lane 6: 200  $\mu\text{M}$  **14b** (8.7%); lane 7: 500  $\mu\text{M}$  **14b** (8.7%); lane 8: 1 mM **14b** (6.1%); lane 9: 2 mM **14b** (not quantified). Condition: UV irradiation at pH8 for 4h.

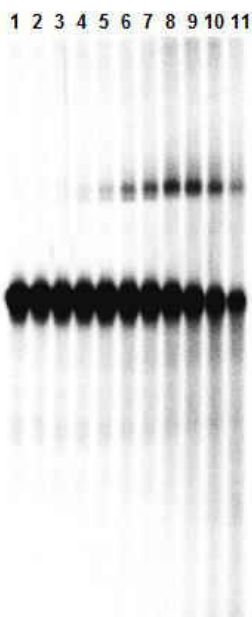


**Figure 4-6.** Time dependence of ICL formation by **14a** upon UV irradiation. Lane 1: no UV irradiation; lane 2: UV for 5 min (cross-linking yield 0.4%); lane 3: 15 min (0.9%); lane 4: 30 min (1.2%); lane 5: 1 h (2.5%); lane 6: 2 h (4.5%); lane 7: 3 h (8.9%); lane 8: 4 h (13.3%); lane 9: 6 h (14.1%); lane 10: 8 h (16.6%); lane 11: 12 h (not quantified). Condition: UV irradiation at pH8.

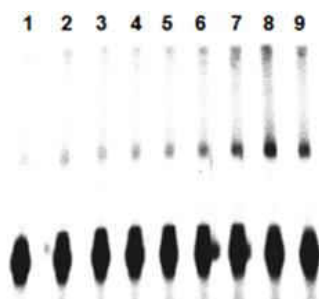


**Figure 4-7.** Time dependence of ICL formation by **14b** upon UV irradiation. Lane 1: no UV irradiation; lane 2: UV for 5 min (cross-linking yield 0.9%); lane 3: 15 min (1.8%); lane 4: 30 min (2.2%); lane 5: 1 h (3.8%); lane 6: 2 h (5.8%); lane 7: 3 h (6.7%); lane 8: 4 h (7.9%); lane 9: 6 h (6.6%). Condition: UV irradiation at pH8.

### 4.2.3. Determination of cross-linking site

We further investigated the heat-stability of purified cross-linked products and monoalkylated single-stranded DNA and determined the cross-linking sites. The ICLs formed from **14a** and **14b** were stable to heating in phosphate buffer while clear DNA cleavage was observed with piperidine treatment. Strong cleavage bands were observed mainly at dG sites upon heating in 1.0 M piperidine which is known to induce cleavage of N-7-alkylated purines according to the Maxam and Gilbert reaction mechanism (Figure 4-9 lanes 1 and 3).<sup>12,13</sup> This indicated that the cross-linking reactions mainly occurred with dGs via alkylation. To confirm this, we applied self-complementary dAT duplex **6** and duplex **7** having only dCs/dTs in one strand and dGs/dAs in the other strand. The DNA ICL formation was observed with duplex **7** but not with **6** when they were treated with **14a** upon photo-irradiation (Figure 4-10), which indicated that cross-linking reactions took place with dG and dC not with dA/dT.

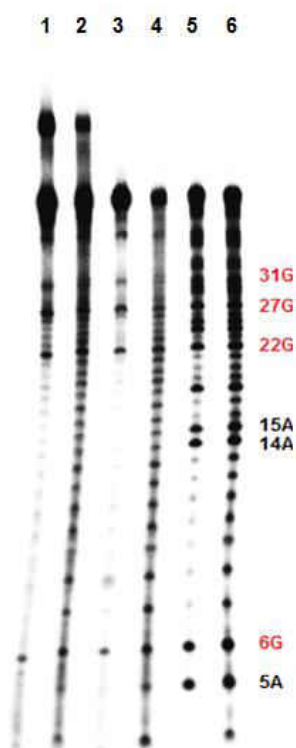


**Figure 4-8.** Determination of cross-linking site of **14a**. Phosphorimage autoradiogram of 20% denaturing PAGE analysis of the isolated ICL products and monoalkylated single stranded DNA (**5a'**) upon heating in piperidine. Lane 1: piperidine treatment of ICL product; lane 2: Fe·EDTA treatment of ICL product; lane 3: piperidine treatment of **5a'**; lane 4: Fe·EDTA treatment of **5a'**; lane 5: G+A sequencing; lane 6: Fe·EDTA treatment of **5**.

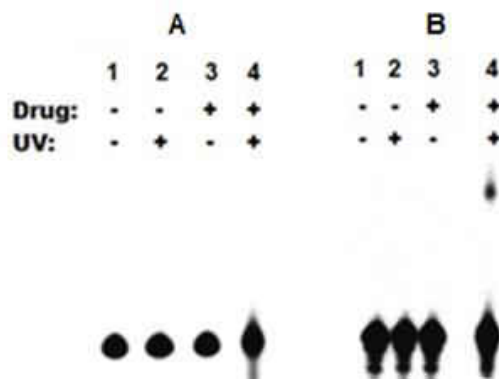
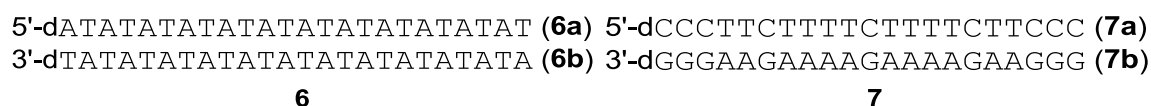


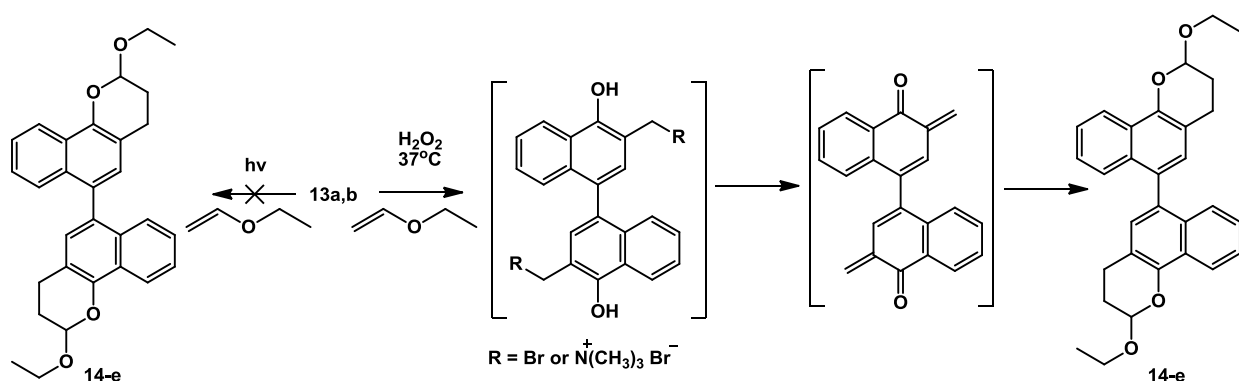
**Figure 4-9.** ICL formation from duplex **7** induced by **14a** upon UV irradiation. Lane 1: DNA only; lane 2: DNA only with UV; lane 3: DNA with 500  $\mu$ M **14a** no UV; lane 4: DNA with 500  $\mu$ M **14a** and UV irradiation. Condition: UV irradiation for 4 h at pH8.

### 4.3. The mechanism of ICL formation induced by **14a,b**

#### 4.3.1. QM formation in the presence of H<sub>2</sub>O<sub>2</sub>

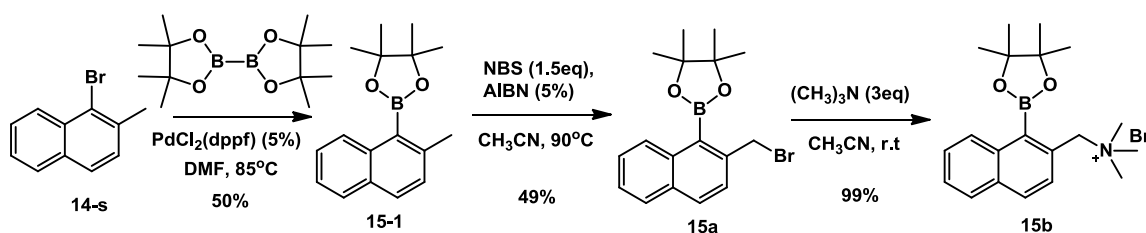
As we described previously,<sup>6,7</sup> QM trapping experiment using excess ethyl vinyl ether (EVE) was applied for determining H<sub>2</sub>O<sub>2</sub>-induced QMs formation. As expected, the QM trapping product **14-e** was isolated when **14a** or **14b** was incubated with H<sub>2</sub>O<sub>2</sub> in the presence of EVE at 37 °C for 24 h (Scheme 4-3). To our surprise, **14-e** was not detected when compounds **14a** and

**14b** were irradiated with 350 nm light in the presence of excess EVE. These results suggested that different from H<sub>2</sub>O<sub>2</sub>-induced DNA cross-linking by **14a** and **14b** where QMs were involved, photo-irradiation of these compounds might lead to formation of other active species capable of cross-linking DNA, such as radicals or cations.



**Scheme 4-3.** QM Trapping reactions with ethyl vinyl ether.

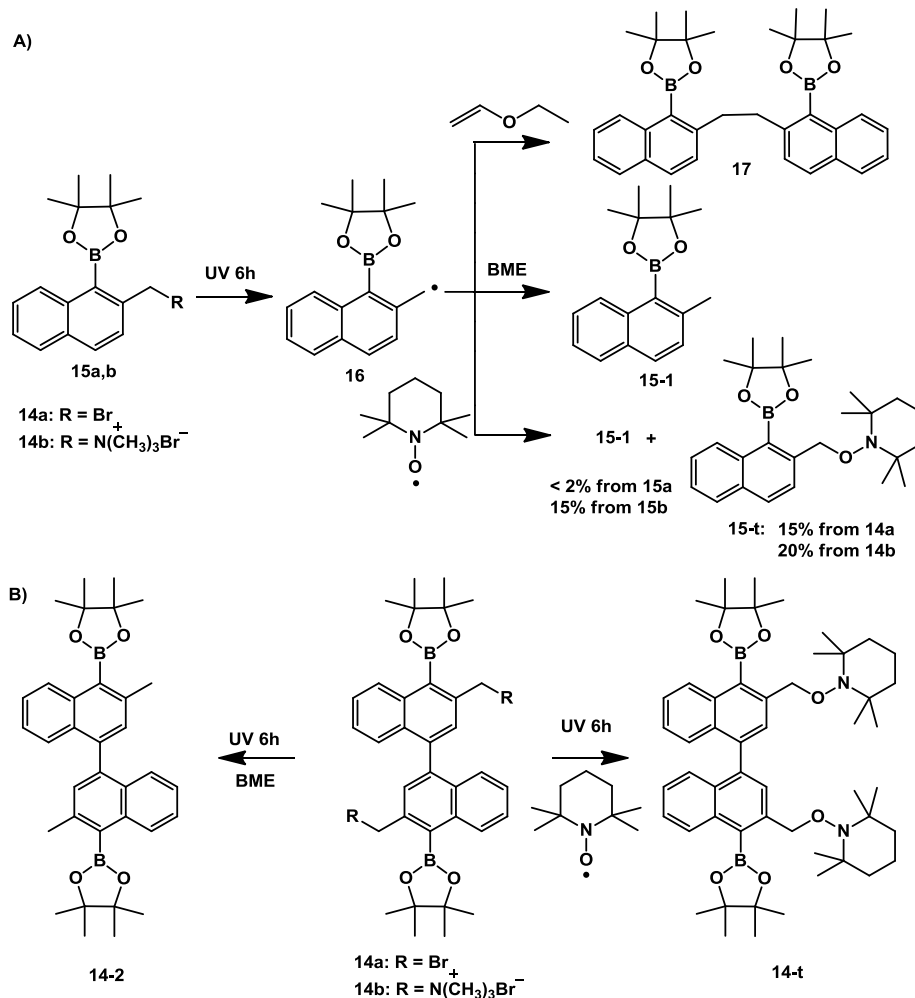
#### 4.3.2. Radical formation upon UV irradiation



**Scheme 4-4.** Synthesis of compounds **15a** and **15b**.

In order to fully investigate the photo-reactivity of naphthaleneboronates and simplify the trapping reaction, we synthesized two simpler models **15a,b** (Scheme 4-4). Then the QM trapping reaction was performed. Similar to the results obtained with **14a** and **14b**, the QM trapping product was not obtained after **15a,b** were irradiated at 350 nm in the presence of EVE (Scheme 4-5 A). However we observed the generation of compound **17** which was considered resulting from the dimerization of the radical **16** (Scheme 4-5 A). Thus, to provide evidence for

formation of **16**, 2-mercaptoethanol (BME) and 2,2,6,6-tetramethylpiperidin-1-oxyl (TEMPO) were chosen as radical trapping agents. As expected, the radical trapping products **15-1** and **15-t** were obtained following photo-irradiation of **15a,b** (Scheme 4-5 A). Encouraged by these data, we further performed radical trapping reactions with **14a** and **14b** upon 350 nm irradiation using BME and TEMPO, which yielded **14-2** and **14-t**, respectively. Clearly, photo-induced DNA ICL formation by **14a** and **14b** was through a radical mechanism not via QM formation. However, we cannot conclude that the DNA ICLs were directly produced from the radical intermediates since the methyl radical could be oxidized or reduced to cation or anion.<sup>9</sup>



**Scheme 4-5.** Radical trapping reactions with BME or TEMPO.

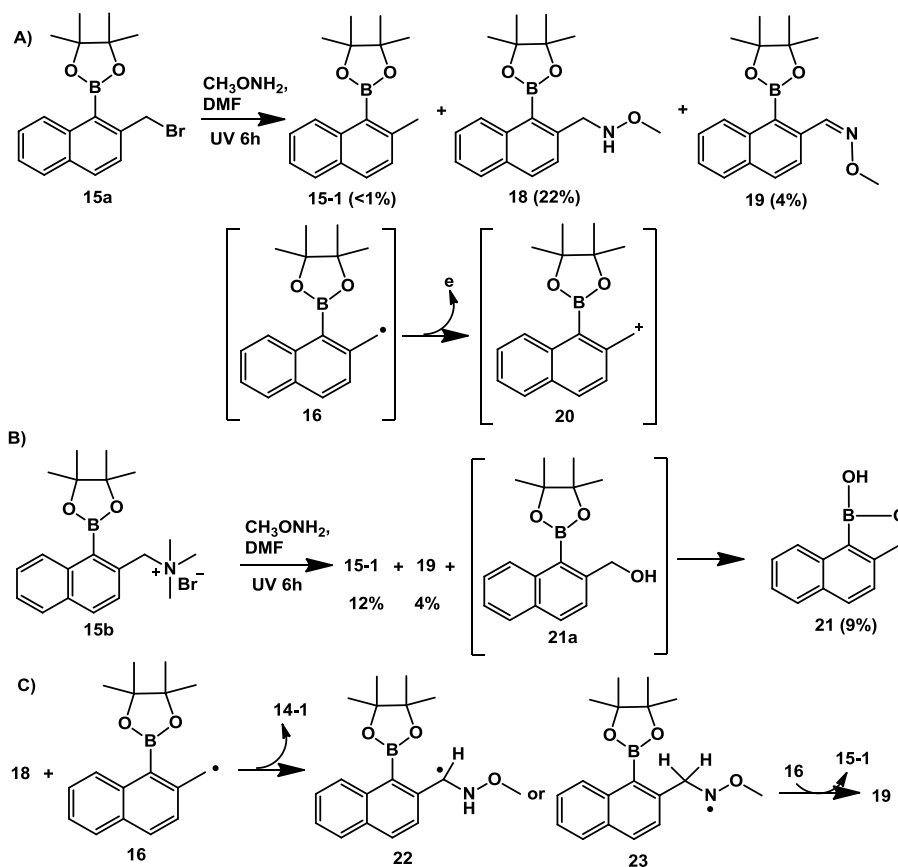
#### 4.3.3. Cation formation from radical through electron transfer

Subsequently, methoxyamine was chosen as trapping agent for carbocation, as it had been successfully employed as a probe for 5-(2'-deoxyuridinyl)methylation.<sup>8</sup> Photo-irradiation of **15a** in the presence of methoxyamine produced the expected cation trapping products **18** and **19**. Meanwhile, **15-1** was also obtained. We considered that compound **19** was generated from oxidation of **18**. Although the exact mechanism for formation of **15-1** and **19** is not clear yet, it is precedent that alkoxyamines can be oxidized to oxime ethers in the presence of radicals.<sup>14</sup> We propose that the reaction might proceed via a H-transfer from either the CH<sub>2</sub> or NH to the radical **16** resulting in **15-1** and the radical intermediate **22** or **23** (Scheme 4-6 C). A second H-transfer from **22** or **23** to **16** would yield **19** and **15-1**.

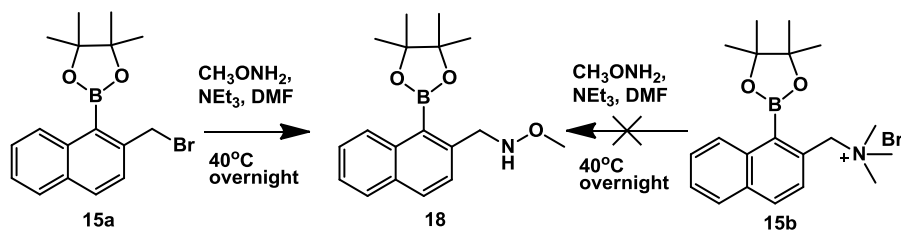
Our further investigation showed that a nucleophilic substitution occurred between **15a** and methoxyamine under heating without UV-irradiation which yielded only **18** but not **15-1** and **19** (Scheme 4-7). This provided evidence that formation of **19** is via a radical mechanism. Similar to **15a**, photo-irradiation of **15b** with methoxyamine yielded compounds **15-1** and **19**. However, alkoxyamine **18** was not isolated in sufficient amount with **15b** but compound **21** was isolated in 9% yield instead. Compound **21** could be generated from a hydroxymethyl intermediate **21a** which might be produced via oxidation of the radical **16** or hydroxylation of the cation **20**. As no direct evidence for H abstraction by **16** to form **20**, we cannot exclude the possibility that another molecule of **16** accepts one electron to generate a methyl anion, which is protonated to form **20**. However, our anion trapping reaction by using D<sub>2</sub>O discriminate against formation of the methyl anion as **20** was generated from photo-irradiation of **15b** in the presence of D<sub>2</sub>O while the deuterated analogue of **20** was not detected (Scheme 4-8). Obviously, **16** is unlikely reduced to



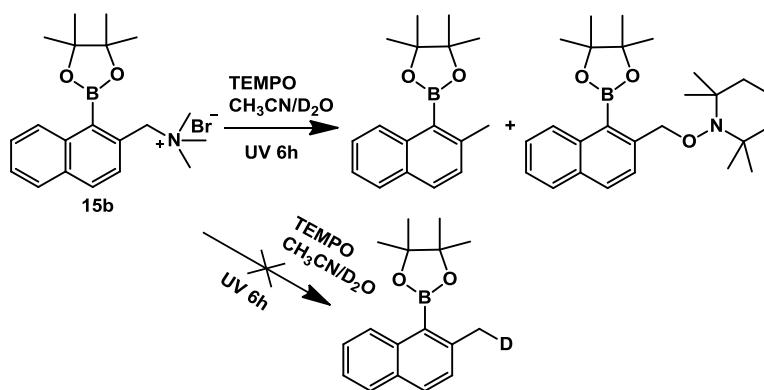
the methyl anion. Thus, we proposed that the bromo radical could be the electron acceptor for formation of **20**.



**Scheme 4-6.** Cation trapping reactions with methoxyamine.

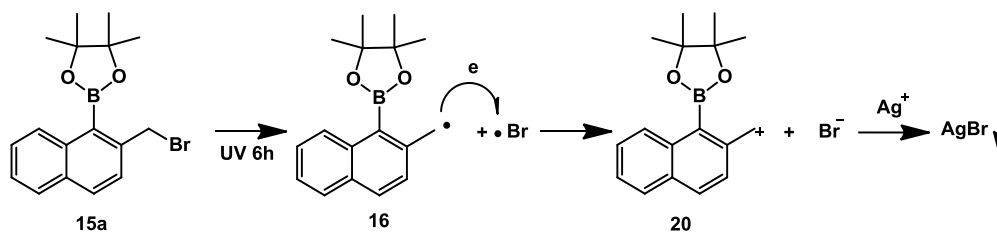


**Scheme 4-7.** Nucleophilic substitution occurred between **15a** and methoxyamine under heating without UV-irradiation.



**Scheme 4-8.** Photo-irradiation of **15b** in the presence of TEMPO and D<sub>2</sub>O.

To test our hypothesis, a AgNO<sub>3</sub> solution was added to a 20 mM **15a** solution in CH<sub>3</sub>CN after 4 h photo-irradiation. The formation of white precipitate AgBr suggested the presence of Br<sup>-</sup> (Scheme 4-10). Collectively, our data confirmed that the naphthelenemethylation **20** as well as the radical **16** were generated from photo-irradiation of **15a,b**.



**Scheme 4-9.** One-electron transfer occurred between the radical **16** and bromo radical.

There are two possible pathways for formation of **20**, either through direct heterolysis of **15a,b** or via electron transfer from **16**. In order to distinguish between these two processes, we performed a trapping experiment by using both methoxyamine and TEMPO. We chose **15b** but not **15a** for this study because of the observation that direct nucleophilic substitution of Br with methoxyamine occurred with **15a** even without UV-irradiation which may lead to non-specific reaction (Scheme 4-9), while such a reaction was not observed with **15b** possibly due to poorer leaving property of trimethylamine than bromo group. Should **20** be directly produced from

heterolysis of **15b**, the presence of TEMPO would not affect generation of compounds **15-1**, **18** and/or **19**. However, if **20** would be produced from the radical **16**, the yields of **15-1**, **18** and/or **19** would be greatly reduced due to the competence of TEMPO for **15** prior to its conversion to **20**.

As trapping the radical **16** by TEMPO is much more efficient than trapping the cation **20** by methoxyamine (Figures 4-14 and 4-15), we used a 10:1 ratio of methoxyamine to TEMPO. The results showed that photo-irradiation of 20 mM **15b** in the presence of 800 mM methoxyamine and 80 mM TEMPO yielded the radical trapping products **15-t** (18%), and **15-1** (11%) with trace amount of **19** (<1%). The greatly reduced yields for the cation trapping products **18** and **19** and formation of large amount of the radical trapping products **15-t** suggested that the cation **20** was more likely formed from **16** via electron transfer.

#### 4.3.4. The effect of trapping agent on DNA cross-link formation

At last, we employed the orthogonal traps, methoxyamine and TEMPO to determine the species responsible for DNA ICL formation. The two traps were then tested separately as competitors for ICL formation upon 350 nm irradiation of **14a** and **14b** with DNA duplex **5**. Should the DNA cross-linking products be directly produced from the cation **20** which is derived from **16**, both methoxyamine and TEMPO would compete with ICL formation. As expected, the cross-linking yields are dependent on the concentration of both methoxyamine and TEMPO. The cross-link yield decreased from 13.5% to 1.6% from 0 mM to 100 mM methoxyamine (Figures 4-10 and Figure 4-12) and from 14.8% to 1.0% from 0 mM to 20 mM TEMPO (Figures 4-11 and Figure 4-13).

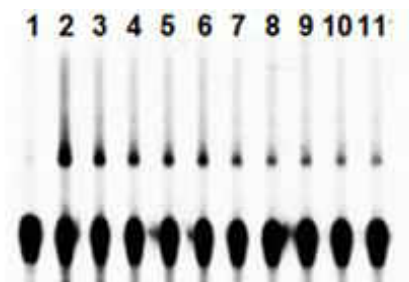


**Figure 4-10.** Effect of methoxyamine on ICL formation by **14a** upon UV irradiation. Lane 1: with DNA only; lane 2: 500  $\mu\text{M}$  **14a** (cross-linking yield 13.5%); lane 3: 500  $\mu\text{M}$  **14a** and 5 mM methoxyamine (6.6%); lane 4: 500  $\mu\text{M}$  **14a** and 10 mM methoxyamine (4.7%); lane 5: 500  $\mu\text{M}$  **14a** and 20 mM methoxyamine (4.0%); lane 6: 500  $\mu\text{M}$  **14a** and 30 mM methoxyamine (4.5%); lane 7: 500  $\mu\text{M}$  **14a** and 40 mM methoxyamine (3.9%); lane 8: 500  $\mu\text{M}$  **14a** and 50 mM methoxyamine (2.7%); lane 9: 500  $\mu\text{M}$  **14a** and 60 mM methoxyamine (2.5%); lane 10: 500  $\mu\text{M}$  **14a** and 80 mM methoxyamine (2.1%); lane 11: 500  $\mu\text{M}$  **14a** and 100 mM methoxyamine (1.6%). Condition: UV irradiation at pH8 for 4 h.

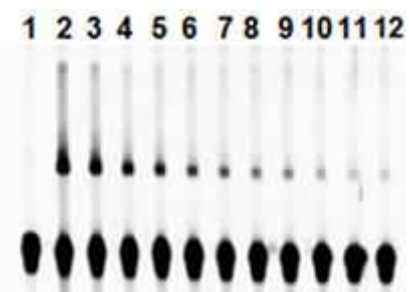


**Figure 4-11.** Effect of TEMPO on ICL formation by **14a** upon UV irradiation. Lane 1: with DNA only; lane 2: 500  $\mu\text{M}$  **14a** (cross-linking yield 14.8%); lane 3: 500  $\mu\text{M}$  **14a** and 500  $\mu\text{M}$  TEMPO (9.8%); lane 4: 500  $\mu\text{M}$  **14a** and 1 mM TEMPO (6.2%); lane 5: 500  $\mu\text{M}$  **14a** and 2 mM TEMPO (4.2%); lane 6: 500  $\mu\text{M}$  **14a** and 3 mM TEMPO (3.3%); lane 7: 500  $\mu\text{M}$  **14a** and 4 mM TEMPO (2.9%); lane 8: 500  $\mu\text{M}$  **14a** and 5 mM TEMPO (2.2%); lane 9: 500  $\mu\text{M}$  **14a** and 7.5 mM TEMPO (2.0%); lane 10: 500  $\mu\text{M}$  **14a** and 10 mM TEMPO (1.7%); lane 11: 500  $\mu\text{M}$  **14a**

and 15 mM TEMPO (1.2%); lane 12: 500  $\mu$ M **14a** and 20 mM TEMPO (1.0%). Condition: UV irradiation at pH8 for 4 h.

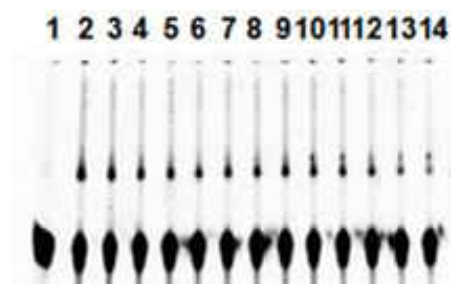


**Figure 4-12.** Effect of methoxyamine on ICL formation by **14b** upon UV irradiation. Lane 1: with DNA only; lane 2: 200  $\mu$ M **14b** (cross-linking yield 7.4%); lane 3: 200  $\mu$ M **14b** and 500  $\mu$ M methoxyamine (6.8%); lane 4: 200  $\mu$ M **14b** and 1 mM methoxyamine (5.8%); lane 5: 200  $\mu$ M **14b** and 2 mM methoxyamine (5.4%); lane 6: 200  $\mu$ M **14b** and 3 mM methoxyamine (4.8%); lane 7: 200  $\mu$ M **14b** and 4 mM methoxyamine (4.5%); lane 8: 200  $\mu$ M **14b** and 5 mM methoxyamine (4.1%); lane 9: 200  $\mu$ M **14b** and 7.5 mM methoxyamine (3.8%); lane 10: 200  $\mu$ M **14b** and 10 mM methoxyamine (3.5%); lane 11: 200  $\mu$ M **14b** and 15 mM methoxyamine (3.2%); lane 12: 200  $\mu$ M **14b** and 20 mM methoxyamine (2.9%); lane 13: 200  $\mu$ M **14b** and 50 mM methoxyamine (2.1%); lane 14: 100  $\mu$ M **14b** and 100 mM methoxyamine (1.4%). Condition: UV irradiation at pH8 for 4 h.

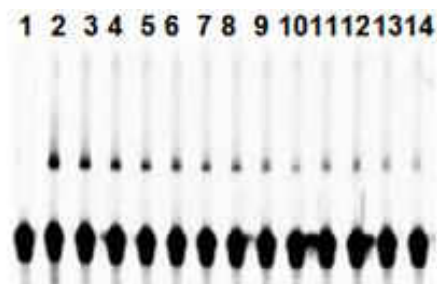


**Figure 4-13.** Effect of TEMPO on ICL formation by **14b** upon UV irradiation. Lane 1: with DNA only; lane 2: 200  $\mu$ M **14b** (cross-linking yield 8.2%); lane 3: 200  $\mu$ M **14b** and 500  $\mu$ M

TEMPO (5.4%); lane 4: 200  $\mu\text{M}$  **14b** and 1 mM TEMPO (3.8%); lane 5: 200  $\mu\text{M}$  **14b** and 2 mM TEMPO (3.0%); lane 6: 200  $\mu\text{M}$  **14b** and 3 mM TEMPO (2.8%); lane 7: 200  $\mu\text{M}$  **14b** and 4 mM TEMPO (2.6%); lane 8: 200  $\mu\text{M}$  **14b** and 5 mM TEMPO (2.1%); lane 9: 200  $\mu\text{M}$  **14b** and 7.5 mM TEMPO (2.0%); lane 10: 200  $\mu\text{M}$  **14b** and 10 mM TEMPO (1.7%); lane 11: 200  $\mu\text{M}$  **14b** and 15 mM TEMPO (1.5%); lane 12: 200  $\mu\text{M}$  **14b** and 20 mM TEMPO (1.2%); lane 13: 200  $\mu\text{M}$  **14b** and 50 mM TEMPO (1.0%); lane 14: 100  $\mu\text{M}$  **14b** and 100 mM TEMPO (0.9%). Condition: UV irradiation at pH8 for 4 h.

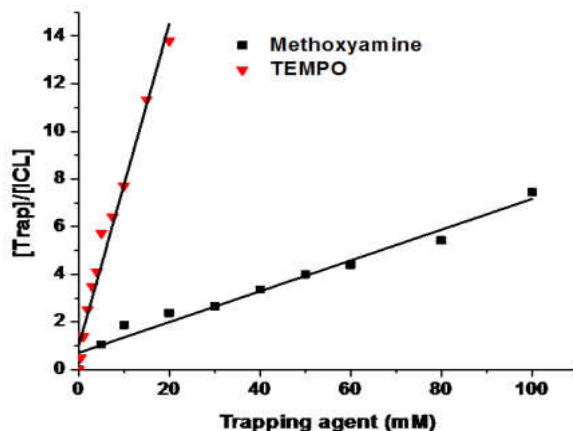


**Figure 4-14.** Effect of methoxyamine and TEMPO on ICL formation by **14a**.

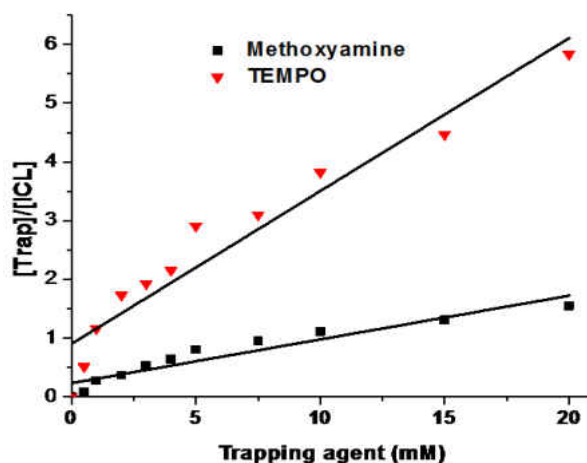
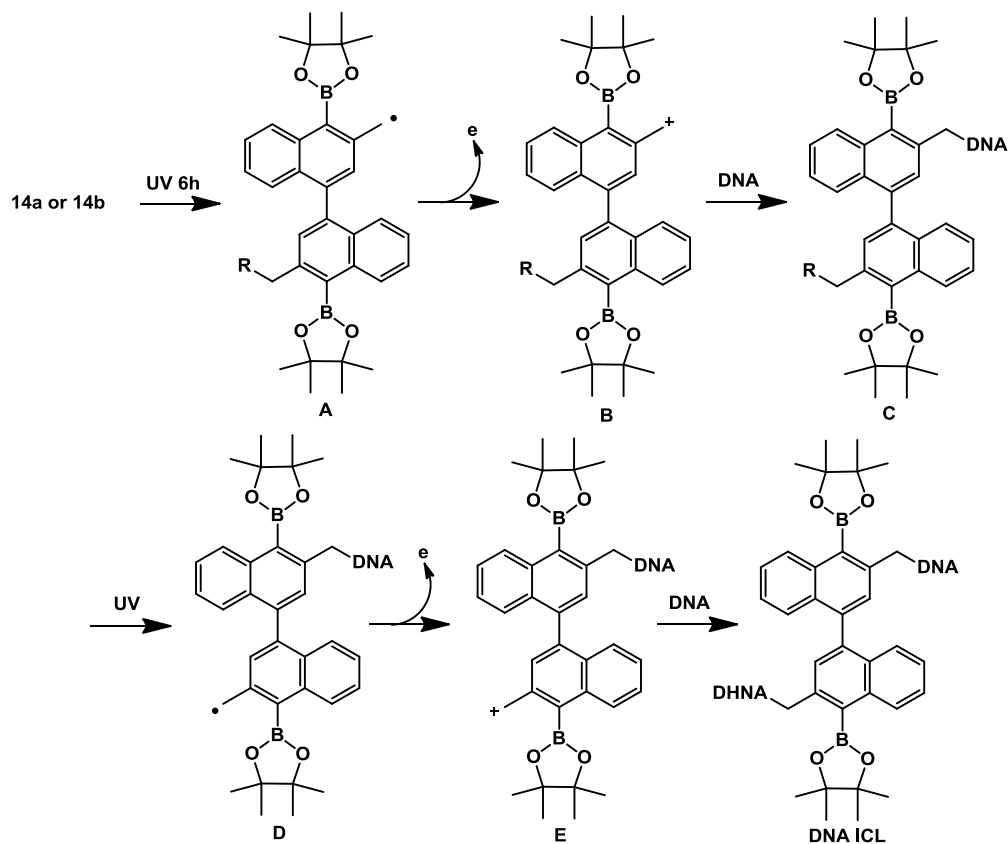


**Figure 4-15.** Effect of methoxyamine and TEMPO on ICL formation by **14b**.

The almost complete quenching of DNA ICL formation by methoxyamine discriminated against that **16** would directly cross-link DNA. On the other hand, TEMPO efficiently inhibited the ICL formation which suggested that a radical would be the precursor for the cation. Collectively, our data suggested that the naphthalenemethylation not the radicals yields DNA ICLs and the cation is derived from the radical not from direct heterolysis of **14a** and **14b**.

#### 4.3.5. Proposed mechanism for ICL formation induced by **14a** and **14b**



**Scheme 4-10.** Proposed mechanism for ICL formation induced by **14a** and **14b**.

Having confirmed formation of the naphthalenemethylation **20** and the radical **16** from photo-irradiation of the naphthalene boronates **15a,b**, we proposed a mechanism for the ICL formation induced by binaphthaleneboronates **14a** and **14b** (Scheme 4-11). Photo-irradiation of **14a** and **14b** produces free radical A which undergoes one-electron transfer to form the cation B directly

alkylating DNA. Departure of the second leaving group followed by electron transfer leads to the second cation product E that alkylates the complementary strand to form ICL products.

#### 4.4. Experimental Section

**General Methods.** Unless otherwise specified, chemicals were purchased from Aldrich or FisherScientific and were used as received without further purification. T4 polynucleotide kinase was obtained from New England Biolabs. Oligonucleotides were synthesized via standard automated DNA synthesis techniques using an Applied Biosystems model 394 instrument in a 1.0  $\mu\text{M}$  scale using commercial 1000Å CPG-succinyl-nucleoside supports. Deprotection of the nucleobases and phosphate moieties as well as cleavage of the linker were carried out under mild deprotection conditions using a mixture of 40% aq.  $\text{MeNH}_2$  and 28% aq.  $\text{NH}_3$  (1:1) at room temperature for 2 h. Radiolabeling was carried out according to the standard protocols.<sup>15</sup> [ $\gamma$ - $^{32}\text{P}$ ]ATP was purchased from Perkin-Elmer Life Sciences. Quantification of radiolabeled oligonucleotides was carried out using a Molecular Dynamics Phosphorimager equipped with ImageQuant Version 5.2 software.  $^1\text{H}$  NMR and  $^{13}\text{C}$  NMR spectra were taken on a Bruker DRX 300 MHz and 500 MHz spectrophotometer. High resolution mass spectrometry was performed at the University of California-Riverside and Shimadzu Laboratory for Advanced & Applied Analytical Chemistry at the University of Wisconsin-Milwaukee.

**Interstrand cross-link formation with duplex DNA 5.** The  $^{32}\text{P}$ -labelled oligonucleotide (0.5  $\mu\text{M}$ ) was annealed with 1.5 equiv of the complementary strand by heating to 65  $^\circ\text{C}$  for 3 min in a buffer containing 10 mM potassium phosphate (pH 7), and 100 mM NaCl, followed by slow-cooling to room temperature overnight. The  $^{32}\text{P}$ -labeled oligonucleotide duplex (2  $\mu\text{L}$ , 0.5  $\mu\text{M}$ ) was mixed with 1 M NaCl (2  $\mu\text{L}$ ), 100 mM potassium phosphate (2  $\mu\text{L}$ , pH 8), 10 mM  $\text{H}_2\text{O}_2$  (2  $\mu\text{L}$ ), and compound **14a** or **14b** (concentration range: 10  $\mu\text{M}$  to 2 mM in 6  $\mu\text{L}$   $\text{CH}_3\text{CN}$ ) and



appropriate amount of autoclaved distilled water were added to give a final volume of 20  $\mu\text{L}$ . The reaction was incubated at room temperature for 24 h and quenched by an equal volume of 90% formamide loading buffer, then subjected to 20% denaturing polyacrylamide gel electrophoresis.

**DNA ICL formation upon UV irradiation.** The  $^{32}\text{P}$ -labelled oligonucleotide (0.5  $\mu\text{M}$ ) was annealed with 1.5 equiv of the complementary strand by heating to 65  $^{\circ}\text{C}$  for 3 min in a buffer containing 10 mM potassium phosphate (pH 7), and 100 mM NaCl, followed by slow-cooling to room temperature overnight. The  $^{32}\text{P}$ -labeled oligonucleotide duplex (2  $\mu\text{L}$ , 0.5  $\mu\text{M}$ ) was mixed with 1 M NaCl (2  $\mu\text{L}$ ), 100 mM potassium phosphate (2  $\mu\text{L}$ , pH range 5-9) and different concentrations of compound **14a** or **14b** (concentration range: 10  $\mu\text{M}$  to 2 mM in 6  $\mu\text{L}$   $\text{CH}_3\text{CN}$ ) and the appropriate amount of autoclaved water to give a final volume of 20  $\mu\text{L}$ . The reaction was irradiated with 350 nm UV light for 1-5 hours and quenched by an equal volume of 90% formamide loading buffer, then subjected to 20% denaturing polyacrylamide gel electrophoresis.

**Trapping assay of oligonucleotides.** The  $^{32}\text{P}$ -labeled oligonucleotide duplex (2  $\mu\text{L}$ , 0.5  $\mu\text{M}$ ) was mixed with 1 M NaCl (2  $\mu\text{L}$ ), 100 mM potassium phosphate (2  $\mu\text{L}$ , pH 8). The stock solution of  $\text{MeONH}_2\cdot\text{HCl}$  (2 M) was titrated with 5 M NaOH solution to adjust the pH to  $\sim 7.0$ . Then, 2  $\mu\text{L}$  was added to the reaction mixture as appropriate for the desired concentration. TEMPO was dissolved in  $\text{CH}_3\text{CN}$ , then 2  $\mu\text{L}$  was added to the reaction mixture as for the desired concentration. Different concentrations of compound **14a** or **14b** (4  $\mu\text{L}$  in  $\text{CH}_3\text{CN}$ ) and the appropriate amount of autoclaved water and  $\text{CH}_3\text{CN}$  were added to give a final volume of 20  $\mu\text{L}$  (6  $\mu\text{L}$   $\text{CH}_3\text{CN}$  with 14  $\mu\text{L}$   $\text{H}_2\text{O}$ ). The reaction was irradiated with 350 nm UV light for 4 hours and quenched by an equal volume of 90% formamide loading buffer, then subjected to 20% denaturing polyacrylamide gel electrophoresis.

**Stability study of ICL product formed with 5.** After the cross-link reaction, the reaction mixtures (0.35  $\mu\text{M}$  DNA duplex, 20  $\mu\text{L}$ ) were coprecipitated with calf thymus DNA (2.5 mg/mL, 5  $\mu\text{L}$ ) and NaOAc (3 M, 5  $\mu\text{L}$ ) in the presence of EtOH (90  $\mu\text{L}$ ) at  $-80\text{ }^\circ\text{C}$  for 30 min, followed by centrifuging for 5 min at 15000 rpm. The supernatant was removed, and the pellet was washed with cold 75% EtOH and lyophilized for 30 min in a Centrivap Concentrator of LABCONCO at  $37\text{ }^\circ\text{C}$ . The dried DNA fragments were dissolved in  $\text{H}_2\text{O}$  (30  $\mu\text{L}$ ) and divided into three portions. One portion (10  $\mu\text{L}$ ) was incubated with piperidine (2 M, 10  $\mu\text{L}$ ) at  $90\text{ }^\circ\text{C}$  for 30 min, and the second portion (10  $\mu\text{L}$ ) was incubated with 0.1 M NaCl and 10 mM potassium phosphate buffer (pH 7, 10  $\mu\text{L}$ ) under the same condition, and the third portion was used as a control sample. The samples were subjected to 20% denaturing polyacrylamide gel electrophoresis.

**Hydroxyl radical reaction (Fe·EDTA reaction).** Fe(II)·EDTA cleavage reactions of  $^{32}\text{P}$ -labelled oligonucleotide (0.1  $\mu\text{M}$ ) were performed in a buffer containing 50  $\mu\text{M}$   $(\text{NH}_4)_2\text{Fe}(\text{SO}_4)_2$ , 100  $\mu\text{M}$  EDTA, 5 mM sodium ascorbate, 0.5 M NaCl, 50 mM sodium phosphate (pH 7.2) and 1 mM  $\text{H}_2\text{O}_2$  for 3 min at room temperature (total substrate volume 20  $\mu\text{L}$ ), then quenched with 100 mM thiourea (10  $\mu\text{L}$ ). Samples were lyophilized, and incubated with 1 M piperidine (20  $\mu\text{L}$ ) at  $90\text{ }^\circ\text{C}$  for 30 min. The mixture was lyophilized again, dissolved in 20  $\mu\text{L}$   $\text{H}_2\text{O}$ : 90% formamide loading buffer (1:1) and subjected to 20% denaturing polyacrylamide gel electrophoresis.

**QM Trapping Assay. General Procedure.** A solution of **14a,b** (20 mg) in a mixture of  $\text{CH}_3\text{CN}$  (2 mL),  $\text{H}_2\text{O}$  (250  $\mu\text{L}$ ), and 1 M potassium phosphate buffer (250  $\mu\text{L}$ , pH 8) was incubated at  $37\text{ }^\circ\text{C}$  for 20 min with excess ethyl vinyl ether (EVE) (80 equiv of **14a,b**). Then  $\text{H}_2\text{O}_2$  (3 equiv of **14a,b**) was added to the reaction mixture. The mixture was stirred at  $37\text{ }^\circ\text{C}$  for 24 h and then evaporated. Water (3 mL) was added to the residue, and the resulting mixture was extracted with ethyl acetate ( $3 \times 2\text{ mL}$ ). The organic phase was combined, dried over anhydrous  $\text{Na}_2\text{SO}_4$ , and

evaporated. The crude product was purified through column chromatography with 0-10% EtOAc in hexane to provide QM-EVE adducts **14-e**.

A solution of **15a,b** in a mixture of CH<sub>3</sub>CN (2 mL), H<sub>2</sub>O (250 μL), and 1 M potassium phosphate buffer (250 μL, pH 8) was irradiated with 350 nm UV light for 6 hours with excess ethyl vinyl ether (EVE) (40 equiv of **15a,b**). Water (3 mL) was added to the residue, and the resulting mixture was extracted with ethyl acetate (3 × 2 mL). The organic phase was combined, dried over anhydrous Na<sub>2</sub>SO<sub>4</sub>, and evaporated. The crude product was purified through column chromatography with 0–10% EtOAc in hexane to provide dimeric adduct **17**.

**2,2'-Diethoxy-3,3',4,4'-tetrahydro-2H,2'H-6,6'-bibenzo[h]chromene (14-e)**. Colorless oil (2.8 mg, 25%). <sup>1</sup>H NMR (300 MHz, CDCl<sub>3</sub>): δ 8.31 (d, *J* = 7.2 Hz, 2H), 7.49-7.37 (m, 4H), 7.31-7.19 (m, 4H), 5.56 (d, *J* = 1.4 Hz, 2H), 4.17-4.03 (m, 2H), 3.87-3.79 (m, 2H), 3.20-3.09 (m, 2H), 2.85-2.79 (m, 2H), 2.23-2.15 (m, 4H), 1.34-1.26 (m, 6H). <sup>13</sup>C NMR (75 MHz, CDCl<sub>3</sub>): δ 146.4, 132.9, 130.5, 129.7, 126.7, 125.4, 125.2, 125.0, 121.2, 115.8, 97.4, 64.0, 26.7, 21.0, 15.2. HRMS (APCI): *m/z* calcd for C<sub>30</sub>H<sub>30</sub>O<sub>4</sub> [M+H]<sup>+</sup> 455.2217, found 455.2220.

**1,2-bis(1-(4,4,5,5-tetramethyl-1,3,2-dioxaborolan-2-yl)naphthalen-2-yl)ethane (17)**.

Colorless oil (1.8 mg, 14%). <sup>1</sup>H NMR (300 MHz, CDCl<sub>3</sub>): δ 8.22 (d, *J* = 3.9 Hz, 2H), 7.81 (s, 2H), 7.78 (s, 2H), 7.52-7.40 (m, 6H), 3.29 (s, 4H), 1.51 (s, 24H). <sup>13</sup>C NMR (75 MHz, CDCl<sub>3</sub>): δ 146.1, 136.8, 131.7, 129.6, 128.1, 127.9, 127.8, 126.0, 124.7, 84.1, 39.9, 25.2. HRMS (ESI): *m/z* calcd for C<sub>34</sub>H<sub>40</sub>O<sub>4</sub>B<sub>2</sub> [M+NH<sub>4</sub>]<sup>+</sup> 552.3451, found 552.3447.

**Radical Trapping Assay. General Procedure.** A solution of **14a,b** and **15a,b** (20 mg) in a mixture of CH<sub>3</sub>CN (2.5 mL) and excess BME (10 equiv of **14a,b** and 5 equiv of **15a,b**) or TEMPO (8 equiv of **14a,b** and 4 equiv of **15a,b**) was irradiated with 350 nm UV light for 6

hours and then evaporated. Water (3 mL) was added to the residue, and the resulting mixture was extracted with ethyl acetate (3 × 2 mL). The organic phase was combined, washed with water, and dried over anhydrous Na<sub>2</sub>SO<sub>4</sub>, and evaporated. The crude product was purified through column chromatography with 0–50% EtOAc in hexane to provide radical trapping adducts **14-1**, **15-t** and **14-t**.

**2,2,6,6-Tetramethyl-1-((1-(4,4,5,5-tetramethyl-1,3,2-dioxaborolan-2-yl)naphthalen-2-yl)methoxy)piperidine (15-t)**. Colorless oil (4.2 mg, 20%). <sup>1</sup>H NMR (300 MHz, CDCl<sub>3</sub>): δ 8.18 (d, *J* = 3.9 Hz, 1H), 7.89 (d, *J* = 4.2 Hz, 1H), 7.83-7.80 (m, 2H), 7.49-7.44 (m, 2H), 5.16 (s, 2H), 1.53 (s, 24H), 1.28 (s, 12H), 1.10 (s, 12H). <sup>13</sup>C NMR (75 MHz, CDCl<sub>3</sub>): δ 142.1, 136.1, 132.4, 129.6, 128.2, 127.9, 126.0, 125.4, 125.1, 84.2, 78.6, 59.9, 39.9, 33.4, 25.2, 20.3, 17.2. HRMS (APCI): *m/z* calcd for C<sub>26</sub>H<sub>38</sub>NO<sub>3</sub>B [M+H]<sup>+</sup> 424.3022, found 424.3029.

**1,1'-(((4,4'-Bis(4,4,5,5-tetramethyl-1,3,2-dioxaborolan-2-yl)-[1,1'-binaphthalene]-3,3'-diyl)bis(methylene))bis(oxy))bis(2,2,6,6-tetramethylpiperidine) (14-t)**. Colorless oil (2.8 mg, 13%). <sup>1</sup>H NMR (300 MHz, CDCl<sub>3</sub>): δ 8.25-8.23 (m, 2H), 7.81 (d, *J* = 7.5 Hz, 2H), 7.54-7.38 (m, 6H), 5.20 (s, 4H), 1.50 (s, 12H), 1.31 (s, 6H), 1.21 (s, 6H). <sup>13</sup>C NMR (75 MHz, CDCl<sub>3</sub>): δ 140.3, 136.2, 128.0, 127.1, 126.1, 125.9, 125.5, 125.2, 84.3, 78.7, 60.0, 39.9, 33.5, 25.3, 20.3, 17.1. HRMS (ESI): *m/z* calcd for C<sub>52</sub>H<sub>74</sub>N<sub>2</sub>O<sub>6</sub>B<sub>2</sub> [M+H]<sup>+</sup> 845.5822, found 845.5806.

**Cation Trapping Assay. General Procedure.** To a solution of MeONH<sub>2</sub>·HCl (40 equiv of **15a,b**) in DMF (1.25 mL), triethylamine (TEA) (44 equiv of **15a,b**) was added. White precipitate was formed upon the addition of TEA. The mixture was stirred at 25 °C for 20 min. A solution of **15a,b** (20 mg) in DMF (1.25 mL) was then added. The mixture was stirred for 20 min and irradiated with 350 nm UV light for 6 hours. Water (3 mL) was added and extracted with ethyl acetate (3 × 2 mL). The organic phases were combined, washed with water, and dried over

anhydrous Na<sub>2</sub>SO<sub>4</sub>, and evaporated. The crude product was purified through column chromatography with 0–50% EtOAc in hexane to provide cation trapping adducts **18**, **19** and **21**.

**O-Methyl-N-((1-(4,4,5,5-tetramethyl-1,3,2-dioxaborolan-2-yl)naphthalen-2-**

**yl)methyl)hydroxylamine (18).** White solid (4.0 mg, 22%). <sup>1</sup>H NMR (300 MHz, CDCl<sub>3</sub>): δ 8.26 (d, *J* = 4.1 Hz, 1H), 7.84 (t, *J* = 8.7 Hz, 2H), 7.50-7.47 (m, 3H), 6.10 (s, 1H), 4.30 (s, 2H), 3.55 (s, 3H), 1.52 (s, 12H). <sup>13</sup>C NMR (75 MHz, CDCl<sub>3</sub>): δ 140.9, 136.5, 132.5, 129.9, 128.2, 128.0, 126.2, 125.4, 84.2, 61.6, 56.7, 25.2. HRMS (ESI): *m/z* calcd for C<sub>18</sub>H<sub>24</sub>NO<sub>3</sub>B [M+H]<sup>+</sup> 314.1925, found 314.1922.

**1-(4,4,5,5-tetramethyl-1,3,2-dioxaborolan-2-yl)-2-naphthaldehyde O-methyl oxime (19).**

White solid (0.6 mg, 4%). <sup>1</sup>H NMR (300 MHz, CDCl<sub>3</sub>): δ 8.68 (s, 1H), 8.29 (d, *J* = 4.7 Hz, 1H), 8.02 (d, *J* = 4.4 Hz, 1H), 7.86-7.82 (m, 2H), 7.51-7.49 (m, 3H), 4.04 (s, 3H), 1.52 (s, 12H). <sup>13</sup>C NMR (75 MHz, CDCl<sub>3</sub>): δ 149.8, 136.4, 135.6, 133.5, 130.3, 128.5, 128.3, 126.6, 126.4, 122.7, 84.6, 62.0, 30.9, 29.7, 25.1. HRMS (APCI): *m/z* calcd for C<sub>18</sub>H<sub>22</sub>NO<sub>3</sub>B [M+H]<sup>+</sup> 312.1769, found 312.1759.

**Naphtho[1,2-*c*][1,2]oxaborol-1(3H)-ol (21).** White solid (0.8 mg, 9%). <sup>1</sup>H NMR (300 MHz, DMSO-*d*<sub>6</sub>): δ 9.24 (s, 1H), 8.32 (d, *J* = 3.6 Hz, 1H), 8.03 (d, *J* = 4.1 Hz, 1H), 7.98 (d, *J* = 3.9 Hz, 1H), 7.63-7.52 (m, 3H), 5.12 (s, 2H). The NMR spectra were consistent with literature values.<sup>16</sup>

**4,4'-Dibromo-3,3'-dimethyl-1,1'-binaphthalene (14-1).** Boron trifluoride diethyl etherate (20 mL) was added to a solution of 1-Bromo-2-methylnaphthalene (17.68 g, 0.08 mol) and lead tetraacetate (19.52 g, 0.044 mol) in acetonitrile (100 mL). The reaction mixture was stirred overnight, then poured into water (300 mL), and the products were extracted with dichloromethane (2 x 300 mL). The organic layer was dried over Na<sub>2</sub>SO<sub>4</sub>, then evaporated to

provide the crude product, which was passed through a short column of basic alumina using hexane as eluant to remove the Pb and highly colored polymeric materials. The crude product was purified through column chromatography (2.5% EtOAc/Hexane) to provide **14-1** (3.09 g, 18%) as white solid. <sup>17</sup>H NMR (300 MHz, CDCl<sub>3</sub>): δ 8.44 (d, *J* = 4.4 Hz, 2H), 7.59 (t, *J* = 4.5 Hz, 2H), 7.39 (s, 2H), 7.32-7.28 (m, 4H), 2.71 (s, 6H).

**2,2'-(3,3'-Dimethyl-[1,1'-binaphthalene]-4,4'-diyl)bis(4,4,5,5-tetramethyl-1,3,2-dioxaborolane) (14-2).** **14-1** (2.19 g, 5 mmol), bis(pinacolato)diboron (5.08 g, 20 mmol), KOAc (5.89 g, 60mmol) and PdCl<sub>2</sub>(dppf) (366 mg, 0.5 mmol) were dissolved in DMF (100mL) under argon atmosphere. The reaction mixture was stirred at 85 °C for 48 hours and cooled to room temperature. Then, water (200 mL) was added and extracted with dichloromethane (3 × 100 mL). The organic layer was washed with water, dried over Na<sub>2</sub>SO<sub>4</sub>, and evaporated to provide the crude product which was purified through column chromatography (2.5% EtOAc/Hexane) to provide **14-2** (1.23g, 46%) as white solid. <sup>1</sup>H NMR (300 MHz, CDCl<sub>3</sub>): δ 8.19 (d, *J* = 4.2 Hz, 2H), 7.43 (t, *J* = 6.9 Hz, 2H), 7.28 (s, 4H), 7.17 (t, *J* = 7.5 Hz, 2H), 2.68 (s, 6H), 1.55 (s, 24H). <sup>13</sup>C NMR (75 MHz, CDCl<sub>3</sub>): δ 140.7, 140.1, 136.7, 130.8, 130.1, 128.5, 127.6, 126.9, 125.9, 124.6, 84.1, 25.2, 22.6. HRMS (APCI): *m/z* calcd. for C<sub>34</sub>H<sub>40</sub>O<sub>4</sub>B<sub>2</sub> [M+H]<sup>+</sup> 535.3197, found 535.3184.

**2,2'-(3,3'-Bis(bromomethyl)-[1,1'-binaphthalene]-4,4'-diyl)bis(4,4,5,5-tetramethyl-1,3,2-dioxaborolane) (14a).** A mixture of CH<sub>3</sub>CN (100 mL), NBS (1.07 g, 6 mmol), AIBN (32.8 mg, 0.2 mmol) and **14-2** (1.07 g, 2 mmol) was refluxed at 90 °C for 4 hours and cooled to room temperature. The mixture was concentrated and purified through column chromatography (5% EtOAc/Hexane) to yield **14a** (0.68 g, 49%) as white solid. <sup>1</sup>H NMR (300 MHz, CDCl<sub>3</sub>): δ 8.39 (d, *J* = 6 Hz, 2H), 7.50 (t, *J* = 6 Hz, 4H), 7.30-7.27 (m, 4H), 5.02 (s, 4H), 1.58 (s, 24H). <sup>13</sup>C

NMR (75 MHz, CDCl<sub>3</sub>):  $\delta$  141.1, 140.6, 136.7, 132.0, 129.3, 128.7, 126.8, 126.6, 126.4, 84.6, 34.2, 25.2. HRMS (ESI):  $m/z$  calcd. for C<sub>34</sub>H<sub>38</sub>O<sub>4</sub>B<sub>2</sub>Br<sub>2</sub> [M+NH<sub>4</sub>]<sup>+</sup> 708.1676, found 708.1663.

**1,1'-(4,4'-Bis(4,4,5,5-tetramethyl-1,3,2-dioxaborolan-2-yl)-[1,1'-binaphthalene]-3,3'-**

**diyl)bis(N,N,N-trimethylmethanaminium) bromide (14b).** A mixture of CH<sub>3</sub>CN (10 mL), 4.2 M trimethylamine (0.72 ml, 3 mmol) in ethanol, and **14a** (346mg, 0.5 mmol) was stirred at r.t.

overnight. The reaction mixture was concentrated to give **14b** (400 mg, 99%) as white solid. <sup>1</sup>H

NMR (300 MHz, DMSO-*d*<sub>6</sub>):  $\delta$  8.43 (d,  $J$  = 4.2 Hz, 2H), 7.71-7.67 (m, 4H), 7.49 (t,  $J$  = 6.9 Hz,

2H), 7.40 (d,  $J$  = 4.1Hz, 2H), 4.81 (s, 4H), 3.15 (s, 18H), 1.53 (s, 24H). <sup>13</sup>C NMR (75 MHz,

DMSO-*d*<sub>6</sub>):  $\delta$  139.7, 136.5, 132.5, 131.5, 131.1, 129.4, 128.3, 127.8, 126.8, 85.7, 69.1, 53.2,

25.4. HRMS (ESI):  $m/z$  calcd. for C<sub>40</sub>H<sub>56</sub>B<sub>2</sub>NO<sub>4</sub>Br<sub>2</sub> [M-Br]<sup>+</sup> 729.3604, found 729.3632.

**4,4,5,5-Tetramethyl-2-(2-methylnaphthalen-1-yl)-1,3,2-dioxaborolane (15-1).** **14-s** (2.21 g,

10 mmol), bis(pinacolato)diboron (5.08 g, 20 mmol), KOAc (5.89 g, 60 mmol) and PdCl<sub>2</sub>(dppf)

(366 mg, 0.5 mmol) were dissolved in DMF (100 mL) under argon atmosphere. The reaction

mixture were stirred at 85 °C for 48 hours and cooled to room temperature. Then, water (200

mL) was added and extracted with dichloromethane (3 × 100 mL). The organic layer was washed

with water, dried over Na<sub>2</sub>SO<sub>4</sub>, and evaporated to provide the crude product which was purified

through column chromatography (2.5% EtOAc/Hexane) to provide **15-1** (1.34 g, 50%). <sup>1</sup>H NMR

(300 MHz, CDCl<sub>3</sub>):  $\delta$  8.13 (d,  $J$  = 4.1 Hz, 1H), 7.80-7.76 (m, 2H), 7.49-7.32 (m, 2H), 7.30 (d,  $J$

= 4.2 Hz, 1H), 2.65 (s, 3H), 1.51 (s, 12H). The NMR spectra were consistent with literature

values.<sup>18</sup>

**2-(2-(Bromomethyl)naphthalen-1-yl)-4,4,5,5-tetramethyl-1,3,2-dioxaborolane (15a).** A

mixture of CH<sub>3</sub>CN (100 mL), NBS (1.33 g, 7.5 mmol), AIBN (41.1 mg, 0.25 mmol) and

compound **15-1** (1.34 g, 5 mmol) was refluxed at 90 °C for 4 hours and cooled to room

temperature. The mixture was concentrated and purified through column chromatography (5% EtOAc/Hexane) to give **15a** (0.85 g, 49%) as white solid. <sup>1</sup>H NMR (300 MHz, CDCl<sub>3</sub>): δ 8.32 (d, *J* = 3.9 Hz, 1H), 7.87 (d, *J* = 4.2 Hz, 1H), 7.82 (d, *J* = 3.8 Hz, 1H), 7.55-7.46 (m, 3H), 4.99 (s, 2H), 1.54 (s, 12H). The NMR spectra were consistent with literature values.<sup>18</sup>

**N,N,N-Trimethyl-1-(1-(4,4,5,5-tetramethyl-1,3,2-dioxaborolan-2-yl)naphthalen-2-yl)methanaminium bromide (15b)**. A mixture of CH<sub>3</sub>CN (10mL), 4.2 M trimethylamine (0.72 ml, 3 mmol) in ethanol and **15a** (347 mg, 1mmol) was stirred at r.t. over night. The reaction mixture was concentrated to give **15b** (400 mg, 99%) as white solid. <sup>1</sup>H NMR (300 MHz, DMSO-*d*<sub>6</sub>): δ 8.30 (d, *J* = 4.8 Hz, 1H), 8.14 (d, *J* = 4.8 Hz, 1H), 8.04 (d, *J* = 4.8 Hz, 1H), 7.69-7.64 (m, 3H), 4.75 (s, 2H), 3.10 (s, 9H), 1.48 (s, 12H). <sup>13</sup>C NMR (75 MHz, DMSO-*d*<sub>6</sub>): δ 136.2, 133.3, 131.5, 131.0, 129.9, 128.8, 127.8, 127.6, 85.5, 69.2, 53.2, 25.4. HRMS (ESI): *m/z* calcd. for C<sub>20</sub>H<sub>29</sub>NO<sub>4</sub>B [M]<sup>+</sup> 326.2290, found 326.2288.

#### 4.5. References

1. Fakhari, F., Rokita, S. E. A walk along DNA using bipedal migration of a dynamic and covalent crosslinker. *Nature communications*, **2014**, *5*, 5591
2. Wang, H., Rokita, S. E. Dynamic cross-linking is retained in duplex DNA after multiple exchange of strands. *Angew. Chem., Int. Ed.* **2010**, *122*, 6093-6096.
3. Peng, X., Hong, I. S., Li, H., Seidman, M. M., Greenberg, M. M. Interstrand cross-link formation in duplex and triplex DNA by modified pyrimidines. *J. Am. Chem. Soc.* **2008**, *130*, 10299-10306.
4. Weng, X., Ren, L., Weng, L., Huang, J., Zhu, S., Zhou, X., Weng, L. Synthesis and biological studies of inducible DNA cross-linking. *Angew. Chem., Int. Ed.* **2007**, *46*, 8020-8023.



5. Wang, P., Liu, R., Wu, X., Ma, H., Cao, X., Zhou, P., Zhang, J., Weng, X., Zhang, X., Qi, J., Zhou, X., Weng, L. A potent, water-soluble and photoinducible DNA cross-linking agent. *J. Am. Chem. Soc.* **2003**, *125*, 1116-1117.
6. Cao, S., Wang, Y., Peng, X. ROS-inducible DNA cross-linking agent as a new anticancer prodrug building block. *Chem. Eur. J.* **2012**, *18*, 3850-3854.
7. Cao, S., Wang, Y., Peng, X. The leaving group strongly affects H<sub>2</sub>O<sub>2</sub>-induced DNA cross-linking by arylboronates. *J. Org. Chem.* **2014**, *79*, 501-508.
8. Weng, L., Horvat, S. M., Schiesser, C. H., Greenberg, M. M. Deconvoluting the reactivity of two intermediates formed from modified pyrimidines. *Organic letters*, **2013**, *15*, 3618-3621.
9. Lin, G., Li, L. Oxidation and Reduction of the 5-(2'-Deoxyuridinyl) methyl Radical. *Angew. Chem., Int. Ed.* **2013**, *52*, 5594-5598.
10. Richter, S. N., Maggi, S., Mels, S. C., Palumbo, M., Freccero, M. Binol quinone methides as bisalkylating and DNA cross-linking agents. *J. Am. Chem. Soc.* **2004**, *126*, 13973-13979.
11. Verga, D., Nadai, M., Doria, F., Percivalle, C., Di Antonio, M., Palumbo, M., Richter, S. N., Freccero, M. Photogeneration and reactivity of naphthoquinone methides as purine selective DNA alkylating agents. *J. Am. Chem. Soc.* **2010**, *132*, 14625-14637.
12. Haraguchi, K., Delaney, M. O., Wiederholt, C. J., Sambandam, A., Hantosi, Z., Greenberg, M. M. Synthesis and characterization of oligodeoxynucleotides containing formamidopyrimidine lesions and nonhydrolyzable analogues. *J. Am. Chem. Soc.* **2002**, *124*, 3263-3269.
13. Peng, X., Hong, I. S., Li, H., Seidman, M. M., Greenberg, M. M. Interstrand cross-link formation in duplex and triplex DNA by modified pyrimidines. *J. Am. Chem. Soc.* **2008**, *130*, 10299-10306.

14. Murarka, S., Wertz, S., Studer, A. Transition-metal-free Oxidative Coupling Reactions for the Formation of C–C and C–N Bonds Mediated by TEMPO and its Derivatives. *CHIMIA International Journal for Chemistry*, **2012**, *66*, 413-417.
15. Maniatis, T., Fritsch, E. F., Sambrook, J. *Molecular Cloning*, Cold Spring Harbor Laboratory, Cold Spring Harbor, NY. **1982**.
16. Baker, S. J., Zhang, Y., Akama, T., Lau, A., Zhou, H., Hernandez, V., Mao, W., Alley, M. R. K., Sanders, Virginia., Plattner, J. J. *J. Med. Chem.* **2006**, *49*, 15.
17. McKillop, A., Turrell, A. G., Young, D. W., Taylor, E. C. *J. Am. Chem. Soc.* **1980**, *102*, 21.
18. Hagadorn, J. R., Bedoya, M. S. PCT Int. Appl. **2012**, WO 2012134615 A1 Oct 04, 2012.

#### 4.6. Appendices C: Characterization of Compounds:

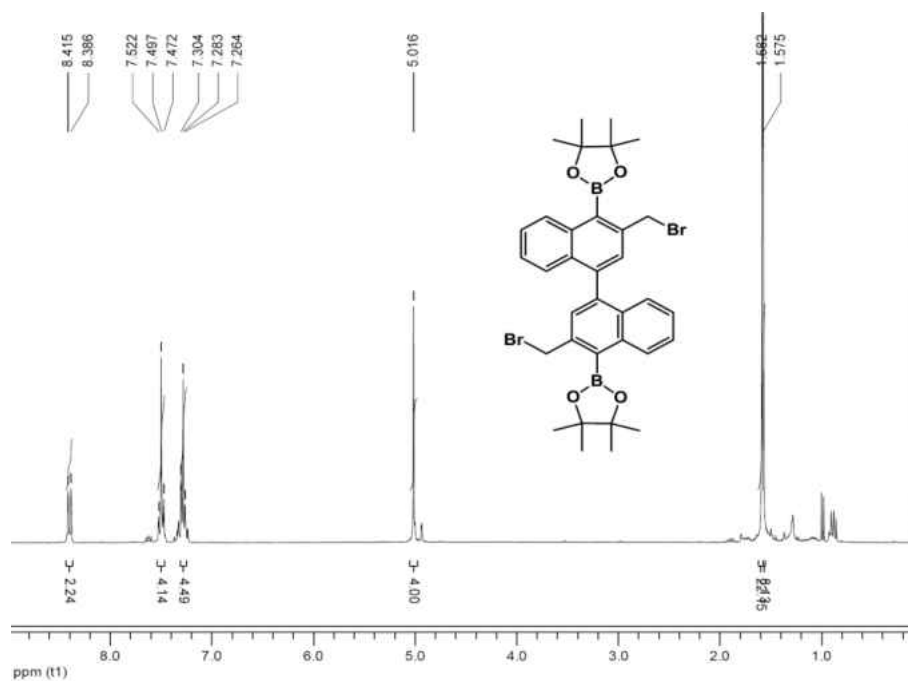


Figure 4-7-1. <sup>1</sup>H NMR spectra of **14a**.

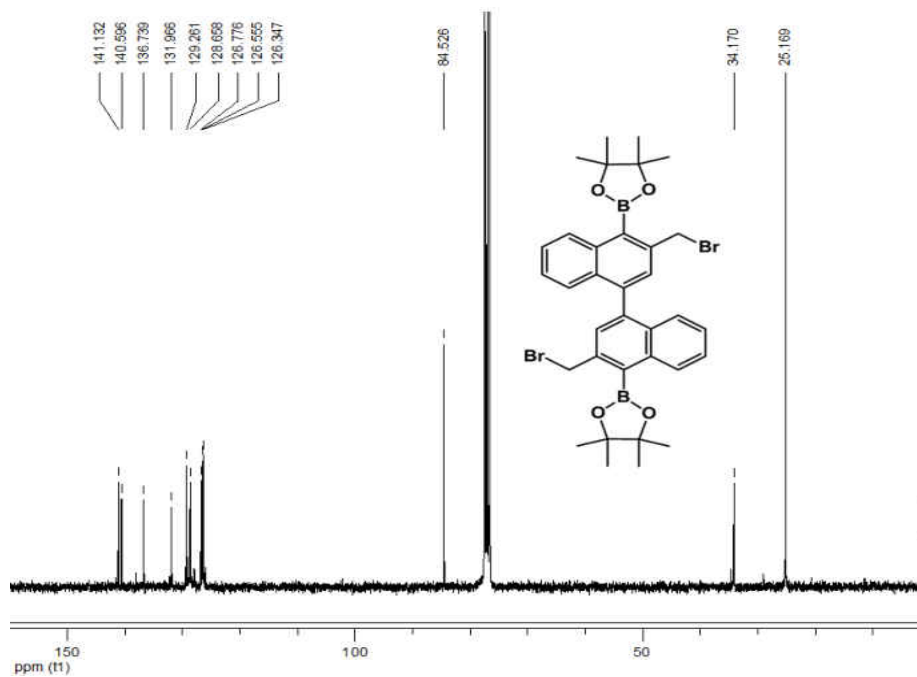


Figure 4-7-2. <sup>13</sup>C NMR spectra of **14a**.

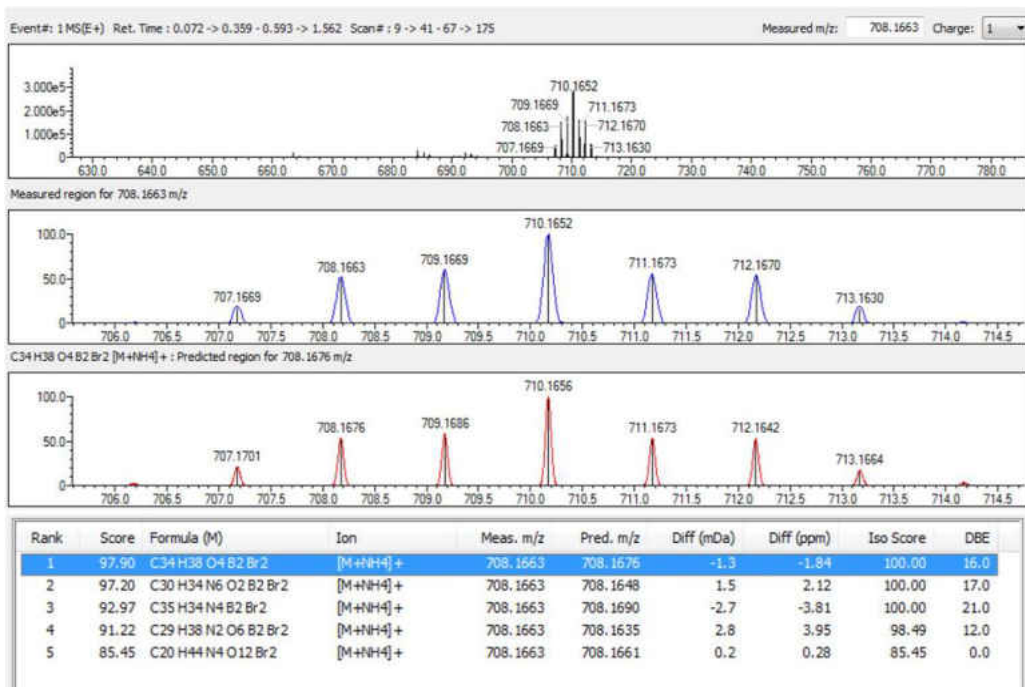


Figure 4-7-3. HRMS (ESI) of **14a**.

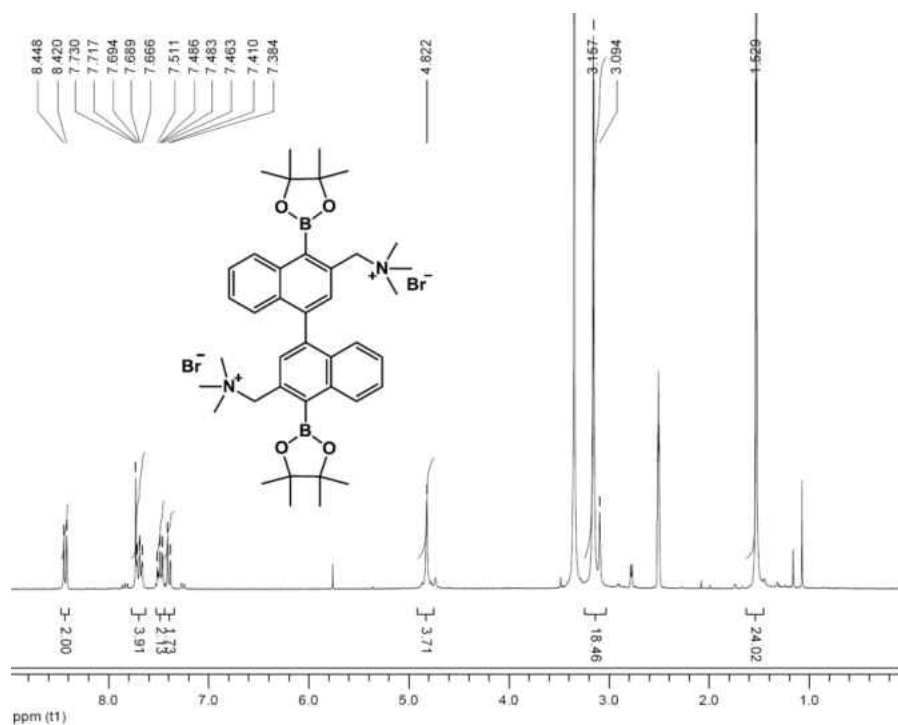


Figure 4-7-4. <sup>1</sup>H NMR spectra of **14b**.

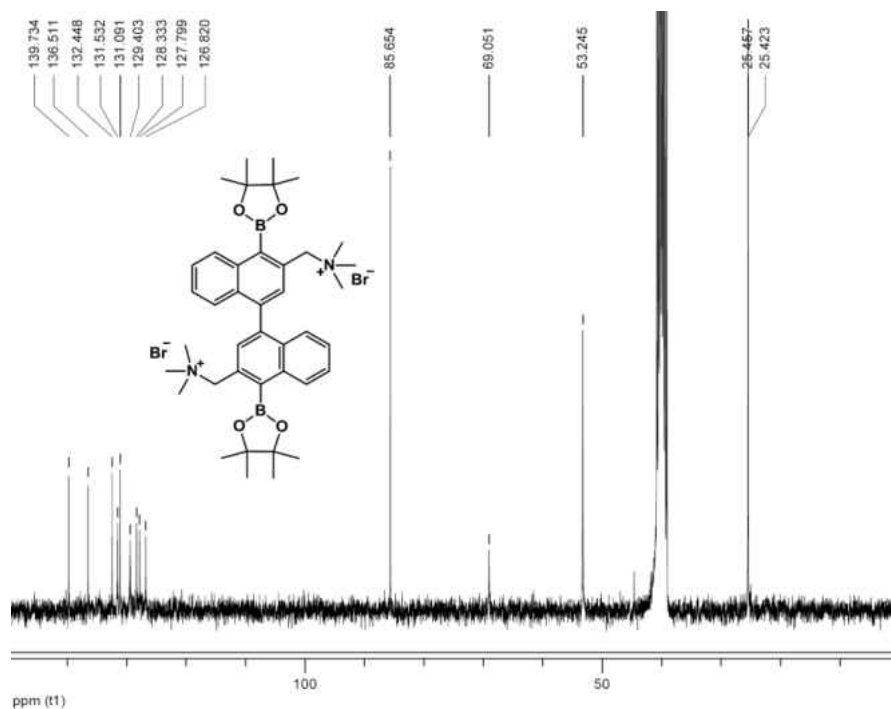


Figure 4-7-5.  $^{13}\text{C}$  NMR spectra of **14b**.

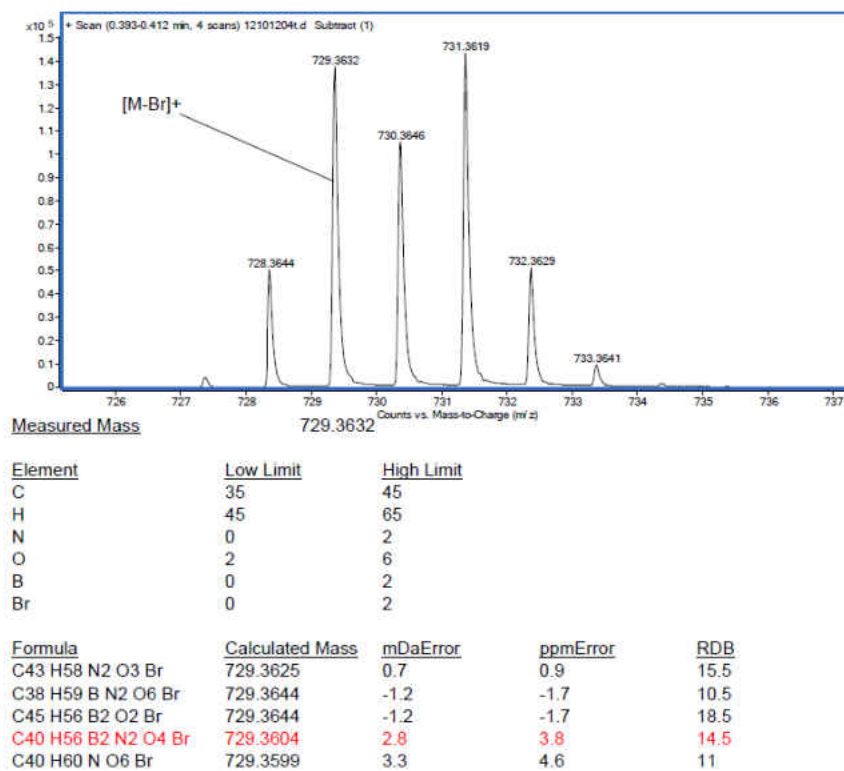


Figure 4-7-6. HRMS (ESI) of **14b**.

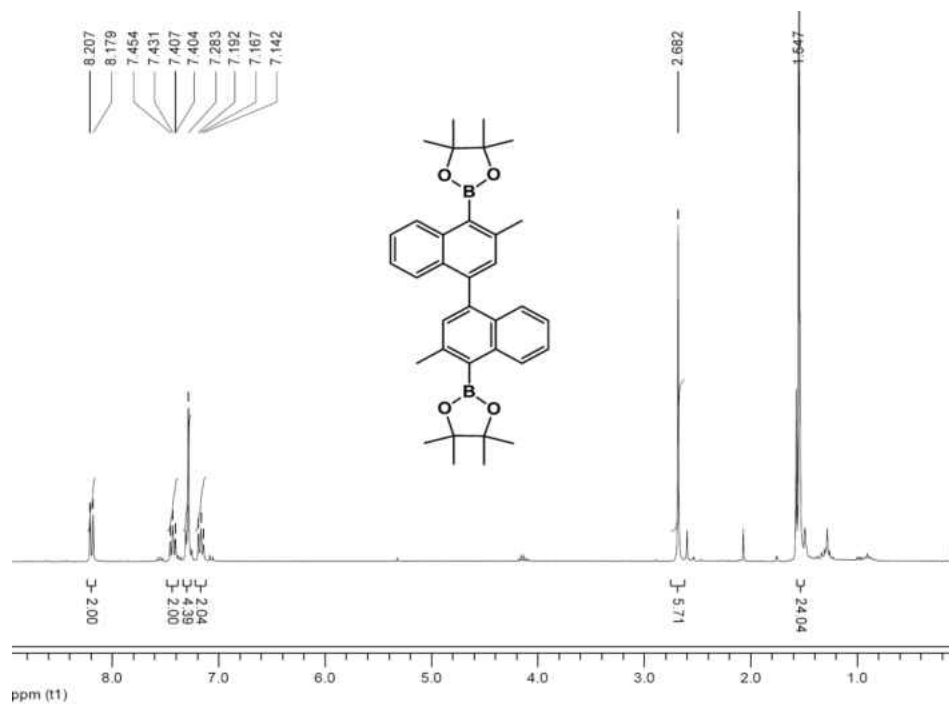


Figure 4-7-7. <sup>1</sup>H NMR spectra of **14-2**.

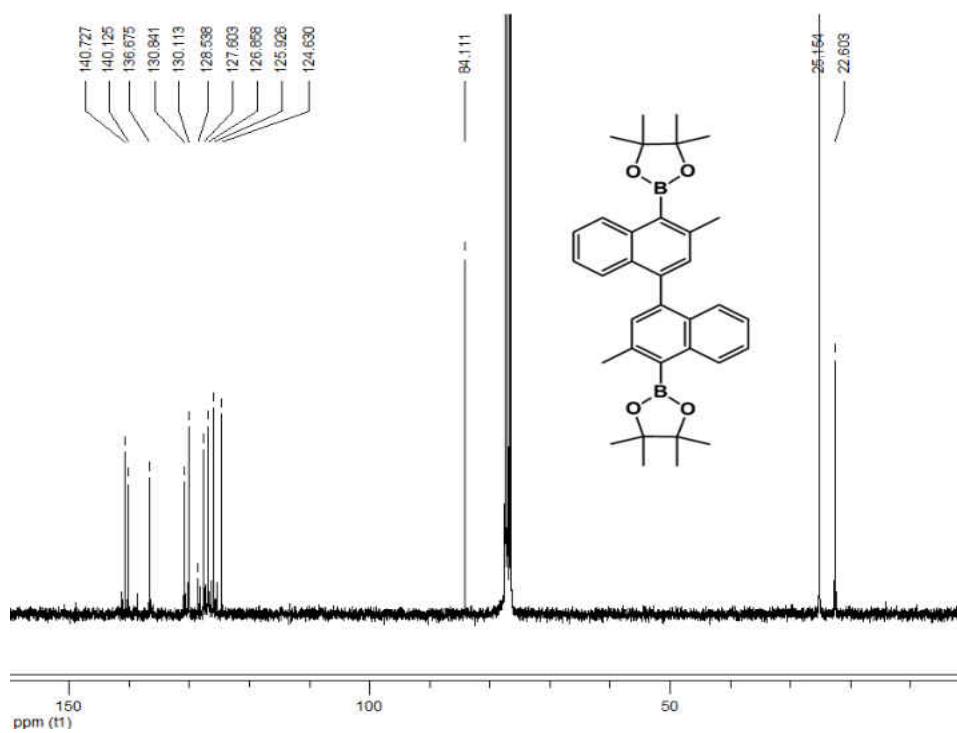


Figure 4-7-8. <sup>13</sup>C NMR spectra of **14-2**.

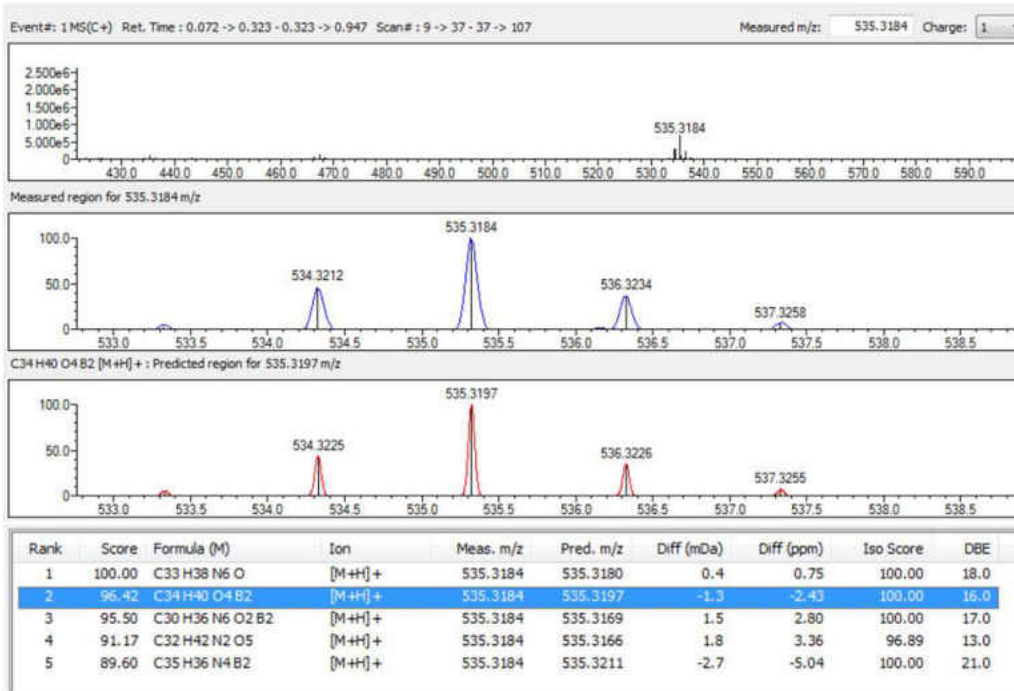


Figure 4-7-9. HRMS (APCI) of **14-2**.

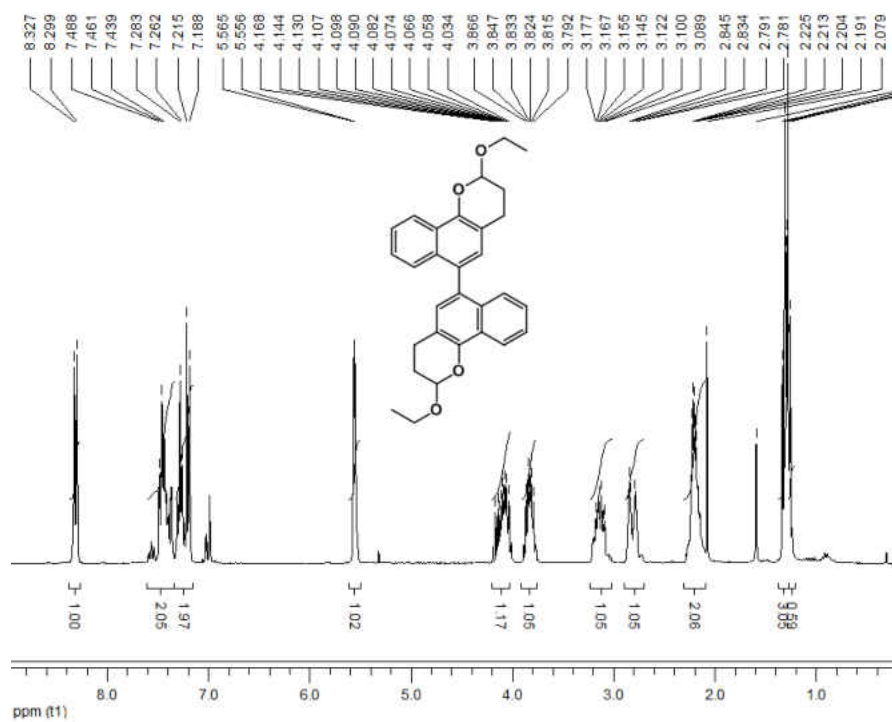


Figure 4-7-10. <sup>1</sup>H NMR spectra of **14-e**.

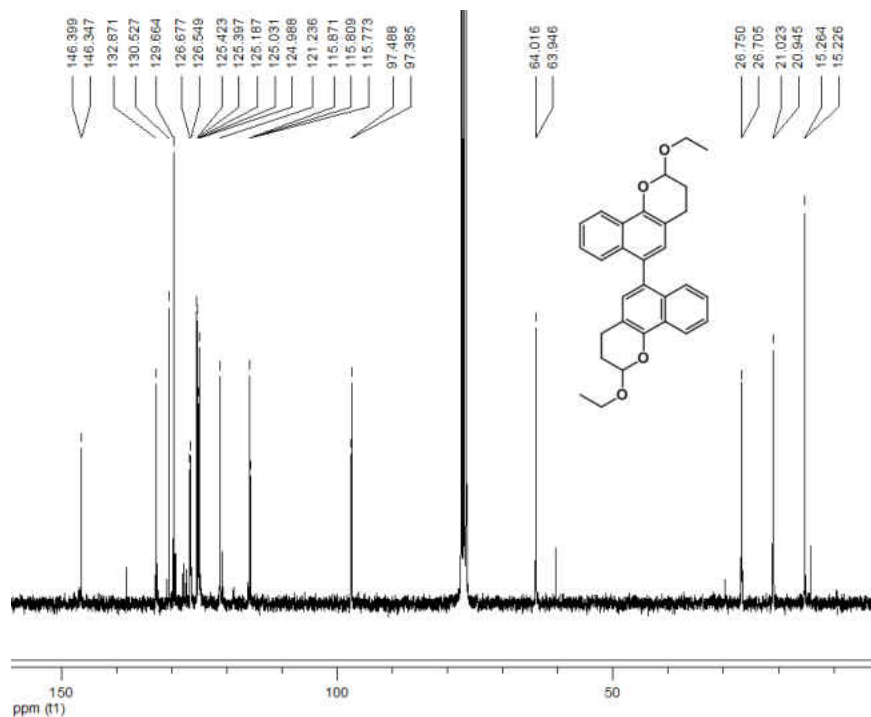
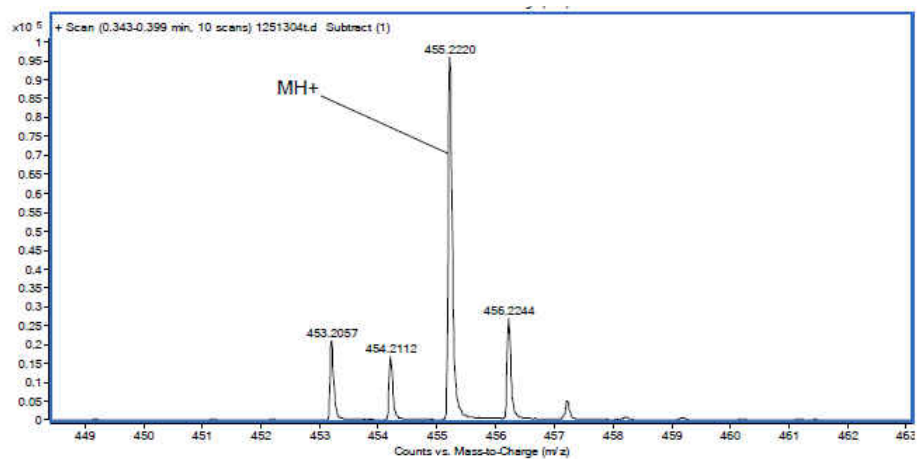


Figure 4-7-11. <sup>13</sup>C NMR spectra of **14-e**.



Measured Mass

455.222

Element	Low Limit	High Limit
C	28	38
H	25	45
O	2	6
11B	0	1

Formula	Calculated Mass	mDaError	ppmError	RDB
C30 H31 O4	455.2217	0.3	0.7	15.5

Figure 4-7-12. HRMS (APCI) of **14-e**.



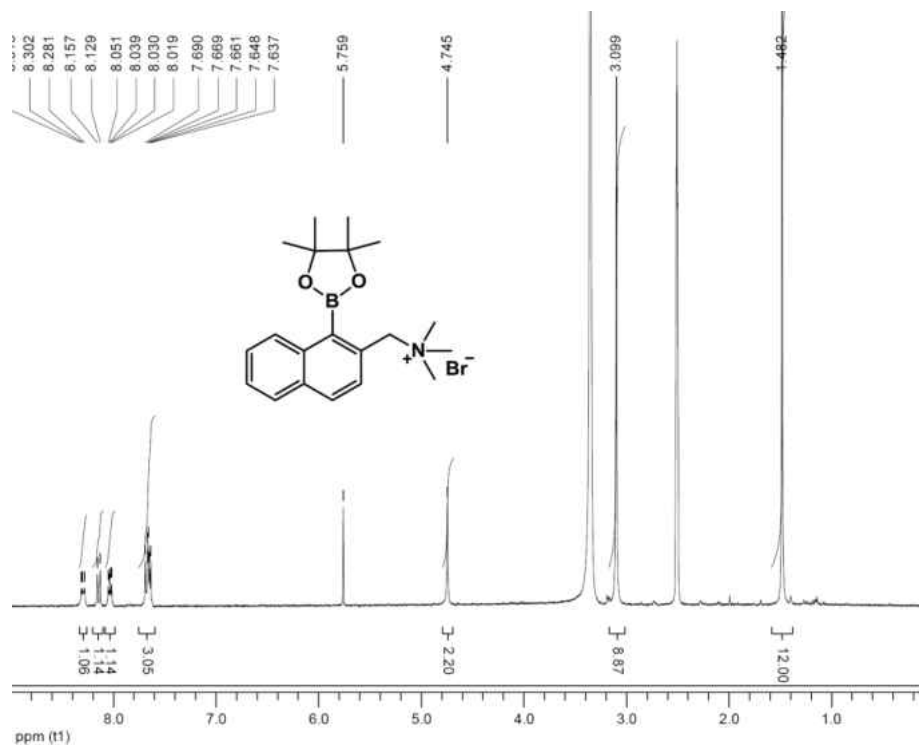


Figure 4-7-13. <sup>1</sup>H NMR spectra of **15b**.

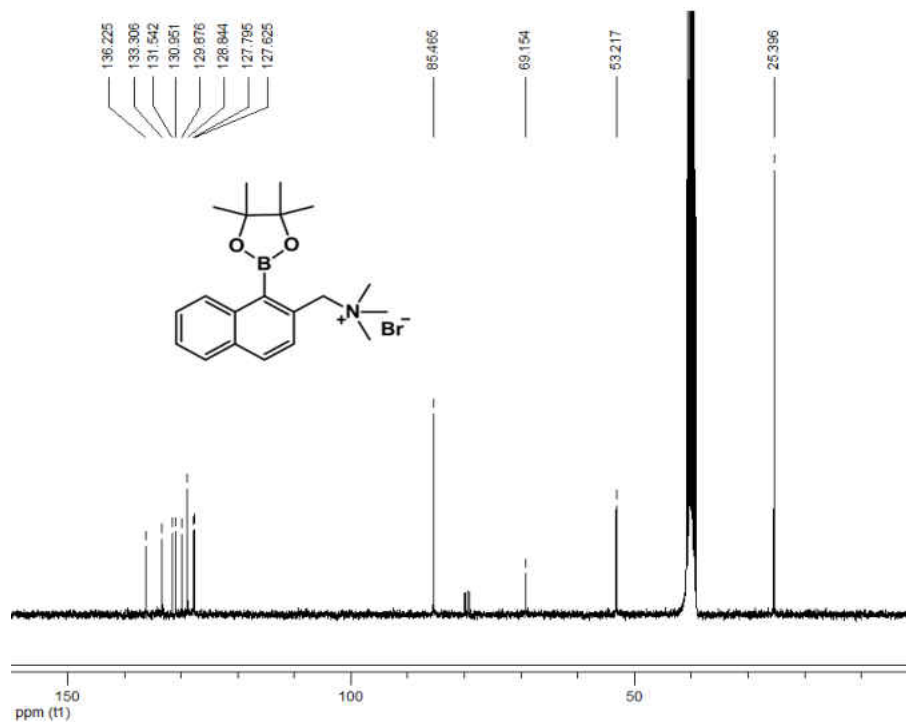


Figure 4-7-14. <sup>13</sup>C NMR spectra of **15b**.

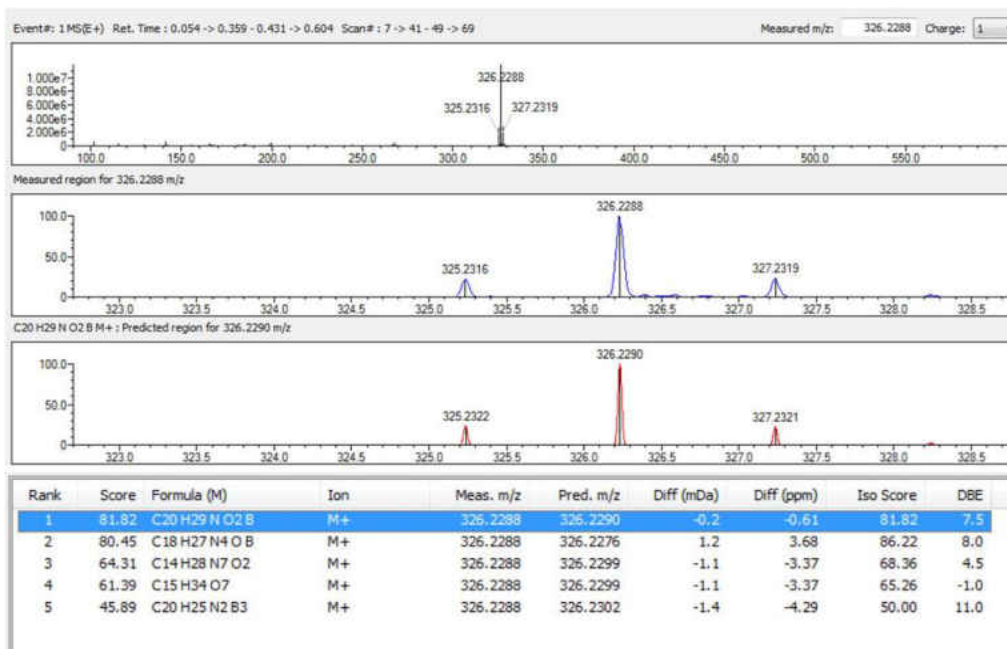


Figure 4-7-15. HRMS (ESI) of **15b**.

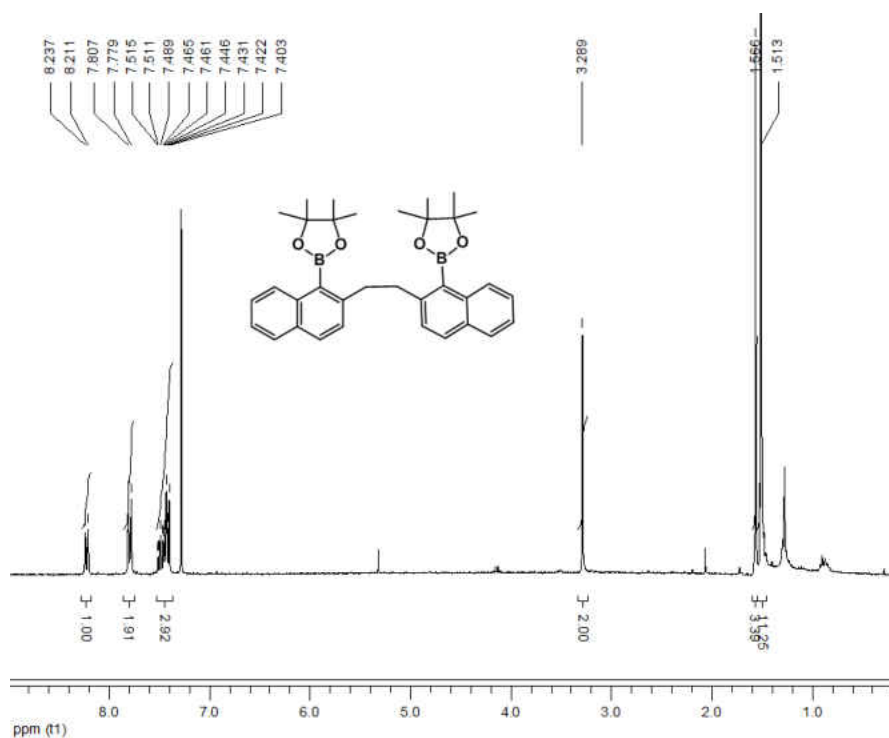


Figure 4-7-16. <sup>1</sup>H NMR spectra of **17**.

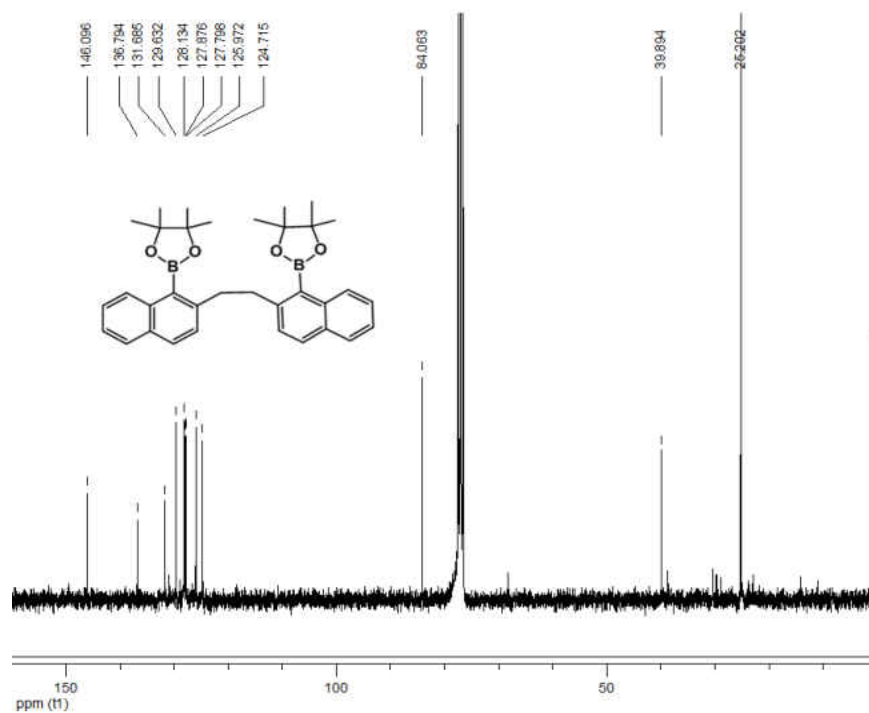


Figure 4-7-17.  $^{13}\text{C}$  NMR spectra of **17**.

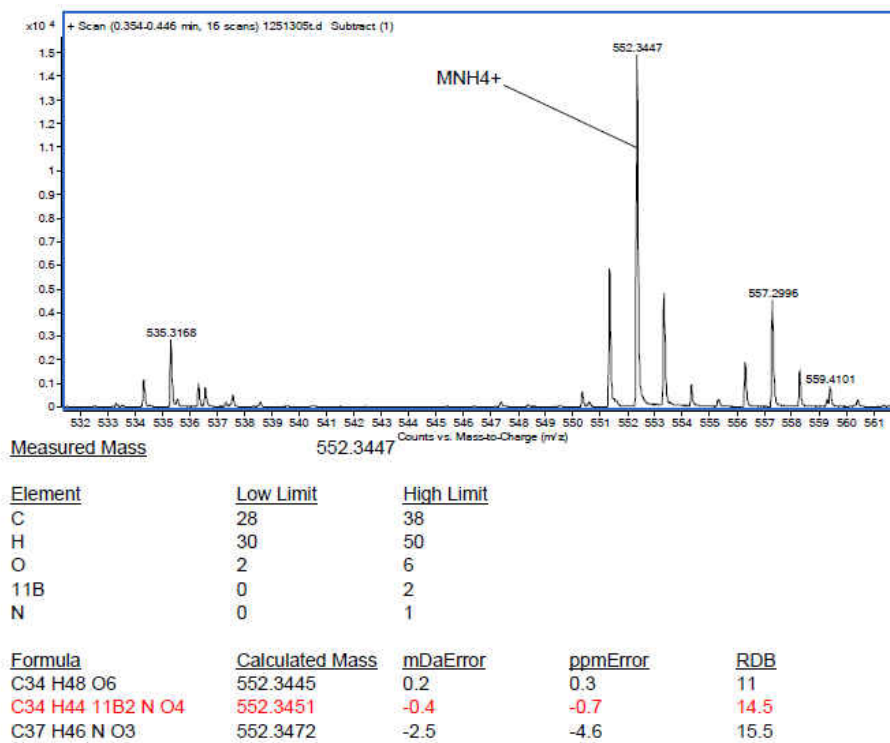


Figure 4-7-18. HRMS (ESI) of **17**.

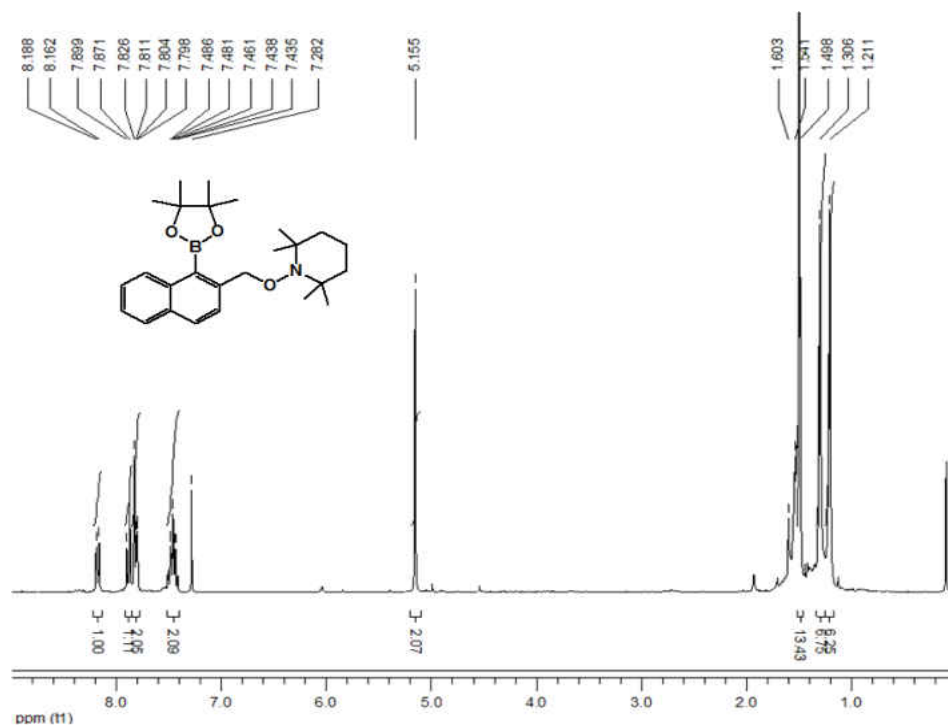


Figure 4-7-19.  $^1\text{H}$  NMR spectra of **15-t**.

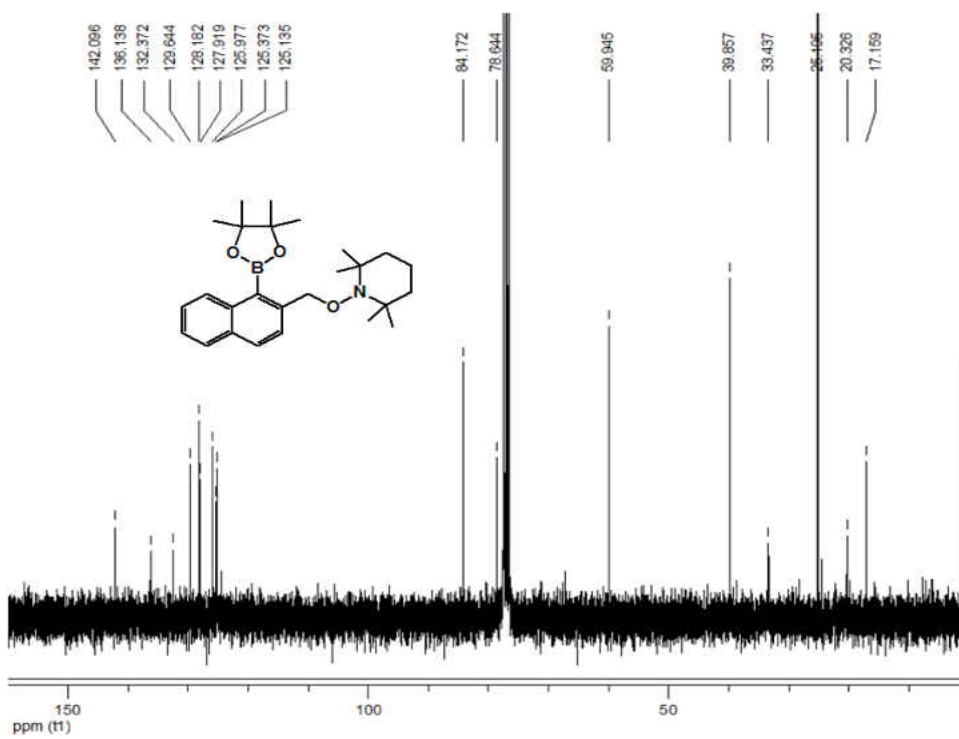


Figure 4-7-20.  $^{13}\text{C}$  NMR spectra of **15-t**.

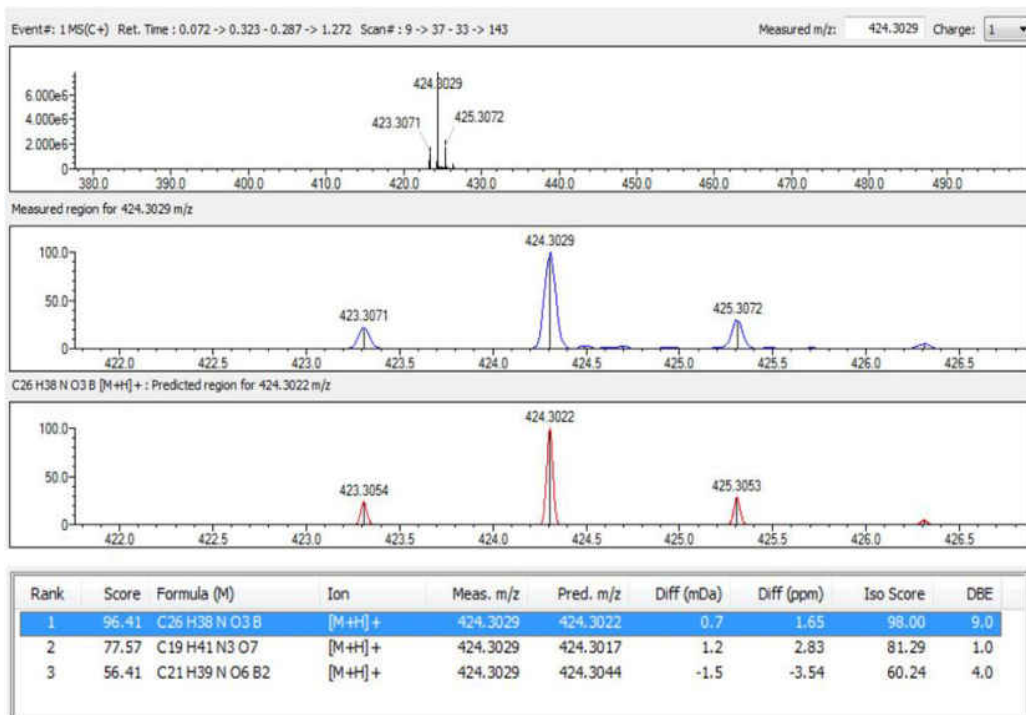


Figure 4-7-21. HRMS (APCI) of **15-t**.

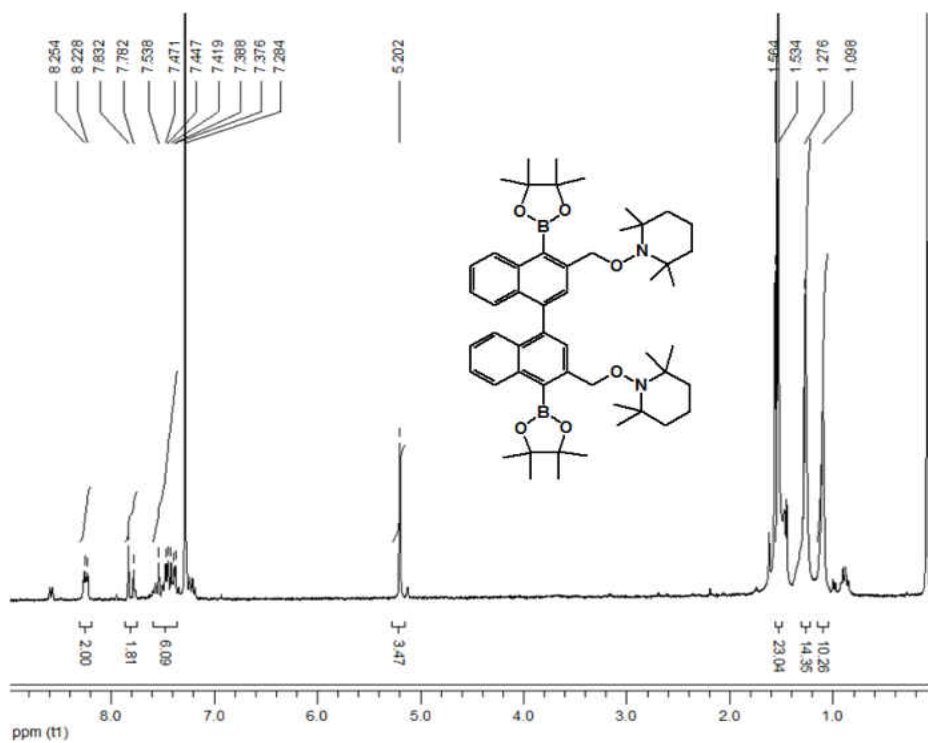


Figure 4-7-22. <sup>1</sup>H NMR spectra of **14-t**.

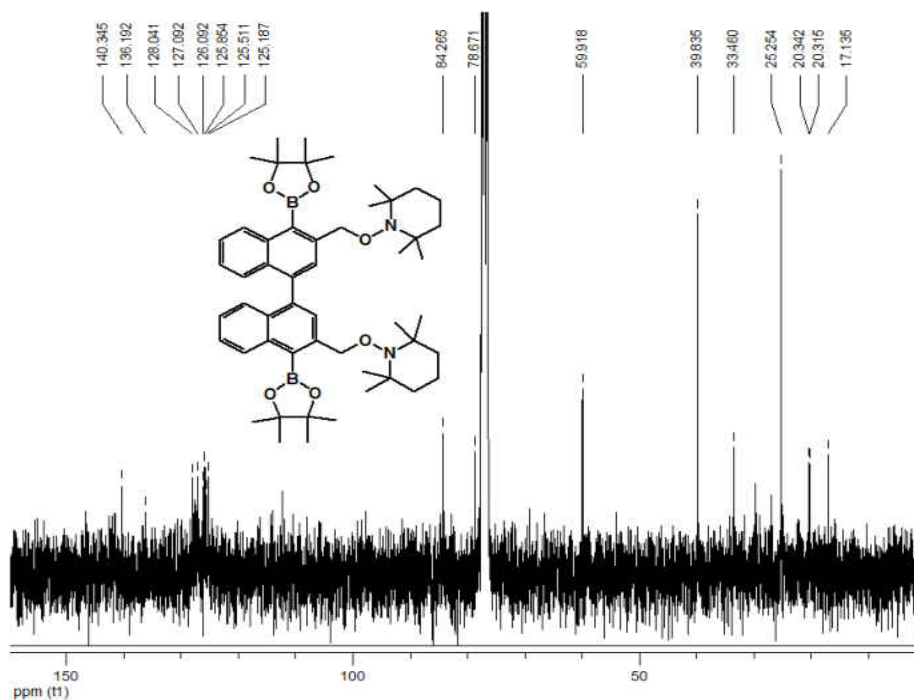


Figure 4-7-23.  $^{13}\text{C}$  NMR spectra of **14-t**.

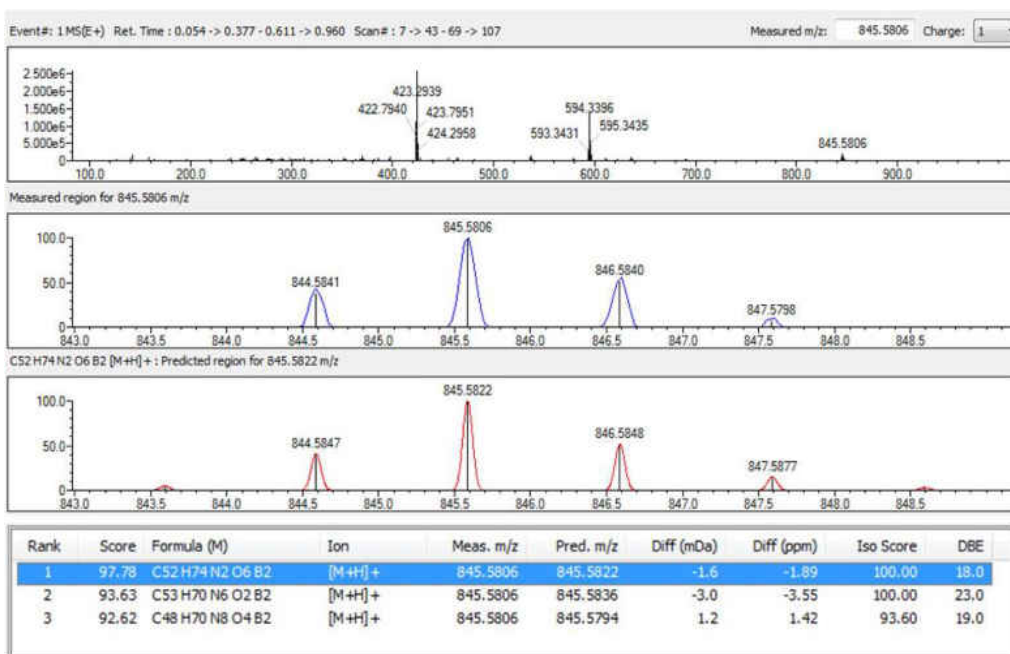


Figure 4-7-24. HRMS (ESI) of **14-t**.

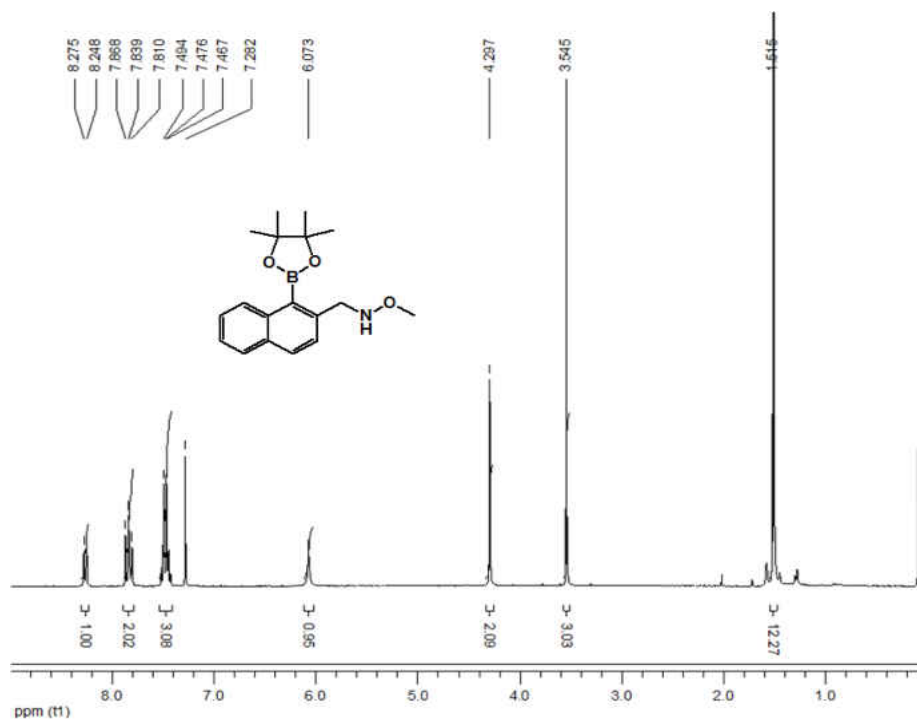


Figure 4-7-25.  $^1\text{H}$  NMR spectra of **18**.

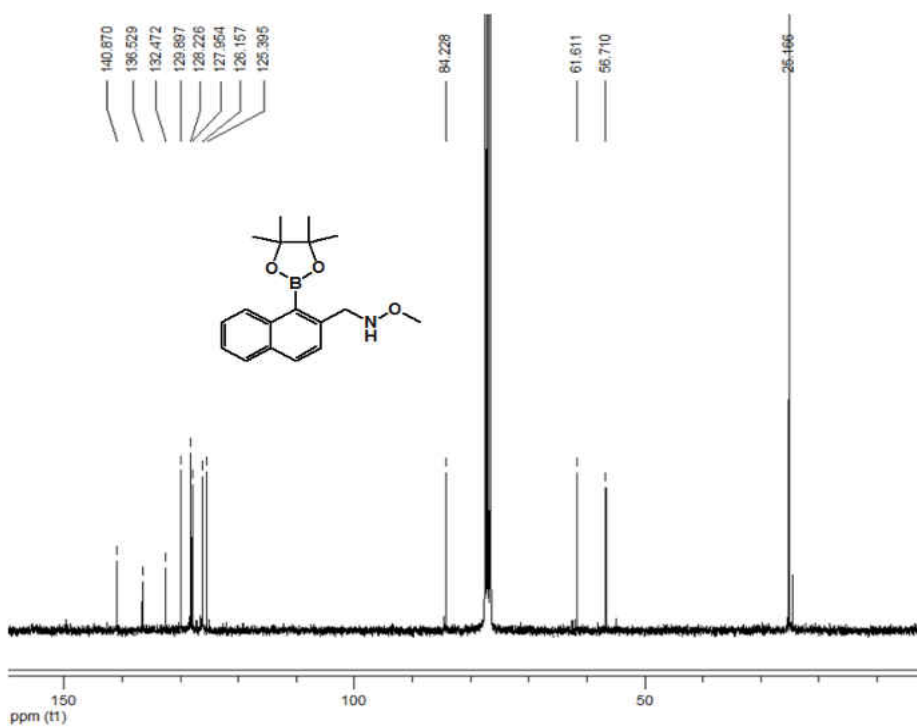


Figure 4-7-26.  $^{13}\text{C}$  NMR spectra of **18**.

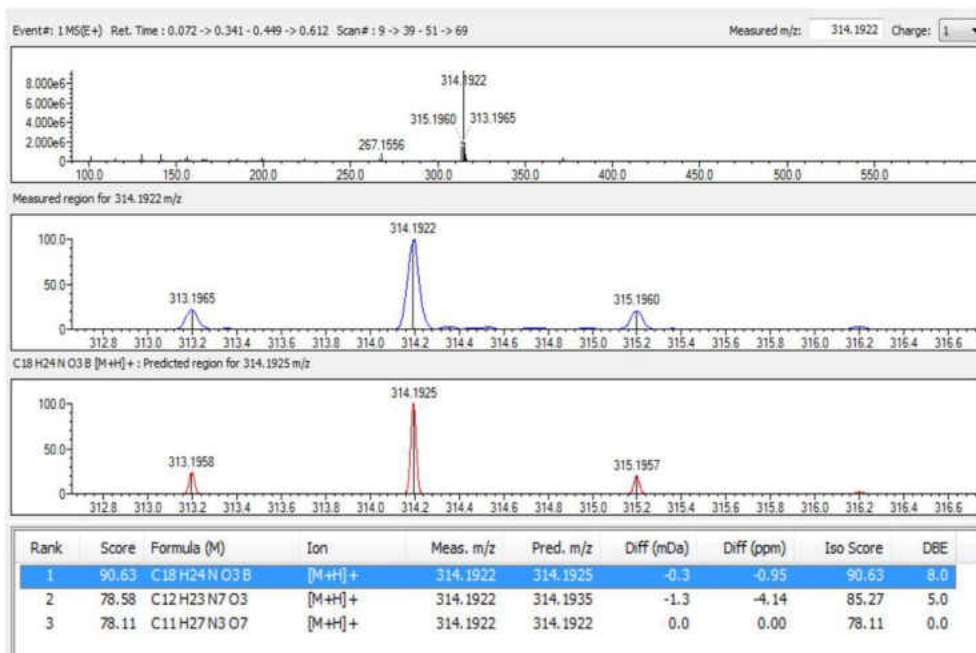


Figure 4-7-27. HRMS (ESI) of **18**.

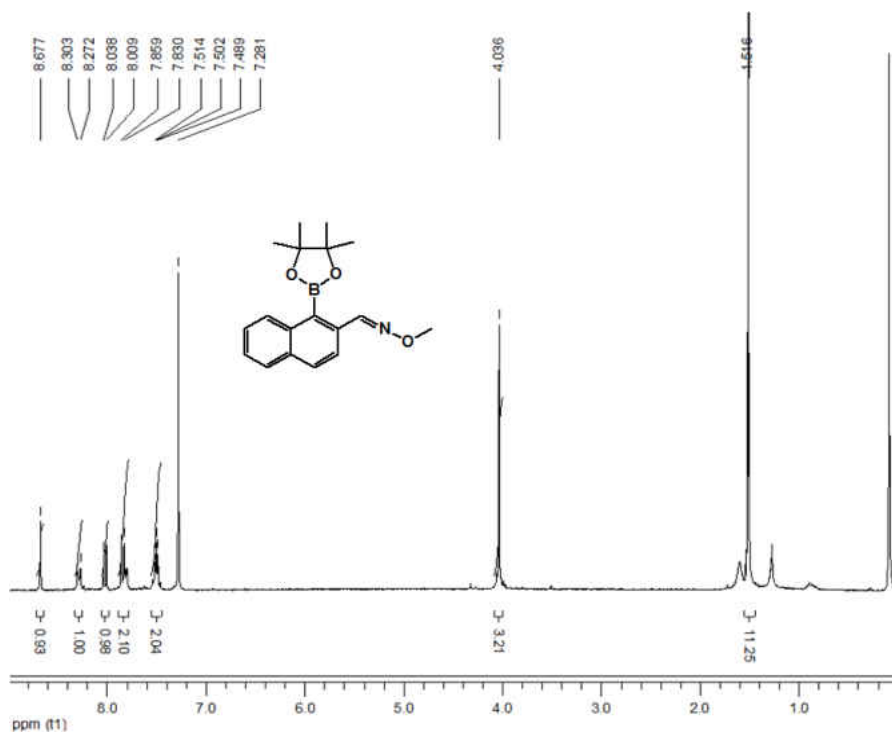


Figure 4-7-28. <sup>1</sup>H NMR spectra of **19**.



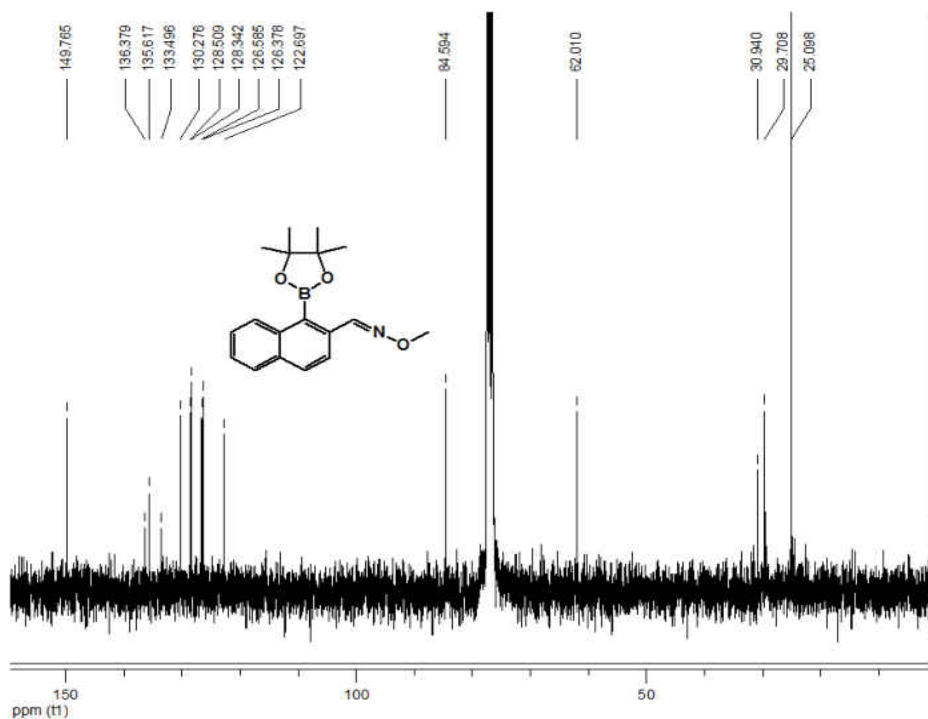


Figure 4-7-29.  $^{13}\text{C}$  NMR spectra of **19**.

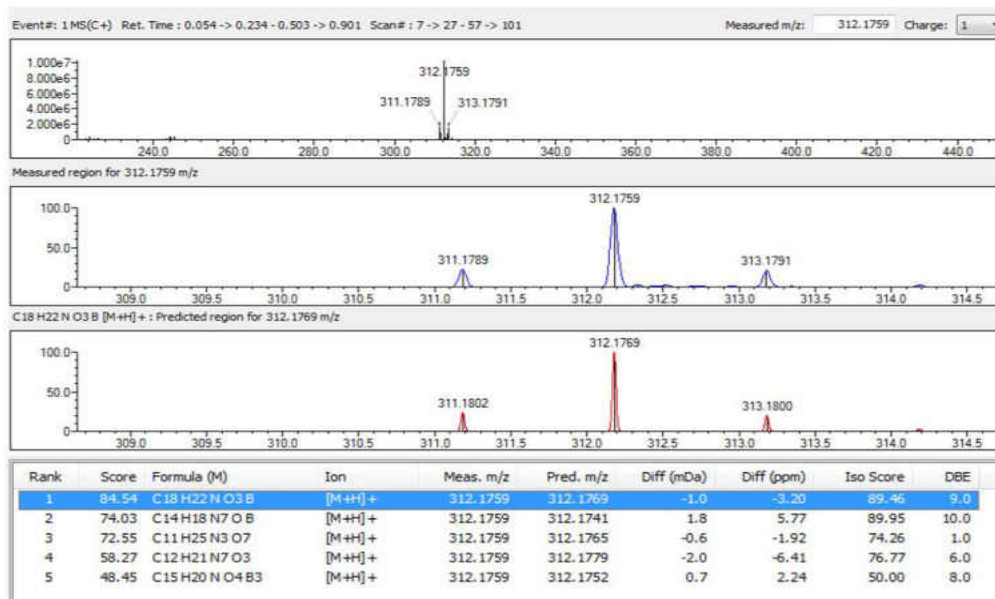


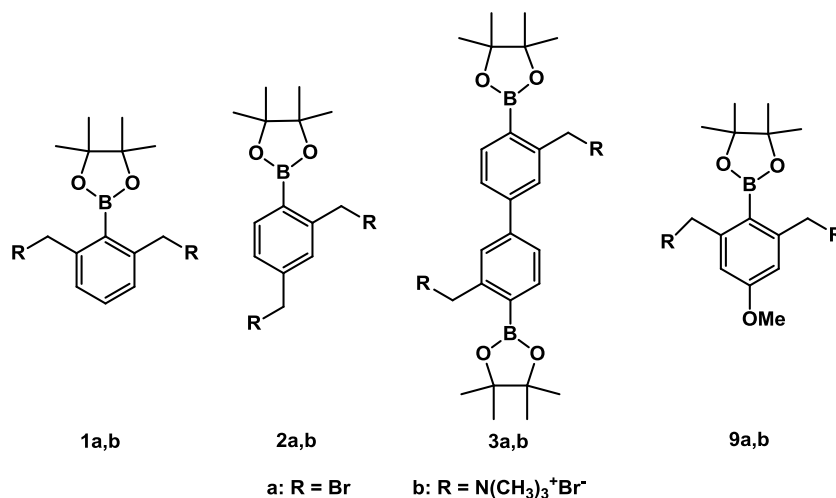
Figure 4-7-30. HRMS (APCI) of **19**.

## Chapter 5. Photo-Induced Interstrand Cross-Link Formation by Phenylboronates

### 5.1. Introduction

Our detailed investigation on the photo reactivity of binaphthalene boronates **14a** and **14b** reveals that the arylboronates can be activated by UV-irradiation to form free radicals which are further oxidized to the corresponding carbocations directly cross-linking DNA. Formation of carbocation is through electron transfer but not heterolysis. This is the first example that a bisaryl derivative undergoes photo-activation to generate a carbocation capable of efficiently cross-linking DNA.

Encouraged by these results, we studied the photo reactivity of all the phenylboronic esters **1-3** and **12** toward DNA and determined the mechanism of DNA cross-linking induced by these phenylboronates upon UV-irradiation.



**Scheme 5-1.** The structures of arylboronates.

### 5.2. DNA cross-linking assay

#### 5.2.1. DNA cross-linking ability of **1-3a,b** upon photo-irradiation

The activity of the phenylboronic esters **1-3** upon photo-irradiation was investigated using DNA duplex **5** in phosphate buffer (pH = 8.0) at 37 °C. DNA ICL formation was not observed with these compounds (Figure 5-1) without UV irradiation. However, irradiation at 350 nm resulted in DNA cross-linking with compounds, **3a** and **1b-3b**. The highest ICL yield was observed with **3b**. Higher concentration of drugs and extended irradiation time led to increased ICL yields (Figure 5-2 to 5-5). This result is different from the H<sub>2</sub>O<sub>2</sub>-induced DNA ICL formation, in which only bromides **1a-3a** but not **1b-3b** induced DNA ICL formation in the presence of H<sub>2</sub>O<sub>2</sub>. These results suggested that the mechanism for UV-induced ICL formation with compounds **1-3** may be different from that of H<sub>2</sub>O<sub>2</sub>-induced DNA ICL formation, which goes through a QM mechanism. We propose that other active species capable of cross-linking DNA may be involved in UV-irradiation of these compounds. A QM trapping experiment using excess EVE provided evidences that QMs were not formed in the photo reaction of compounds **1-3** as QM trapping products were not detected.

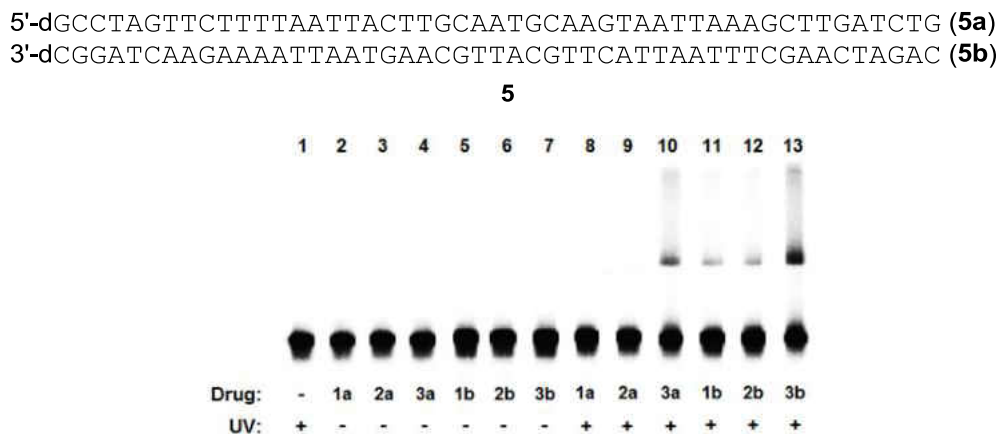


**Figure 5-1.** UV-induced DNA cross-link formation by compounds **1a,b-3a,b**. Lane 1: DNA only; lane 2: 2 mM **1a**; lane 3: 2 mM **2a**; lane 4: 2 mM **3a** (cross-linking yield 6.9%); lane 5: 2 mM **1b** (2.3%); lane 6: 2 mM **2b** (3.5%); lane 7: 2 mM **3b** (14.3%). Condition: UV irradiation at pH8 for 8 h.

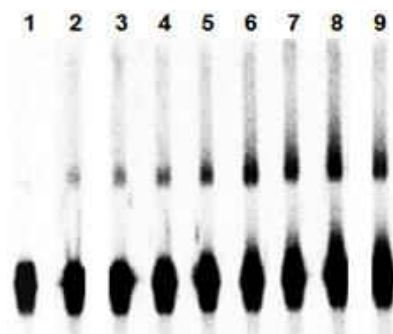


**Figure 5-2.** Concentration dependence of ICL formation by **3a** upon UV irradiation. Lane 1: with DNA only; lane 2: 20  $\mu\text{M}$  **3a** (cross-linking yield 1.7%); lane 3: 50  $\mu\text{M}$  **3a** (2.6%); lane 4: 100  $\mu\text{M}$  **3a** (3.9%); lane 5: 200  $\mu\text{M}$  **3a** (4.7%); lane 6: 500  $\mu\text{M}$  **3a** (8.5%); lane 7: 1 mM **3a** (8.3%); lane 8: 2 mM **3a** (7.5%); lane 9: 5 mM **3a** (7.3%). Condition: UV irradiation at pH8 for 8 h.

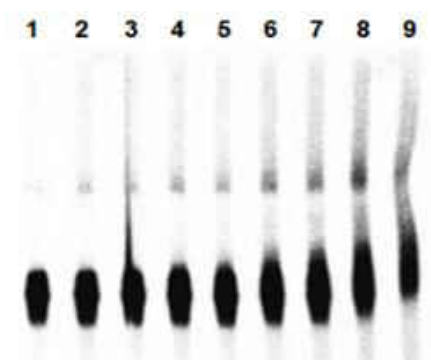


**Figure 5-3.** Concentration dependence of ICL formation by **3b** upon UV irradiation. Lane 1: with DNA only; lane 2: 20  $\mu\text{M}$  **3b** (cross-linking yield 2.2%); lane 3: 50  $\mu\text{M}$  **3b** (3.1%); lane 4: 100  $\mu\text{M}$  **3b** (3.6%); lane 5: 200  $\mu\text{M}$  **3b** (4.0%); lane 6: 500  $\mu\text{M}$  **3b** (6.0%); lane 7: 1 mM **3b** (8.5%); lane 8: 2 mM **3b** (14.0%); lane 9: 5 mM **3b** (24.1%). Condition: UV irradiation at pH8 for 8 h.

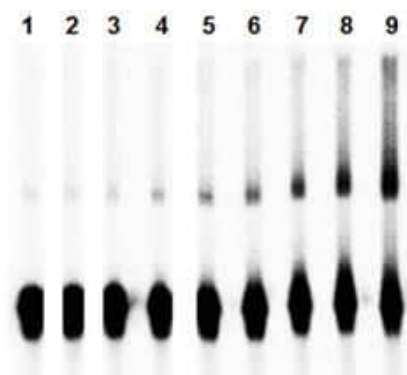


**Figure 5-4.** Time dependence of ICL formation by **3a** upon UV irradiation. Lane 1: no UV irradiation; lane 2: UV for 30 min (cross-linking yield 1.3%); lane 3: 1 h (1.9%); lane 4: 2 h (2.4%); lane 5: 4 h (3.5%); lane 6: 6 h (5.2%); lane 7: 8 h (7.3%); lane 8: 12 h (11.8%); lane 9: 24 h (25.0%). Condition: 2 mM **3a** upon UV irradiation at pH8.

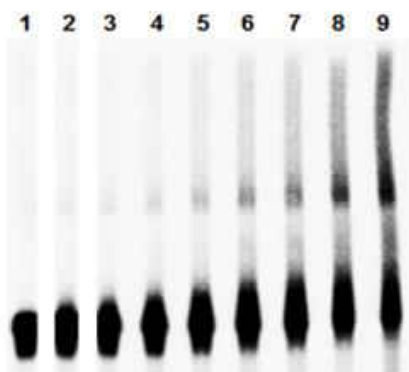


**Figure 5-5.** Time dependence of ICL formation by **3b** upon UV irradiation. Lane 1: no UV irradiation; lane 2: UV for 30 min (cross-linking yield 0.8%); lane 3: 1 h (1.8%); lane 4: 2 h (3.1%); lane 5: 4 h (6.1%); lane 6: 6 h (10.2%); lane 7: 8 h (14.2%); lane 8: 12 h (24.2%); lane 9: 24 h (38.6%). Condition: 2 mM **3b** upon UV irradiation at pH8.

### 5.2.2. Determination of cross-linking site

The photoreactivities of **3a,b** towards DNA were further investigated by determining the heat-stability of purified cross-linked products. The ICLs formed from **3a** and **3b** were stable to

heating in phosphate buffer while DNA cleavage was observed with piperidine treatment. Cleavage bands were observed mainly at dG sites upon heating in 1.0 M piperidine which indicated that the cross-linking reactions mainly occurred with dGs via alkylation (Figure 5-6 and 5-7). In the same condition, DNA interstrand cross-links were observed with duplex **7** but not with **6** can further confirm that alkylation took place only with dG and dC (Figure 5-8).

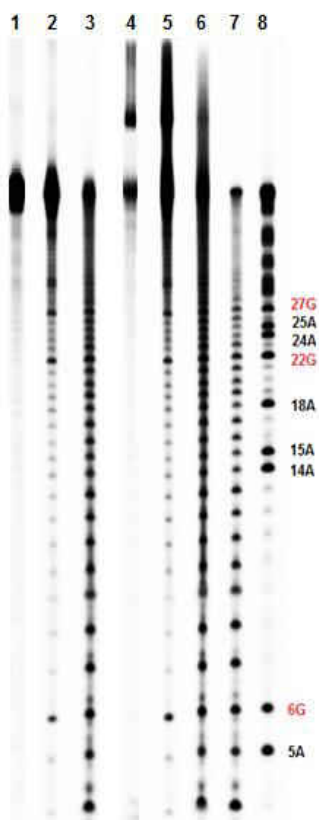


**Figure 5-6.** Determination of cross-linking site of **3a**. Phosphorimage autoradiogram of 20% denaturing PAGE analysis of the isolated ICL products and monoalkylated single stranded DNA (**5a'**) upon heating in piperidine. Lane 1: heating treatment of **5a'**; lane 2: piperidine treatment of **5a'**; lane 3: Fe·EDTA treatment of **5a'**; lane 4: heating treatment of ICL; lane 5: piperidine treatment of ICL; lane 6: Fe·EDTA treatment of ICL; lane 7: Fe·EDTA treatment of **5**; lane 8: G+A sequencing.

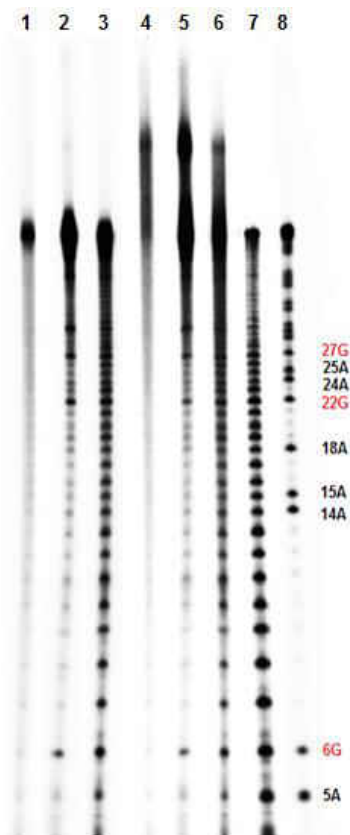


**Figure 5-7.** Determination of cross-linking site of **3b**. Phosphorimage autoradiogram of 20% denaturing PAGE analysis of the isolated ICL products and monoalkylated single stranded DNA (**5a'**) upon heating in piperidine. Lane 1: heating treatment of **5a'**; lane 2: piperidine treatment of **5a'**; lane 3: Fe·EDTA treatment of **5a'**; lane 4: heating treatment of ICL; lane 5: piperidine treatment of ICL; lane 6: Fe·EDTA treatment of ICL; lane 7: Fe·EDTA treatment of **5**; lane 8: G+A sequencing.

5'-dATATATATATATATATATATATATAT (6a) 5'-dCCCTTCTTTTCTTTTCTTCCC (7a)  
 3'-dTATATATATATATATATATATATATA (6b) 3'-dGGGAAGAAAAGAAAAGAAGGG (7b)

6

7

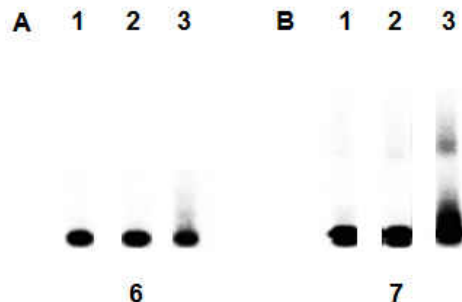


**Figure 5-8.** ICL formation from duplex **7** induced by **3b** upon UV irradiation. Lane 1: DNA only; lane 2: DNA only with UV; lane 3: DNA with 2 mM **3b** no UV; lane 4: DNA with 2 mM **3b** and UV irradiation. Condition: UV irradiation for 8 h at pH8.

### 5.2.3. The mechanism of ICL formation induced by **3a,b**

Based on our previous investigation of the photo-activity of the naphthalene boronates, we propose that the phenylboronic esters **1b-3b** and **3a** undergo a similar reaction mechanism, which involves formation of a free radical followed by conversion to a carbocation directly alkylating DNA.

In order to test our hypothesis, we performed the radical and cation trapping reactions with **3a** and **3b** upon UV irradiation. However, no trapping products could be isolated and the resulting products were too complicated to identify. Thus, we investigated the effect of trapping agents on DNA ICL formation with DNA duplex **5**. First, 2-mercaptoethanol (BME) and 2,2,6,6-tetramethylpiperidin-1-oxyl (TEMPO) were employed as free radical trapping agents, which act as competitors for ICL. As expected, the DNA cross-linking yields induced by **3a** were dependent on the concentration of both BME and TEMPO (Figure 5-9 and 5-10). To our surprise, only BME but not TEMPO inhibited ICL formation induced by **3b** upon UV-irradiation (Figure 5-11 and 5-12). TEMPO did not affect ICL formation, which indicated that free radicals were not generated when **3b** was irradiated at 350 nm. The inhibiting effect of BME on DNA cross-



linking might be due to the capability of BME on trapping cation as both SH and OH are good nucleophiles. These results suggested that carbocation but not free radical was generated by UV-irradiation of **3b**.

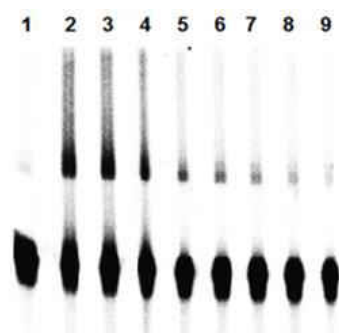


**Figure 5-9.** Effect of TEMPO on ICL formation by **3a** upon UV irradiation. Lane 1: with DNA only; lane 2: 2 mM **3a** (cross-linking yield 20.8%); lane 3: 2 mM **3a** and 1 mM TEMPO (18.5%); lane 4: 2 mM **3a** and 2 mM TEMPO (11.0%); lane 5: 2 mM **3a** and 5 mM TEMPO (5.9%); lane 6: 2 mM **3a** and 10 mM TEMPO (4.1%); lane 7: 2mM **3a** and 20 mM TEMPO (3.1%); lane 8: 2 mM **3a** and 50 mM TEMPO (2.2%); lane 9: 2 mM **3a** and 100 mM TEMPO (1.1%). Condition: UV irradiation at pH8 for 24 h.

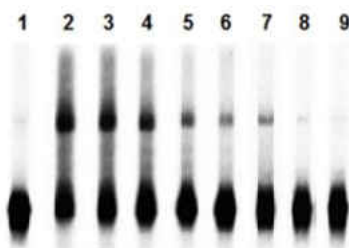


**Figure 5-10.** Effect of BME on ICL formation by **3a** upon UV irradiation. Lane 1: with DNA only; lane 2: 2 mM **3a** (cross-linking yield 21.2%); lane 3: 2 mM **3a** and 1 mM BME (18.1%); lane 4: 2 mM **3a** and 2 mM BME (13.5%); lane 5: 2 mM **3a** and 5 mM BME (7.1%); lane 6: 2 mM **3a** and 10 mM BME (3.9%); lane 7: 2 mM **3a** and 20 mM BME (2.7%); lane 8: 2 mM **3a**

and 50 mM BME (1.9%); lane 9: 2 mM **3a** and 100 mM BME (0.9%). Condition: UV irradiation at pH8 for 24 h.

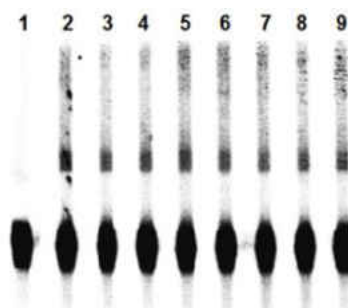


**Figure 5-11.** Effect of TEMPO on ICL formation by **3b** upon UV irradiation. Lane 1: with DNA only; lane 2: 2 mM **3b** (cross-linking yield 32.3%); lane 3: 2 mM **3b** and 1 mM TEMPO (30.8%); lane 4: 2 mM **3b** and 2 mM TEMPO (31.4%); lane 5: 2 mM **3b** and 5 mM TEMPO (30.6%); lane 6: 2 mM **3b** and 10 mM TEMPO (29.5%); lane 7: 2 mM **3b** and 20 mM TEMPO (27.1%); lane 8: 2 mM **3b** and 50 mM TEMPO (26.2%); lane 9: 2 mM **3b** and 100 mM TEMPO (22.1%). Condition: UV irradiation at pH8 for 24 h.

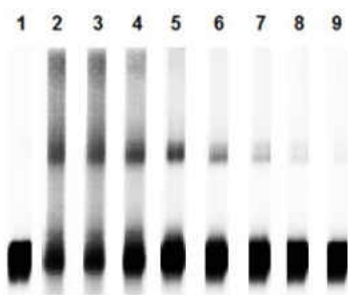


**Figure 5-12.** Effect of BME on ICL formation by **3b** upon UV irradiation. Lane 1: with DNA only; lane 2: 2 mM **3b** (cross-linking yield 34.1%); lane 3: 2 mM **3b** and 1 mM BME (31.1%); lane 4: 2 mM **3b** and 2 mM BME (28.3%); lane 5: 2 mM **3b** and 5 mM BME (19.7%); lane 6: 2 mM **3b** and 10 mM BME (7.9%); lane 7: 2 mM **3b** and 20 mM BME (4.3%); lane 8: 2 mM **3b** and 50 mM BME (2.2%); lane 9: 2 mM **3b** and 100 mM BME (1.0%). Condition: UV irradiation at pH8 for 24 h.

In order to provide evidence for formation of carbocation, methoxyamine was chosen as a trapping agent for DNA ICL formation. As expected, ICL formation was inhibited by methoxyamine when **3a** and **3b** were irradiated with duplex **5** (Figure 5-13 and 5-14). Increasing concentration of methoxyamine gradually decreased the ICL yield. 100 mM methoxyamine resulted in complete quenching of interstrand cross-link formation (Figure 5-13 and 5-14 lane 9). Clearly, carbocations were produced in the photo reactions of **3a** and **3b**.

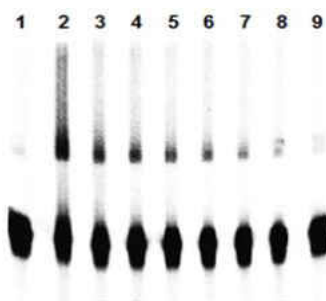


**Figure 5-13.** Effect of methoxyamine on ICL formation by **3a** upon UV irradiation. Lane 1: with DNA only; lane 2: 2 mM **3a** (cross-linking yield 20.8%); lane 3: 2 mM **3a** and 1 mM methoxyamine (10.1%); lane 4: 2 mM **3a** and 2 mM methoxyamine (7.7%); lane 5: 2 mM **3a** and 5 mM methoxyamine (6.4%); lane 6: 2 mM **3a** and 10 mM methoxyamine (4.3%); lane 7: 2 mM **3a** and 20 mM methoxyamine (3.0%); lane 8: 2 mM **3a** and 50 mM methoxyamine (2.0%); lane 9: 2 mM **3a** and 100 mM methoxyamine (0.5%). Condition: UV irradiation at pH8 for 24 h.

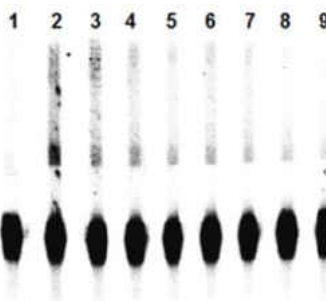


**Figure 5-14.** Effect of methoxyamine on ICL formation by **3b** upon UV irradiation. Lane 1: with DNA only; lane 2: 2 mM **3b** (cross-linking yield 32.3%); lane 3: 2 mM **3b** and 1 mM

methoxyamine (20.1%); lane 4: 2 mM **3b** and 2 mM methoxyamine (14.7%); lane 5: 2 mM **3b** and 5 mM methoxyamine (11.6%); lane 6: 2 mM **3b** and 10 mM methoxyamine (7.8%); lane 7: 2 mM **3b** and 20 mM methoxyamine (5.1%); lane 8: 2 mM **3b** and 50 mM methoxyamine (2.5%); lane 9: 2 mM **3b** and 100 mM methoxyamine (1.1%). Condition: UV irradiation at pH8 for 24 h.

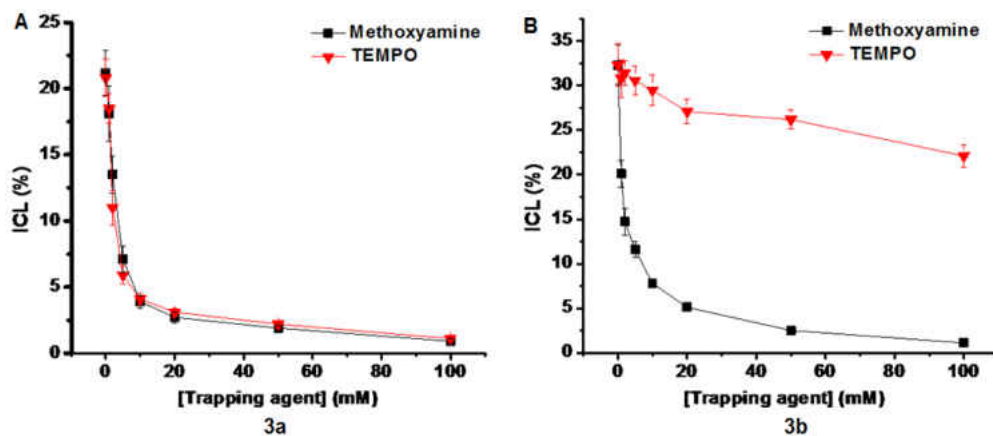


**Figure 5-15.** Effect of TEMPO and methoxyamine on ICL formation by **3a** and **3b**.

We propose that different reactivity of **1b-3b** may be related to their UV absorption. Thus, the UV absorption spectra of **1b-3b** were measured. Compounds **1b** and **2b** showed a strong absorbance at 225 nm but almost no absorption after 300 nm. However the maximum absorption of **3b** was shifted to a longer wavelength of 270 nm (Figure 5-16). These results indicated that **3b** is more sensitive to irradiation at longer wavelength than **1b** and **2b**, thus leading to a higher cross-linking yield with 350 nm irradiation.

Further study showed that the leaving group affected the reaction mechanism. For example, the cross-linking yield of **3a** was affected by both methoxyamine and TEMPO, which is similar to the naphthalene boronates discussed in Chapter 4. This indicated that formation of free radicals followed by conversion to carbocation was possible for **3a** having a Br as leaving group.

However, ICL formation of **3b** with a trimethylamine salt was only affected by methoxyamine but not TEMPO, which suggested that a carbocation was directly generated by heterolysis of C-N bond but not from free radicals.

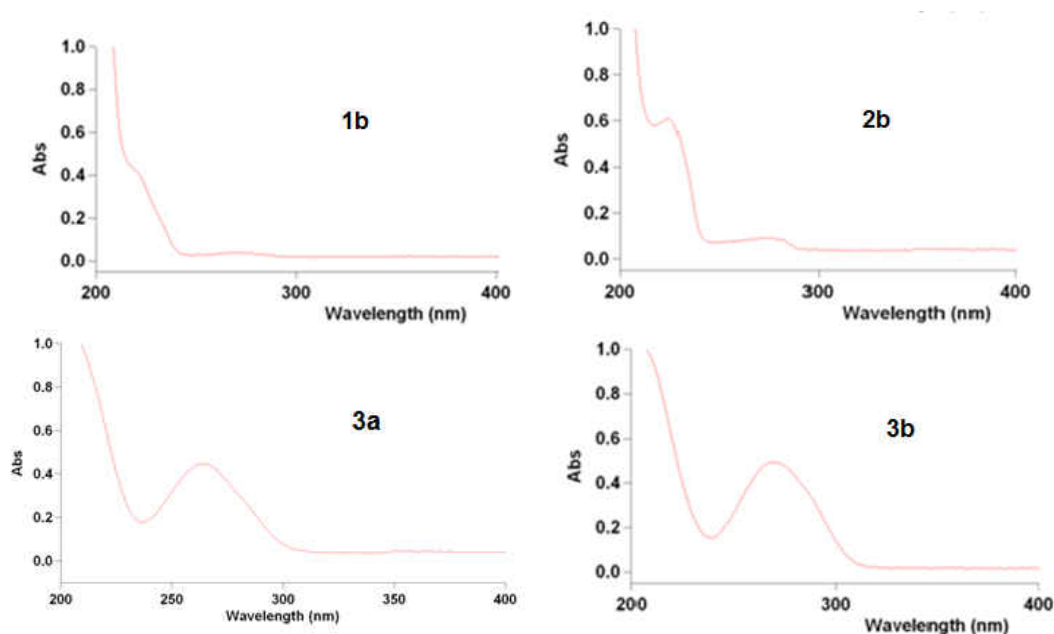
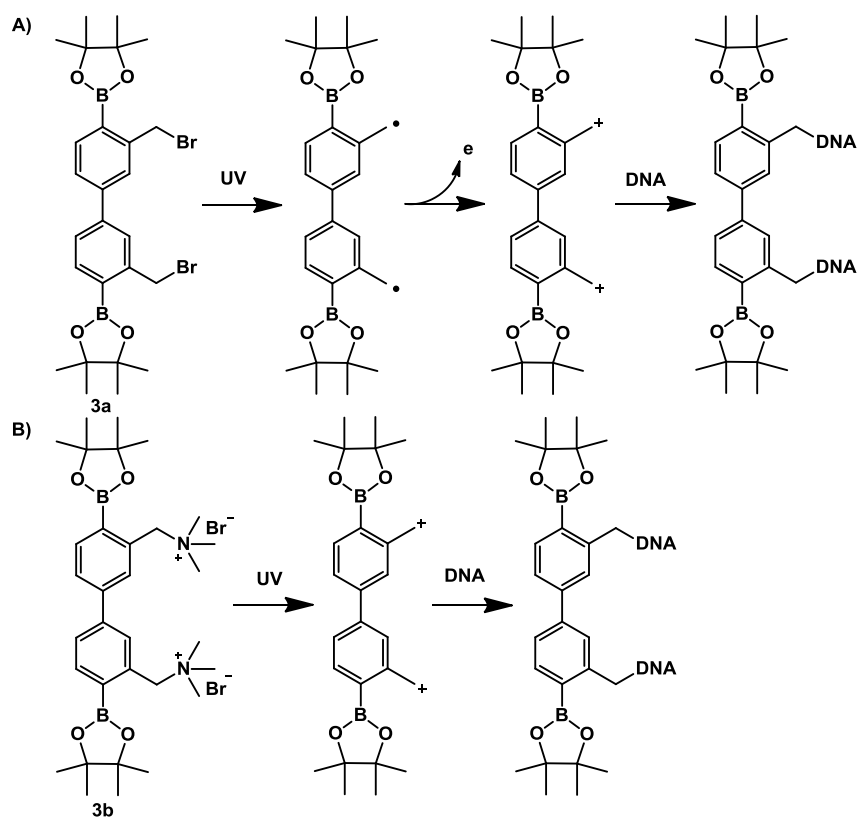


**Figure 5-16.** Absorbance of **1b**, **2b** and **3a,b**.

In summary, 350 nm irradiation of bromide **3a** and ammonium salts **1b-3b** induced DNA ICL formation. A different reaction mechanism was observed for **3a** having Br as a leaving group and that of **1b-3b** with a trimethylamine salt as a leaving group. Photo-irradiation of **3a** generates free radicals which go through one-electron transfer to produce carbocation alkylating DNA, while direct heterolysis occurs with photo-irradiation of **3b** at 350 nm to produce carbocations cross-linking DNA (Scheme 5-2).



**Scheme 5-2.** Proposed mechanism for ICL formation induced by **3a** and **3b**.

#### 5.2.4. DNA cross-linking ability of **9a** and **9b**

In order to see the generality of the leaving group effect on DNA cross-linking, we investigated the photo-reactivity of compounds **9a** and **9b**. Both compounds contain an electron-donating group ( $\text{OCH}_3$ ) in the aromatic ring and show a strong absorbance peak at  $\lambda = 280$  nm (Figure 5-17), while they have different leaving groups.

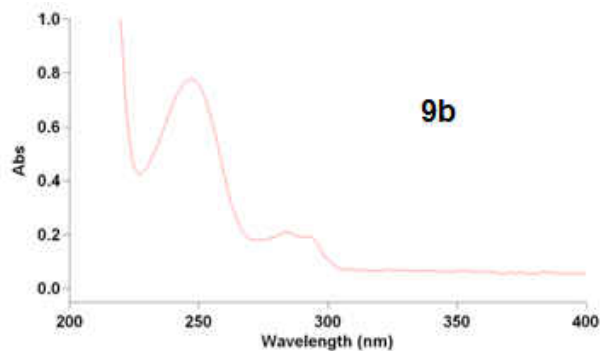


**Figure 5-17.** Absorbance of **9b**.

Similar with **3a** and **3b**, the ICL yield depends on the concentration and the irradiation time.

Higher cross-linking yield was obtained with higher concentration of drug and extended irradiation time (Figure 5-18 to 5-21). However, the ICL yields induced by **9a** (23% for 2 mM **9a**) and **9b** (51% for 2 mM **9b**) were much higher than **3a** (8% for 2 mM **3a**) and **3b** (14% for 2 mM **3b**).

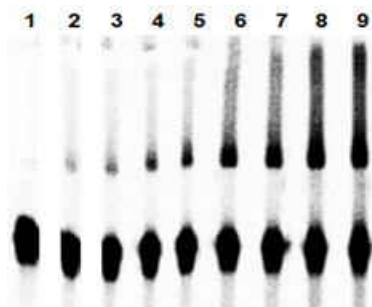


**Figure 5-18.** Concentration dependence of ICL formation by **9a** upon UV irradiation. Lane 1: with DNA only; lane 2: 20  $\mu\text{M}$  **9a** (cross-linking yield 1.1%); lane 3: 50  $\mu\text{M}$  **9a** (1.9%); lane 4: 100  $\mu\text{M}$  **9a** (3.1%); lane 5: 200  $\mu\text{M}$  **9a** (4.7%); lane 6: 500  $\mu\text{M}$  **9a** (11.3%); lane 7: 1 mM **9a** (15.8%); lane 8: 2 mM **9a** (23.1%); lane 9: 5 mM **9a** (28.1%). Condition: UV irradiation at pH8 for 8 h.

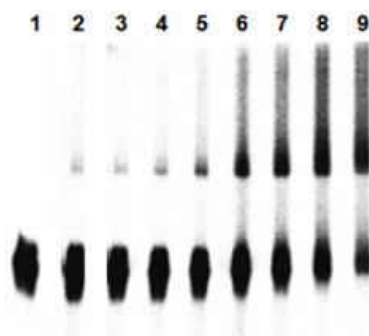


**Figure 5-19.** Concentration dependence of ICL formation by **9b** upon UV irradiation. Lane 1: with DNA only; lane 2: 20  $\mu\text{M}$  **9b** (cross-linking yield 0.9%); lane 3: 50  $\mu\text{M}$  **9b** (1.5%); lane 4: 100  $\mu\text{M}$  **9b** (5.0%); lane 5: 200  $\mu\text{M}$  **9b** (9.3%); lane 6: 500  $\mu\text{M}$  **9b** (22.3%); lane 7: 1 mM **9b** (33.4%); lane 8: 2 mM **9b** (51.1%); lane 9: 5 mM **9b** (65.5%). Condition: UV irradiation at pH8 for 8 h.

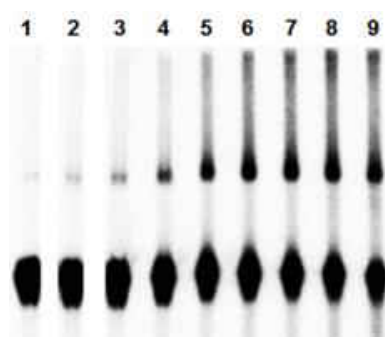


**Figure 5-20.** Time dependence of ICL formation by **9a** upon UV irradiation. Lane 1: no UV irradiation; lane 2: UV for 30 min (cross-linking yield 1.4%); lane 3: 1 h (3.4%); lane 4: 2 h (6.3%); lane 5: 4 h (12.8%); lane 6: 6 h (19.7%); lane 7: 8 h (23.5%); lane 8: 12 h (27.3%); lane 9: 24 h (31.8%). Condition: 2 mM **9a** upon UV irradiation at pH8.



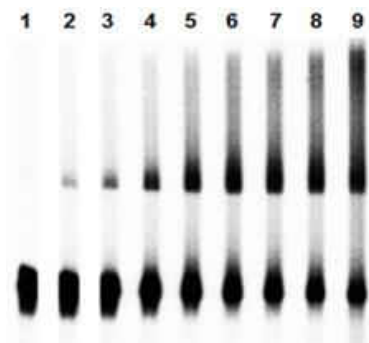


**Figure 5-21.** Time dependence of ICL formation by **9b** upon UV irradiation. Lane 1: no UV irradiation; lane 2: UV for 30 min (cross-linking yield 4.3%); lane 3: 1 h (9.9%); lane 4: 2 h (20.1%); lane 5: 4 h (35.6%); lane 6: 6 h (45.0%); lane 7: 8 h (49.0%); lane 8: 12 h (54.4%); lane 9: 24 h (60.6%). Condition: 2 mM **9b** upon UV irradiation at pH8.

In order to investigate the reaction mechanism, the radical and carbocation trapping experiments were performed by using TEMPO and methoxyamine as trapping agents. As expected, the cross-linking yields were dependent on the concentration of TEMPO (Figure 5-22) and methoxyamine (Figure 5-23) by **9a**, which is similar to **3a**. However, ICL formation induced by **9b** only depended on methoxyamine but not TEMPO (Figure 5-24 and 5-25), which is similar to **3b**. These results provided further evidence on that the leaving groups affected the reaction mechanism for ICL formation. Photo irradiation of compounds with Br as leaving group, such as **3a** and **9a**, generates free radical which is converted to carbocation via one-electron transfer. However, compounds with trimethyl amine salts as leaving groups, such as **3b** and **9b**, undergo direct heterolysis upon photo-irradiation to form carbocation which directly producing DNA ICLs.

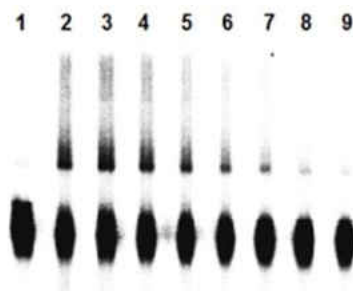


**Figure 5-22.** Effect of TEMPO on ICL formation by **9a** upon UV irradiation. Lane 1: with DNA only; lane 2: 2 mM **9a** (cross-linking yield 22.9%); lane 3: 2 mM **9a** and 1 mM TEMPO (18.8%); lane 4: 2 mM **9a** and 2 mM TEMPO (15.3%); lane 5: 2 mM **9a** and 5 mM TEMPO (10.1%); lane 6: 2 mM **9a** and 10 mM TEMPO (7.4%); lane 7: 2 mM **9a** and 20 mM TEMPO (4.8%); lane 8: 2 mM **9a** and 50 mM TEMPO (2.9%); lane 9: 2 mM **9a** and 100 mM TEMPO (1.7%). Condition: UV irradiation at pH8 for 8 h.

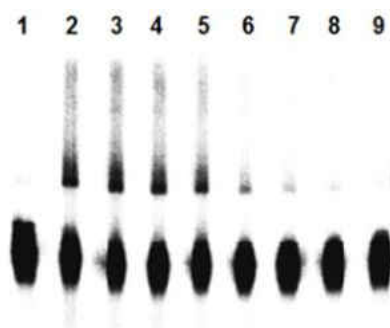


**Figure 5-23.** Effect of methoxyamine on ICL formation by **9a** upon UV irradiation. Lane 1: with DNA only; lane 2: 2 mM **9a** (cross-linking yield 22.9%); lane 3: 2 mM **9a** and 1 mM methoxyamine (19.0%); lane 4: 2 mM **9a** and 2 mM methoxyamine (14.5%); lane 5: 2 mM **9a** and 5 mM methoxyamine (11.1%); lane 6: 2 mM **9a** and 10 mM methoxyamine (4.8%); lane 7: 2 mM **9a** and 20 mM methoxyamine (3.1%); lane 8: 2 mM **9a** and 50 mM methoxyamine (1.8%); lane 9: 2 mM **9a** and 100 mM methoxyamine (0.9%). Condition: UV irradiation at pH8 for 8 h.

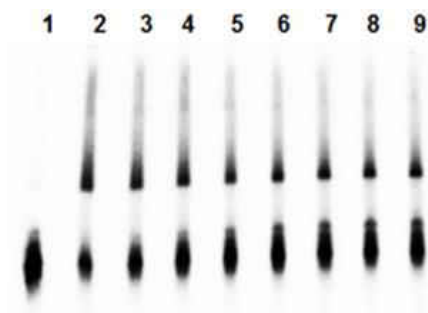


**Figure 5-24.** Effect of TEMPO on ICL formation by **9b** upon UV irradiation. Lane 1: with DNA only; lane 2: 2 mM **9b** (cross-linking yield 54.4%); lane 3: 2 mM **9b** and 1 mM TEMPO (49.1%); lane 4: 2 mM **9b** and 2 mM TEMPO (44.6%); lane 5: 2 mM **9b** and 5 mM TEMPO (38.1%); lane 6: 2 mM **9b** and 10 mM TEMPO (36.1%); lane 7: 2 mM **9b** and 20 mM TEMPO (35.8%); lane 8: 2 mM **9b** and 50 mM TEMPO (36.2%); lane 9: 2 mM **9b** and 100 mM TEMPO (35.8%). Condition: UV irradiation at pH8 for 8 h.

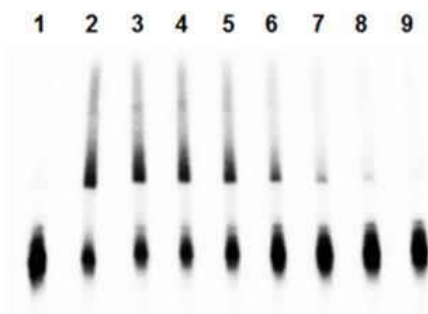


**Figure 5-25.** Effect of methoxyamine on ICL formation by **9b** upon UV irradiation. Lane 1: with DNA only; lane 2: 2 mM **9b** (cross-linking yield 54.4%); lane 3: 2 mM **9b** and 1 mM methoxyamine (52.0%); lane 4: 2 mM **9b** and 2 mM methoxyamine (45.0%); lane 5: 2 mM **9b** and 5 mM methoxyamine (39.7%); lane 6: 2 mM **9b** and 10 mM methoxyamine (22.4%); lane 7: 2 mM **9b** and 20 mM methoxyamine (5.6%); lane 8: 2 mM **9b** and 50 mM methoxyamine (2.5%); lane 9: 2 mM **9b** and 100 mM methoxyamine (1.1%). Condition: UV irradiation at pH8 for 8 h.

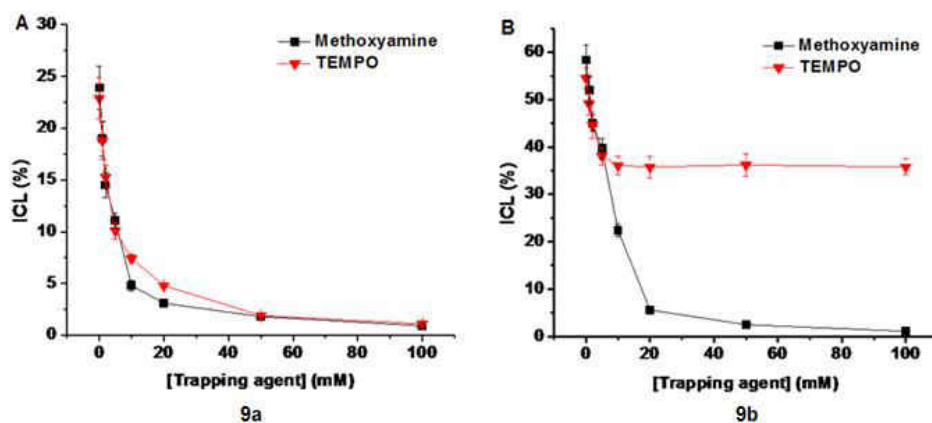


**Figure 26.** Effect of TEMPO and methoxyamine on ICL formation by **9a** and **9b**.

### 5.3. Experimental Section

**General Methods.** Unless otherwise specified, chemicals were purchased from Aldrich or FisherScientific and were used as received without further purification. T4 polynucleotide kinase was obtained from New England Biolabs. Oligonucleotides were synthesized via standard automated DNA synthesis techniques using an Applied Biosystems model 394 instrument in a 1.0  $\mu$ M scale using commercial 1000Å CPG-succinyl-nucleoside supports. Deprotection of the nucleobases and phosphate moieties as well as cleavage of the linker were carried out under mild deprotection conditions using a mixture of 40% aq. MeNH<sub>2</sub> and 28% aq. NH<sub>3</sub> (1:1) at room temperature for 2 h. Radiolabeling was carried out according to the standard protocols.<sup>1</sup> [ $\gamma$ -<sup>32</sup>P]ATP was purchased from Perkin-Elmer Life Sciences. Quantification of radiolabeled oligonucleotides was carried out using a Molecular Dynamics Phosphorimager equipped with ImageQuant Version 5.2 software. <sup>1</sup>H NMR and <sup>13</sup>C NMR spectra were taken on a Bruker DRX 300 MHz and 500 MHz spectrophotometer. High resolution mass spectrometry was performed at the University of California-Riverside and Shimadzu Laboratory for Advanced & Applied Analytical Chemistry at the University of Wisconsin-Milwaukee.

**Interstrand cross-link formation with duplex DNA 5 upon UV irradiation.** The  $^{32}\text{P}$ -labelled oligonucleotide (0.5  $\mu\text{M}$ ) was annealed with 1.5 equiv of the complementary strand by heating to 65  $^{\circ}\text{C}$  for 3 min in a buffer containing 10 mM potassium phosphate (pH 7), and 100 mM NaCl, followed by slow-cooling to room temperature overnight. The  $^{32}\text{P}$ -labeled oligonucleotide duplex (2  $\mu\text{L}$ , 0.5  $\mu\text{M}$ ) was mixed with 1 M NaCl (2  $\mu\text{L}$ ), 100 mM potassium phosphate (2  $\mu\text{L}$ , pH range 5-9) and different concentrations of compound **1-3b** or **9a,b** (concentration range: 20  $\mu\text{M}$  to 5 mM in 6  $\mu\text{L}$   $\text{CH}_3\text{CN}$  or  $\text{H}_2\text{O}$ ) and the appropriate amount of autoclaved water to give a final volume of 20  $\mu\text{L}$ . The reaction was irradiated with 350 nm UV light for 1-24 hours and quenched by an equal volume of 90% formamide loading buffer, then subjected to 20% denaturing polyacrylamide gel electrophoresis.

**Trapping assay of oligonucleotides.** The  $^{32}\text{P}$ -labeled oligonucleotide duplex (2  $\mu\text{L}$ , 0.5  $\mu\text{M}$ ) was mixed with 1 M NaCl (2  $\mu\text{L}$ ), 100 mM potassium phosphate (2  $\mu\text{L}$ , pH 8). The stock solution of  $\text{MeONH}_2\cdot\text{HCl}$  (2 M) was titrated with 5 M NaOH solution to adjust the pH to  $\sim 7.0$ . Then, 2  $\mu\text{L}$  was added to the reaction mixture as appropriate for the desired concentration. TEMPO was dissolved in  $\text{CH}_3\text{CN}$ , then 2  $\mu\text{L}$  was added to the reaction mixture as for the desired concentration. Different concentrations of compound **3** or **9** (4  $\mu\text{L}$  in  $\text{CH}_3\text{CN}$ ) and the appropriate amount of autoclaved water and  $\text{CH}_3\text{CN}$  were added to give a final volume of 20  $\mu\text{L}$  (6  $\mu\text{L}$   $\text{CH}_3\text{CN}$  with 14  $\mu\text{L}$   $\text{H}_2\text{O}$ ). The reaction was irradiated with 350 nm UV light for 4 hours and quenched by an equal volume of 90% formamide loading buffer, then subjected to 20% denaturing polyacrylamide gel electrophoresis.

**Stability study of ICL product formed with 6.** After the cross-link reaction, the reaction mixtures (0.35  $\mu\text{M}$  DNA duplex, 20  $\mu\text{L}$ ) were coprecipitated with calf thymus DNA (2.5 mg/mL, 5  $\mu\text{L}$ ) and NaOAc (3 M, 5 $\mu\text{L}$ ) in the presence of EtOH (90  $\mu\text{L}$ ) at -80  $^{\circ}\text{C}$  for 30 min, followed by

centrifuging for 5 min at 15000 rpm. The supernatant was removed, and the pellet was washed with cold 75% EtOH and lyophilized for 30 min in a Centrivap Concentrator of LABCONCO at 37 °C. The dried DNA fragments were dissolved in H<sub>2</sub>O (30 µL) and divided into three portions. One portion (10 µL) was incubated with piperidine (2 M, 10 µL) at 90 °C for 30 min, and the second portion (10 µL) was incubated with 0.1 M NaCl and 10 mM potassium phosphate buffer (pH 7, 10 µL) under the same condition, and the third portion was used as a control sample. The samples were subjected to 20% denaturing polyacrylamide gel electrophoresis.

**Hydroxyl radical reaction (Fe·EDTA reaction).** Fe(II)·EDTA cleavage reactions of <sup>32</sup>P-labelled oligonucleotide (0.1µM) were performed in a buffer containing 50 µM (NH<sub>4</sub>)<sub>2</sub>Fe(SO<sub>4</sub>)<sub>2</sub>, 100 µM EDTA, 5 mM sodium ascorbate, 0.5 M NaCl, 50 mM sodium phosphate (pH 7.2) and 1 mM H<sub>2</sub>O<sub>2</sub> for 3 min at room temperature (total substrate volume 20 µL), then quenched with 100 mM thiourea (10 µL). Samples were lyophilized, and incubated with 1 M piperidine (20 µL) at 90 °C for 30 min. The mixture was lyophilized again, dissolved in 20 µL H<sub>2</sub>O: 90% formamide loading buffer (1:1) and subjected to 20% denaturing polyacrylamide gel electrophoresis.

## CURRICULUM VITAE

Yibin Wang

Place of birth: Beijing, China

### **Education:**

*Ph.D.*, University of Wisconsin-Milwaukee, December 2015

Major: Organic Chemistry, Minor: Biochemistry, (Advisor: Prof. Xiaohua Peng)

*M.S.*, University of Wisconsin-Milwaukee, December 2012

Major: Organic Chemistry, Minor: Biochemistry, (Advisor: Prof. Xiaohua Peng)

*B.S.*, University of Science and Technology of China (China), July 2007

Major: Analytical Chemistry, (Advisor: Prof. Qingde Su)

**Publications:**

Cao, S., Wang, Y., Peng, X. The leaving group strongly affects H<sub>2</sub>O<sub>2</sub>-induced DNA cross-linking by arylboronates. *J. Org. Chem.* **2014**, *79*, 501-508.

Cao, S., Wang, Y., Peng, X. ROS-inducible DNA cross-linking agent as a new anticancer prodrug building block. *Chem. Eur. J.* **2012**, *18*, 3850-3854.

Wang, Y., Chen, W., Fan, H., Sun, H., Fan, Y., Peng, X. Photo-induced DNA interstrand cross-link formation by naphthalene boronates via a carboncation. (In preparation)

Wang, Y., Fan, H., Chen, W., Cao, S. Fan, Y., Sun, H., Kelly, T., Arnold, L. A., Peng, X. Electron-donating group greatly facility H<sub>2</sub>O<sub>2</sub>-induced DNA cross-linking and improved the cytotoxicity by arylboronates. (In preparation)

Wang, Y., Fan, Y., Fan, H., Sun, H., Chen, W., Peng, X. Photo-induced interstrands cross-links formation by arylboronates. (In preparation)

**Patent:**

Peng, X., Kuang, Y., Cao, S., Chen, W., Wang, Y.(2013) U. S. Pat. Appl. Publ., US 20130045949A120130221.

**Awards:**

UW-Milwaukee Chancellor's Graduate Fellowship, UW-Milwaukee, 2010.9-Present.

University Outstanding Undergraduate Researcher Award, USTC, CHINA, 2007